An investigation into the function and mechanism of a GRK5-L41 polymorphism using human pluripotent cell-derived cardiomyocytes.

Submitted by

Ngoc Nguyen Vo Thi, BSc MSc

School of Medicine

Department of Cancer & Stem Cells

The University of Nottingham

March 2020

Thesis submitted to The University of Nottingham for the degree of Doctor of Philosophy

I would like to dedicate this thesis to my Dad, Dr Vo Van Hiem, for giving me unconditional love and always supporting my dream of becoming a scientist. I love you, mom and dad.

I also want to send a special appreciation to my Sun, who always stand by me and keep me alive. I could not go this far without you.

Vietnamese translation:

Tôi giành tặng bản luận văn này cho ba mẹ của tôi, đã luôn động viên và giúp tôi hoàn thành ước mơ của mình là trở thành một nhà khoa học chân chính. Con cám ơn ba và mẹ rất nhiều. Con nhớ và yêu mẹ nhiều.

Anh đã luôn ở bên em trong những khoảnh khắc khó khăn nhất. Em sẽ không thể hoàn thành hành trình này nếu không có sự động viên của anh.

Declaration

I hereby declare that this thesis has been composed by myself and has not been submitted for any other degree previously. Acknowledgements of specific procedures not performed by myself are stated; otherwise, the work described is my own.

Ngoc Nguyen Vo Thi _____

Date:

Acknowledgements

First and foremost, I would like to thank my supervisor, Professor Chris Denning, for his patience and supports throughout my study. This work would not be accomplished without his supervision and inspiration. I believe your guidance will stand me in good stead for the rest of my career.

I am also grateful to Dr Minh Duc Hoang, who trained me labwork skills and put initial steps for this project by generating all GRK5-Q41L cell lines. Furthermore, I would also like to express my gratitude to Sasha, Dr Alexander Kondrashov, for his excellent guidance in molecular works. I want to send my thanks to Dr Robert Markus and Dr David Onion for training in Microscopy (SLIM) facility and Flow Cytometry facility respectively. Special thanks to Puspita Katili and Nurul Mohd Yusof for training in CellOPTIQ and CardioECR.

My gratitude extends to Cardio group, in past and present, who always encourage me and see me grow up over the past few years: Dr Diogo Mosqueira, Dr Jamie Bhagwan, Dr James Smith, Dr Liz Scott, Dr Aishah Nasir, Dr Vinoj George, Dr Mine Bakar Dogu, Dr James Crutchley, Dr Gary Duncan, Dr Luke Flatt, Dr Spandan Karla, Dr Lazaros Fotopoulos, and Mr Ralph Hyde. To Maria Muñoz, Penny Howick, Jayson Bispham and Katarzyna Lis-Slimak, I appreciate your technical supports. I would also like to acknowledge Caroline Reffin, who always encourage me during my PhD.

I thankfully never had to all of my CBS family: Lara, Sara PG, Ashley, Maria, Emma, Zubair, Peggy, Paulina, Analy, Paige, Sara, Anna, Jordan, Nigel, Kavita, Ben and Liam. Your supports and encouragement go above and beyond in terms of mentorship.

Finally, I'd like to thank my parent, for supporting my dream being a scientist and my Sun, for always believing in me and encouraging me to pursue my goals.

Abstract

A single-nucleotide polymorphism (SNP) in G protein-coupled receptor kinase 5 (termed GRK5-Q41L) was reported to be associated with a low mortality rate for patients with heart failure and cardiac ischemia (Liggett et al., 2008). An *in vitro* study on transfected cells and transgenic mice suggested that this GRK5-Q41L polymorphism enhances β-adrenergic receptors (β-AR) desensitisation to prevent adverse effects of chronic β-AR stimulation.

An area of need is for a relevant *in vitro* human cellular model to further characterise phenotype and explore mechanism for the gain-of-function of GRK5-Q41L SNP. This was the aim of my thesis, wherein I used the tractability of human pluripotent stem cell-derived cardiomyocytes (hPSC-CMs) to provide a valuable tool.

Nickase CRISPR/Cas9 genome editing technology had previously been used in our lab to generate Q41L SNP on the GRK5 loci in HUES7 line to generate the isogenic HUES7-GRK5-Q41L model. Also, in separate experiments, human induced pluripotent stem cells (hIPSCs) harbouring homogenous GRK5-Q41 and GRK5-L41 had been generated from lymphoblastoid cells by episomal reprogramming technology; however, this hIPSC GRK5-Q41L model has heterogenic background.

The isogenic HUES7-GRK5-Q41L model and heterogenic hIPSC GRK5-Q41L model were characterised for pluripotency criteria and differentiated to hPSC-CMs for further phenotype and mechanism analysis.

Phenotype analysis of contractility and cell survival response of GRK5-Q41L variant exhibited preserved contractility functions and lower cell death induced during chronic catecholamine stress. Analysis for nuclear translocation of GRK5-Q41L illustrated a noncanonical function, wherein the L41 variant prevented nuclear GRK5 accumulation relative to the Q41

variant. This phenotype was also associated with the higher BNP induction in HUES7-GRK5-L41 CMs, which suggested a compensation response during chronic catecholamine stress. However, the increase of nuclear GRK5 fraction was not observed in the heterogenic hIPSC GRK5-Q41L model, which highlighted the potential effects of genetic background on phenotypic study for SNPs. This observation suggested that affects of GRK5-Q41L SNP on noncanonical functions of GRK5 maybe not the main pathway accounting for the cardioprotection phenotype of the GRK5-L41 variant.

Further experiments studying the mechanism of GRK5-Q41L polymorphism on the isogenic model showed that GRK5 was responsible for the activation of extracellular signal-regulated kinases (ERK1/2) during isoprenaline (ISO) stimulation. The higher phosphorylated ERK1/2 activation in GRK5-L41 suggested an association with cardioprotection phenotypes. The GRK5-L41 variant was hypothesised to exert gain-of-function during catecholamine stress by (1) accelerating GRK5-mediated β-ARs phosphorylation and desensitisation to reduce adverse effects of chronic β-AR induction; and (2) promoting higher phosphorylated ERK1/2 activation via the β-arrestin dependent pathway.

Overall, the hPSC-CM model harbouring GRK5-Q41L SNP recapitulated cardioprotection phenotype in contractility and cell survival response during chronic catecholamine stress induced by ISO exposure. Molecular analysis also explored the mechanism for the gain-of-function of GRK5-Q41L SNP. Despite limitations of technique and phenotype, this thesis shows that an hPSC-CM model carrying GRK5-Q41L SNP provides a relevant human *in vitro* platform for the study of phenotypes and mechanisms of specific SNPs.

Abbreviations

Abbreviation	Description
AAV	Adeno-associated virus
AM	Acetoxymethyl ester
ANOVA	Analysis of variance
BL15	Biotin-lenti clone 15
bp	Base pairs
bpm	Beats per minute
β-MHC	Beta myosin heavy chain
BMP	Bone morphogenic protein
BSD	Blasticidin-S deaminase
CAG	CMV early enhancer/chicken β-actin promoter
CaM	Calmodulin
CaMKII	Ca^{2+}/calmodulin-dependent kinase II
CCD	Charge-coupled device
cDNA	Complementary DNA
ChR2	Channelrhodopsin-2
CICR	Calcium-induced calcium release
CM	Cardiomyocyte
CPVT	Catecholaminergic polymorphic ventricular tachycardia
CRISPR	Clustered Regularly Interspaced Short Palindromic Repeats
crRNA	CRISPR RNA
DAD	Delayed after-depolarisation
DAPI	Di-amino phenyl-indole
DMEM	Dulbecco's (Modified Eagle's) minimal essential medium
DMSO	Dimethyl sulfoxide
DNA	Deoxyribonucleic acid
dNTP	Deoxyribonucleotide triphosphate
DSB	Double-strand break
DPBS	Dulbecco’s Phosphate Buffered Saline
E8	Essential 8 medium
EDTA	Ethylene diamine tetra-acetic acid
ELISA	Enzyme-linked immunosorbent assay
EMCCD	Electron-multiplying CCD
ESPT	Excited state proton transfer

ex/em	Excitation/ Emmision
F/F_0	Fluorescence intensity signal-to-noise ratio
FP	Fluorescent protein
FRET	Förster resonance energy transfer
FRT	Flippase recombinase target
FWD	Forward
gDNA	Genomic DNA
GECI	Genetically encoded calcium indicator
GECO	Genetically encoded calcium indicator for optical imaging
GEVI	Genetically encoded voltage indicator
GFP	Green fluorescent protein
HBSS	Hank's Buffered Salt Solution
HCM	Hypertrophic Cardiomyopathy
HDR	Homology-directed repair
hESC	Human embryonic stem cell
hESC-CM	Human embryonic stem cell derived cardiomyocyte
hiPSC	Human induced pluripotent stem cell
hiPSC-CM	Human induced pluripotent stem cell derived cardiomyocyte
hPSC	Human pluripotent stem cell
hPSC-CM	Human pluripotent stem cell derived cardiomyocyte
KO	Knock out
iPSC	Induced pluripotent stem cell
IRES	Internal ribosome entry site
kb	Kilobases
mESC	Mouse embryonic stem cell
mRNA	Messenger RNA
MW	Molecular weight marker
MUT	Mutant
NTC	No template control
NEAA	Non-essential amino acids
NHEJ	Non-homologous end joining
NpHR	Halorhodopsin from Natronomonas
P2A	Porcine teschovirus-1 2A
PAM	Protospacer adjacent motif
PBS	Phosphate buffered saline
PCR	Polymerase chain reaction
Puro	Puromycin

RB	RPMI 1640 with B27 supplement
REV	Reverse
RFP	Red fluorescent protein
RGEN	RNA-guided endonuclease
RLU	Relative luminescence units
RNA	Ribonucleic acid
ROCKi	Rho-associated kinase inhibitor
RT	Room temperature
RT-PCR	Reverse transcriptase PCR
SCD	Sudden cardiac death
SD	Standard deviation of the mean
SEM	Standard error of the mean
SERCA	Sarcoplasmic reticulum Ca^{2+}-ATPase
sgRNA	Single guide RNA
SNP	Single nucleotide polymorphism
SR	Sarcoplasmic reticulum
T2A	Thoseaasigna virus 2A
TALEN	Transcription activator-like effector nuclease
TAE	Tris-acetate-EDTA
tracrRNA	Transactivating CRISPR RNA
VTN	Vitronectin-N truncated protein
WT	Wild-type
ZFN	Zinc finger nuclease
%	Percentage
^{0}C	Degree Celsius

Table of Contents

List of Figures

List of Tables

Chapter 1 Introduction

1.1 G-Protein Coupled Receptors (GPCRs).

G-protein coupled receptors (GPCRs) are seven-transmembrane domain receptors with an extracellular amino terminus and an intracellular carboxyl terminus (Muthumala et al., 2008; Pierce et al., 2002) (**Figure 1.1**). GPCRs function via their interaction with guanine nucleotide-binding proteins (G-protein) inside cells and form the largest protein superfamily in the mammalian system. There are approximately 800 human GPCRs, and they are grouped into five main families; Rhodopsin, Glutamate, Adhesion, Secretin and Frizzled/taste2 (Fredriksson et al., 2003). GPCRs respond to a variety of extracellular signals, including small molecules, peptides and proteins to regulate most physiological responses and disease development, such as cardiovascular diseases, metabolism, inflammation, cancer and infectious disease (Pierce et al., 2002, Katritch et al., 2013). Therefore, they have become a major pharmaceutical target for intervention with approximately 34% of all drugs approved by the US Food and Drug Administration targeting GPCRs, creating a global market value of at least $180 billion annually (Hauser et al., 2018).

1.1.1 Overview of GPCR signalling

GPCR signalling contains three main components, including a seven-transmembrane-spanning receptor, an intracellular heterotrimeric G-protein complex and effectors (Pierce et al., 2002; Wang Jialu et al., 2018) (**Figure 1.1**). The trimeric G-protein complex comprises α, β and γ subunits - Gαβγ, that can bind to both guanosine triphosphate (GTP) and guanosine diphosphate (GDP) nucleotides (Dolatshad et al., 2015; Pierce et al., 2002). The α subunit is responsible for GDP to GTP conversion, while the β and γ subunits are associated as βγ complex. To date, 16 Gα subunits have been

identified, 5 Gβ subunits and 12 Gγ subunits have also been revealed in the human genome. GPCR signalling is primarily mediated via the receptor G-protein α-subunits, including Gαs, Gαi, Gαq, and Gα12/13. Each class also consists of multiple subtypes.

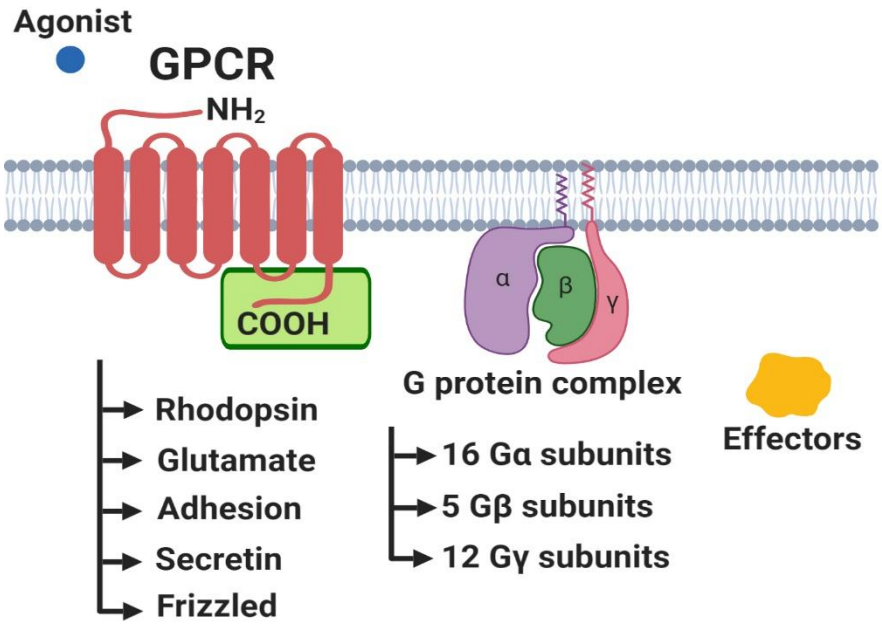

Figure 1.1 G protein-coupled receptor signalling

A representative GPCR with extracellular amino terminus (NH_2), seven-transmembrane domains (Red), and intracellular carboxy-terminus (COOH). Intracellular G protein coupling domains that can be phosphorylated by GRKs are shown by the green rectangle.

1.1.2 Agonist-mediated activation of GPCR

In the resting state, GPCRs and Gαβγ are not associated (Pierce et al., 2002; Wang Jialu et al., 2018). Once the agonist binds, Gαβγ associates with the receptor at the intracellular C-terminal domain of the receptor and is followed by GDP-GTP conversion. The binding of α subunit to GTP results in Gα and Gβγ dissociation from the receptor with its respective effector proteins leading to activation of downstream signalling pathways, including adenylyl cyclase (AC), phospholipases, or ion channels. The deactivation of agonist-bound GPCRs is mainly accomplished via phosphorylation of G

protein-coupled receptor kinases (GRKs) via a process called desensitisation, which leads to a reduction of receptor responsiveness. Phosphorylation of the receptor induces receptor conformational changes and subsequent β-arrestin binding. β-arrestin binding prevents receptor-Gα interaction and promotes internalisation of phosphorylated receptors which are subsequently sorted for proteasome degradation or recycling back to the sarcolemmal membrane (Katritch et al., 2013; Pierce et al., 2002) (**Figure 1.2**).

1.1.3 GPCR in the heart

Adrenergic signalling is one of the major stress-response systems in the human body, and their receptors belong to the rhodopsin family, which has the largest number of GPCRs (Dorn, 2010a; Fredriksson et al., 2003). The biogenic amine receptor group includes α1-adrenergic receptors (α1-ARs), α2-adrenergic receptors (α2-ARs) and β-adrenergic receptors (β-ARs). The AR system regulates heart functions in response to the stress induced by catecholamines (Lohse et al., 2003; Katritch et al., 2013). The three β-ARs subtypes, β1-ARs, β2-ARs and β3-ARs, are all expressed in cardiomyocytes to varying extents and they are also found in the myocardium, vascular smooth muscle and adipose tissue, respectively.

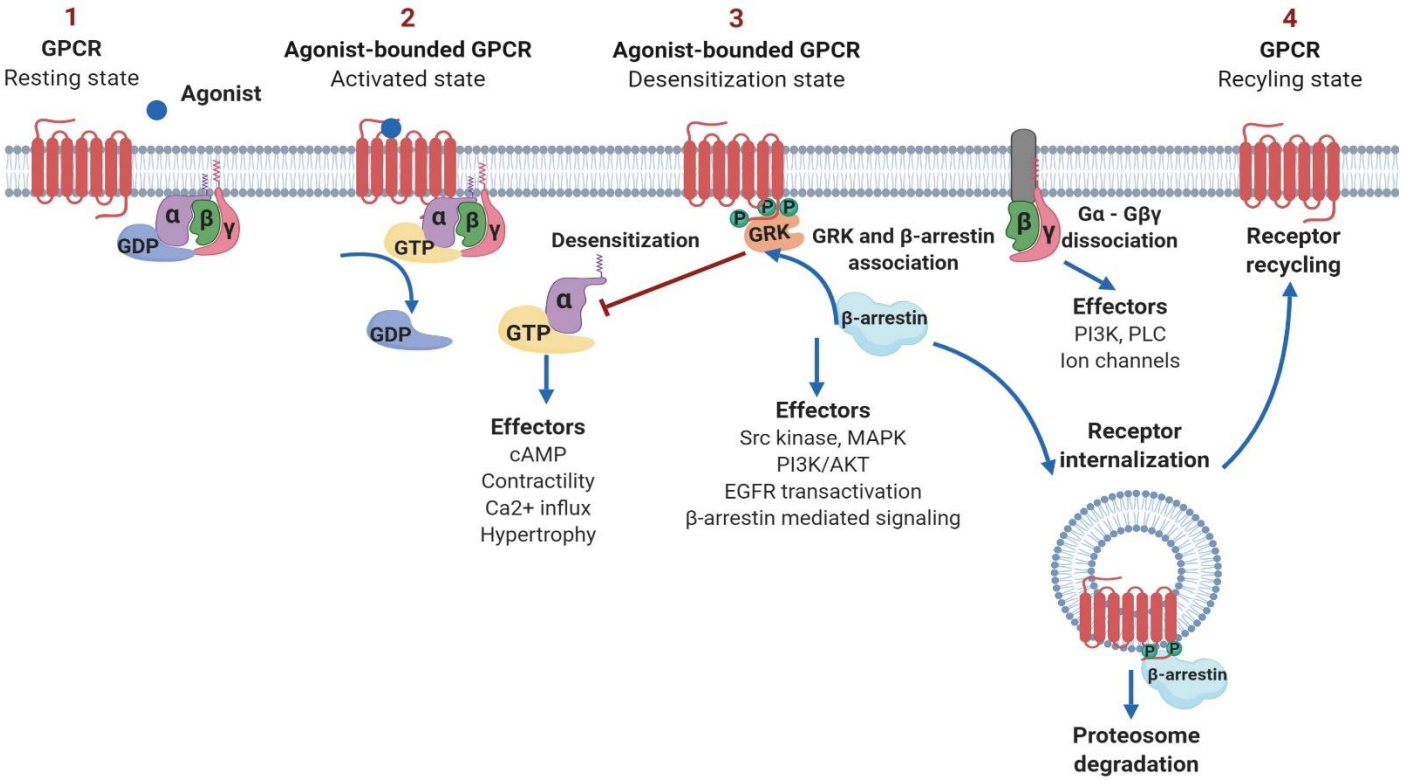

Figure 1.2 The activation of G protein-coupled receptor signalling pathway

At resting state (1), Gαβγ complex is bounded to GTP and is not associated with GPCR. Upon agonist binding (2), Gαβγ associates with the receptor. (3) Gα and Gβγ dissociate from the receptor with its respective effector proteins leading to down downstream signalling. At the activated receptor, GRK binds and phosphorylate the receptor leading to receptor conformation changes and subsequent β-arrestin binding. (4) β-arrestin bounded receptors are then primed for clathrin-mediated endocytosis and sorted for proteasome degradation or receptor recycling.

1.2 β-adrenergic signalling (β-ARs)

1.2.1 β-ARs functions in the heart

As the adrenergic system is the major regulator of immediate stress responses in the human body, stimulation of β-AR signalling is the early response of the body to enhance cardiac output (Dorn, 2010a; Kang et al., 2016; Lohse et al., 2003b). Among three groups of adrenergic receptors, the β-AR family plays a vital role in the control of the contractile machinery, such as heart rate (chronotropy), contractility (inotropy) and relaxation speed (lusitropy) (Andersson et al., 2011; Dorn, 2010a; Lohse et al., 2003a). The consequence of β-AR signalling stimulation is increased cardiac output by enhanced cardiac muscle contraction (positive inotropy), heart rate (positive chronotropy) as well as relaxation time (positive lusitropy). In normal ventricle myocardium, β1-ARs and β2-ARs are expressed in a ratio of 80 %: 20 %, and β3-ARs are less than 1 %. But this ratio changes in heart failure (HF) myocardium to approximately 60 %: 40 % with the down regulation of β1-ARs (Bristow et al., 1986; Lohse et al., 2003b). This indicates a pivotal role of β2-ARs during the development of HF. β1-ARs and β2-ARs play major roles in modulating cardiac output (inotropy and chronotropy) and blood pressure, while β3-AR roles have not been well studied (Lucia et al., 2018). Balligand et al. claimed that the β3-AR expression is increased during heart failure and its activation results in the reduction of positive inotropic response in the failing heart (Balligand, 2013).

β-AR signalling plays a central role in the regulation of cardiac contractility. In cardiomyocytes, catecholamines, which are released by the sympathetic (adrenergic) nervous system, bind to β-ARs receptors resulting in stimulation through Gαs (Gs) (Lohse et al., 2003b; Pierce et al., 2002). Gs signalling stimulates the effector AC to convert adenosine triphosphate (ATP) into a second messenger cyclic adenosine monophosphate (cAMP),

leading to activation of the cAMP-dependent protein kinase – protein kinase A (PKA). The Gs-Ac-cAMP signalling cascade can be mediated by both β1-AR and β2-AR (Muthumala et al., 2008) (**Figure 1.3**).

The increase of PKA leads to the phosphorylation of a wide variety of intracellular proteins that results in a significant increase in free intracellular Ca^{2+}, which is the main regulator of cardiac contraction. PKA can elicit enhanced inotropy, lusitropy, hypertrophy (growth) and apoptosis (death) (Lohse et al., 2003b; Yang Jason H. et al., 2011). Major targets of PKA phosphorylation are essential for cardiac function, such as L-type calcium channels (LTCC), ryanodine receptors (RyRs), phospholamban (PLB), troponin I, myosin-binding protein-C (MyBP-C) and protein phosphatase inhibitors-1 (Lohse et al., 2003b). Phosphorylation affects cardiomyocyte contraction by increasing Ca^{2+} influx (LTCC), Ca^{2+} reuptake (PLB) and modulating myofilament Ca^{2+} sensitivity (Troponin I, MyBP-C).

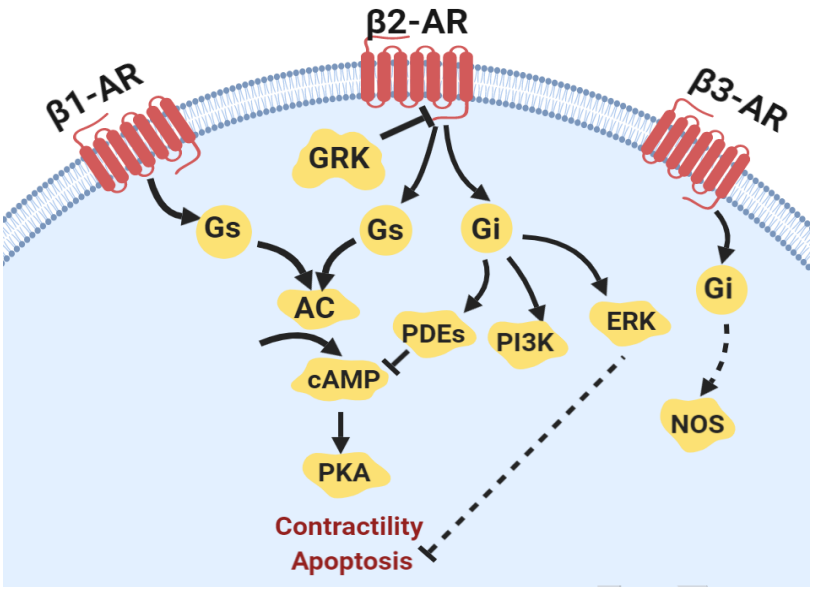

Figure 1.3 ***Signalling properties of β-adrenergic receptor subtypes.***

GRK indicates G protein-coupled receptor kinase; AC, adenylyl cyclase; βArr, β-arrestin; cAMP, cyclic adenosine monophosphate; ERK, Extracellular signal-regulated kinase; NOS, nitric oxide synthase; PDE, phosphodiesterase; and PI3K, phosphatidylinositol 3-kinase (Adapted from Lohse et al., 2003)

1.2.2 Sustained β-AR signalling related to the apoptosis of cardiomyocytes during Heart Failure.

Chronic stimulation of the Gs-Ac-cAMP cascade via β1-AR stimulation can cause harmful effects resulting in HF. β2-ARs and β3-ARs can couple to Gαi (Gi) to suppress activation of the $G\alpha_s$-Ac-cAMP cascade as a negative feedback loop (Lucia et al., 2018; Sato et al., 2015a). Moreover, chronic stimulation of β-ARs also develops a receptor desensitisation process mediated by GRKs, followed by β-arrestin binding, which prevents receptor-Gs interaction and promotes internalisation of desensitised β-ARs.

At the early stage of reduced cardiac function, an increase of β-ARs signalling preserves cardiac output (Bristow, 2000; Lohse et al., 2003b). However, sustained induction of β-AR signalling may lead to further pathogenic changes in the heart. During HF, the Gs-Ac-cAMP cascade, especially through β1-ARs signalling, may cause harmful effects leading to apoptosis in cardiomyocytes through activation of the downstream cAMP/PKA signalling, as well as fibroblast hyperplasia and proarrhythmia (El-Armouche and Eschenhagen, 2008; Engelhardt et al., 1999; Mann et al., 1992). This cAMP/PKA signalling is counterbalanced by cAMP phosphodiesterase (PDE). The hydrolysis of cAMP in the heart is mediated by $G\alpha_i$ through β-AR activation (Ding et al., 2005).

During β-AR signalling in cardiomyocytes, PDEs play crucial roles in regulating cardiac contraction amplitude, beating duration, and compartmentalisation of cAMP (El-Armouche and Eschenhagen, 2008; Lohse et al., 2003b). PDE3 enzymes play a major role in regulating cAMP metabolism in the cardiovascular system, where downregulation of PDE3A isoform in failing hearts was suggested to have a causative role in the progression of HF (Yan et al., 2007). In particular, persistent upregulation of inducible cAMP early repressor (ICER) and downregulation of PDE3A via

cAMP/PKA cascade was proven to activate the positive feedback loop, which promotes cardiac myocyte dysfunction and apoptosis due to suppression of Bcl-2 transcription (Tomita et al., 2003).

One type of apoptotic response in cells is mediated through the mitochondria pathway and involves members of the BCL-2 family protein. The protein family regulates cell death via directly binding to the mitochondrial membrane (Kale et al., 2018; Shamas-Din et al., 2013). This binding then regulates mitochondrial membrane permeabilisation (MOMP) resulting in the release of intermembrane space proteins and subsequent caspase activation and apoptosis. This protein family can be divided into three groups named Group I proteins, consisting of anti-apoptotic BCL2 protein, Group II and III pro-apoptotic proteins, consisting of BAX and BAK (Kale et al., 2018; Zhao et al., 2014). Homodimer formation of BAX or BAK could open the mitochondrial membrane resulting in the release of Cytochrome C and Reactive Oxygen Species (ROS), which in turn trigger cell apoptosis (Kolenko et al., 2013). Further studies have reported that β-ARs subtypes regulate apoptosis response in cardiomyocytes associated with BCL2 suppression and increased ROS production (Saito et al., 2000; Shin et al., 2014; Tomita et al., 2003; Wang et al., 2015). Induction of β1-AR signalling induced apoptosis via the cAMP/PKA cascade results in reduction of BCL2 levels. In contrast, induction of β2-AR signalling could reduce programmed cardiomyocyte death by switching sequentially from Gs to Gαi-coupled signalling pathway (Dorn, 2010b; Shin et al., 2014). This study highlights the role of β2-AR in apoptosis response during HF.

The activation of β-AR signalling results in an increase of intracellular Ca^{2+} following by its downstream signalling, including Calcineurin - Calmodulin-dependent protein kinase II (CaMKII). Both of these signalling pathways contribute to cardiac remodelling during HF (Lohse et al., 2003b; Yang et al., 2014). Exaggerated CaMKII activation increases mitochondrial cytochrome C release as well as activating pro-apoptotic factor Bcl10 and pro-apoptotic protease AP24 (Wright et al., 1997). The excessive stimulation of β-ARs via Gs-Ac-cAMP cascade leads to the increase of Ca^{2+} followed by the activation CaMKII dependent signalling and causes an increase of Reactive Oxygen Species (ROS) production and reduced *BCL2* transcription, which induce apoptosis in cardiomyocytes (Corbi et al., 2013; Dries et al., 2016; Kang et al., 2016; Zhang and Brown, 2004).

The induction of β-AR signalling also activates nicotinamide adenine dinucleotide phosphate (NADPH) oxidases and promotes ROS production, which is an important activator in the Mitogen-activated protein kinases (MAPKs) cascade (Lohse et al., 2003b; Yang et al., 2014). Activation of cardiac MAPK signalling also adds more complexity in the regulation of apoptosis during sustained β-AR stimulation. The MAPKs are cytosolic signalling proteins and consist of three classical members, which are protein kinase p38 (p38 MAPK), extracellular signal-regulated kinases (ERK1/2) and c-Jun N-terminal kinases (JNK). Activation of MAPK via β-AR stimulation involves PKA-mediated phosphorylation of β2-AR, which then induces the switch from Gs to Gi and leads to an increased ERK activation and associated anti-apoptotic signals (Lohse et al., 2003b; Shin et al., 2014). Activation of ERK1/2 signalling via β-Arrestin-dependent, G Protein-dependent pathways has been well established during β2-AR activation (Jean-Charles et al., 2017; Shenoy et al., 2006). In contrast, JNK activation exerts pro-apoptotic effects,

while p38 MAPK-mediated effects on apoptosis are controversial (Rose et al., 2010; Zhai et al., 2012).

Activation of the β-AR signalling also induces an increase in phosphoinositide 3-kinase (PI3K) activity, which has been proven to play important roles in cell survival (Fujio Yasushi et al., 2000; Yang et al., 2014). Gi coupling via β2-AR has protective functions in cardiomyocytes, which not only help to reduce the Gs stimulated signalling pathway but also activates the PI3K-Akt signalling pathway (**Figure 1.3**). IGF-1, which is downstream of PI3K-Akt signalling, has been shown to promote survival in cardiomyocytes (Fujio Yasushi et al., 2000; Mockridge et al., 2000). Akt signalling has cardioprotective effects by phosphorylating pro-apoptotic molecule BAD to prevent BAD from binding to BCL2 and BCL-xL (Chen et al., 2012, p. 2; Fujio Yasushi et al., 2000; Wu et al., 2000).

1.3 GRKs and their roles in deactivating GPCRs

1.3.1 Overview of GRK family

G protein-coupled receptor kinases (GRKs) are a family of serine/threonine-protein kinases that specifically recognise and phosphorylate agonist-activated GPCRs (Ribas et al., 2007; Sato et al., 2015a). Phosphorylation of activated GPCRs by GRKs initiates receptor internalisation and induces recruitment and phosphorylation of cytosolic protein β-arrestins, which binds to the receptor and terminates further G-protein coupling in a process termed desensitisation. The GRK family is composed of seven members and is divided into three main subcategories based on their sequence similarity and gene structure analysis, including rhodopsin (or visual) kinase subfamily (comprising of GRK1 and GRK7), β-AR kinase subfamily (consisting of GRK2 and GRK3), and GRK4 subfamily (comprising of GRK4, GRK5 and GRK6) (Sato et al., 2015) (**Figure 1.4**). The GRK family contain shared structural and functional hallmarks that are

evolutionarily conserved among GRKs in nematodes, insects, and mammals, indicating their biological significance (Pfleger et al., 2019a; Sato et al., 2015a).

The structure of these protein kinases is composed of three essential regions, consisting of 25-residue proximal NH2 terminal regions followed by a regulator of G protein signalling (RGS) homology region (RH), a centrally located ~500 to 520 amino acid catalytic domain, which flanked by large amino- and carboxyl-terminal regulatory domains (Pfleger et al., 2019a; Ribas et al., 2007). The catalytic domain performs Ser/Thr kinase activities. The NH2 terminal regions of GRKs share a common structure, while the carboxyl terminus is the most diverse component among GRK subfamilies (Ribas et al., 2007; Sato et al., 2015).

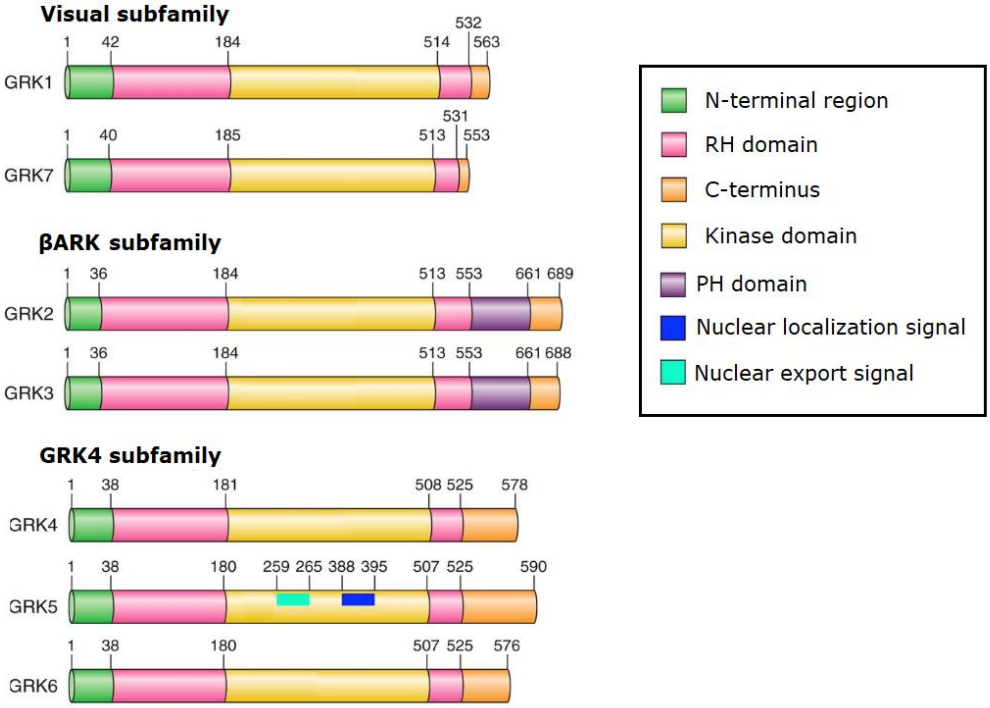

Figure 1.4.GRK topology *and* subfamily.

All GRKs are comprised of a NH2-terminal region (green), followed by an RH domain (pink) interrupted by a kinase domain (yellow) and a COOH terminus (orange). Visual or rhodopsin-kinases subfamily comprises of GRK1 and GRK7. The βARK subfamily comprises of GRK2 and GRK3. The GRK4 subfamily is comprised of GRK4, GRK5, and GRK6. GRK5 has a unique nuclear localisation signal (blue) and nuclear export signal (turquoise) (Adapted from Sato et al., 2015a).

1.3.2 GRKs functions in the heart

Most GRKs are ubiquitously expressed, but there is still tissue-specific distribution (Pfleger et al., 2019a; Sato et al., 2015a). GRK1 and GRK7 are primarily expressed in retinal photoreceptor cells, while GRK4 is highly expressed in the testes. GRK2, GRK3 and GRK5 are ubiquitously expressed with varying extents in different tissue. In the heart, GRK5 and GRK2 are most abundant, whereas GRK3 and GRK6 are found at low levels.

In the heart, GRK2 and GRK5 are directly involved in the regulation of the adrenergic functions (Hullmann et al., 2016; Pfleger et al., 2019a). GRK2s are cytosolic proteins and contain a pleckstrin homology (PH) domain suggesting that these GRKs confer the ability to associate with Gβγ subunits or anionic phospholipids (Johnson et al., 2013). The GKR5 kinase is a membrane-bound protein with a phospholipid-binding domain. Interestingly, GRK5 is the only GRK that has both a nuclear localisation sequence (NLS) domain and a nuclear export signal (NES) domain (Johnson et al., 2013) (**Figure 1.4**).

The canonical function of GRKs is mediating the uncoupling and internalisation of activated GPCRs, and so all GRKs are primarily localised in the cytosol and plasma membrane (Grisanti et al., 2018; Pfleger et al., 2019a; Sato et al., 2015a). GRK1 and GRK7 can attach to the plasma membrane due to prenylation consensus sequences within the C terminal. In contrast, GRK2 and GRK3 are localised to the cytosol. These kinases contain pleckstrin homology domain in the C terminus, which binds to the membrane-anchored Gβγ subunit after dissociation from the G-protein heterotrimer, resulting in membrane translocation after receptor stimulation. Both GRK4 and GRK6 contain a palmitoylation site, while GRK5 contains a phospholipid-binding domain. These components allow for their membrane localisation. In addition, GRK5, with the presence of NLS and NES domains,

is able to localise in the nucleus (Sato et al., 2015a). Indeed, GRK5 nuclear import was found to be controlled by calcium/calmodulin-binding to its CaM binding domain in the amino-terminus (Hullmann et al., 2016; Komolov et al., 2015; Sato et al., 2015a). Recent studies have shown that GRK2 can also be found to localise in mitochondria (Fusco et al., 2012; Mayor et al., 2018; Sorriento et al., 2019).

1.3.3 GRKs and their roles in heart failure conditions

The distribution of variants of GRKs is different among heart cells, GRK2 and GRK5 are expressed in almost all cardiac cells, while GRK3 is only found in cardiac myocytes (Penela et al., 2006; Vinge et al., 2007). During HF, GRK3 level is not altered; however, Vinge *et al.* suggested that GRK3 may play roles in cardiac growth and hypertrophy (Vinge et al., 2007). Many studies have proved that GRK2 and GRK5 are the primary regulators of β1-AR and β2-AR desensitisation in response to catecholamine stress, and their expression is upregulated during HF (Dorn, 2009; Pfleger et al., 2019a; Ribas et al., 2007). The deactivation of agonist-bound GPCRs prevents prolonged activation of Gs signalling and the subsequent activation of cAMP. Hence, increased GRK activity switches the receptor equilibrium towards the inactive state, which in turn, creates a condition of reduced receptor responsiveness to catecholamines (Dorn, 2009; Grisanti et al., 2018). Continued activation of β-ARs in cardiomyocytes during HF leads to the increase in GRK2 and GRK5 expression, which results in receptor downregulation and reduction of β-AR signalling pathways (Penela et al., 2006). However, HF studies have reported that increasing GRK activities in both the heart and sympathetic nervous system further enhanced these pathological events (Lobmeyer et al., 2011).

1.3.3.1 GRK2

GRK2 is the best-studied isoform among GRK isoforms. GRK2 is proven to play a pivotal role in normal and pathological cardiac regulation and function (Dorn, 2009; Mangmool et al., 2018; Sato et al., 2015a). Chronic administration of catecholamine stress by ISO leads to β-AR desensitisation and upregulation of GRK2 levels. Chronically enhanced GRK2 activity leads to blunted β-AR signalling, however chronically enhance GRK2 activity leads to blunted β-AR signalling and decreased inotropic and contractility reserves (Penela et al., 2006; Pfleger et al., 2019a; Ribas et al., 2007; Ungerer et al., 1993). Studies of reduction in GRK2 levels, both in expression and activity, showed enhanced cardiac contractility function. Knockout (KO) of GRK2 in mice significantly prevented mortality during chronic HF (Raake Philip W. et al., 2012, 2008). Inhibition of GRK2 activity by a small peptide, βARKct, in transgenic mice also showed enhanced contractility and increased sensitivity to β-AR stimulation (Koch et al., 1995).

GRK2 was also involved in the regulation of cell metabolism and apoptosis. GRK2 localised to the mitochondria was shown to regulate mitochondrial biogenesis and ATP generation (Fusco et al., 2012). GRK2 overexpression leads to increased oxidative stress and promotes cell death in ischemic myocytes, while its inhibition showed an increase in ATP production and had a cardioprotective effect (Chen Mai et al., 2013; Sato et al., 2015a). The cardioprotective effects of GRK2 inhibition could also be due to removing of its inhibition of Akt signalling and MEK1/ERK activation (Liu et al., 2005; Ribas et al., 2007). GRK2 is reported to associate directly with the serine-threonine kinase Akt, which is an important mediator of cardiomyocyte survival during stress. Also, the binding of GRK2 to MEK is reported to have an inhibiting effect on MEK/ERK activation (Jiménez-Sainz et al., 2005). Together, upregulation of GRK2 showed it has pathological

roles during HF and is associated with the dysfunction of β-AR mediating signalling.

1.3.3.2 GRK5

GRK5 is ubiquitously expressed in the body; however, the expression level of GRK5 is highest in the myocardium compared to other tissues, and it is the most commonly found GRK in transplanted and the failing hearts (Dorn, 2009; Mangmool et al., 2018; Sato et al., 2015a). Studies on zebrafish and mice showed that GRK5-KO is not embryonic lethal, but GRK5 is believed to play role in cardiac development (Burkhalter et al., 2013; Gainetdinov et al., 1999; Philipp et al., 2014; Rockman et al., 1996). GRK6 may compensate for GRK5-KO as double KO of GRK5 and GRK6 is embryonic lethal (Gainetdinov et al., 1999; Philipp et al., 2014). Overexpression of GRK5 in the heart showed attenuation of β-AR signalling and function. However, cardiac hypertrophy and HF phenotypes were detected in cardiac-specific overexpression of GRK5 in transgenic mice, due to its translocation to the nucleus (Martini et al., 2008). Conversely, GRK5 was also reported to promote cardiomyocytes survival during catecholamine-induced β-AR stimulation (Noma et al., 2007). These beneficial effects were due to the canonical roles of GRKs in terminating GPCR signalling by mediating the uncoupling and internalisation of GPCRs.

GRKs could also phosphorylate nonreceptor substrates, which has been defined as noncanonical functions of GRKs. Indeed, recent studies have reported that nuclear localisation of GRK5 in cardiomyocytes is attributed to the development of hypertrophy and the progression of HF (Gold et al., 2013; Hullmann et al., 2014; Traynham et al., 2015). The accumulation of GRK5 in the nucleus, mediated in a Gαq - dependent manner, acts as a class II histone deacetylase 5 (HDAC5) kinase to activate hypertrophic transcription factors - myocyte enhancer factor-2 (MEF2) (Hullmann et al.,

2014; Sato et al., 2015a; Traynham et al., 2015). While the canonical role of GRK5 to phosphorylate agonist bound GPCRs occurred at the plasma membrane is associated with cardioprotective effects, noncanonical actions of GRK5 is induced by its nuclear accumulation resulting in pathological hypertrophy (Traynham et al., 2016).

1.4 Polymorphisms in GRK5 and β-ARs and their effects during heart failure.

1.4.1 Polymorphisms in GRK5

Genetic polymorphisms are defined as variants that occur at a locus with an allelic frequency of greater than or equal to 1%. Both the susceptibility for the development of heart failure and the efficacy of therapeutic interventions, including β-blocker therapy, are associated with polymorphisms. There is considerable variation in HF susceptibilities to pharmacological β-blocker treatments, whereby genetic predisposition is proposed to be responsible for the susceptibility to HF and inter-individual variability (Cipolletta et al., 2013; Dorn, 2010a). Importantly for GRK-targeted therapeutic intervention, polymorphisms can affect GRK regulation of adrenergic signalling. No polymorphisms were detected in GRK2, but four uncommon variants were identified in GRK5 (Liggett et al., 2008). Nucleotide changes results in Single Nucleotide Polymorphism (SNP) that are detected at nucleic acid positions 122 (A/T), 840 (G/A), 1274 (C/T) and 1624 (C/G), resulting in amino acid changes at position 41 (glutamine - Q to leucine - L), 304 (arginine - R to histidine - H), 425 (threonine - T to methionine - M) and 542 (proline - P to alanine - A). Among four of these SNPs, GRK5-Q41L is the only allele frequency greater than 2% in any ethnic group.

The CaM binds to N- and C-terminal regions of GRK5 at amino acid 20–39 and 546–562 residues, respectively (Komolov et al., 2015). These regions also overlap with the membrane-binding determinants, which resides at

amino acid 22–35 residues. The GRK5-Q41L variant, which resides at the α1 helix of the RH domain, is close to the membrane-binding determinant and CaM binding domain in the N-terminal. The position of GRK5-Q41L polymorphism is illustrated in **Figure 1.5**.

This polymorphism showed enhancement of β1-AR desensitisation. A study of transgenic mice expressing human GRK5-Q41 and GRK5-L41 showed that GRK5-L41 expressing mice were protected from adverse ventricle remodelling caused by catecholamine stress (isoproterenol) and acted as though they had been treated with the β-blocker propranolol (Dorn and Liggett, 2013; Liggett et al., 2008). Interesting, this GRK5-Q41L variant is more common in African Americans affecting approximately 40 % compared to the Caucasian population with just around 2 % (Dorn and Liggett, 2013). This may suggest some evolutionary impact.

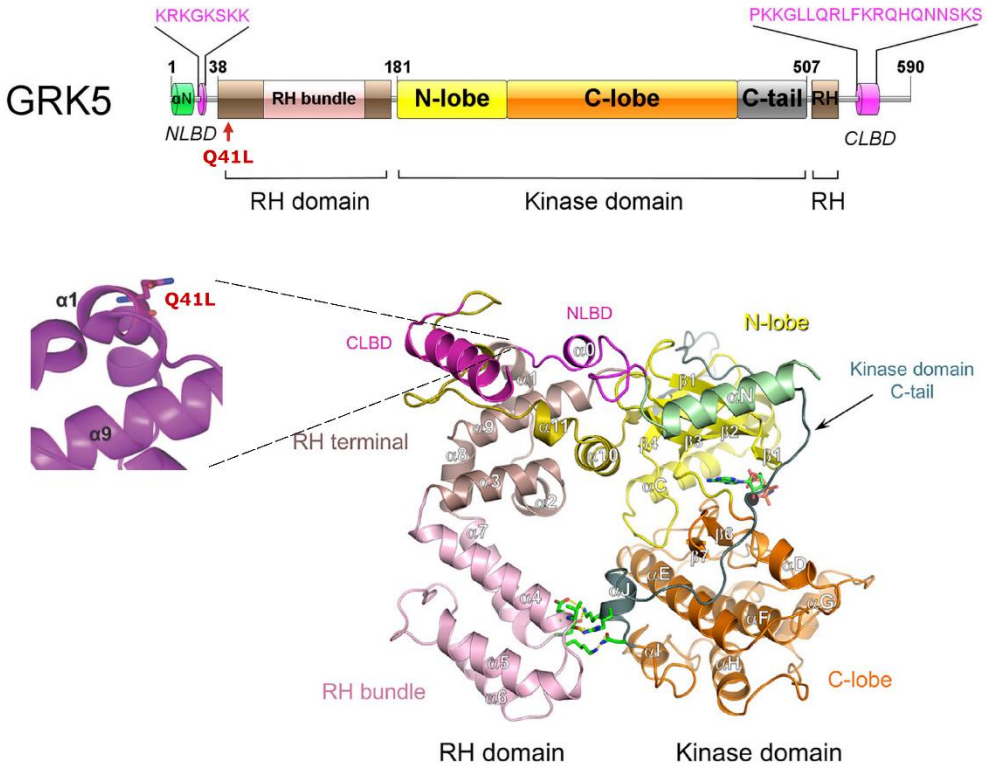

Figure 1.5.Position of the GRK5-Q41L polymorphism in GRK5 protein.

The GRK5-Q41L polymorphisms reside in α1 helix of the RH domain. Structural schematic of GRK5 includes RH bundle and terminal subdomains, catalytic C-lobe and N-lobe subdomains, N-terminal lipid-binding domain (NLBD) and C-terminal lipid-binding domain (CLBD) (Adapted from Komolov and Benovic, 2018).

1.4.2 Polymorphisms in β-ARs

1.4.2.1 β1-ARs

Polymorphisms in GPCRs also alter susceptibility and mortality of patients during HF and β-blocker treatment, where they were reported to influence receptor expression level, responses and receptor recycling (Brodde, 2008; Dorn, 2010a; Dorn and Liggett, 2009; Liggett, 2010). Numerous genetic polymorphisms of β-ARs have been identified (Table 1). *ADRB1* is polymorphism with 9 SNPs reportedly associated with human disease (Dorn, 2010a; Liggett, 2010). The two most studied SNPs that result in amino acid changes in β1-AR are at residues 49 (Serine – S to Glycine – G) in the extracellular amino-terminus and 389 (Arginine – R to Glycine – G)

in the intracellular carboxy-terminus. The ADRB1-S49G polymorphism affects agonist-mediate downregulation, where ADRB1-G49 variant has much more rapid downregulation compared to ADRB1-S49 variant (Brodde, 2008, 2007). The ADRB1-R389 variant has three-to-four fold higher ISO-stimulation AC than ADRB1-G389 variant. Interestingly, the ADRB1-S49G and ADRB1-R389G have a strong linkage disequilibrium. G49 is almost always homozygous with R389, while G389 is nearly always homozygous with S49. The combination of G49G389 appears not to occur natively (Brodde, 2008, 2007; Dorn, 2010a). These studies stated that ADRB1-R389G seems to determine heart rate and blood pressure in response to β1-blocker, and patients carrying homozygous ADRB1-R389 have better responses and survival compared to homozygous ADRB1-G389 during β1-blocker carvedilol or metoprolol.

1.4.2.2 β2-ARs

The *ADRB2* gene is highly polymorphic and plays pivotal roles in HF, which make it an ideal prototype for studying links between receptor polymorphisms, drug response and susceptibility to HF (Dorn, 2010a; Sotoodehnia et al., 2006). The *ADRB2* gene has been identified with 49 SNPs, but only 5 of β2-AR SNPs code for amino acid changes (Cipolletta et al., 2013). The replacement of arginine - R by glycine - G at position 16 (R16G) and the substitution of glutamine - Q with glutamate - E at position 27 (Q27E) of the encoded protein are the two most commonly studied polymorphisms in β2-ARs which affect agonist-stimulated receptor down-regulation (Dorn, 2010). Clinical studies reported that the G16 polymorphism is associated with increased agonist-promoted desensitisation while E27 polymorphism is resistant to down-regulation. β2-ARs also play a critical role in modulating myocardial contractility in the failing heart, suggesting these ADRB2 SNPs are attractive candidates for risk factor and

predictive response to treatments (Cipolletta et al., 2013). Also, a clinical study of cardiovascular health reported that ADRB2-Q27 but not ADRB2-G16 polymorphism has an increased risk of sudden cardiac death (Sotoodehnia et al., 2006). This highlights the importance of SNPs in β2-ARs as risk factors of cardiac death.

Genetic information			**Population frequencies of the rare allele**		
Nucleotide position	Amino acid	Common → rare allele	Caucasians	African-Americans	Asian
β1-AR SNPs					
145	49	A → G	12-16%	13-15%	15%
1165	389	R → G	24-34%	39-46%	20-30%
B2-AR SNPs					
-47	-19	C → R	35%	21%	8-12%
46	16	G → R	38-46%	49-51%	54-59%
79	27	Q → E	35-46%	20-27%	7-20%
491	164	T → I	2-4%	2-4%	0-1%
GRK5 SNPs					
122	41	Q → L	2%	40%	

Table 1.1. Summary of clinically relevant β-Adrenergic receptor polymorphisms, with an emphasis on the specific location of genetic mutations.

1.4.3 Current models for studying GRKs and GPCRs

The current models studying GRK and GPCR functions and their polymorphisms are transgenic animals, immortalised cell lines and primary adult tissues. Human embryonic kidney cells (HEK 293) is an immortalised cell line, which has been widely used due to their proliferation capacity and ease of culture (Bourque et al., 2018). Although HEK 293 has been used as the generic model to study GPCR signallings, the physiology differences make them unrepresentative for cardiovascular study. Besides, HEK293s often exhibit chromosomal aberrations from extended passaging.

Rodent models and cardiomyocytes isolated from neonatal rats/mice are the most widely used *in vivo* and *in vitro* models in cardiovascular research due to their easy handling, low maintenance cost and availability

for genetic manipulation (Overington et al., 2006; Savoji et al., 2019). Since the first knockout mouse model study (KO of GRK1) was published by Koch et al. in 1995, various mouse models have been established to functions of GPCRs and GRKs (Burkhalter et al., 2013; Gainetdinov et al., 1999; Koch et al., 1995).

The physiological differences between these animal models and humans are the main concerns for the relevance of these models. For example, conflicting data sets on β-AR signalling have been obtained in inter-species models and in the immortalised HEK 293 cells making these studies insufficient to reach an agreement (Hill and Baker, 2003; Lewin et al., 2009; Watson et al., 2007). In particular, studies of human β-AR signalling showed that β1-AR does not internalise upon agonist stimulation because it is resistant to GRK-mediated desensitisation and has a lower affinity to β-arrestins (Shiina et al., 2000; Suzuki et al., 1992) whereas β1-ARs internalisation is observed in the mouse.

Human primary cells derived from donors are the gold standard model for representing human cardiomyocytes. However, their usage is restricted due to non-proliferative capacity, finite lifespan, limited viable source from small biopsies and difficult to maintain in culture (Khan et al., 2013; Overington et al., 2006; Savoji et al., 2019). In the study of a rare genotype, such as GRK5-L41, accessing patient samples with this genotype could be challenging when less than 2% of the population carry this SNP. Until recently, only two studies have been performed for studying GRK5-Q41L functions on transgenic cells and transgenic mice (Liggett et al., 2008; Zhang et al., 2011). Therefore, there is a need for an appropriately physiological and functional model to understand the impacts and the underlying mechanism of GRK5-Q41L polymorphism.

1.5 Human pluripotent stem cell-derived cardiomyocytes

As mentioned above, transgenic animals, immortalised cell lines and human primary cells present a serious limitation to the studies performed. Human pluripotent stem cell (hPSCs) have been regarded as a promising solution to these limitations (Bourque et al., 2018; Fermini et al., 2016; Savoji et al., 2019). Human pluripotent stem cell-derived cardiomyocytes (hPSC-CMs) can provide unlimited cell source due to the proliferation potential of hPSCs. Unlike immortalised cells, hPSC-CMs are non-transformed, genetically stable and physiologically relevant. In this study, the use of hPSC-CMs eliminated differences in receptor subtypes, distribution and signalling among species compared to animal models (Brito-Martins et al., 2008). Moreover, the accessibility of genetic modification in hPSCs makes them a valuable model for *in vitro* model and drugs screening. In addition, the use of hPSC-CMs models is also adequate to the "3R principle" - replace, refine, and reduce the use of animals in research testing.

1.5.1 Derivation and characterization of hPSC

Pluripotent stem cells are defined as cells that are self-replicating and able to develop into three primary germ layers, including endoderm, mesoderm and ectoderm (Yu and Thomson, 2008). The first derivation of human embryonic stem cells (hESCs) from the blastocyst of preimplantation embryos was established in 1998 (Thomson et al., 1998). Although hESCs suggested an attractive model for study human biology and development, several ethical issues restricted their uses as a research model. In 2007, Yamanaka and Thomson successfully demonstrated the establishment of human-induced pluripotent stem cell (hiPSC) reprogramming from somatic cells by just 4 genetic factors (Takahashi et al., 2007). These findings created a new paradigm for modern science and regenerative medicine. The reprogramming of somatic cells has been further developed with the use of

free-genome integration technique using Sendai virus or episomal plasmid (Ban et al., 2011; Fusaki et al., 2009; Yu et al., 2011).

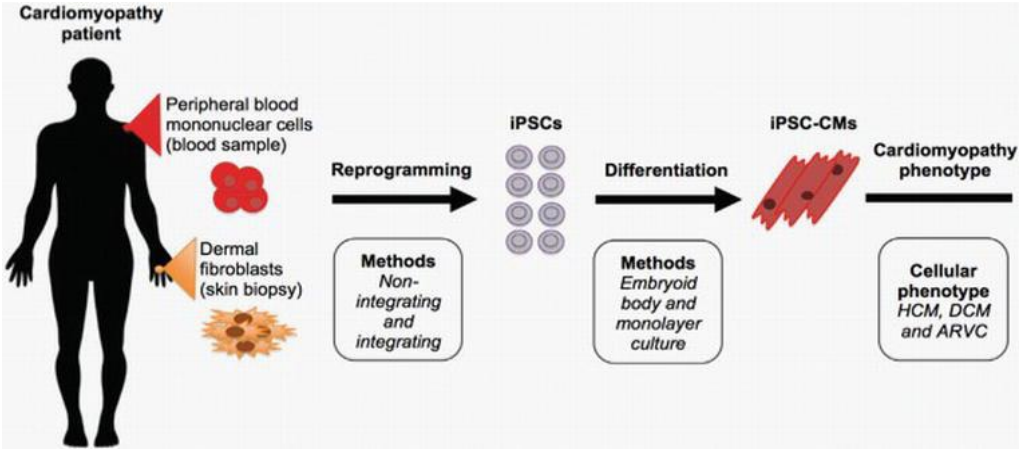

Figure 1.6. Generation of hIPSC-CMs for in vitro cardiomyopathies modelling

Somatic cells are isolated from patients and reprogrammed back to hiPSCs. hiPSCs then differentiate to hIPSC-CMs, which can be used for disease modelling or drug screening experiments. HCM, hypertrophic cardiomyopathy; DCM, dilated cardiomyopathy; ARVC, arrhythmogenic right ventricular cardiomyopathy (Adapted from Liu et al., 2017)

Both hESCs and hiPSCs, which are both defined as hPSCs, express transcription factors OCT4, NANOG, SOX2 in the cell nucleus (De Los Angeles et al., 2015; Denning et al., 2006). They also express the embryonic antigens (SSEA-3/4) and keratin sulfate-related antigens (TRA-1-60 and TRA-1-81) on the cell surface. The high telomerase activity of hPSCs allows their unlimited proliferation.

1.5.2 Differentiation of hPSC towards a cardiomyocyte fate.

1.5.2.1 Recapitulating cardiac development

To generate a relevant cardiac model to study the function of specific SNP, hPSCs need to differentiate into cardiomyocytes. The development of cardiac differentiation protocols relies on recapitulating *in vivo* embryonic heart development. This development process broadly consists of mesoderm induction, cardiac specification and cardiomyocyte maturation (Burridge et al., 2012). After gastrulation, epithelial-to-mesenchymal (EMT) transition precedes the formation of the cardiac mesoderm. This process is induced by NODAL, which encourages BMP4 and WNT3 expression in surrounding germ layers (Burridge et al., 2012; Später et al., 2014). Once cardiac mesoderm has been formed, the formation of the first and second heart fields occurs. During this process, the inhibition of Wnt/β-catenin signalling is required for cardiac progenitor formation (Spater et al., 2014). During the formation of heart fields, expression of transcription factor *NKX2.5*, TBX5 and ISL1 in cardiac progenitors is initiated. Cardiomyocytes developed from the first and second heart fields express key transcription factors such as NKX2.5, GATA4 and MEF2 (Burridge et al., 2012; Später et al., 2014)

1.5.2.2 Cardiac differentiation protocols

By recapitulating cardiac development using biological cues, hPSCs undergo a series of sequential differentiation steps (mesoderm, cardiac mesoderm, cardiac progenitors). During this process, the temporal activation/ inhibition of different signalling pathways are regulated by different growth factors to drive cardiac differentiation of hPSCs to cardiomyocytes (Mummery Christine L. et al., 2012; Später et al., 2014).

By using biological cues discovered in the field of developmental biology, several approaches for generating hPSC-CMs have been established and divided into 4 main classes: i) embryoid body (EB), ii) monolayer culture

iii) inductive co-culture,and iv) suspension culture (Mummery Christine L. et al., 2012; Talkhabi et al., 2016). EB and monolayer approaches are the most commonly used protocols.

The EB protocols are based on the suspension culture of hPSC to generate the formation of three-dimensional aggregates of pluripotent stem cells. This protocol, however, was inefficient and had a poor purity cardiomyocyte (~50%) (Anderson et al., 2007; Burridge et al., 2011). In the monolayer culture, growth factors and small molecules are diffused to guide hPSCs towards a cardiomyocyte fate. Our laboratory has developed a monolayer cardiac differentiation protocols generating cardiomyocytes of which > 80 % of cells are α–actinin^{+}, figure 3.11 (Duncan et al., 2017; Kondrashov et al., 2018).

1.5.3 Immaturity of hPSC-CMs

Despite the efficient generation of a large number of cardiomyocytes, generated hPSC-CMs exhibit the fetal morphological and functional characteristics compared to adult cardiomyocytes (Khan et al., 2013; Robertson et al., 2013). However, this is a defining drawback shared by the whole field.

In general, differences between hPSC-CMs and adult CMs range from morphological and gene expression. Several hallmarks of immaturity phenotypes of hPSC-CMs include disorganised sarcomere, rounded shape, slower conduction velocity and a negative force-frequency relationship, **table 1.2** (Denning et al., 2016; Giacomelli et al., 2017; Parikh et al., 2017). In particular, hPSC-CMs lack ultrastructural transverse tubules (T-tubules) and have low expression of key sarcoplasmic reticulum accessory proteins.

Parameters		hiPSC-CMs	Adult CMs
Morphology	Shape	Round	Rod-shaped
	Sarcomere alignment	Unaligned	Aligned
	Sarcomere length	~1.6 μm	~2.2 μm
Structure	T-tubules	No	Yes
	Sarcoplasmic reticulum	Disorganised	Highly organised
Energy & Force	Mitochondria	Mainly perinuclear occupies a small fraction of cell volume	Regularly distributed; occupies 20-40% of cell volume
	Metabolism	Glucose, lactate, fatty acids	Fatty acids
	Beating	Spontaneous	Quiescent
	Force-frequency relationship	Negative	Positive
	Conduction force	0.8-1.2 mN/mm^2	40-80 mN/mm^2

Table 1.2. Characteristics of hiPSC-CMs compared to adult CMs reveal a lack of maturity in hiPSC-CMs.

1.6 Thesis rationale and objective:

Studies into the putative functions of GRK5-Q41L polymorphism have only been performed on transfected cells and transgenic mice. Results of these studies suggested that this GRK5-Q41L SNP enhances β-AR desensitisation to prevent adverse effects of chronic β-AR stimulation. Human PSC models harbouring GRK5-Q41L SNP had been previously established in our lab. This thesis employs hPSC-GRK5-Q41L models to characterise phenotype and explore mechanism for the gain-of-function of GRK5-Q41L SNP. The following objectives will need to be achieved:

- Validate the established hPSC models harbouring GRK5-Q41L polymorphism
- Validate the utility of hPSC-CMs as a relevant *in vitro* human cellular model for studying phenotype of GRK5-Q41L variants
- Develop functional assays to study effects of GRK5-Q41L variants on contractility and cell survival response during chronic catecholamine stress.
- Investigate effects of GRK5-Q41L SNP on the nuclear translocation of GRK5 by quantifying subcellular GRK5 distribution change.
- Develop molecular assays to further explore the mechanism of GRK5-Q41L.

Chapter 2 Methods

2.1 Molecular Biology

2.1.1 DNA extraction

All cellular DNA (genomic DNA, gDNA) of hPSCs were extracted from frozen cell pellets using a DNeasy Blood and Tissue kit (QIAGEN, # 69504) following the manufacture's protocol. The DNA was eluted in 50 µL of Molecular Graded water. The DNA concentration was measured using NanoDrop DN100 spectrophotometer and stored at -20°C.

2.1.2 Polymerase Chain Reaction (PCR)

Fragments of targeted genes were amplified by PCR using GoTaq G2 DNA Polymerase (Promega,# M7845) with forward and reverse primers (**Table 2.1**). The DNA concentration did not exceed 250 ng. The total volume of each PCR reaction was 50 µL by topping up with molecular grade water. The PCR conducted followed the conditions as described in the table below. The PCR products were next conducted to agarose gel electrophoresis and the remaining samples were kept at -20°C for long-term storage. Confirmed PCR products were purified with a QIAquick PCR purification kit (QIAGEN, # 28104) before sending for sequencing conducted by Source Bioscience Sequencing.

Component	**Volume**	**PCR condition**	
		Cycle	**Condition**
Forward Primer (10 µM)	2.5 µL	Initial denaturation	94°C for 5 minutes
Reverse Primer (10 µM)	2.5 µL	35 amplify cycles	
dNTP	1 µL	Denaturation	94°C for 30 seconds
5X GoTag Buffer	10 µL	Annealing	59°C for 30 seconds
Tag Polymerase	0.5 µL	Extension	72°C for 1 minute
DNA (<250ng)	2 µL	Final extension	72°C for 10 minutes
dH_2O	Up to 50 µL	Storage	4°C

Table 2.1. Composition of the PCR reaction mixture using Tag Polymerase and PCR conditions.

Targeted genes	Polymorphism	Strand	Sequences (5' to 3')
ADRB1	49	Forward	CCGGGCTTCTGGGGTGTTCC
		Reverse	GGCGAGGTGATGGCGAGGTAGC
	389	Forward	CGCTCTGCTGGCTGCCCTTCTTCC
		Reverse	TGGGCTTCGAGTTCACCTGCTATC
ADRB2	16 and 27	Forward	GCTGAGTGTGCAGGACGAGT
		Reverse	ATGGCAAAGTAGCGATCCAC
GRK5	41	Forward	AGCGCAAAGGGAAAAGCAAG
		Reverse	ACTGACATCCCCAGCAAGTG

Table 2.2. ***Primer sequences used in PCR.***

2.1.3 Agarose gel electrophoresis

Agarose gel was made by adding Agarose powder to a TEA buffer (1X), containing 40 mM Tris Acetate and 1 mM EDTA. The agarose powder was dissolved by heating it in a microwave and was then cooled down at room temperature (RT) before adding Ethidium bromide (EtBr) at 0.4 µg/ml. The gel was poured into a clean tray with combs and solidified at RT for 45 minutes. The loading dye was added into the PCR samples with ratio 1:6 (v/v) before loading into the gel. The gel was run at 85V for 90 minutes in the electrophoresis tank containing TEA buffer. A Fujifilm LAS-1000CCD camera was used to capture the signal from the gel.

2.1.4 Total RNA extraction and cDNA synthesis

The total RNA was extracted according to the manufacture of the Nucleospin RNA kit (Macherey-Nagel, # 12373368). The RNA was eluted in 30 µL of RNase free water and this water was used as the blank calibration for the RNA concentration measurement by the NanoDrop DN100 spectrophotometer. The RNA negative sample (RNA-, no cells) was used as a control to evaluate the RNA contamination during the extraction procedure. The extracted RNA was stored at -80°C.

To convert RNA to complementary DNA (cDNA) for quantitative PCR (qPCR), the first-strand cDNA synthesis master mix SuperScript® VILO™

(Invitrogen, # 11755050) containing SuperScript III Reverse Transcriptase was used to synthesize the cDNA template. 500ng of RNA extraction was used for the cDNA synthesis by adding 4 µL of the master mix, topped up with RNase free water up to 20 µL for the total volume. The cDNA synthesis was conducted with the first incubation at 25°C for 10 minutes followed by 60 minutes incubation at 42°C before the termination reaction at 85°C for 5 minutes. Once all reactions had completed, the samples were diluted with 80 µL of molecular grade water to make up the total volume of 100 µL. All the samples have their relative Reverse transcriptase negative controls (RT-) and the cDNA negative control. The cDNA samples were stored at -20^{o}C.

2.1.5 qPCR gene expression analysis

To investigate the gene expression change, qPCR was performed. The qPCR reaction was conducted by TaqMan Fast Advanced Master Mix (Thermo Fisher, # 4444963). The real-time PCR reaction was performed using the Applied Biosystems 7500 Fast Real-time PCR template. The relative expression of genes was calculated and expressed as $2-\Delta\Delta Ct$.

Components	Volume
Master Mix (2X)	10 µL
TagMan Assay (20X)	1 µL
cDNA template	2 µL
dH_2O	7 µL

***Table 2.3. Composition of qPCR reaction mixture using TaqMan Fast Advanced Master* Mix.**

2.1.6 Subcellular extraction of nuclear and cytoplasmic protein.

The Thermo Scientific NE-PER Nuclear and Cytoplasmic Extraction Reagent (Thermo Fisher, # 78835) was used to separate the nuclear and cytoplasm protein extracts of the cultured cells. The cells were first washed in cold Dulbecco's Phosphate Buffered Saline (DPBS) and were then collected by using a scraper. The cytoplasm and nuclear protein extraction from the cell pellets was conducted following the manufacturer's protocol.

All the centrifugation steps were performed at 4°C. All protein extracts were snap-frozen and stored at -80°C.

2.1.7 Total protein extraction.

RIPA Lysis and Extraction Buffer (Thermo Fisher, # 89900) were used to extract the total protein of the cells following the manufacturer's protocol. The cells were first washed in cold DPBS and were then collected by using a scrapper. All the centrifugation steps were performed at 4°C. All protein extracts were snap-frozen and stored at -80°C.

2.1.8 Bradford assay for protein concentration measurement

The Bradford assay (Thermo Fisher; # 23236) containing Coomassie G-250 dye was used to measure the total protein concentration of the protein extracts. A serial dilution of BSA (2000 µg/mL), ranging from 0 – 2000 µg/mL was prepared in molecular grade water and was then mixed with 200 µL of Bradford solution to make the standard curve. The total protein concentration of all samples was incubated with Bradford solution for 10 minutes at RT. The measurement was performed at 595 nm by the Tecan Infinite 200 PRO plate reader.

2.2 Cell culture

All cell culture was conducted in sterile, non-antibiotic conditions, in a Class II biological safety cabinet. Cells were incubated at 37°C, 5% CO_2 in a humidified environment. All tissue culture reagents were purchased from Invitrogen and Thermo Fisher, and all chemicals and pharmaceutical drugs were from Sigma unless otherwise stated. All cell culture vessels were tissue culture-treated unless otherwise stated.

2.2.1 Chemical defined culture condition of hPSCs

For the routine culture of hPSCs, growth factor reduced Matrigel™ (Corning: 354234) was used as an extracellular matrix substrate. In brief, Matrigel™ was diluted 1:100 in cold DMEM for coating tissue culture-treated

vessels for 1 h at RT. The hPSCs were first thawed in a cryotube in water bath for 2 minutes and were then resuspended in 9ml of BGK medium. The cells were centrifuged at 160g for 4 minutes. The cell pellet was gently resuspended in Essential 8 (E8, ThermoFisher, #A1517001) medium supplemented 10μM Y-27632 (RockI, Tocris Bioscience, # 1254/10) and plated on the Matrigel-coated vessels. The culture medium was changed every day until the cells reached more than 80% confluence. The densely compact cells in a T25 flask were passaged using 1 ml of TrypLE Select enzyme (ThermoFisher, #12563029) for 3 minutes at 37°C. The dissociated cells were then resuspended in 9 ml of BGK to neutralise the TrypLE enzyme and centrifuged at 160g for 4 minutes. The cell pelleted was then mixed gently with 5ml E8-RockI medium and plated into a new Matrigel-coated flask for the first 24 h. Cells were maintained with daily E8 medium changes and the confluent cells in T25 flask were regularly split at a 1:5 ratio every 2 days.

Components	Stock concentration	Final concentration	Volume
DMEM-F12	N/A	1X	500 ml
KSR	100%	15%	90 ml
Glutamax	100X	1X	6 ml
NEAA	100X	1X	6 ml
β-mercaptoethanol	1 M	10 μM	60 μl

Table 2.4. Composition of BGK medium.

2.2.2 Pluripotency Characterization:

2.2.2.1 Growth curve

To generate the growth curve and calculate the population doubling (PD) time, established hPSCs were seeded at 1 x 10^6 cells/ T25 flask. The cells were dissociated every 2 days using the method described in section 2.2.1. The total cell number was manually counted or was conducted using a Cedex HiRes counter (Roche). The total cell counts were recorded for 5 passages in each line. The population doublings (PDs) were calculated by

using the formula below (Denning et al., 2006). The cumulative PD was summed across the 5 passages to plot the growth curve relative to the time in test culture, using linear regression best fit curve:

$$\text{Cumulative Population Doubling Time (CPD)} = \frac{\text{Log10 (total cell counts/cells seeded)}}{\text{Log10 (2)}}$$

$$\text{Population Doubling Time (h)} = \frac{\text{H in test culture}}{\text{CPD}}$$

2.2.2.2 Sample Preparation for Karyotype

To investigate the genomic stability of hPSCs during prolonged culture, a Karyotype analysis of all hPSC lines was performed after 10 passages in normal culture conditions. The hPSCs were seeded at $1x10^6$ cells to capture the maximum number of hPSCs in the metaphase. The cells were cultured for 24 h and then incubated with KaryoMAX Colcemid (100 ng/ml) for 30 minutes. Cells were harvested by TrypLE as described above. The cell pellet was gently mixed by adding drop-wise 0.6% sodium citrate with vortex and incubated at RT for 20 minutes followed centrifuged at 300g for 5 minutes. The pellets were then fixed by adding dropwise 10 ml of Methanol: Glacial Acetic acid (5:1, v/v) with vortex and centrifuged at 300g for 5 minutes. This fixing step was repeated three times. In the third spinning time, 1 ml of fixing solution remained after aspirating the supernatant. The samples were stored at -20^{o}C. The karyotype at 30 metaphase spreads and G-banding analysis was conducted and analysed by Mr Nigel Smith in Nottingham University Hospital NHS Trust in accordance with the International System for Human Cytogenetic Nomenclature International Guidance (ISCN, 2005)

2.2.2.3 Immunofluorescence analysis of nuclear pluripotent-associated transcription factors

To analyse the immunofluorescence analysis of nuclear pluripotent-associated transcription factors, the hPSCs were seeded at 20,000 cells/cm^2 in Matrigel-coated 96-well plates. The 50% confluency culture was fixed with

4% paraformaldehyde (PFA) for 12 minutes, then permeabilized with 0.05% Triton X-100 in DPBS for 15 minutes and rinsed with 0.5% Tween 20 in DPBS. After 1 h incubation with 4% goat serum (Sigma, # G9023) in DPBS (blocking solution), hPSCs were incubated overnight at 4°C with primary antibodies (OCT4, NANOG and SOX2) made in blocking solution and diluted using DPBS. Cells were washed three times with 0.5% Tween-20 for 10 minutes in each wash and were performed for 2 h incubation at RT with secondary antibodies, as shown in table 6. Nuclei were revealed by staining for 15 minutes with 4,6-diamidino-2-phenylindol (DAPI, 100 ng/mL) then imaged using the Operetta High-content imaging system (PerkinElmer).

Primary Antibody & supplier	Dilutions	Secondary Antibody	Dilutions
OCT4 (SantaCruzBiotech,#sc-5279)	1:200	AlexaFluor 488	1:1000
NANOG (R&D Systems, #AF1997)	1:200	AlexaFluor 488	1:1000
SOX2 (R&D Systems, #AF2018)	1:200	AlexaFluor 488	1:1000

Table 2.5. ***List of antibodies used for stem cell characterisation.***

2.2.3 Cardiac differentiation

2.2.3.1 Cardiac differentiation of hPSCs in the E8 culture

To initiate the cardiac differentiation process, the hPSCs were seeded at 25,000 – 40,000 cells/cm^2 in the Matrigel-coated T25 flasks and maintained in E8 culture for 2 days. When the cells reached approximately 70% confluency and compaction, the culture was preconditioned with the StemPro34 (SP34) containing Matrigel (1:100 dilution) and BMP4 (1 ng/ml) for 12h to 18h. After the preconditioning step, day 0 of cardiac differentiation was started when the preconditioned culture was exposed to SP34 medium, supplemented with 10 ng/ml BMP4 and 8 ng/ml Activin-A (termed SP34-AB medium) for 48 h. On day 2, the culture was switched to an RPMI medium contained B27 supplement minus Insulin (termed RB27 –Ins, Thermo Fisher, # A1895601), 10uM KY02111, and 10μM XAV939 (termed KYX). On day 4,

the medium was changed into RPMI medium with B27 supplement (termed RB27, Thermo Fisher, # 17504-044) and KYX (10μM) for the next 48 h. From day 6 onwards, the culture was maintained in RB27 medium with medium changes every 2 – 3 days.

2.2.3.2 Dissociation of monolayer cardiomyocytes using Collagenase II

On day 12 – day 15 post differentiation, cardiomyocytes beat synchronously and started to detach from the culture surface indicating that they needed to dissociate. One day before dissociation, the culture media was refreshed with RB27 to enhance the survival rate of the cardiomyocytes. hPSC-CMs and were dissociated and seeded in different culture vessels, which were coated with vitronectin-N (VTN, ThermoFisher, # A14700). The monolayer of cardiomyocytes was washed twice with calcium- and magnesium-free Hank's Balanced Salt Solution (HBSS, ThermoFisher, # 14170112). Cardiomyocytes were then incubated with dissociation solution, containing 200 units/ml collagenase II (Worthington,# LS004176) dissolved in HBSS, supplemented with 10 μM RockI, 30 nM *N*-Benzyl-*p*-toluenesulphonamide (BTS, TCI chemicals, # B3082), and 1 mM HEPES (Sigma, # H4034). Cells were incubated in dissociation solution in an incubator at 37°C, 5% CO_2 for 3 h. Cells were then harvested and the enzyme neutralised with RPMI basal medium supplemented with 24 μg/ml DNaseII (Sigma,# D8764). Cell count was manually performed or automatically performed by Cedex HiRes counter. The harvested cell solution was centrifuged at 100g for 15 minutes. Cells were then resuspended and seeded in RP27 medium, supplemented with 10 μM RockI for 24 h. On the next day, plated cardiomyocytes were changed to fresh RB27.

2.2.3.3 Characterization of hPSC-derived cardiomyocytes using immunofluorescence analysis

Immunofluorescence staining with cardiac markers (anti-human cardiac troponin T, cTNT, or α-Actinin) was used to identify cardiomyocyte purity. Cardiomyocytes dissociated by Collagenase enzyme were seeded into a Matrigel-coated 96-well plate at 30,000 cells/well. Cells were maintained 3 days before fixing them with 4% PFA for 10 minutes at RT. Cells were then permeabilized with 0.05% Triton X-100 in PBS and blocked with 4% goat serum in PBS, following the standard immunofluorescence staining procedure**,** as described in section 2.2.2.3. Cardiomyocytes were incubated overnight at 4°C with primary antibodies, followed by the incubation of the appropriate secondary antibodies (Table 2.5) for 2 h at RT the next day. The cell nuclei were then stained with DAPI 1:500 dilution for 15 minutes at RT. The immunofluorescence samples were then imaged and analysed using the Operetta High-content imaging system (PerkinElmer).

Primary Antibody & supplier	Dilutions	Secondary Antibody	Dilutions
α-actinin (Sigma, #A7811)	1:800	AlexaFluor 488	1:1000
cTnT (Abcam, #45932)	1:400	AlexaFluor 647	1:1000
ProBNP (Abcam, #13115)	1:500	Alexa Fluor 488	1:1000
GRK5 (Abcam, # ab64943)	1:800	Alexa Fluor 647	1:1000

Table 2.6. ***List of antibodies used for cardiomyocytes.***

2.2.3.4 qPCR analysis of GPCRs and GRKs in hPSC-CMs.

qPCR analysis expression profiles of GPCRs and GRKs in hPSC-CMs were performed at different culture intervals, including day 0 (d0), day 20 (d20), day 30 (d30), day 40 (d40), day 50 (d50) and day 60 (d60) post-cardiac differentiation. Commercial ventricle human samples (VHH) were used as the relative control for the physiological expression level. Expression values were normalised to the average expression of the housekeeping gene 18S. Taqman assay IDs for *18S*, *GAPDH, ADRB1, ADRB2, GRK5, AGTR1* and

EDNRA are 4333760F, Hs02330048_s1, Hs00240532_s1, Hs00176395_m1,Hs00992173_m1, Hs00258938_m1 and Hs03988672_m1.

2.2.4 Phenotyping Analysis

2.2.4.1 Analysis contractility response using CellOPTIQ™ platform

hPSC-CMs at day 25 + were dissociated and plated onto a Vitronectin-coated 96-well plate at a seeding density of 100,000 cells/$cm^{2,}$ to generate a partially confluent monolayer. 3 - 5 days after plating, contractility experiments were carried out on hPSC-CMs using the CellOPTIQ™ (Clyde Biosciences) platform at 37C, 5% CO_2. Bright-field images were captured for 10-second periods using an ORCA-Flash4.0 digital CMOS camera (Hamamatsu,# C11440). Contraction analysis was performed by ImageJ Macro provided by Clyde BioSciences.

2.2.4.2 Real-time analysis contractility response using CardioECR platform

The 48 CardioECR E-plate coated with Fibronectin (1:100, Sigma, #F1141) was specifically used for the CardioECR system. Fibronectin was coated in an incubator at 37C, 5% CO_2 and the Fibronectin-coated CardioECR E-plate needed to be calibrated before seeding cells. HUES7-Q41L CMs at day 25+ were dissociated and seeded at 180,000 cells/cm^2 to generate a fully confluent monolayer of cardiomyocytes in a 48 CardioECR E-plate. 3 – 5 days post-plating, baseline measurements for the contractility responses of cells were recorded before starting the experiment. Real-time contractility responses of hPSC-CMs were recorded with the CardioECR system (xCELLigence) at 37C, 5% CO_2. Contractility and cell index responses were analysed using RTCA CardioECR Data Analysis software provided by xCELLigence.

2.2.4.3 Live-dead analysis using flow cytometry .

Around day 15, hPSC-CMs were dissociated with Collagenase enzyme and plated in a Vitronectin-coated 6 well plate at 150,000 cell/cm^2. hPSC-CMs from day 30+ were conducted to 1 µM ISO treatment after 0 h, 24 h, 48 h, 72 h and 96 h incubation. Cardiomyocytes treated with 0.4µM HCl were considered at vehicle-treated control (0h), while 10 µM Doxorubicin (Dox, Sigma, #D1515) was used as the positive control for dead cardiomyocytes. Treated cardiomyocytes were dissociated with a TrypLE enzyme. In brief, treated-cardiomyocytes were washed twice with DPBS before incubating 1 mL of TrypLeE for 7 minutes. The cells were gently harvested and neutralised with 9 mL of warm RPMI. The collected cells were quickly centrifuged at 300g for 5 minutes. The cell pellets were gently mixed in 1mL of the assay master mix, containing RB27 medium, supplemented with 50 µM calcein-AM (Cal AM) and 2 mM ethidium homodimer-1 (EthD-1). The cells were incubated with assay master mix for 15–20 minutes at RT and protected from light. The stained cells were quickly sent for fluorescence analysis for live cells using Cal AM dye (ex/em ~495 nm/~515 nm) and dead cells using EthD-1 dye (ex/em ~495 nm/~635 nm). Unstained and single colour stain for either Cal AM or EthD-1 was applied and later used for standard compensation.

2.2.4.4 Subcellular distribution of GRK5 analysis by Zeiss LSM780 confocal microscope.

In this experiment, day 25 + hPSC-CMs were dissociated using a Collagenase enzyme and plated in Vitronectin-coated MatTek dishes at 150,000 cell/cm^2. The treated cardiomyocytes were fixed with 4% PFA at the end of the experiment and conducted to the immunofluorescence process, as described in section 2.2.2.3, using GRK5 and α-actinin antibodies (table 2.6). Imaging of immunostained samples of treated hPSC-CMs was performed using the Zeiss LSM780 confocal microscope (Zeiss). Images

were processed by ZEN Black or ZEN Blue software and further analysis was performed by ImageJ.

2.2.4.5 Western Blot Analysis of targeted proteins.

On day 15, hPSC-CMs were dissociated using a Collagenase enzyme, before seeding in different culture vessels coated with Vitronectin. hPSC-CMs at day 30 + were subjected to a different treatment. The cells were then collected by using a scraper in cold DPBS and the protein extraction was performed, as described in section 2.1.6 & 2.1.7.

In the subcellular quantification of GRK5 distribution (section 4.3.2), 15 µg of cytoplasmic and nuclear extracts were used for Western blot using the NuPAGE™ 10% Bis-Tris Protein Gels system (Thermo Fisher, # NP0315BOX) following the manufacturer's guidelines. The nitrocellular membrane was blocked with 5% skimmed milk in a TBST buffer (Table 2.6). The western bots were incubated with a primary antibody made up of 5% skimmed milk at 4^{o}C in a cold room overnight. The next day, the membranes were washed with TBST buffer three times for 15 minutes for each wash. The membranes were then incubated with secondary Horseradish Peroxidase (HRP) antibodies at RT for 1 h. These membranes were next washed with TBST buffer three times, 15 minutes for each wash. The western membranes were incubated with the chemiluminescent signal developing solution from ECL™ Prime Western Blotting System (GE Healthcare, #RPN2232). Chemiluminescent signals of the targeted protein were produced from reactions between HRP enzymes and developing solution and these signals were detected by Fujifilm LAS-1000CCD camera.

The stripping process was conducted with ReBlot Plus Mild Antibody Stripping Solution (Millipore, #2502). The membranes were incubated with the stripping solution at RT for 15 minutes. The stripped membranes were next washed twice with TBST for 10 minutes for each wash. The membrane

needed to incubate with the blocking solution at RT for 1 h before reprobing with primary antibody in a cold room at 4°C overnight. The incubation with secondary HRP antibodies and the signal development of membrane were performed as previously described.

In section 5.3, 10 µg of the total protein extracts were used in a western blot analysis for phosphorylated ERK (pERK) and total ERK (TERK). The membrane was firstly probed with a pERK antibody. The stripping process was required to reprobe with Total ERK1/2 antibody, using a similar procedure to the one previously described.

Primary Antibody & supplier	Dilutions	Secondary Antibody & supplier	Dilutions
GRK5 (Abcam, # ab64943)	1:1000	Goat anti-Rabbit HRP (Invitrogen, # 1529610)	1:10000
Tubulin (Cell Signalling Technology,#2128P)	1:2000	Goat Anti-Mouse HRP (Abcam, # 1529618)	1:10000
Lamin A/C (Cell Signalling Technology,#4777T)	1:2000	Goat anti-Rabbit HRP (Invitrogen, # 1529610)	1:10000
β-Actin antibody (Abcam, # 8226)	1:1000	Goat Anti-Mouse HRP (Abcam, # 1529618)	1:10000
TATA-binding protein (TBP, Abcam, # 51841)	1:2000	Goat Anti-Mouse HRP (Abcam, # 1529618)	1:10000
α-actinin (Sigma, #A7811)	1:1000	Goat Anti-Mouse HRP (Abcam, # 1529618)	1:10000
cTnT (Abcam, #45932)	1:1000	Goat anti-Rabbit HRP (Invitrogen, # 1529610)	1:10000
Phospho-p44/42 MAPK (ERK1/2) (Cell Signalling Technology, #4370)	1:1000	Goat anti-Rabbit HRP (Invitrogen, # 1529610)	1:10000

Table 2.7. List of antibodies used for western blot.

2.2.4.6 Immunofluorescence analysis of hypertrophic response in hPSC-CMs.

On day 15, the hPSC-CMs were dissociated and seeded at 40,000 cells/well of the Vitronectin coated 96-well plate. The hPSC-CMs were maintained until day 30, post-differentiation process when the experiment was performed. The hPSC-CMs were then treated with ISO and hypertrophic

drugs Endothelin-1 (ET-1) for incubation periods of 0 h, 24 h, 48 h, and 72 h. Drugs were prepared and changed fresh every 24 h. Brefeldin A (BFA, Sigma, # B7651) at 10 µg/ml were added to the cell culture medium and incubated for 3 h. Other hypertrophic drugs Angiotensin II (AngII) and Phenylephrine (PE) were also tested during the 18-h induction. The cells were then fixed and followed the immunofluorescence process as described in section 2.2.2.3, using anti-human BNP antibody at (Abcam, # 13115, Table 2.6).

2.2.4.7 Statistical analysis

All data are presented as mean with standard error. Statistical analysis was performed using GraphPad software.

For comparing multiple data sets to a single control column, one-way ANOVA and two-way ANOVA with Dunnett's multiple comparison test was chosen. Significance tests were based on p-values as follows: * $p < 0.05$; ** $p < 0.01$.

Chapter 3 Study phenotyping of GRK5-Q41L in hPSC-CM models during catecholamine stress.

3.1 Introduction:

3.1.1 Introduction:

This chapter briefly explains the establishment of the isogenic HUES7-GRK5-Q41L model and hIPSC-GRK5-Q41L models, which were all generated by Dr Hoang Minh Duc. All undifferentiated hPSC lines of these two models were examined for standard pluripotency characterization, their differentiation into cardiomyocytes was demonstrated and their phenotypes *in vitro* were explored. GRK5-L41 is known to have cardioprotective effects associated with low mortality during HF or heart transplantation. This chapter explores how these hPSC-CMs with GRK5-Q41L polymorphisms can be used to study its effects during chronic catecholamine stress *in vitro*. Different platforms and assays were used to investigate contractility response and cell death response of hPSC-CMs harbouring these polymorphisms.

3.1.2 Generation of hPSC models harbouring GRK5-Q41L variants.

The current models used to study polymorphisms in GRK5 as well as the β-AR system, like other signalling pathways, are transgenic animals, immortalised cell lines and primary adult tissues. Animal physiology and immortalised cell lines are significantly different from humans. For example, conflicting data sets have been obtained in inter-species models and in the immortalised HEK 293 cells, making these studies insufficient to reach an agreement (Hill and Baker, 2003; Lewin et al., 2009; Watson et al., 2007). In particular, studies of human β-AR signalling using HEK 293 cells showed that β1-AR does not internalise upon agonist stimulation because β1-ARs are resistant to GRK-mediated desensitisation and have lower affinity to β-arrestins (Shiina et al., 2000; Suzuki et al., 1992). Primary human cardiomyocytes are considered the "gold standard" for studying cardiac

signalling, but these cell sources are scarce and difficult to maintain in culture (Khan et al., 2013). Therefore, there is a need for an appropriately physiological and functional model to understand the impact and the underlying mechanism of polymorphisms in β-AR signalling.

These current models required to obtain relevance and each model has value for specific questions. hPSC-CMs could address many of these issues because, unlike immortalised cells, they are non-transformed, genetically stable and physiologically relevant. Using hPSC-CM models can eliminate differences in receptor subtypes, distribution and signalling among species, compared to animal models (Brito-Martins et al., 2008). Since the discovery of human embryonic stem cells (hESC), hESC-derived cardiomyocytes (hESC-CMs) have been characterized and show similarities to human cardiomyocytes in terms of receptor response, electrophysiology and calcium handling (Khan et al., 2013). In the case of studying a specific SNP or genotype of interest with an extremely low frequency in the population, gene editing can be employed to introduce single nucleotide change. Isogenic lines of human disease models are populations of identical cells that undergo "editing" to create desired genetic modifications that are present in specific patient populations. The isogenic model of a certain gene has an identical genetic background, with the only difference being the desired genetic modification. In this context, producing SNPs from an isogenic background can give a better understanding of their effects and activity by eliminating the impacts of variable genetic backgrounds (Merkle and Eggan, 2013). However, the immature phenotype of hPSC-CMs makes them not a perfect model. Multiple models required to obtain relevance and each model has value for specific questions.

Dr Hoang Minh Duc explored two different strategies to generate the isogenic set and heterogenic hIPSC sets, harbouring GRK5-Q41L variants

(**figure 3.1**). To investigate the physiological effects of GRK5 SNPs, "foot-print-free" isogenic HUES7 ESC models were established. The strategy for the HUES7-GRK5 platform is summarized in **figure 3.1.A**. The parental HUES7 line has glutamine (Q) at position 41 and is termed HUES7-GRK5-Q41. Work was done in the lab before I arrived (courtesy of Dr Hoang Minh Duc). Dr. Hoang used a Nickase/CRISPR-PiggyBac approach to create homozygote (bi-allelic gene editing) isogenic sets that represent the GRK5 position 41 variants found in the human population (Kondrashov et al., 2018). The homozygous line was modified using Nickase/CRISPR to produce homozygote HUES7-GRK5-L41 (Leucine, L) and heterozygote HUES7-GRK5-Q/L41 lines for studying the effects of these variants on heart function (**figure 3.1.B**).

Also, the second strategy employing episomal reprogramming plasmids was used to generate heterogenic hIPSC-GRK5-Q41L lines (courtesy of Dr Harry Hoang Minh Duc). This time, lymphoblast harvested from patients carrying homozygous GRK5-Q41 or GRK5-L41 were sourced from the Corriell cell bank in the USA (**figure 3.1.C**). Episomal reprogramming, which is an integration-free method, was employed to generate human-induced pluripotency stem cells (hiPSCs) from each of these lymphoblast lines, to use these in parallel to the Cas9/CRISPR sets produced above.

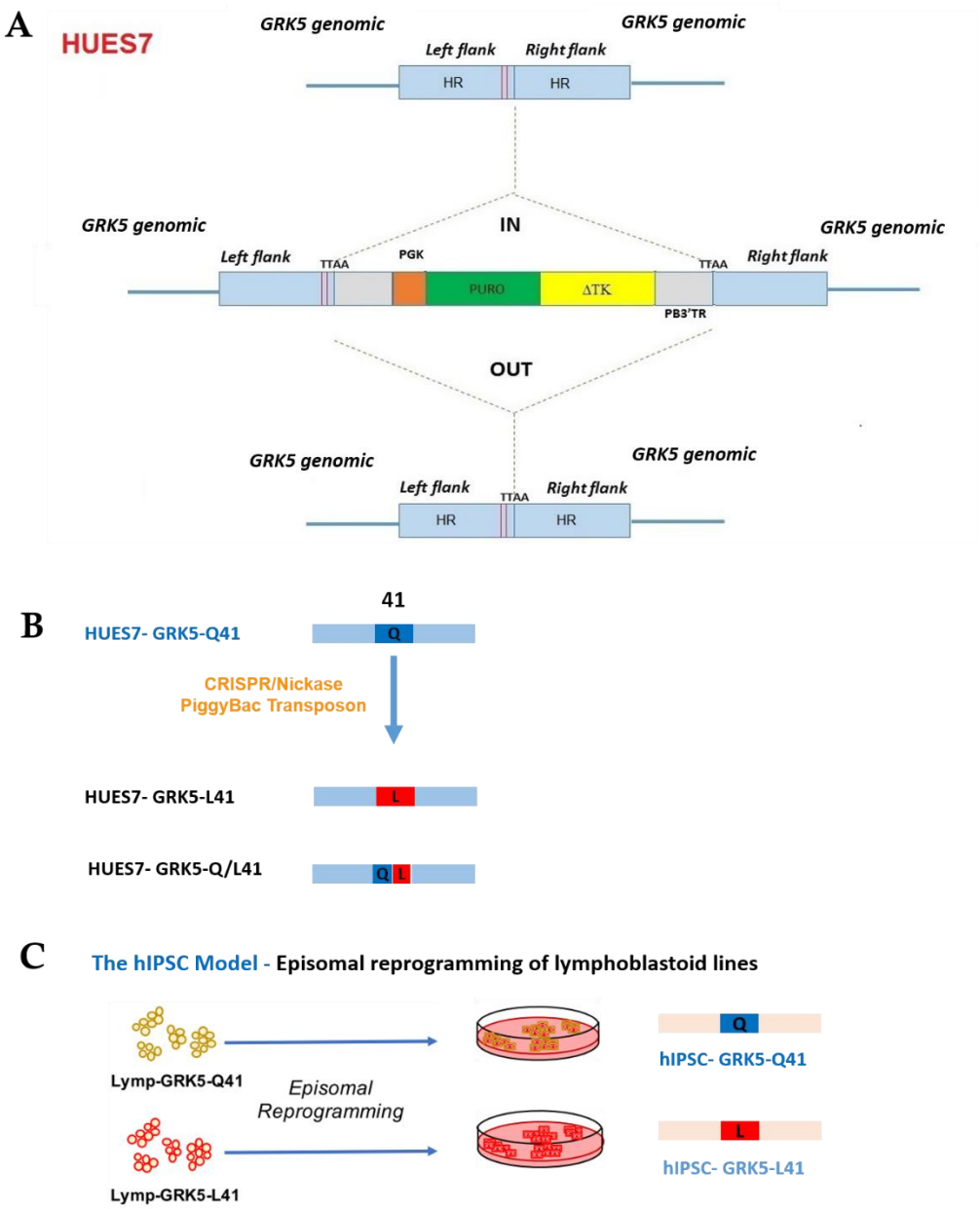

Figure 3.1.Footprint-free CRISPR/Cas strategy to establish the isogenic models for the GRK5 gene.

Schematic diagram demonstrating a two-step gene-editing approach generating amino acid substitutions in the ADRB2 locus and the derivation of edited HUES7-β2 from the parental HUES7-hESCs. Top line, the structure of *GRK5* gene in the parental HUES7 lines. Second line, the homogenous insertion of PiggyBac transposon carrying a PGK-puroΔtk cassette on the *GRK5* locus. Third line, the excision of the PiggyBac transposon generating seamless single amino acid substitution in the *GRK5* locus of HUES7 to create the edited HUES7-GRK5 lines. (B) The isogenic HUES7-GRK5 models, including the primary line HUES7- GRK5-Q41L and three edited lines: HUES7-GRK5-Q41, HUES7-GRK5-L41 and HUES7-GRK5-L41. (C) The lymphoblastoid hIPSC-GRK5-Q41L system using episomal reprogramming.

3.1.3 Monolayer cardiac differentiation:

hPSCs have been widely applied in *in vitro* disease modelling. To investigate phenotypes in cardiac pathologies, relevant cell types must be generated and an efficient cardiac differentiation protocol is required to produce large numbers of cardiomyocytes. *In vitro* cardiac differentiation protocols mainly rely on recapitulating embryonic heart development to generate hPSC-CMs in suspension or in 2D monolayer culture (Dunn and Palecek, 2018; Giacomelli et al., 2017). In this study, a monolayer cardiac differentiation, developed and modified in our lab, was used to generate the large number of cardiomyocytes required for phenotyping of GRK5-Q41L SNP (Duncan et al., 2017; Kondrashov et al., 2018). The protocol efficiently generates cardiomyocytes with high purity (≥ 80% α-actinin$^+$ cells) across hESC and hIPSC lines.

3.1.4 β-AR signalling control cardiac contraction:

During HF progression, reduced contractility, hypertrophy and apoptosis are observed as phenotypes in cardiomyocytes (Kang et al., 2016; Lohse et al., 2003b). Apoptosis and hypertrophy responses in cardiomyocytes are regulated by the intercellular signalling pathways, while cardiac contractility is regulated by both ion channel activity and signalling pathways. In the early stage of HF, cardiac output (supply) is decreased due to pathogenic remodelling of the heart (apoptosis, hypertrophy and malfunction contractility), where the β-AR and angiotensin II (Ang II) signalling pathways are activated to enhance cardiac output as a compensation response to meet the demands of the body. As the adrenergic system is the immediate stress response in the human body, stimulation of β-AR signalling is the early response of the body to the reduction of cardiac function (Dorn, 2010a; Kang et al., 2016; Lohse et al., 2003b). Stimulation

of this signalling pathway has positive inotropic and chronotropic effects on adult human cardiomyocytes. The mechanism of these effects in response to β-AR stimulation is due to an increase of cAMP leading to PKA phosphorylation of cardiac contractility regulators, including RyRs, LTCC, PLB, troponin I, MyBP-C and phosphatase inhibitors (Lohse et al., 2003b).

β-AR agonists could be selective for specific β-AR subtypes or non-selective. Dobutamine is a selective agonist for β1-AR, while the selective β2-AR agonists commonly used are formoterol and salbutamol (Hanania et al., 2002; Warne et al., 2019). Isoprenaline (or Isopretepronol, ISO), which is analogous to the endogenous adrenaline hormone with an additional isopropylamine group, is a non-selective β-AR agonist. The structural similarity of ISO to the endogenous positive chronotrope, adrenaline, means that is commonly used to modulate cardiac excitation-contraction or to mimic catecholamine stress during HF (Ginsburg and Bers, 2004; Wang et al., 2016).

3.1.5 Cardiac death during HF.

Although the activation of β-AR signalling is beneficial in the acute phase, sustained β-AR stimulation induces a cascade of alterations at the cellular level, resulting in apoptosis of cardiomyocytes and reduced cardiac contractility (Ding et al., 2005; Mangmool et al., 2010; Pitt and Marx, 2014; Saito et al., 2000; Wang Wang et al., 2004). As cardiomyocytes are terminally differentiated cells, they are almost not proliferative after birth (Lucia et al., 2018; Madamanchi, 2007). Loss of cardiomyocytes permanently leads to the reduction of functioning contractility of the myocardium, where cardiac death has been proven to contribute to the HF progression (Communal et al., 1999; Empel and Windt, 2004; Kang et al., 2004; Sheng et al., 2015).

As explored in the introduction (section 1.3), sustained activation of β-AR signalling causes cardiomyocyte death, which is a feature of cardiac pathophysiology and progressive HF (Ho et al., 2010; Marín-García, 2016). The main mechanism of β-AR signalling inducing apoptosis is via cAMP/PKA cascade, which then modulates downstream targets, regulating cardiac myocyte apoptosis, including BCL2 protein family, MAPKs and PI3K-Akt cascades (Chen et al., 2012; Fujio Yasushi et al., 2000; Lohse et al., 2003b). Chronic activation of β-AR signalling also induces cardiomyocyte death via Ca^{2+}/CaMKII signalling and mitochondria-dependent pathways (Corbi et al., 2013; Dries et al., 2016; Kang et al., 2016; Kolenko et al., 2013).

Genetic association studies have shown that patients harbouring the GRK5-L41 variant associated with a higher survival rate during cardiac ischemia and HF. *In vitro* studies of the GRK5-L41 SNP, using transgenic mice, Chinese hamster ovary (CHO) or Chinese hamster fibroblasts (CHW-1102 cells), showed an enhancement of β-AR desensitisation, which is similar to the effects of β-blockers, to downregulate β-AR signalling during catecholamine stress (Liggett et al., 2008, p. 5; Wang et al., 2008). This function is suggested to be linked with improved survival of HF patients. In this chapter, different assays were used to access cell death responses in cardiomyocytes of the isogenic and hiPSC model, during chronic catecholamine stress induced by ISO.

3.1.6 Methods for investigating contraction response in hPSC-CMs.

3.1.6.1 Direct measurement of catecholamine effects on cardiomyocyte contractility

Excessive β-AR signalling emerges as a key factor during the progression of HF (Madamanchi, 2007). During HF, the increased catecholamine outflow induces increases in contractility and heart rate as

the consequences for the activation of the β-AR system. In this chapter, the use of the xCELLigence RTCA CardioECR system (CardioECR) and Clyde's CellOPTIQ™ system (CellOPTIQ) has functional screening platforms to access the contractility features of cardiomyocytes is described. Indeed, the CellOPTIQ platform was used for optical recording to quantify the contractility responses of hPSC-CMs (contraction amplitude, contraction time and relaxation time) whereas the CardioECR platform was used to investigate cell viability and other contractility features via impedance measurement, including beat rate and impedance beating amplitude. As the CardioECR platform was only available for a short-term (on loan from ACEA Biosciences), this system was only used for isogenic models in focused experiments, which verify phenotype results from CellOPTIQ. Nevertheless, other cell-based assays were also applied to investigate the viability and apoptosis response of the cells.

3.1.6.2 xCELLigence RTCA CardioECR and its principle of impedance and field potential detection

The CardioECR platform was used to investigate cell viability and other contractility features of hPSC-CMs in this study. The application of hiPSC-CMs in cardiac safety evaluation was proposed and demonstrated by the Comprehensive *In Vitro* Proarrhythmia Assay (CiPA) initiative, launched by the Cardiac Safety Research Consortium (CSRC), Health and Environment Sciences Institute (HESI) and Food and Drugs Administration (FDA) (Fermini et al., 2016; Mulder et al., 2018). The aim of this initiative is to establish a mechanism-based standard for evaluating the arrhythmogenicity of drugs development, where the CardioECR system is one of the four representative impedance/multi-electrode array (MEA) platforms used for the cardiotoxicity assessment of hiPSC-CMs. The introduction of the CardioECR platform

provides access for real-time and non-invasive measurement of cardiomyocyte contractility and viability (Xi et al., 2011; Zhang et al., 2016). This instrument records cellular impedance (presented as Cell Index, CI) and electrical field potential (presented as extracellular recording, ECR) in parallel as proprietary MEA technology (**figure 3.2.A**). The xCELLigence system requires a compatible sensor plate (CardioECR 48 E-plate), in which each well contains gold microelectrode arrays integrated into the bottom of the plate (**figure 3.2.B**). The multiple impedance microelectrodes in each well are linked together to form two main interdigitating arrays. At the centre of the well and in between two impedance microelectrode arrays, there is a distinct pair of electrodes to measure field potential (FP) (**figure 3.2.B**). The sampling frequency is termed as a sweep, defined as the number of times during an experimental run that the beating is sampled. The block duration is defined as the duration of time that the contractility is measured. After data acquisition, the RTCA CardioECR Analysis Software is used to calculated different contractility parameters, such as cell index, beating rate, contraction amplitude and field potential duration.

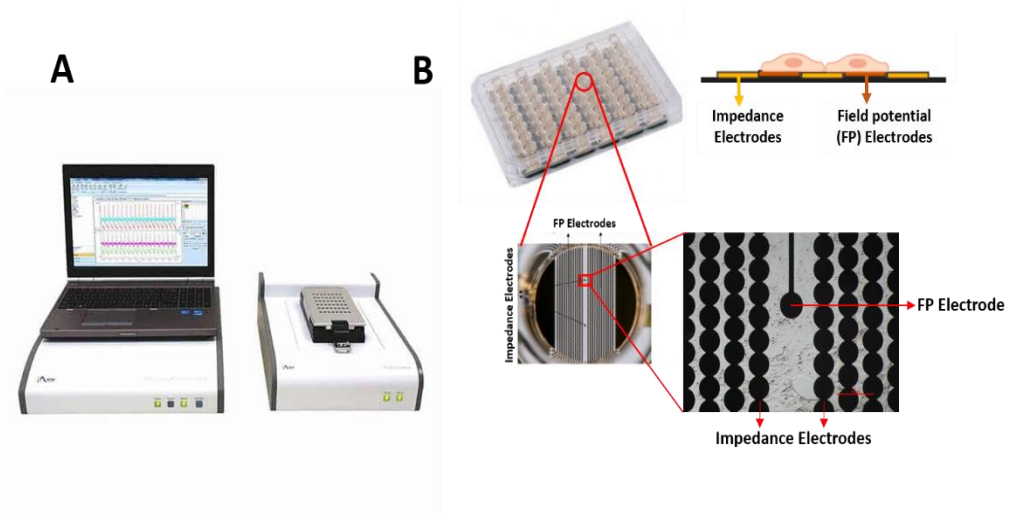

Figure 3.2. xCELLigence RTCA CardioECR system

(A) The system contains a 48-well microtiter plate format placed inside a standard CO2 cell culture incubator and interfaces via a cable with analysis and control units that are placed outside the incubator. (B) Details of E-Plate CardioECR 48. Each well within an E-Plate CardioECR contains arrays

interdigitated impedance (IMP) electrodes and a separated pair of field potential (FP) electrodes.

Through cellular impedance measurement, the CardioECR system records the impedance of the cells by imposing a small excitation voltage between electrodes, which does not affect cell health and behaviour (Xi et al., 2011). This electric potential goes through the hPSC-CM monolayer and then picks up the current released from the culture. The contact of cells with the electrodes produces a signal of electrical cell impedance, which is termed CI and calculated by the following formula:

$$Cell\ Index\ (CI) = Impedance\ Tn - Impedance\ T0$$

Where Tn is the time point being measured, and T0 is time point zero in the absence of cells with just medium. CI is a dimensionless unit that represents the electrical resistance of the surface with cells in relation to the background surface, without cells at a given time point for each well. Because of this, CI, therefore, correlates to the cell numbers or cell morphology of hPSC-CMs attaching to the sensor surface (**figure 3.3.A**). These value can illustrate the real-time changes of the cell numbers via cell attachment response of viable cells, however, it could not alternate for the direct measurement of viable cells. The CI measurement was also used to quantify the relative contractile state of the cell monolayer (**figure 3.3.B**). The RTCA CardioECR Data Analysis Software was used to convert CI signals to beating waveforms. A cardio analysis template was used to quantify 13 impedance parameters: normalized impedance amplitude (N/A), beating rate (bpm), beating period (ms), rising time (ms), falling time (ms), rising slope (1/ms), falling slope (1/ms), beating pattern similarity (N/A), beating rhythm irregularity (N/A), irregularity/ regular beat ratio (N/A), irregularity/ total beat ratio (N/A), individual beating duration - IBD (ms), the area under the curve (N/A) and CI (N/A). In this thesis, the CardioECR analysis was

thereby used to investigate changes in beating rate (bpm), impedance contraction amplitude (N/A) as well as cell viability via CI measurement (N/A).

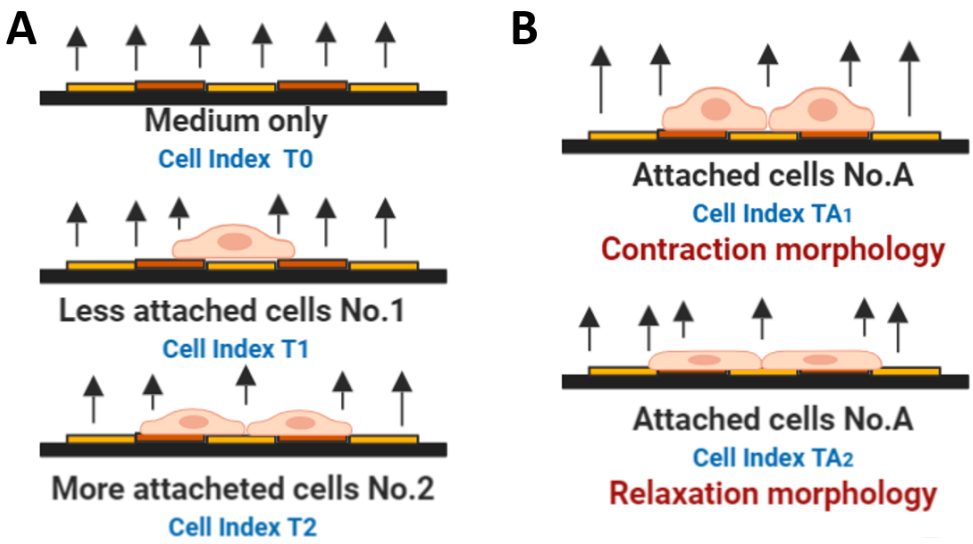

Figure 3.3 ***Principle of impedance-based label-free cellular assays.*** (A) The arrows indicate the electric potential releasing from electrodes. The attached cells generate impedance by changing the electric potential across the electrodes. Before the seeding of cells, the baseline impedance at T0 is Z0. As cells adhere to the electrodes, impedance increases proportionally. (B) Changes in cell morphology also directly reflected in the impedance profile, which is used to investigate the contractility response of hPSC-CMs.

3.1.6.3 CellOPTIQ

The CellOPTIQ system (CellOPTIQ™, Clyde Biosciences) is a custom-built platform for contractility, voltage and Ca^{2+} measurement. This platform offers CO_2 and temperature control, recapitulating physiological conditions (**figure 3.4.A**). Besides the CardioECR system, the CellOPTIQ system has also been demonstrated as an effective platform for evaluating drug-induced arrhythmias in hiPSC-CMs (Blinova et al., 2018, 2017; Denning et al., 2016). The CellOPTIQ assesses the contractility response of 2D monolayer hPSC-CMs over a 10 second period by recording bright-field images of the beating cardiomyocytes at 100 frames per second (**figure 3.4.B**). These images are then analysed offline using the proprietary Contractility Tool software. This software uses the sum of absolute algorithm differences, which is a measure of similarity between images frames (**figure 3.4.C, D**). The contraction amplitude can be calculated through changes in pixel intensity by taking the absolute difference between pixels in the original frame and comparing it against the pixels in the corresponding frame. This software was used to plot contractility over 10 seconds and calculate average contraction parameters, including amplitude, contraction time (Up90 – upstroke time) and relaxation time (Dn90 – downstroke time), contraction duration (CD). These parameters are illustrated in the sample trace (**figure 3.4.E &F**).

CellOPTIQ can also be used to assess electrophysiology and calcium handling. Voltage-sensitive dyes, which penetrate inside the cell membrane, are used to measure changes in the membrane action potential. Fura-4F, AM and Fluo-4, AM can be used for CellOPTIQ to assess intercellular calcium handing of hPSC-CMs by detecting changes in the fluorescent signals, which are analysed with delicate proprietary software provided with CellOPTIQ.

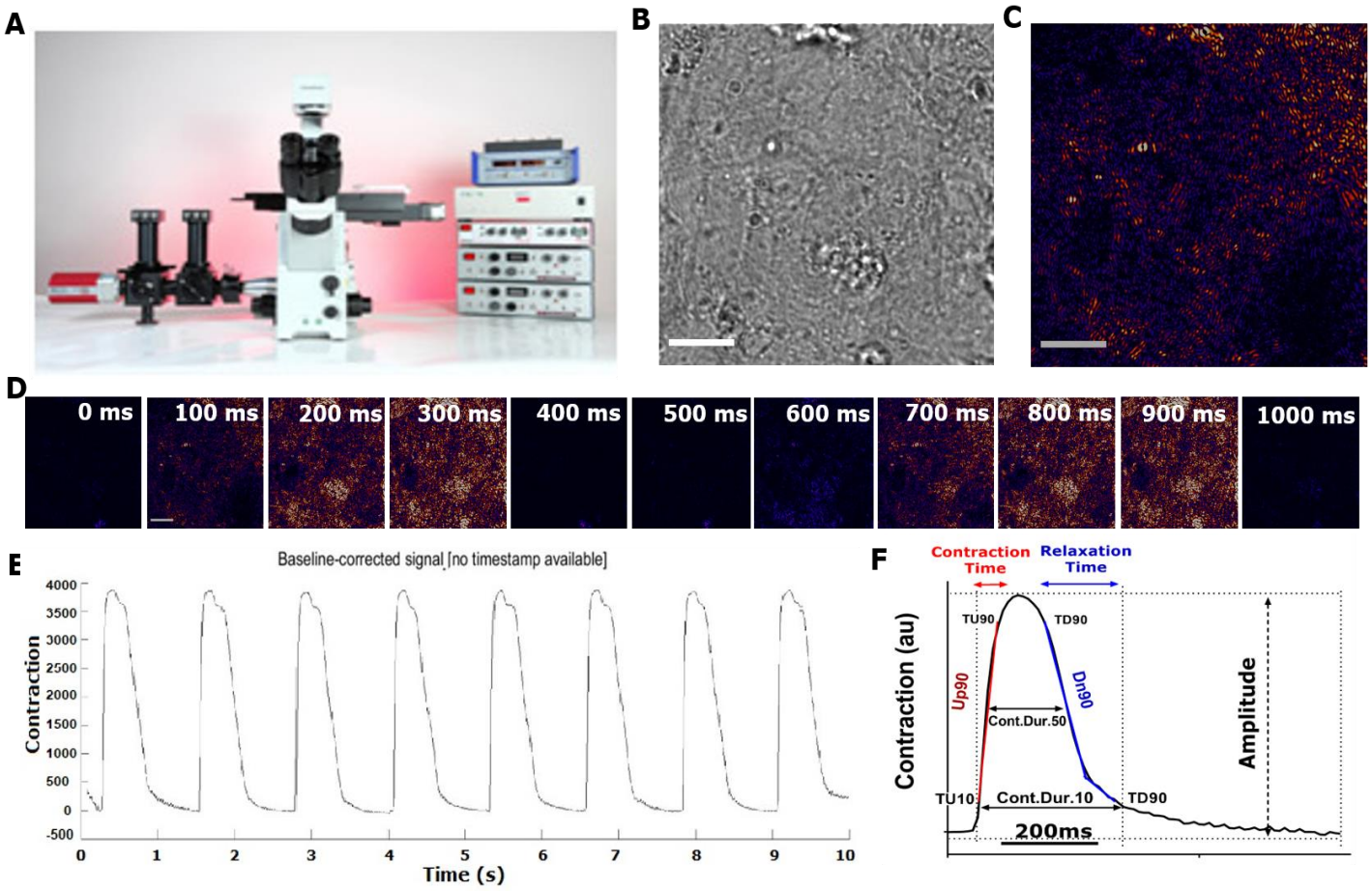

Figure 3.4. Contractility Quantification by CellOPTIQ™

(A) The CellOPTIQ instrument. (B) Bright-field images of the beating CMs captured by the CellOPTIQ. (C) Proprietary image-analysis by Contractility Tool software, the arise of colour indicate for the changes of pixel intensity, scale bars = 20 µm. (D, E) Pixel displacement of 1000 frame images was calculated to plot contraction parameters. (F) Contraction parameters that are calculated by CellOPTIQ software. Up90 – upstroke time, Dn90 – downstroke time.

3.2 Chapter Aims and Objectives:

This chapter aims are to describe the investigation into the effects of GRK5-Q41L on cardiac contractility response and cardiotoxicity response during chronic catecholamine stress and to validate the uses of hiPSC-CM models to study SNPs function in *in vitro* modelling cardiac diseases. The objectives were:

1. Characterise the hESC isogenic model and hiPSC model harbouring GRK5-Q41L variants.
2. Generate cardiomyocytes for all hPSC lines and characterise hPSC-GRK5-Q41L-CM models.
3. Develop assays to study the phenotype of GRK5-Q41L SNP in contractility response during chronic catecholamine stress.
4. Develop assays to evaluate cardiotoxicity responses of GRK5-Q41L SNP during chronic catecholamine stress.

3.3 Results:

3.3.1 Pluripotency characterisation of the β2-AR isogenic hESC models:

To validate all established hPSC lines, standard pluripotency characterisation was conducted using immunocytochemistry technique to evaluate the expression of nuclear pluripotency markers (OCT4, SOX2 and NANOG), the proliferation rates and karyotype.

All the gene-edited HUES7-GRK5-Q41L lines (known as isogenic set) showed typical pluripotency stem cell morphology with defined border colonies and a high nuclear-to-cytoplasm ratio (**figure 3.5.A**). Pluripotency marker analysis by immunofluorescence was performed in the cells cultured in E8 medium after 3 passages from thawing. Immunocytochemistry staining for the nuclear pluripotency markers OCT4, NANOG, SOX2 demonstrated that established hPSC cultures uniformly expressed these markers, and the stain was specifically revealed in the nucleus stained with DAPI (**figure 3.5.B**).

G-banding analysis of all cell lines after 10 passages in E8 culture showed normal male 46, XY karyotypes in the engineered hESC lines, while both the hiPSC lines had normal female 46, XX karyotypes (**figure 3.5.C**). Karyotype analysis results indicated that the genetic stability of engineered hESC lines was retained during TrypLE passaging culture. The stability of all cell lines was further confirmed with the average population doubling (PD) intervals of HUES7-GRK5-Q41, HUES7-GRK5-L41, HUES7-GRK5-Q/L41, hIPSC-GRK5-Q41 and hIPSC-GRK5-L41 over 5 passages were 23.3h ± 0.9, 22.8h ± 1.3, 23.5h ± 1.3, 21.7h ± 0.9 and 21.7h ± 1.4 respectively (**figure 3.5.D**). These data, taken together, demonstrate that our engineered hPSC lines conform to the criteria required for a standard pluripotency hPSCs.

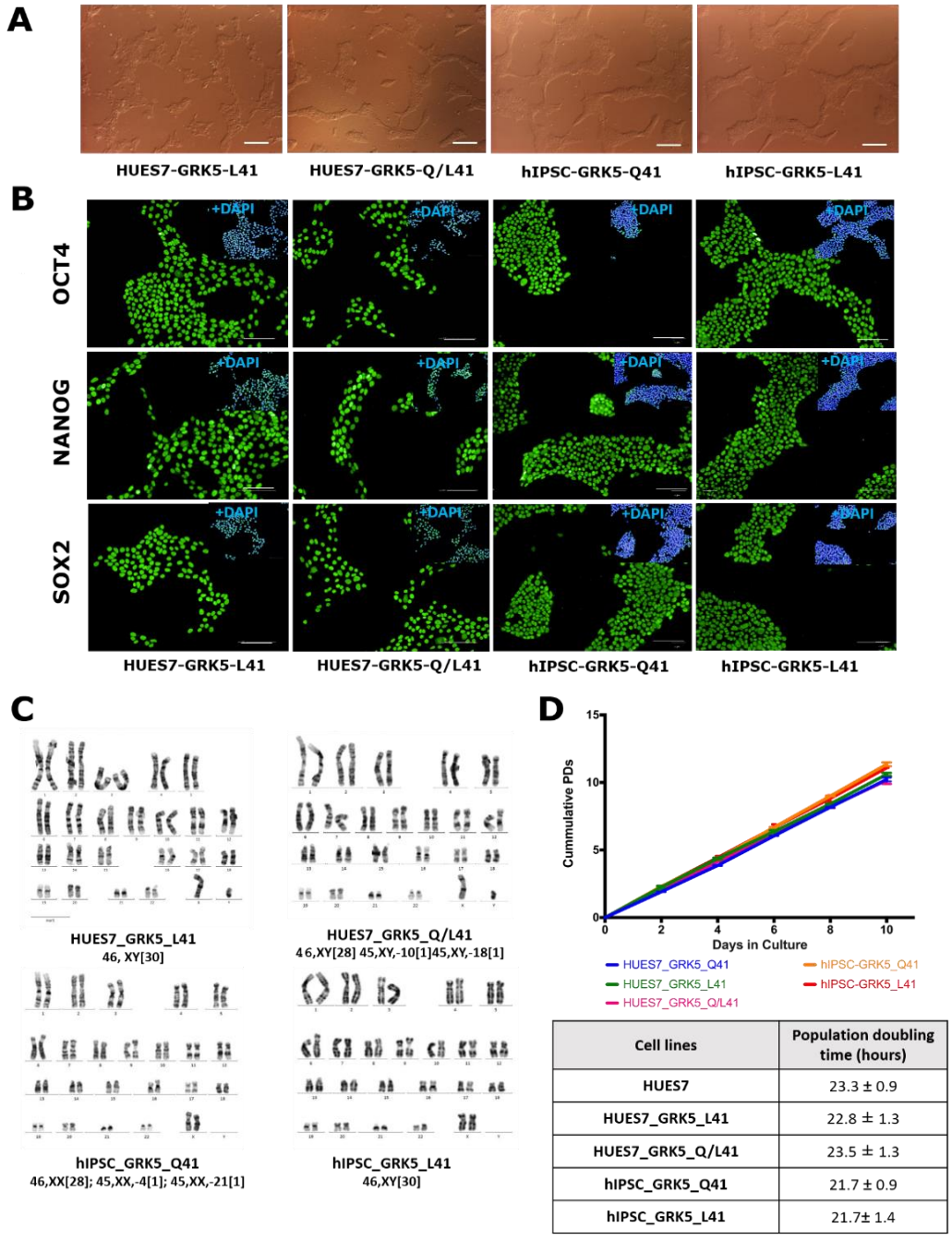

Cell lines	Population doubling time (hours)
HUES7	23.3 ± 0.9
HUES7_GRK5_L41	22.8 ± 1.3
HUES7_GRK5_Q/L41	23.5 ± 1.3
hIPSC_GRK5_Q41	21.7 ± 0.9
hIPSC_GRK5_L41	21.7± 1.4

Figure 3.5. Pluripotency characterization of the GRK5's hPSC lines.

(A) Morphology of hPSC lines in E8 medium cultured on Matrigel. (B) Immunofluorescence staining of OCT4, NANOG and SOX2 (Green) demonstrated the specific expression of these pluripotency markers in the nucleus, which is stained with DAPI (Blue), scale bar: 100μm (C) Representative karyograms of the tested lines after 10 passages cultured in E8 medium showed normal 46XY in the isogenic engineered hESC lines and 46XX karyotypes in the hIPSC lines. (D) Linear growth curves demonstrated the proliferation rate of the tested lines in E8 culture condition. All the engineered hESC lines and hIPSC lines exhibited a similar growth rate to HUES7 around 23.3h, the cumulative PD was summed across the 5 passages to plot the growth curve relative to the time in test culture. The PD times were presented as mean ± SE.

3.3.2 Genotyping of isogenic and hIPSC models:

To check the presence of corrected GRK5 genotypes in the isogenic and hIPSC models, PCR amplification of specific GRK5 loci containing SNPs were sent for sequencing. First, GRK5 amplicons of all cell lines were obtained at the correct size at 638bp (**figure 3.6.A**). These PCR products were collected and sent for Sanger DNA Sequencing to confirm the genotype.

The change of the nucleotide at position 142 from A to T of the coding sequence caused a substitution in amino acid 41 with Glutamine (Q) into Leucine (L) in HUES7 hESCs to create the isogenic GRK5 model in HUES7 with either the homozygous L41 line or the heterozygous Q/L41 line (**figure 3.6.C**). Genetic screening of GRK5 loci in hIPSC lines showed the expected genotypes in hIPSC-GRK5-Q41 and hIPSC-GRK5-L41 (**figure 3.6.B**). A summary of encoded amino acid 41 in GRK5 protein in all the hPSC lines is shown in **figure 3.6.D**.

GRK5 is involved in the phosphorylation of agonist-activated β-AR receptors, which is one of the central systems regulating cardiac contractility. Genetic studies of polymorphisms in β-ARs have shown its correlation to patient survival as β-AR polymorphisms affect desensitization and downregulation of β-AR signalling in *in vitro* studies (Ahles and Engelhardt, 2014; Dorn, 2010a; Sotoodehnia et al., 2006). Therefore, knowing what β-AR polymorphisms are in our isogenic and hIPSC models would help to understand their effects on GRK5 function.

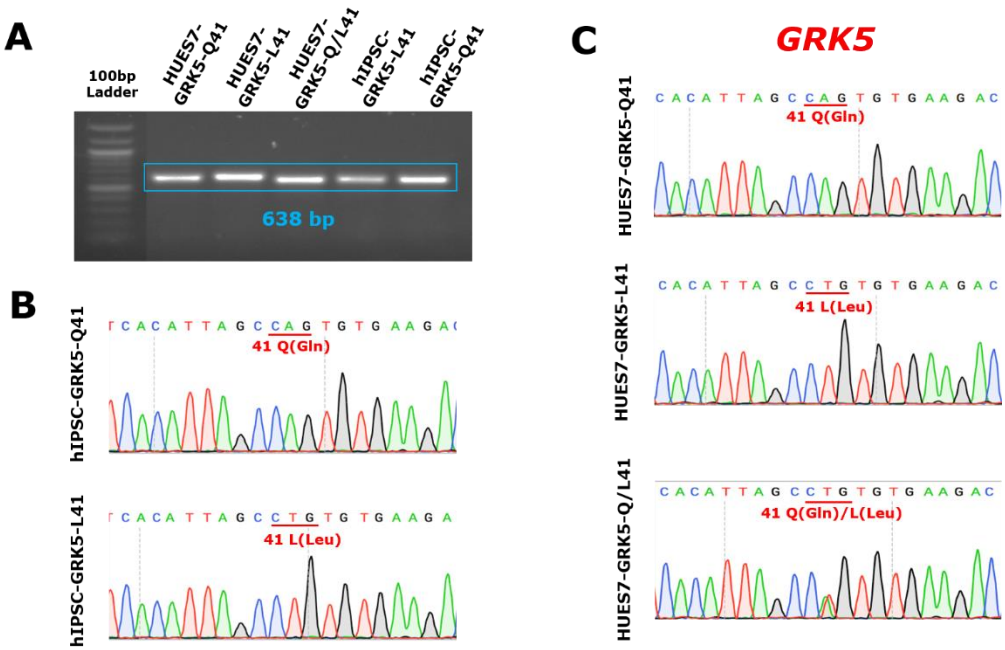

D

Gene	GRK5
Cell lines	41
hiPSC-GRK5-Q41	Q41
hiPSC-GRK5-L41	L41
HUES7-GRK5-Q41	Q41
HUES7-GRK5-L41	L41
HUES7-GRK5-Q/L41	Q/L41

Figure 3.6. Validation of polymorphisms in GRK5

(A) PCR analysis of GRK5 showed the correct band size at 638bp. Sequence analysis of the GRK5 locus demonstrated the expected polymorphisms in hIPSC-Q41L lines (B) and in the isogenic HUES7-Q41L lines (C), where a single nucleotide substitution resulted in an alteration in the codon triplet encoding for Glutamine (Q) into Leucine (L) at amino acid positions 41 (c.A122T - c.Q41L) in the GRK5 protein. (D) A summary of encoded amino acid 41 from the sequencing results of in GRK5 protein all the hPSC lines.

The two most relevant SNPs found in the β1-AR (ADRB1) were 49(S/Q) variant and 389(R/G) variant. The PCR analysis using primer pairs spanning individual *ADRB1* variant was performed and PCR amplicons of *ADRB1_SNP49* and *ADRB1_SNP389* were obtained at 564bp and 530bp, respectively (**figure 3.7.A**). DNA sequencing analysis of *ADRB1* variants showed the homozygous presence of S in the HUES7 isogenic set and hIPSC-GRK5-Q41 at amino acid 49 and G at amino acid 389 (**figure 3.7.B**), whereas hIPSC-GRK5-L41 possesses heterozygous alleles at amino acid 49 (A/G) and 389 (R/G).

The two most commonly studied polymorphisms in β2-AR (*ADRB2*) were 16 (R16G) variant and 27 (Q27E) variant, which affect agonist-stimulated receptor down-regulation (Dorn, 2010). PCR amplifying specific *ADRB2* loci containing SNP for genotyping were conducted in all the lines established, including the isogenic and the hIPSC models. PCR of all cell lines was obtained at the corrected size at 1.2 kb (**figure 3.7.C**). DNA sequencing results by Sanger sequencing showed the genotype of isogenic HUES7-GRK5-Q41L lines are homozygous in G at amino acid 16 and E acid at in amino acid 27 (**figure 3.7.D**). Genetic screening of *ADRB2* loci in hIPSC-GRK5-Q41 and hIPSC-GRK5-L41 showed the homozygous presence of Q27 in the encoded protein sequences but were heterozygous of at amino acid 16. A summary of encoded amino acids at polymorphic positions in β1-AR and β2-AR protein of all the cell lines are shown in **figure 3.7.E**.

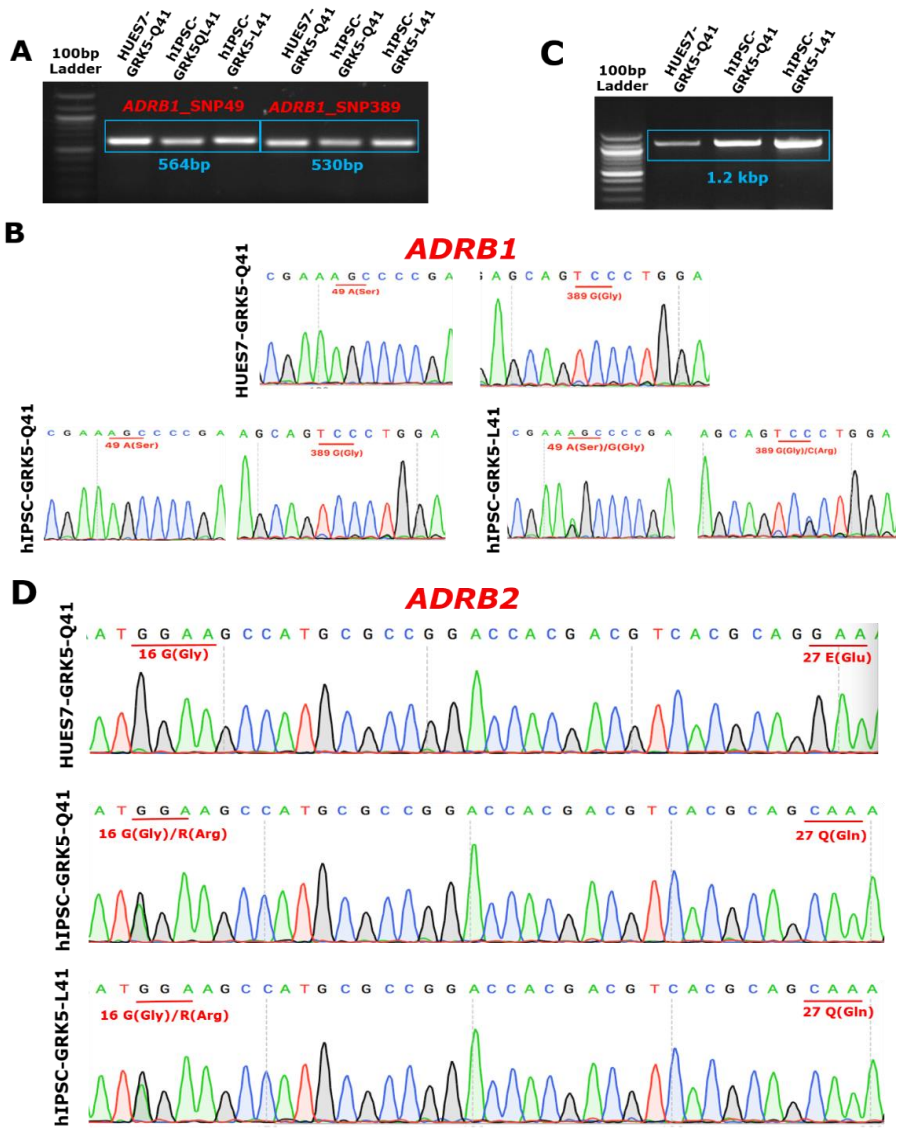

E

Gene	*ADRB1*		*ADRB2*	
Cell lines	**49**	**398**	**16**	**27**
hiPSC-GRK5-Q41	S49	G389	R/G16	Q27
hiPSC-GRK5-L41	S/G49	G/R389	R/G16	Q27
HUES7-GRK5-Q41	S49	G389	G16	E27
HUES7-GRK5-L41	S49	G389	G16	E27
HUES7-GRK5-Q/L41	S49	G389	G16	E27

Figure 3.7. Validation of polymorphisms in ADRB1 and ADRB2 gene in HUES7 and hIPSC lines.

(A) Gel electrophoresis demonstrated the ADRB1 PCR products for SNP49 and SNP389 (B) Sequencing analysis of the ADRB1 locus showed genotypes of the nucleotides encoding amino acid 49 and 389 (C) Gel electrophoresis of the ADRB2 PCR products for SNP16 and SNP27 genotype. (D) Sequencing analysis of the ADRB2 locus containing polymorphisms at amino acid 16 and 27 (E) A summary of encoded amino acids from the sequencing results in *ADRB1* and *ADRB2* genes in the hIPSC lines and the isogenic HUES7 lines.

3.3.3 Cardiac differentiation of hPSCs:

To generate the relevant platform for studying the effects of GRK5-Q41L variants on cardiac contractility function, all the hPSC lines were differentiated to cardiomyocytes (**figure 3.8.A**). Cardiomyocytes were successfully generated across the cell lines. The high purity of cardiomyocytes is important to prove that the results from the following experiments are representative of cardiomyocytes. Cardiomyocytes after d15 post differentiation were dissociated by Collagenase and were stained with α-actinin (or cardiac troponin T; cTnT) to define the percentage of the α-actinin$^+$ cells. Purity quantification for cardiac differentiation is explained in **figure 3.8.B**. The α-actinin$^+$ cells illustrate the high purity of hPSC-CMs, which were all above 90%. The results confirmed that all the established cell lines were able to differentiate to cardiomyocytes with high purity.

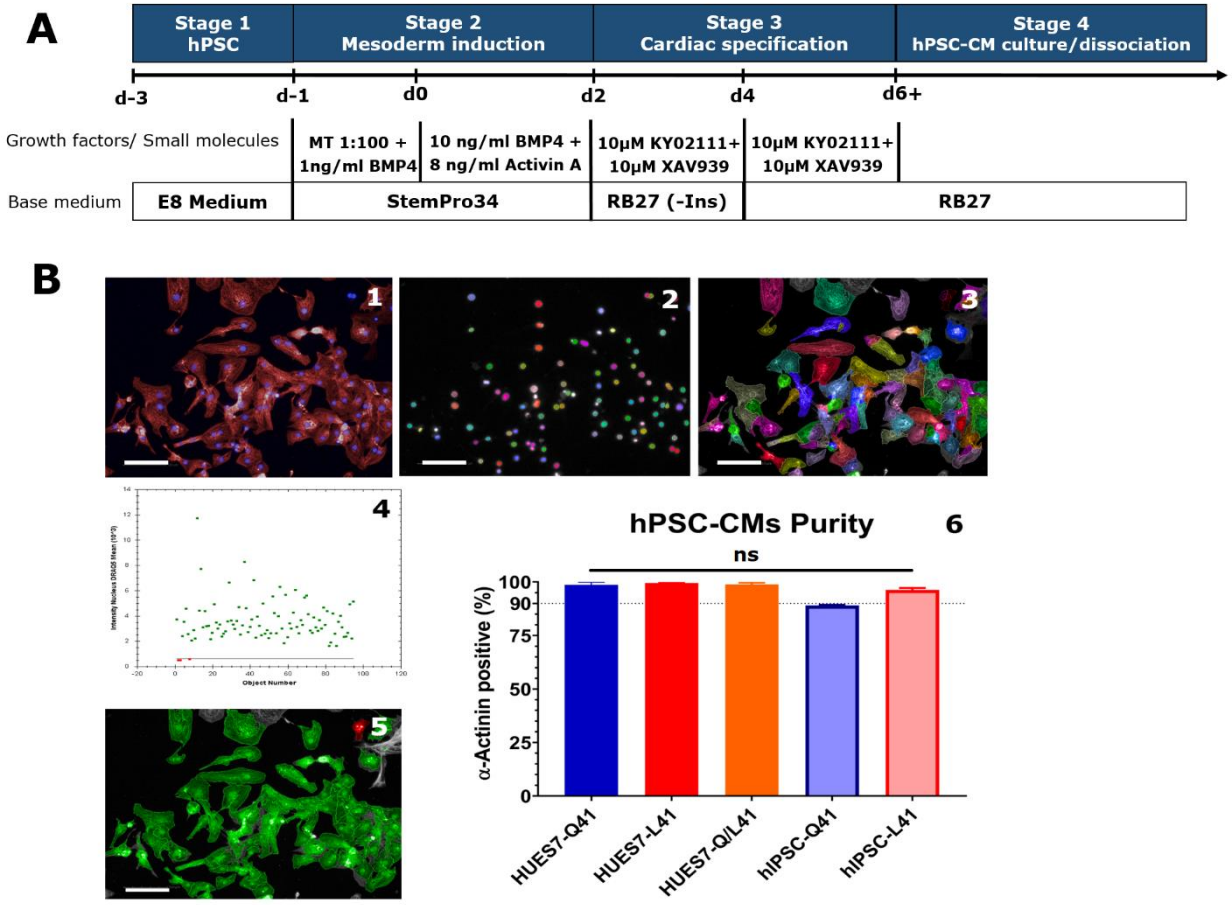

Figure 3.8. Determination of hPSC-CM purity by high-content imaging.

(A) The schematic depicts the procedures of the cardiac differentiation protocol, including media and concentration of growth factors and small molecules. (B) Confocal imaging (Operetta) algorithm to quantify purity of α-actinin immunostained hPSC-CMs 1) immunofluorescence images of hPSC-CMs staining with α-actinin (Green), DAPI nuclear dye (Blue) 2) find nuclei using DAPI stain 3) find cytoplasm using cell region around defined nuclei and measure α-actinin intensity signal 4) apply a determined signal threshold using secondary Alexa 488 control (negative control) 5) counted cardiomyocytes (Green) and non-cardiomyocytes (Red). 6) Purity of all hPSC-CMs lines showed successful differentiation with ~90% α-Actinin positive cells, represent means ± SEM, n≥5 biological. Scale Bar: 100μm.

3.3.4 Gene expression profile of hPSC-CMs:

Human PSC-CMs exhibit foetal-like phenotypes in gene expression (Khan et al., 2013; Robertson et al., 2013). Therefore, it is important to investigate mRNA expression of *GRK5* and different GPCRs, in which GRK5 is involved, such as β-AR (*ADRB1, ADRB2*), angiotensin II type 1 receptor (*AGTR1*) and endothelin receptor (*EDNRA*). To define when will be the earliest time for studying the functions of GRK5-Q41L variants, cardiomyocytes of our hPSC models were collected on different days, ranging from day 20 to day 60 post-differentiation to check the mRNA expression of associated genes.

A ventricle human heart sample (VHH) was also included as the physiological expression control. Time-course measurement of mRNA expression of *GRK5* and other associated GPCRs, including *ADRB1, ADRB2, EDNRA* and *AGTR1* was performed for all cell lines. 18S was used for endogenous control. All negative controls, including RNA negative, reverse transcriptase (RT) negative and cDNA negative samples were run prior to the samples, while non-template controls (NTC) were performed for every qPCR experiments.

Expression of *GRK5* was upregulated during cardiac differentiation (**figure 3.9**). *GRK5* mRNA levels started increasing on day 20 and were stabilised on day 30, post-differentiation afterwards with ~ 10-fold increase compared to day 0. There was no significant difference in the *GRK5* expression across the lines, indicating that SNPs did not alter the basal expression of *GRK5* ($p>0.05$). Expression levels on day 30 were also close to the GRK5 expression level in VHH (**figure 3.10**). Therefore, it was decided to perform a phenotyping study of the effect of the GRK5-Q41L variant on hPSC-CM day 30-post differentiation.

Similar to the expression level of *GRK5*, *ADRB2* and *EBNRA*, mRNA expression levels were upregulated during cardiac differentiation and started to be stable after day 30 with ~ 10-fold increase compared to day 0 (**figure 3.9**). Significant increases of *ADRB2* mRNA were detected at day 30 in HUES7-Q41 and HUES7-L41 but was not observed in hIPSC lines (*$p < 0.05$, **$p<0.01$). While significant upregulations of *EBNRA* mRNA were observed on day 20 in most of the cell lines (*$p < 0.05$, **$p<0.01$). However, the expression level of *ADRB1* significantly increased during hPSC-CMs culture, expression was ~ 10-fold higher on day 30 and was significant ~80-fold higher on day 60 cell lines (*,$p < 0.05$). Interestingly, Angiotensin receptor type II (*AGTRII*) was silent in our hPSC-CMs both for the HUES7-GRK5-CM models and hIPSC-CM models, when Ct value was undetected or detected after cycle 35 (data not shown).

The general observation showed that hPSC-CMs on day 30 post-differentiation could be used for studying the effects of GRK5-Q41L SNP on β-AR and ET, signalling that the expression levels of *GRK5*, *ADRB2* and *EBNRA* in 30-days hPSC-CMs were upregulated and relatively close to the expression level in VHH (**figure 3.10**). The absence of *AGTRII* mRNA showed that we could not study GRK5-Q41L SNP functions in this signalling system.

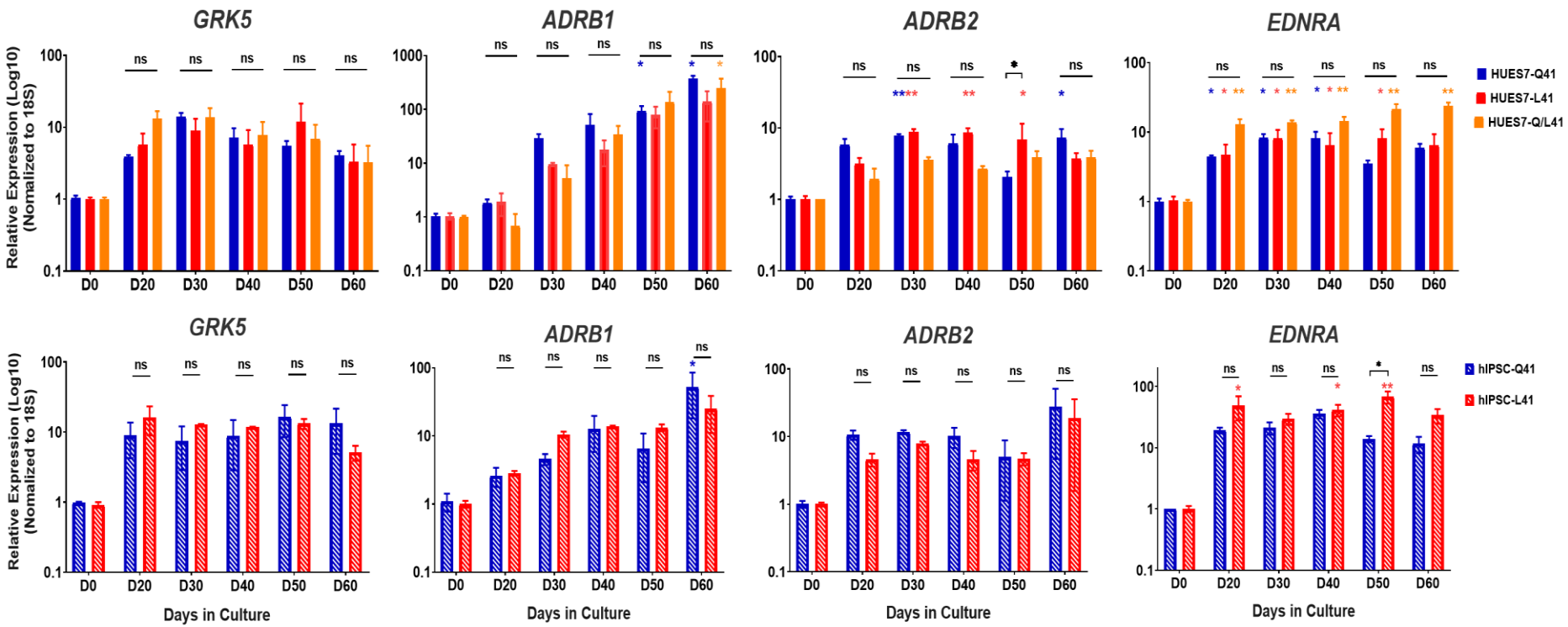

Figure 3.9. **Gene expression profiles of hPSC-CMs.**

q-PCR analysis of *GRK5* and associated GPCRs, including *ADRB1, ADRB2,* and *EDNRA* in (A) the isogenic HUES7-Q41L model and (B) the hIPSC-Q41L model, represent means ± SEM, n=3 biological replicates, ns: no significant, *p<0.05, **p<0.01. Colour-coded according to duration treatment compared within the same cell lines; black asterisk indicates cross-comparison between Q41 and L41 variants. Two-way ANOVA with Dunnett's multiple comparison test.

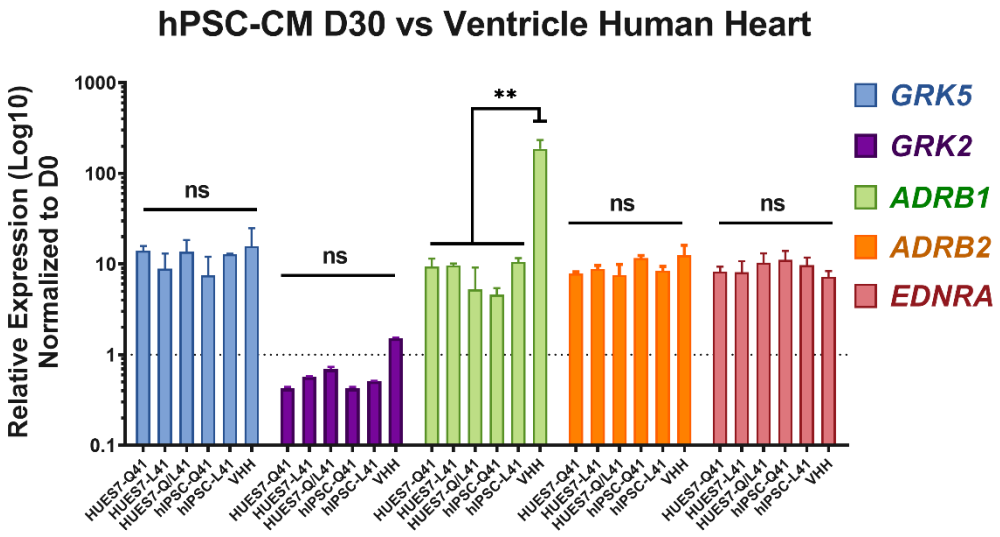

Figure 3.10. Comparison of gene expression between hPSC-CMs d30 and human left ventricular cardiomyocytes (VHH)

q-PCR analysis of GRK5 and associated GPCRs, including ADRB1, ADRB2, EDNRA and AGTRII in hPSC-GRK5-Q41L cardiomyocytes and ventricle human heart (VHH), represent means ± SEM, n=3 biological replicates. *p<0.05, **p<0.01; One-way ANOVA with Dunnett's multiple comparison test.

3.3.5 HUES7-L41 cardiomyocytes exhibited beneficial effects in contractile performances during chronic catecholamine stress

Contractility dysfunctions in long term β-AR stimulation have been the subject of investigation for several decades, while a decrease in inotropic and chronotropic responses has been observed in animal models as well as hPSC-CM models (Dolatshad et al., 2015; Madamanchi, 2007). As explored in the introduction (section 3.1.5), several methods have been optimised in our lab to investigate the contractility responses of hPSC-CMs. In this project, we used the optical CellOPTIQ™ and xCELLigence RTCA CardioECR platforms to measure the contractility of the isogenic HUES7-GRK5-Q41L CMs model and hIPSC-GRK5-Q41L CMs during chronic β-AR stimulation, induced using ISO. 100nM of ISO is present at the physiological level of β-adrenergic stimulation in the human body. The presence of ISO at high concentration will be not specifically activated β-adrenergic, as ISO (> 10μM) could α-adrenergic receptors (Tanimura et al., 1999). All experiments in this study were conducted at 100nM and 1μM of ISO.

3.3.5.1 Optical analysis of contractility response from isogenic HUES7-GRK5-Q41L CMs model and hIPSC-GRK5-Q41L CMs during chronic β-AR stimulation using CellOPTIQ™

In order to determine the effects of the GRK5-Q41L variant on contractility responses during chronic β-AR stimulation, we used CellOPTIQ to capture the spontaneous beatings of all hPSC-CM lines, which were treated with ISO for 24h, 48h, 72h, 96h. The vehicle treatment was considered as 0h. The 10mM ISO stock was prepared in 4 mM HCl to maintain its stability. Therefore, the vehicle control was medium, supplemented with 0.4 μM HCl (~ 1μM ISO).

Bright-field images of spontaneous beating cardiomyocytes of different lines were captured by CellOPTIQ and then calculated into contraction parameters using Contractility Tool software (**figure 3.11.A**). The plating density of 150,000 cells/cm^2, where cell count was conducted by an automated CEDEX HiRes counter, generated a thick and fully confluent monolayer of hIPSC-CMs for the CellOPTIQ experiment. However, these dense layers of cardiomyocytes exhibited abnormal contraction traces, with different contraction peaks observed in every contraction event (**figure 3.11.B**). This issue of cell plating density could cause false-negative results and highlights the importance of seeding density optimisation based on the assay properties. The optimal seeding density for CellOPTIQ contractility assay was obtained at 100,000 cells/cm^2 to generate a partially confluent monolayer of hIPSC-CMs (**figure 3.11.C**).

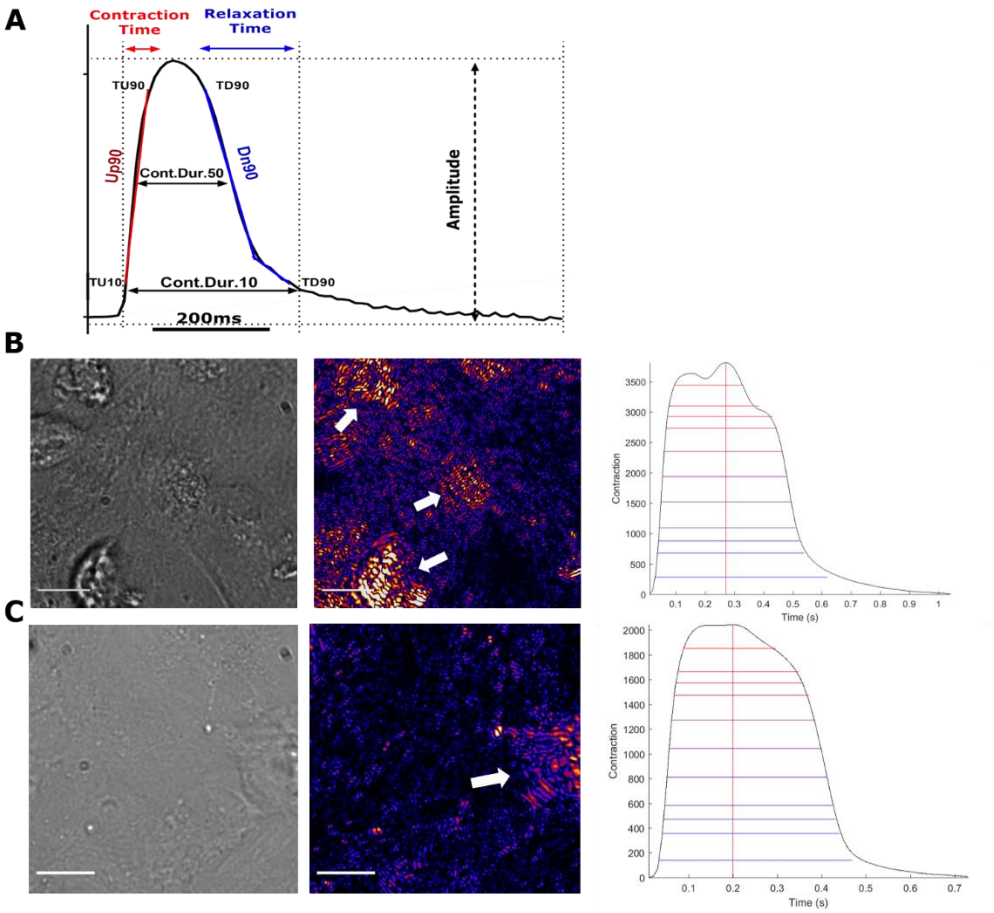

Figure 3.11. Optimization for CellOPTIQ

(A) Contraction parameters that are calculated by CellOPTIQ software. Up90 – upstroke time, Dn90 – downstroke time. (B) Bright-field image and pixel converted image of a dense hPSC-CM layer exhibited several maximum peaks in every contraction event (C) Bright-field image and pixel converted image of a partially confluent monolayer of cardiomyocytes generated standard contraction traces. Scale bar: 20 µm.

Upon analysis with a Contractility Tool, optical contraction traces of HUES7-GRK5-Q41 CMs were generated to compare with its isogenic pair homozygous GRK5-L41 and heterozygous GRK5-Q/L41 CMs, at different exposure durations of ISO at 100 nM and 1 μM. The spontaneous beating of three lines harbouring different GRK5-Q41L variants exhibited different contraction baselines (**figure 3.12 and 3.13**). Indeed, seeding density, the viability of post-dissociated cardiomyocytes and batch-to-batch variation of cardiomyocytes could introduce different baseline measurements among cell lines or even between replicates of the same cell line.

To investigate GRK5-Q41L variant effects during long-term ISO exposure induction, the contractility signal measurement was normalized to the vehicle control (**figure 3.14**), termed as 0 h, and then cross-compared among haplotypes at 72h and 96h (**figure 3.15**). Interestingly, catecholamine stress by ISO induced a significant reduction in contractility of HUES7-GRK5-Q41 CMs in a time- and concentration-dependent manner (**figure 3.14**) while there were no marked differences observed in contraction traces of HUES7-GRK5-L41 and HUES7-GRK5-Q/L41 CMs during chronic ISO exposure at both 100 nM and 1 μM. Indeed, contraction amplitude of HUES7-GRK5-Q41 CMs significantly reduced from 2508 (vehicle control) to 1550 (96h) amplitude unit (au) (**figure 3.12**), a reduction of approximately 38.2 % after 96h exposed to 100 nM of ISO (**figure 3.14.A**, * $p < 0.05$). The effect of catecholamine stress of ISO at 1 μM on HUES7-GRK5-Q41 CMs contractility was more severe where its contraction amplitude significantly decreased, ranging from 1805 to 1372 au (~ 28 % - 45.3 %) between 48h and 96h exposure to ISO (**figure 3.13 & 3.14.A**, * $p < 0.05$, ** $p < 0.01$). Conservative contraction responses of HUES7-GRK5-L41 and HUES7-GRK5-Q/L41 CMs during chronic ISO stress were observed when these haplotypes prevented the significant reduction in contraction

amplitude at both low and high ISO concentrations (**figure 3.12** - **3.15)**. The best illustration of these phenotype differences obtained at 72h and 96h exposure to ISO is a significant reduction in contraction amplitude (> -35%) in Q41 CMs but less than 10 % change in contraction amplitude in L41 and Q/L41 CMs (**figure 3.15.A**). These phenotype differences of GRK5-Q41L SNPs obviously indicate the gain-of-function of GRK5-L41 SNP in contractility.

Decreased contraction time (Up 90) was observed in all lines of isogenic models (**figure 3.14.B**). This indicates the positive chronotropic effects of ISO on contractility responses of hPSC-CMs; however, positive inotropic effects of ISO were not observed at any GRK5-Q41L variants (**figure 3.14.A**). This could be explained by the foetal phenotype of hPSC-CMs which has been found in other studies (Chang and Mummery, 2018; Keung et al., 2014; Ribeiro et al., 2015). Even though ISO induced reduction of contraction time across all lines, HUES7-GRK5-Q41 CMs exhibited more pronounced reduction compared to HUES7-GRK5-L41 and HUES7-GRK5-Q/L41 CMs at 48h and 72h post ISO exposure (**figure 3.14.B & 3.15.B)**. There were no significant differences observed in the relaxation time (Dn 90) during long-term ISO stress among the variants (**figure 3.14.C & 3.15.C**).

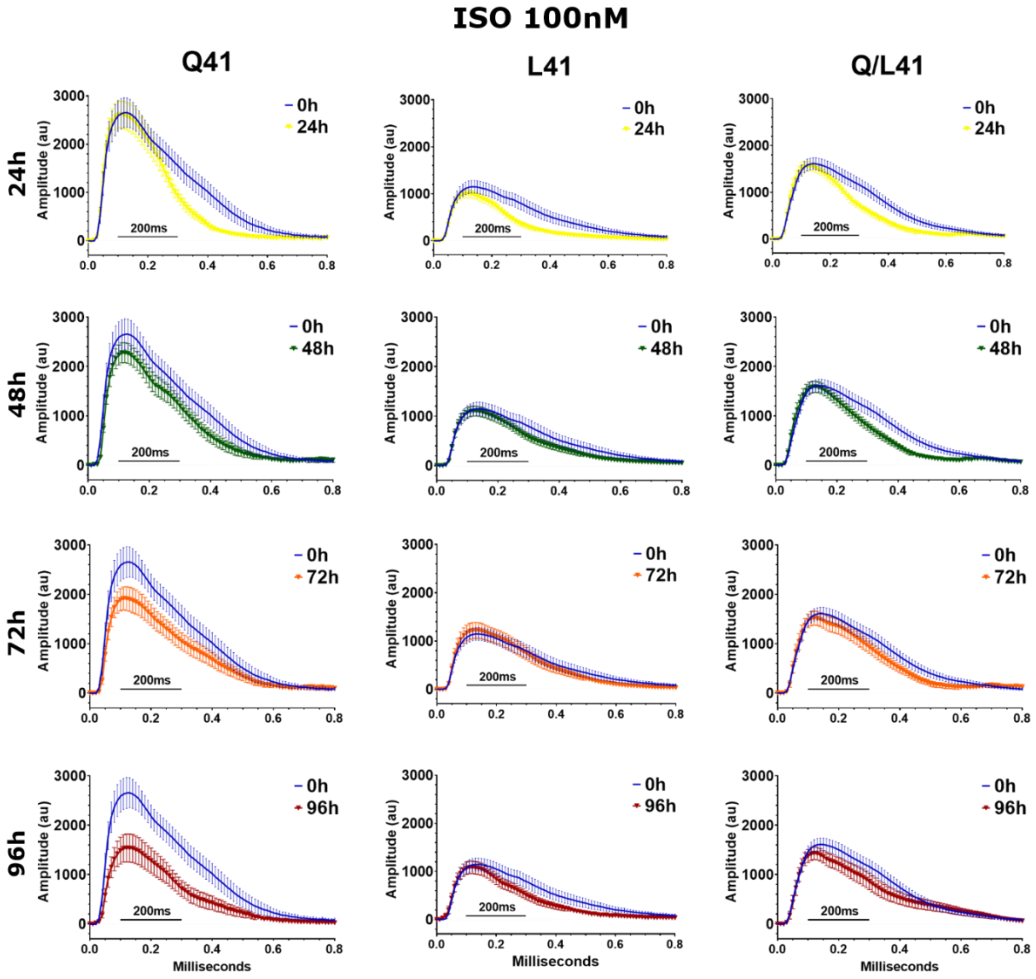

Figure 3.12. Contraction traces of isogenic HUES7-GRK5-Q41L CM models at 100 nM ISO.

Contraction traces of HUES7-GRK5-Q41L CMs generated by Contractility Tool software during exposure to 100 nM ISO for 0 h (blue), 24 h (yellow), 48 h (green), 72 h (orange) and 96 h (red), represent means ± SEM, n=4 biological replicates.

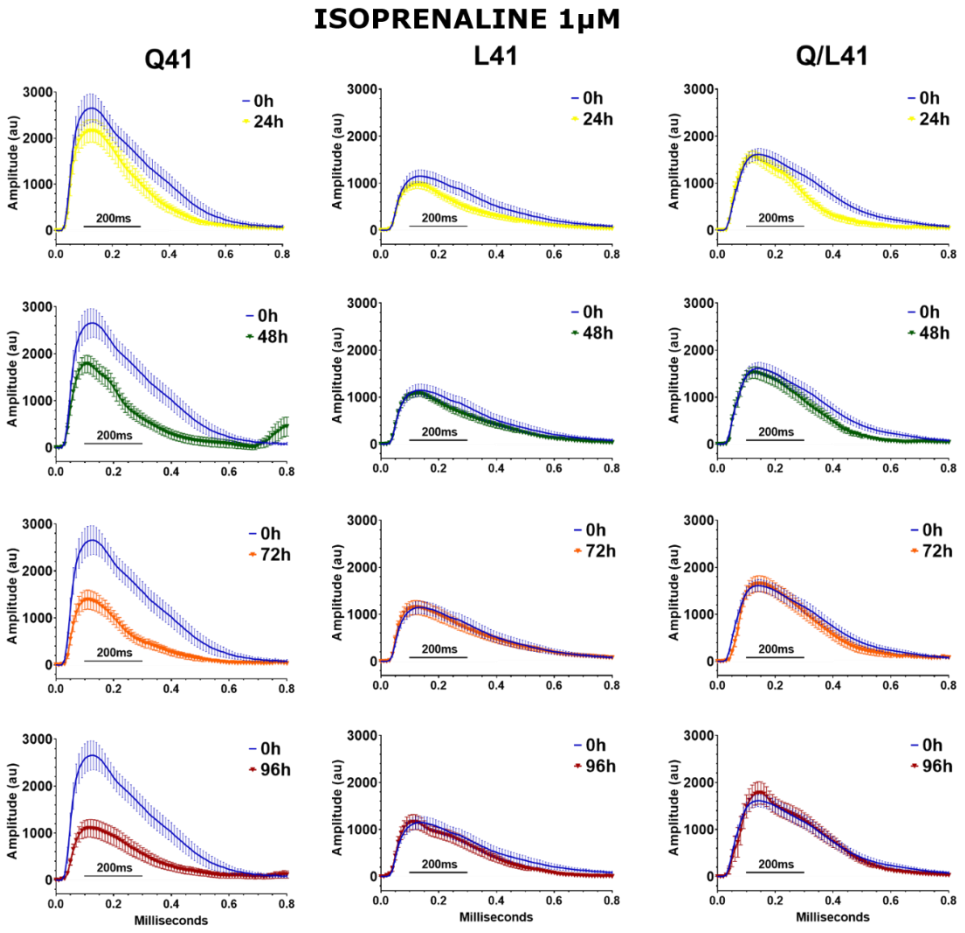

Figure 3.13. Contraction traces of isogenic HUES7-GRK5-Q41L CM models at 1 μM ISO.

Contraction traces of HUES7-GRK5-Q41L CMs generated by Contractility Tool software during exposure to 1 μM ISO for 0 h (blue), 24 h (yellow), 48 h (green), 72 h (orange) and 96 h (red), represent means ± SEM, n=4 biological replicates.

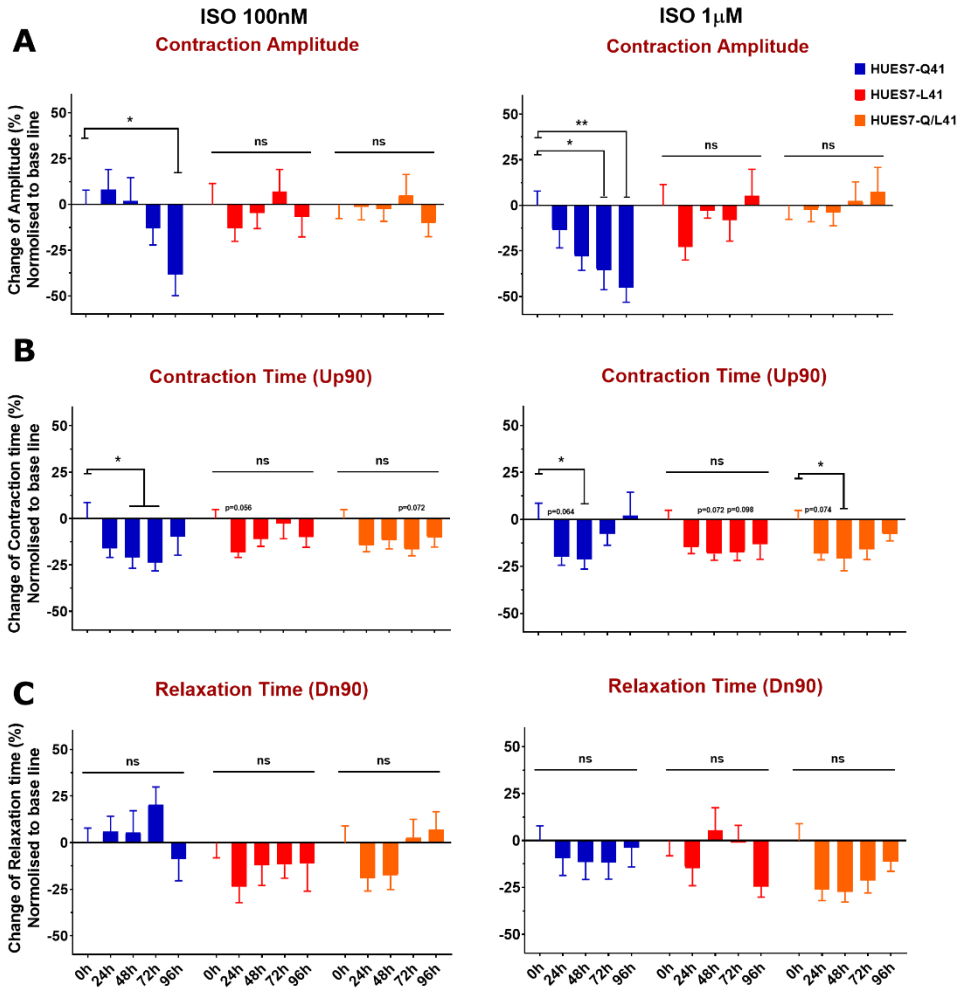

Figure 3.14. Quantification of contractility parameters in isogenic HUES7-GRK5-Q41L CM models during chronic ISO exposure.

Quantification of contraction amplitude (A), contraction time (B) and Relaxation time (C) of HUES7-Q41 CMs (blue), HUES7-L41 CMs (red) and HUES7-Q/l41 CMs (orange), represent means ± SEM, n=4 biological replicates. ns not significant difference, *p<0.05, **p<0.01. Two-way ANOVA with Dunnett's multiple comparison test.

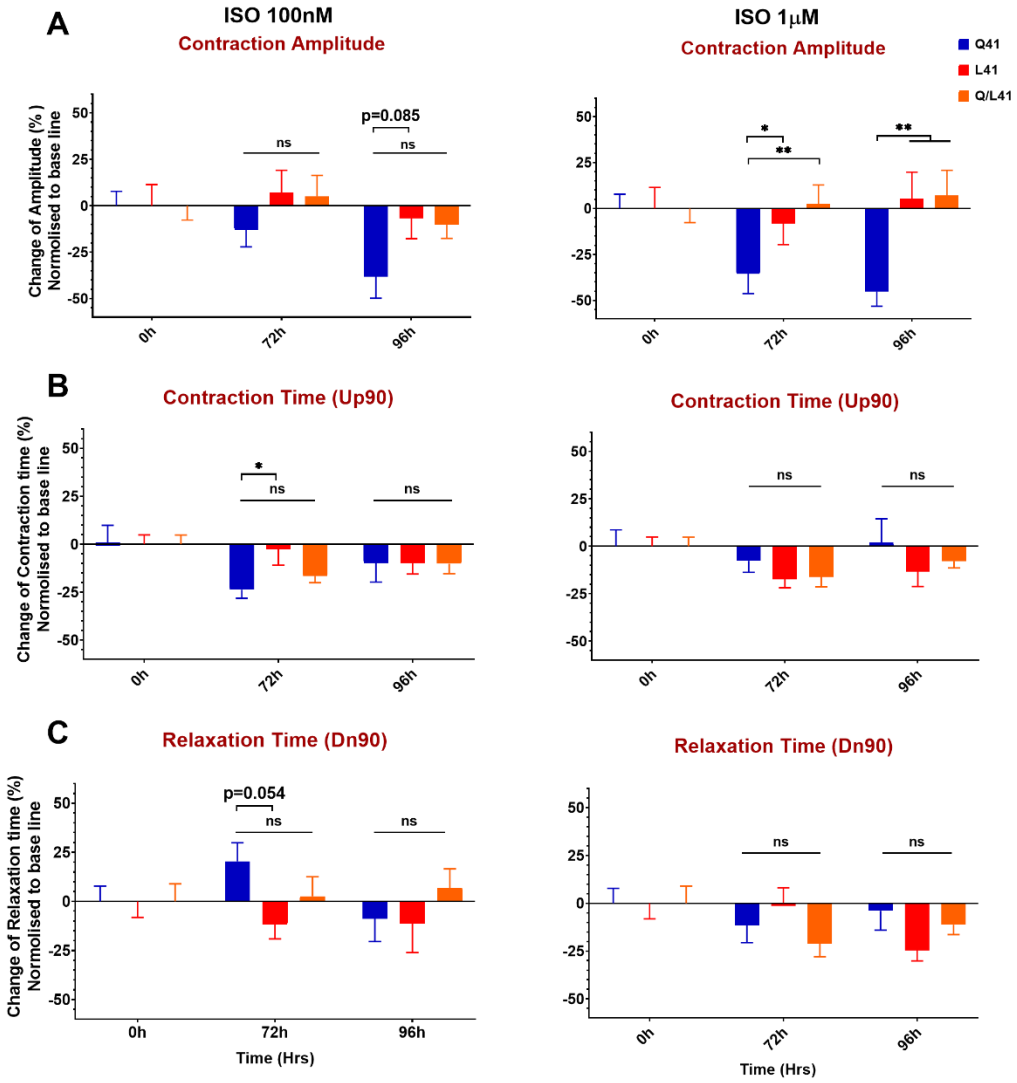

Figure 3.15. GRK5-L41 polymorphism exhibited conservative effects to maintain contractility function during chronic ISO exposure at 72 and 96 h in the isogenic HUES7-Q41L CM model.

Cross comparison changes of contraction amplitude (A), contraction time (B) and Relaxation time (C) among HUES7-Q41 CMs (blue), HUES7-L41 CMs (red) and HUES7-Q/l41 CMs (orange), represent means ± SEM, n=4 biological replicates. ns not significant difference, *p<0.05, **p<0.01. Two-way ANOVA with Dunnett's multiple comparison test.

Interestingly, the hIPSC-GRK5-Q41L CMs model also exhibited a similar trend of change in contractility responses to the isogenic model. While hIPSC-GRK5-Q41 CMs showed a reduced pattern in contraction traces during prolonged ISO exposure, hIPSC-GRK5-L41 CMs can maintain normal contractility function at both low and high ISO concentrations (**figure 3.16 & 3.17**). The contraction amplitude of hIPSC-GRK5-Q41 CMs showed a consistent reduction from 2884 to 2002 au, approximately 15.6 % to 32.3 % reduction during sustained ISO induction and when ISO concentration increased. This declining trend was not significantly observed when compared to the baseline at 0 h (**figure 3.18.A**, p_{96h} = 0.09); however, a cross-comparison between Q41 and L41 phenotype changes at 72h and 96h post ISO exposure showed significant differences (**figure 3.19.A**, * $p < 0.05$). The reduction trend in contraction amplitude was not shown in hIPSC-GRK5-L41 CMs, confirming the gain-of-function of this variant during long-term catecholamine stress. Reproducibly, the contraction time of Q41 CMs in the hIPSC-CM model also decreased ~ 20 % - 35 % during ISO induction, with a significant difference observed at 48h and 72h (**figure 3.18.B**, ** $p < 0.01$). Compared to hIPSC-GRK5-L41 CMs, the contraction time of the Q41 variant decreased more considerably (**figure 3.19.B**, p_{72h} =0.076). However, the relaxation times of these two variants did not show obvious changes during the experiment (**figure 3.18.C & 3.19.C**). These responses were reproducible to the phenotypes we observed in the isogenic models.

The positive chronotropic response of our hPSC-CMs to ISO exposure showed that we could use our models to study the effects of GRK5-Q41L variants in contractility response during catecholamine stress. The reproducible results obtained in both isogenic and heterogenic models demonstrate the gain of function of GRK5-L41 SNP in contractility responses, which is correlated with enhanced cardiac contractility function and low

mortality of patients harbouring this variant in clinical studies (Dorn and Liggett, 2009; Liggett et al., 2008).

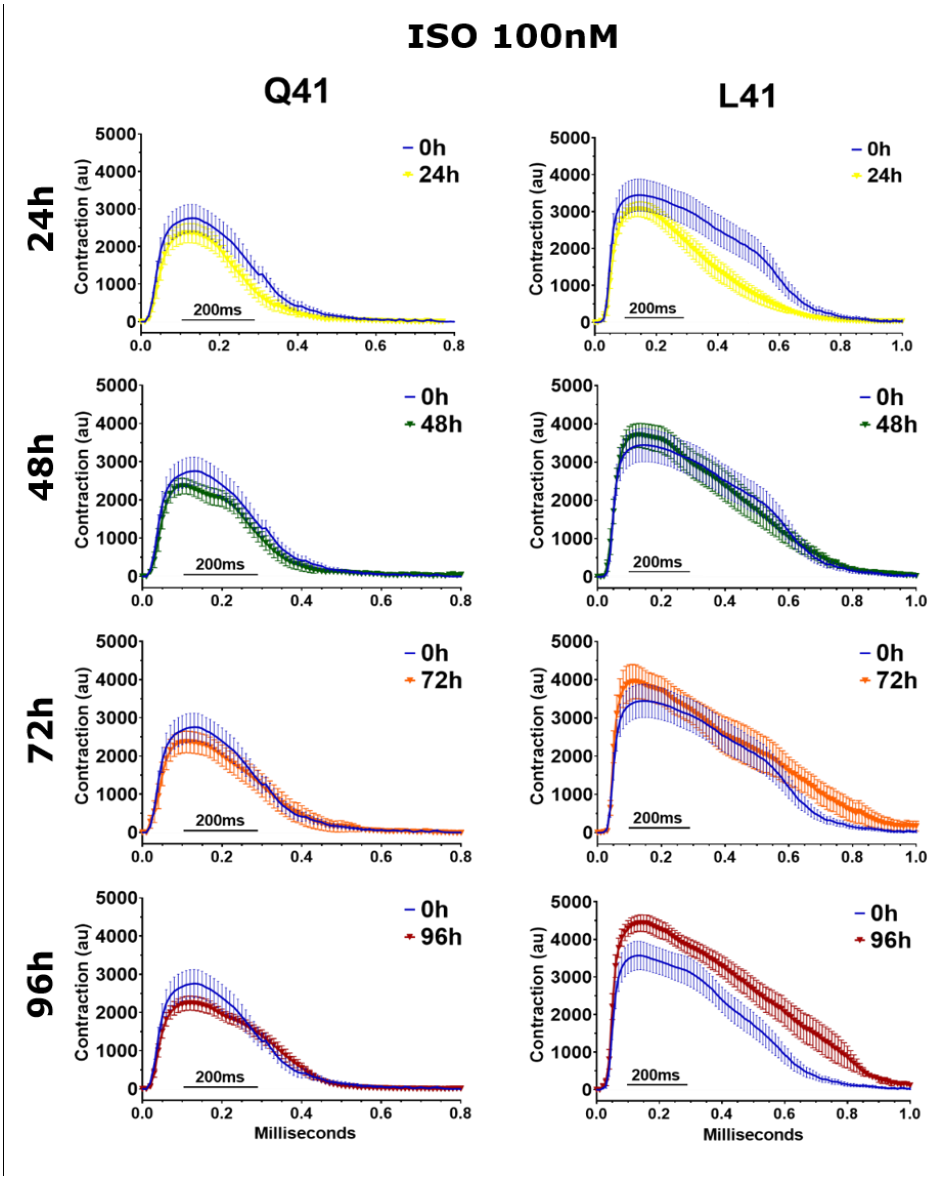

Figure 3.16. Contraction Traces of isogenic hIPSC-GRK5-Q41L CM Models at 100nM ISO

Contraction traces of hIPSC-GRK5-Q41L CMs generated by Contractility Tool software during exposure to 100 nM ISO for 0 h (blue), 24 h (yellow), 48 h (green), 72 h (orange) and 96 h (red), representing means ± SEM, n=4 biological replicates.

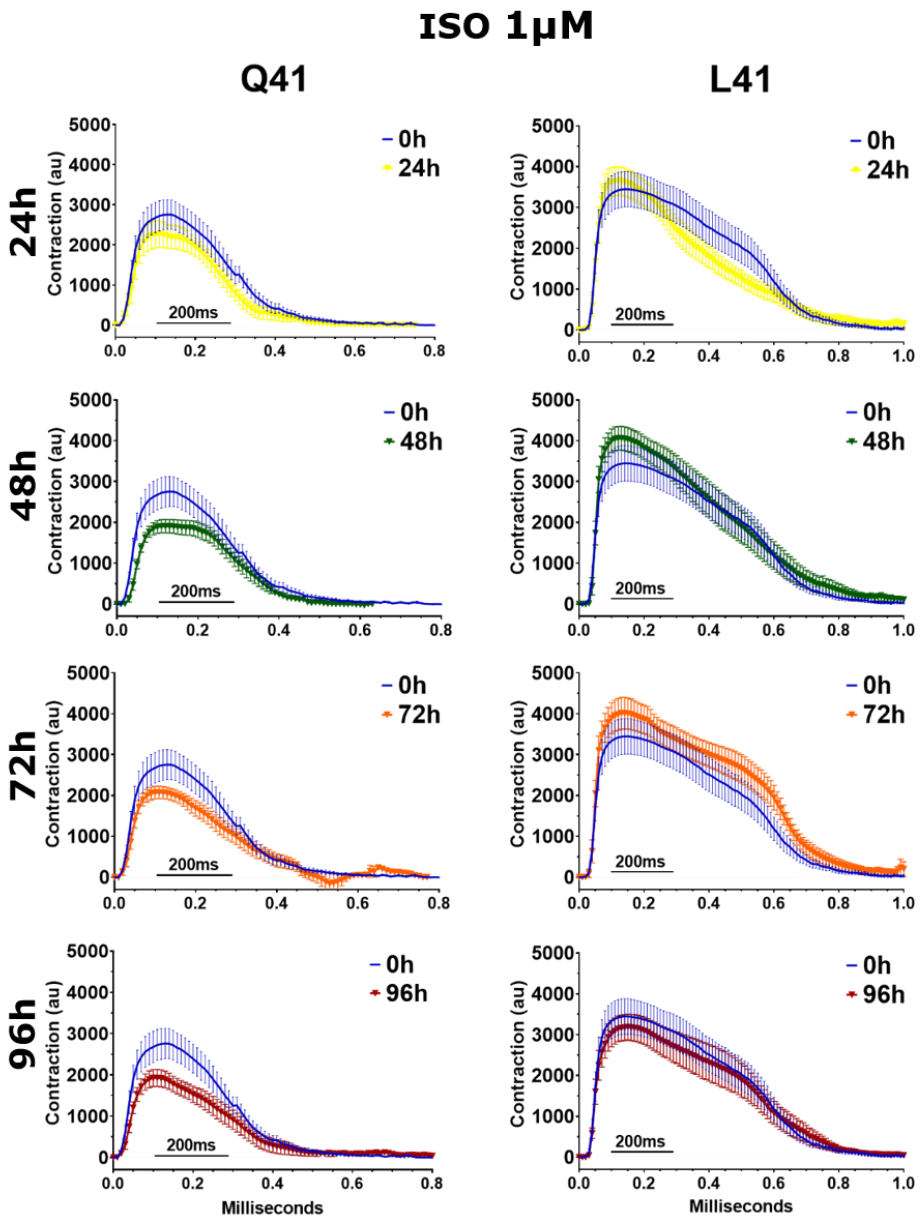

Figure 3.17. Contraction Traces of isogenic hIPSC-GRK5-Q41L CM Models at 1μM ISO

Contraction traces of hIPSC-GRK5-Q41L CMs generated by Contractility Tool software during exposure to 1 μM ISO for 0 h (blue), 24 h (yellow), 48 h (green), 72 h (orange) and 96 h (red), representing means ± SEM, n=4 biological replicates.

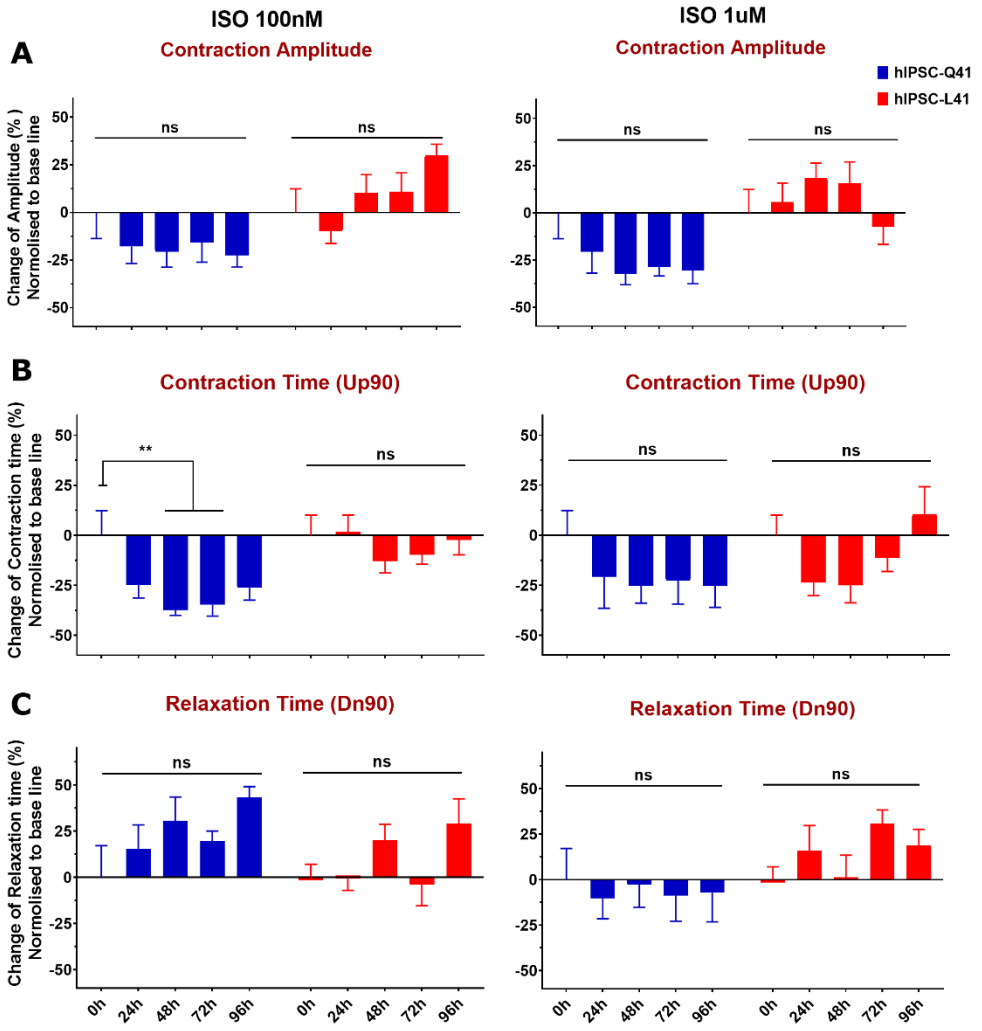

Figure 3.18. Reduced contractility response in isogenic hIPSC-GRK5-Q41L CM Models

Quantification of contraction amplitude (A), contraction time (B) and relaxation time (C) of hIPSC-Q41 CMs (blue) and hIPSC-L41 CMs (red), representing means ± SEM, n=4 biological replicates. ns not significant difference, *p<0.05, **p<0.01. Two-way ANOVA with Dunnett's multiple comparison tests.

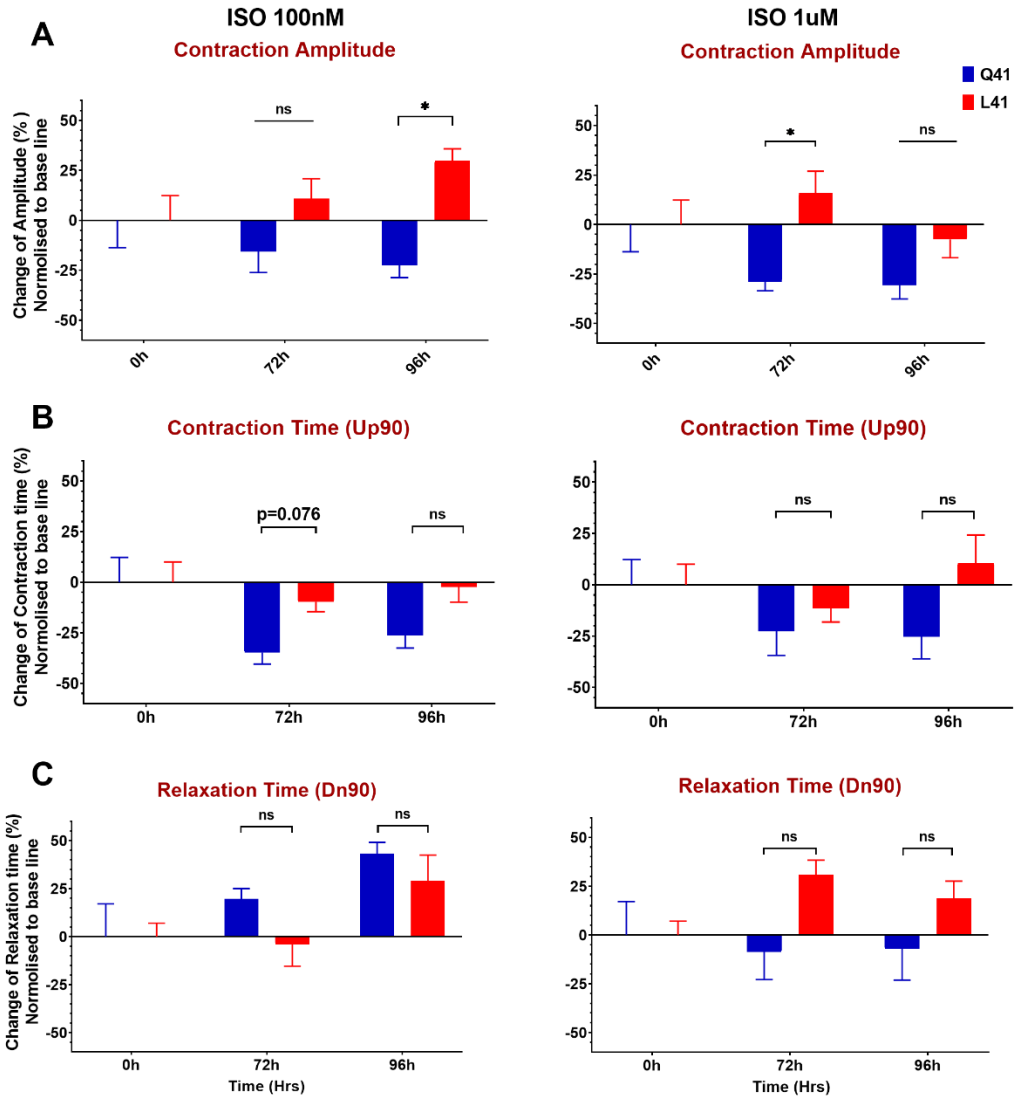

Figure 3.19. Consistent conservative effects GRK5-L41 polymorphism maintained contractility function during chronic ISO exposure at 72 and 96 h in hIPSC model.

Cross comparison changes of contraction amplitude (A), contraction time (B) and relaxation time (C) among hIPSC-Q41 CMs (blue) and hIPSC-L41 CMs (red), representing means ± SEM, n=4 biological replicates. ns not significant difference, *p<0.05, **p<0.01. Two-way ANOVA with Dunnett's multiple comparison test.

3.3.5.2 Real-time analysis of cardiac contractility responses in the isogenic HUES7-GRK5-Q41L-CMs.

Real-time analysis of contractility responses of GRK5-Q41L SNPs was performed by CardioECR. In the CellOPTIQ experiment, phenotype differences in contractility responses of GRK5-Q41 CMs were more significant in the isogenic model than in the hIPSC model. Therefore, in this real-time CardioECR experiment, we focused on investigating the contractility responses of the isogenic HUES7-Q41L CM model by accessing changes in beating rate and contraction amplitude during chronic ISO exposure.

High purity HUES7-Q41L-CMs on day 25+ were used which were dissociated and seeded in the 48 CardioECR E-plate from 3 to 5 days prior to the experiment. Generating a complete monolayer of beating hPSC-CMs is important for signal measurements by CardioECR because these measurements are based on cell and electrode contacts. The optimal seeding density for CMs on CardioECR plates was 180,000 cells/ cm^2.

Contractility signals were detected 48 h after cell seeding. HUES7-Q41 and HUES7-L41 CMs exhibited relatively consistent contractility functions with the spontaneous beat rate at ≥ 30 bpm and rhythmic irregularity at about 10 % (**table 3.1**). Contraction amplitude by impedance measurement of HUES7-Q41L-CMs was ≥ 0.1. There was no significant difference in spontaneous beating between the two haplotypes under the vehicle-treated control during 72h experimental time.

	Beating rate (bpm)	**Beating Amplitude (NA)**	**Irregular beating ratio (%)**
HUES7-Q41 CM day 30+	41.0 ± 3.4	0.143 ± 0.011	10.4 ± 2.7
HUES7-L41 CM day 30+	43.9 ± 2.8	0.151 ± 0.009	10.9 ± 2.8

Table 3.1. Summary of contractility feature of HUES7-Q41L cardiomyocytes on day 30+, n ≥4.

The real-time analysis of beat rate in HUES7-GRK5-Q41L CMs at the vehicle treatment and ISO treatments for 72h is illustrated in **figure 3.20**. The technical variation could introduce very different baselines, which could alter or hide phenotype differences. Internal controls in the real-time contractility experiment using Cardio ECR could be beneficial to avoid this technical variation issue.

HUES7-GRK5-Q41 and HUES7-GRK5-L41 CMs in the vehicle treatment showed similar beating rate pattern during the experimental time, where slight reductions, around 25 %, were observed in beating rate and beating amplitude at the endpoint of the experiment (**figure 3.21.A & B**). These observations showed that the CardioECR system could be used for long-term experiments at about 10 days in duration. For experiments lasting more than 2 weeks, further optimisation for seeding density may be required since the detachment of the beating monolayer of CMs was observed at different levels after 10 days post-seeding.

The chronotropic effects of ISO were observed immediately after ISO was added when the maximum levels of beat rate were observed during the first 1h after induction. Beat rate of both HUES7-Q41 and HUES7-L41 haplotypes both increased about 140 % to the basal beat rate at 100 nM ISO; the increase of ISO concentration to 1 µM also enhanced the beat rate up to 150 % and 170 % in HUES7-Q41 CMs and HUES7-L41 CMs, respectively (**figure 3.21. A** * $p < 0.05$, ** $p < 0.01$). Surges in beat rate were observed in the first 4h during ISO induction; the beat rate of cardiomyocytes of both variant then slowed down and stabilised after 8h post-ISO treatment. However, the beat rate of these two cell lines was still maintained at a high level, around 120% compared to the basal beat rate, after 24h (**figure 3.21. A)**. These results indicate that the bioactivity of ISO

at 100 nM and 1 μM was maintained during 2h. ISO was refreshed every 24h to maintain consistent ISO induction. Similar to CellOPTIQ results, no inotropic responses were observed in either of the two hPSC-CM variants to ISO at both acute response at 1h and chronic response after 24h. There was no significant difference between these two variants in beat rate or beat amplitude in the first 24h of ISO induction (**figure 3.21. A & B**).

A gradual reduction in the beat rate of HUES7-GRK5-Q41 CMs was observed during long term ISO exposure. Indeed, significant decreases of 54.9 % and 62.5 % in beating rate and beating amplitude were detected respectively, after 72h exposure to 100 nM ISO compared to vehicle control (**figure 3.20** ** $p < 0.01$). At 1 μM ISO, this reduction in contractility was more pronounced, with significant reductions of 63.7% and 69.81% in beat rate and beating amplitude obtained at 72h time point. Beat rate and beat amplitude of HUES7-GRK5-Q41 CMs were significantly reduced compared to HUES7-GRK5-L41 CMs after 72h exposure at 100 nM ISO and after 48 h exposure at 1 μM ISO (**figure 3.20,** ** $P < 0.01$). These phenotypes are comparable to CellOPTIQ results, but the amplification changes are more pronounced. These results confirm that the contractility responses of HUES7-Q41 CMs are reduced during ISO stress in a time- and concentration-dependent manner, while HUES7-L41 CMs exhibited conservative effects to maintain contractility functions (beat rate and beating amplitude) during this chronic stress.

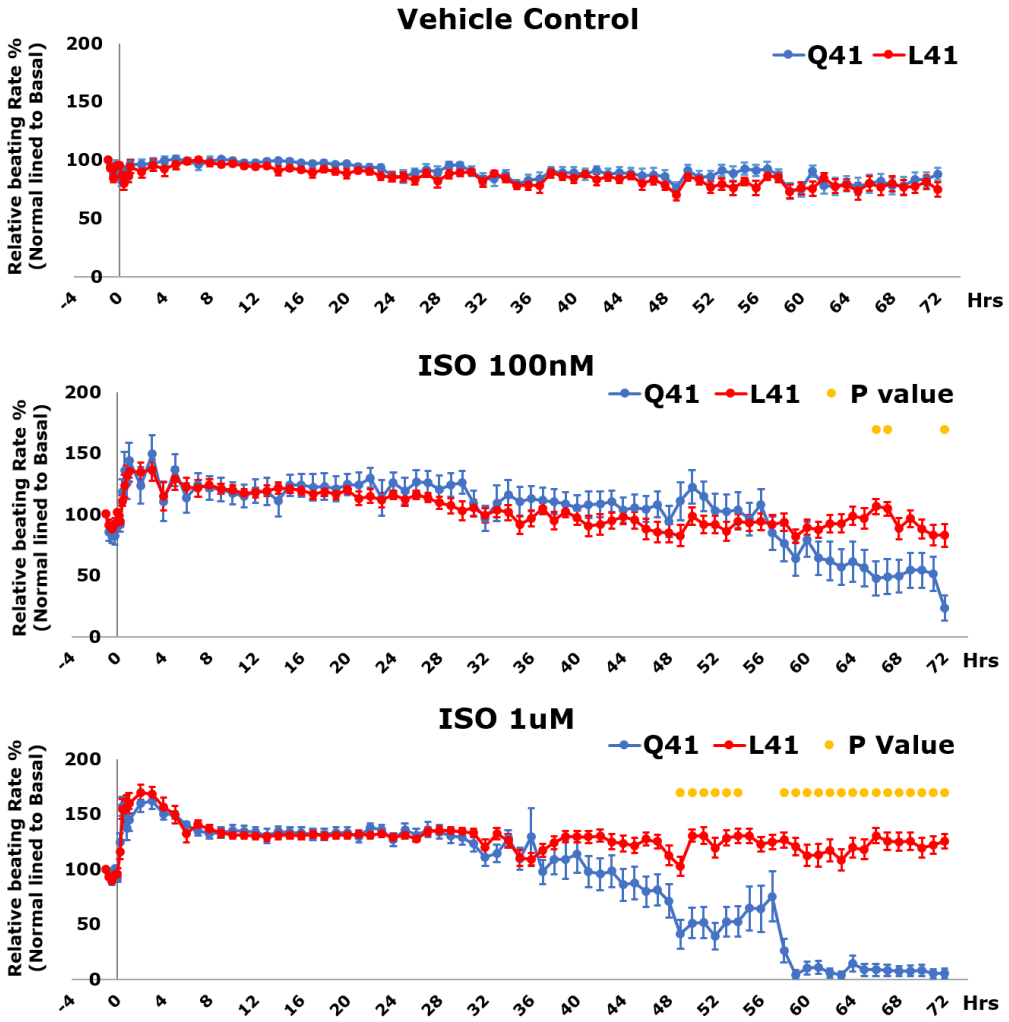

Figure 3.20. Real-time measurement of beat rate of HUES7-GRK5-Q41L CMs during chronic ISO stress.

Real-time analysis of beat rate in HUES7-Q41 CMs (blue) and HUES7-L41 (red) CMs at vehicle treatment, 100 nM ISO and 1 μM ISO for 72 h, representing means ± SEM, n = 5 biological replicates, P-value indicates significant differences between Q41 and L41 variants (yellow), *p<0.05. Two-way ANOVA with Dunnett's multiple comparison tests.

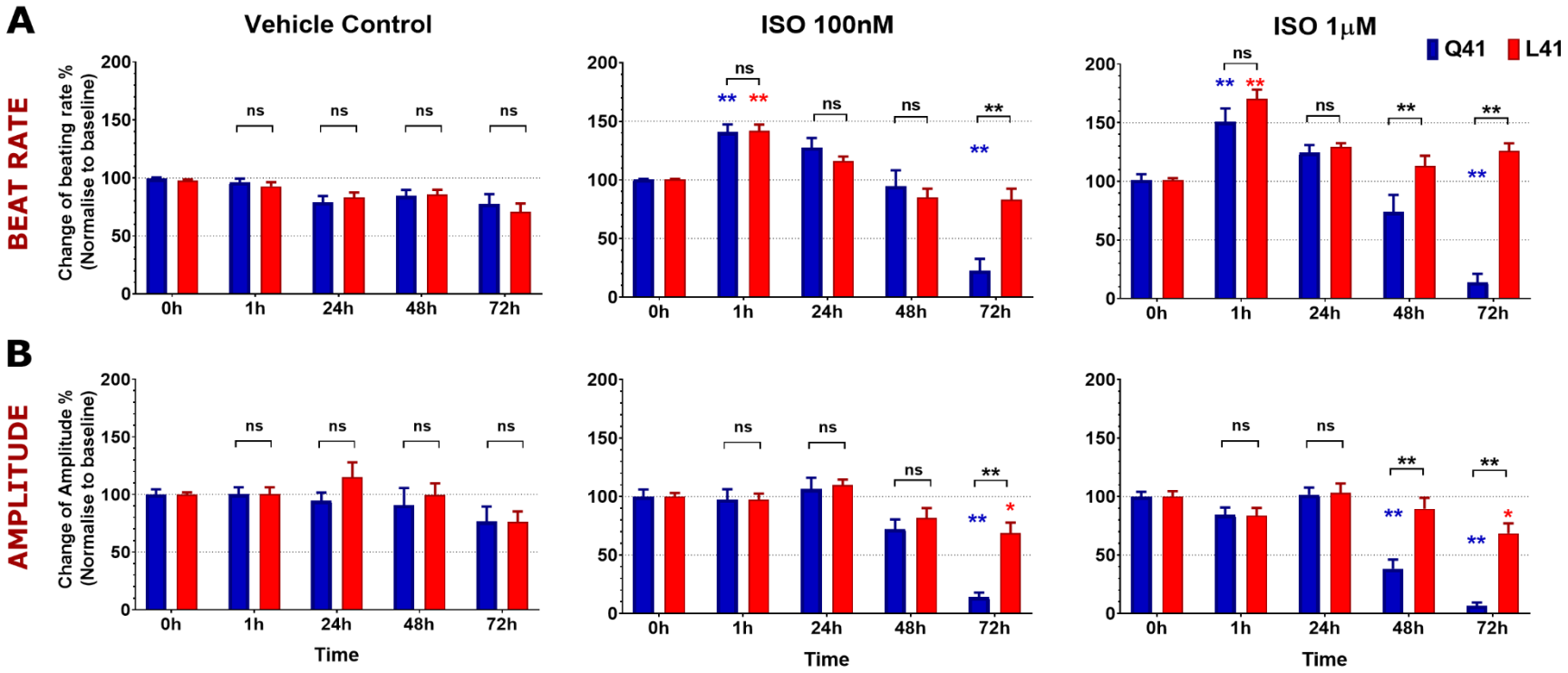

Figure 3.21. Analysis of beat rate and beating amplitude in HUES7-GRK5-Q41L CMs during chronic ISO stress using CardioECR.

Analysis of beat rate (A) and beating amplitude (B) in HUES7-Q41 CMs (blue) and HUES7-L41 CMs (red) at vehicle treatment, 100 nM ISO and 1 μM ISO for 72 h, representing means ± SEM, n = 4 biological replicates. *p<0.05, **p < 0.01. Two-way ANOVA with Dunnett's multiple comparison tests. Colour-coded according to duration treatment compared within the same cell lines; black asterisk indicates cross comparison between Q41 and L41 variants.

The harmful effects of chronic ISO stress in HUES7-GRK5-Q41 CMs are due to sustained β-AR signalling activation. The blockade of different β-AR systems was applied to rescue the contractility phenotype of HUES7-GRK5-Q41L CMs during ISO stress administration. CGP-20712A (CGP), ICI-118551 (ICI) and propranolol are blockers of β1-AR, β2-AR and non-selective β-AR respectively. These blockers were incubated for 1h with cardiomyocytes before and during ISO induction (**figure 3.22)**.

ISO is a non-selective agonist for β-AR systems. By blocking individual components of the β-AR system, it was possible to investigate the contributions of β1-AR and β2-AR responses in the isogenic hPSC-CM model during ISO induction. The blocking of the β-AR system with 200 nM propranolol completely removed the ISO effects with no increases in beat rate or beat amplitude during 100 nM ISO induction (**figure 3.22**). The harmful effects of sustained β-AR activation were abrogated by propranolol treatment in HUES7-GRK5-Q41 CMs. Propranolol treatment showed no effects on HUES7-GRK5-L41 CMs. In the presence of ICI, only a small increase in beat rate to 108.1 % and 104 % was observed in HUES7-GRK5-Q41 CMs and HUES7-GRK5-L41 CMs, compared to their baseline (**figure 3.23**). These increases in beat rate indicated for β1-AR responses during ISO induction. These results illustrated that β1-ARs were present but they were not the main response component to ISO. Blocking of β1-AR activity by CGP showed β2-AR responses to ISO induction with noticeable increases of beat rate to 117.3 % and 113.2 % in HUES7-GRK5-Q41 CMs and HUES7-GRK5-L41 CMs at 1h post-ISO treatment. During long-term ISO treatment, CMs supplemented with CGP blockers maintained a 10 % higher beat rate level compared to vehicle-treated CMs. This data shows that β2-AR but not β1-AR is the dominant subtype in our hPSC-CMs. This observation is also

consistent with other studies using hPSC-CMs, which could be explained by the foetal-like phenotype of hPSC-CMs.

Interestingly, propranolol and ICI treatments showed protective effects, rescuing the contractility of HUES7-GRK5-Q41 CMs during ISO stress, with almost no significant reduction in beat rate or beat amplitude, observed after 72h of 100 nM ISO exposure (**figure 3.22, figure 3.23.A & B)**. CGP treatment during ISO induction, however, could not completely rescue HUES7-GRK5-Q41 CMs, where a 40 % beat rate reduction and 27 % beat amplitude decrease were observed after 72h of exposure to ISO. This result indicates that β2-AR was the main subtype to respond to ISO stress and may be responsible for deleterious effects during chronic ISO induction. Activation of β2-AR did not show negative chronotropic effects during catecholamine exposure. HUES7-GRK5-L41 CMs maintained contractility functions and exhibited similar responses to propranolol or ICI treatments, which confirms the beneficial effects of the GRK5-L41 variant during long term catecholamine stress induced by ISO.

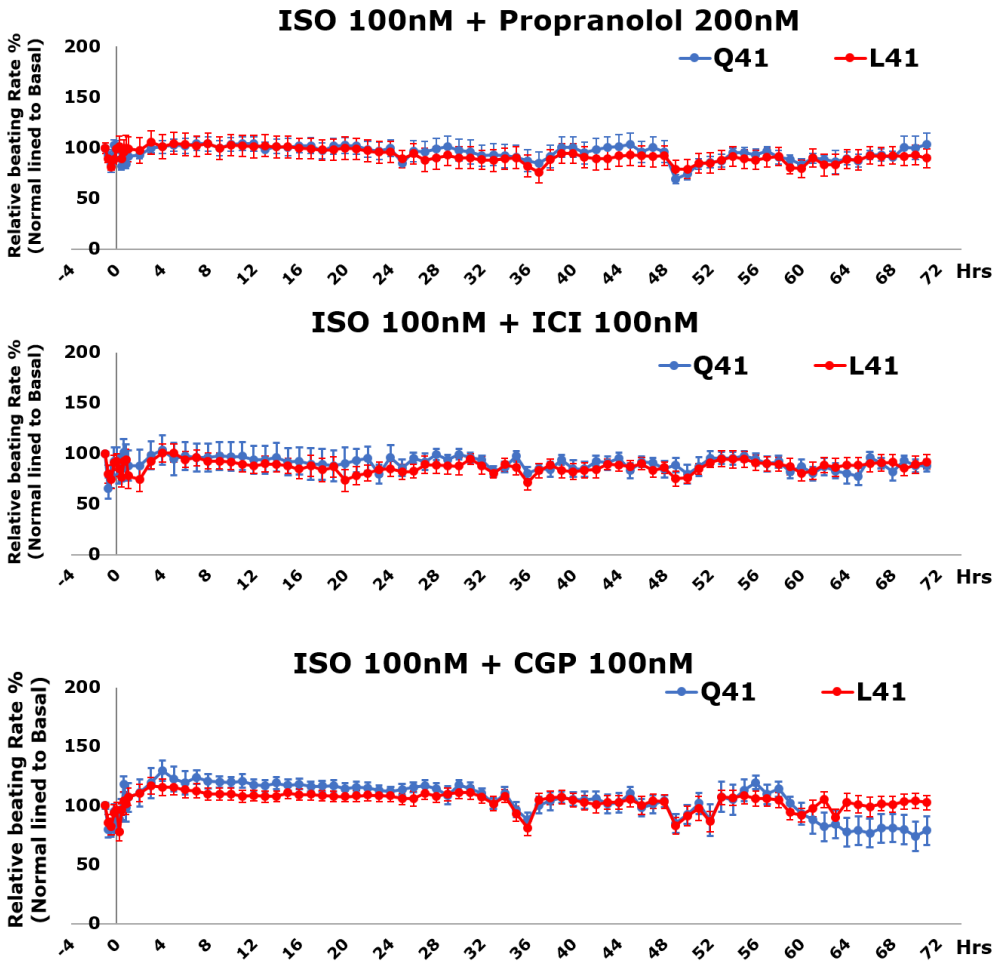

Figure 3.22. Real-time analysis of beat rate of HUES7-GRK5-Q41L CMs during chronic ISO stress in presence of β-blockers.

Real-time analysis of beat rate in HUES7-Q41 CMs (blue) and HUES7-L41 (red) CMs during 72 h exposure of 100 nM ISO in presence of propranolol, ICI and CGP, representing means ± SEM, n = 5 biological replicates.

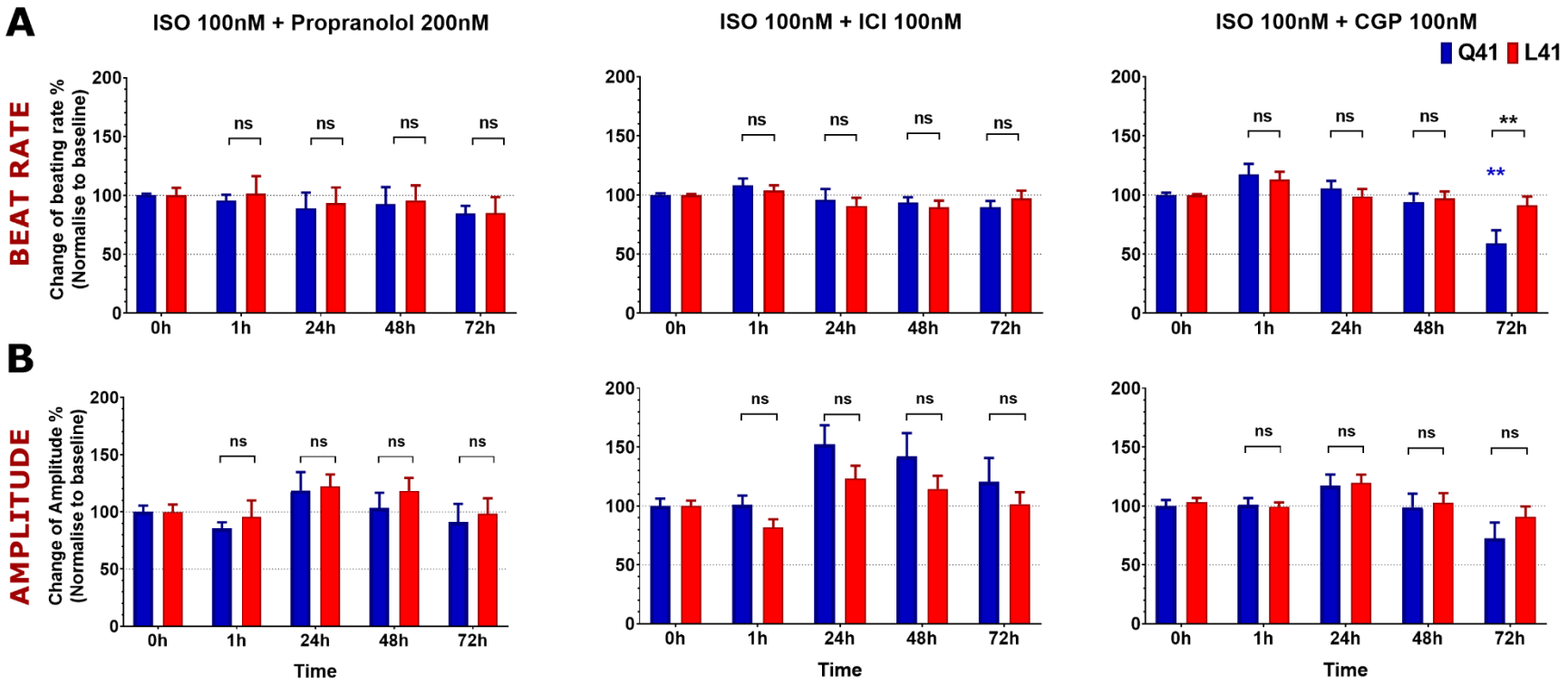

Figure 3.23. Analysis of beat rate and beating amplitude in HUES7-GRK5-Q41L CMs during chronic ISO stress with presence of β-blockers.

Analysis of beat rate (A) and beating amplitude (B) in HUES7-Q41 CMs (blue) and HUES7-L41 (red) CMs during 72 h exposure of 100 nM ISO in presence of propranolol, ICI and CGP, representing means ± SEM, n = 5 biological replicates. *p<0.05, **p < 0.01 Two-way ANOVA with Dunnett's multiple comparison tests. Color-coded according to duration treatment compared within the same cell lines; black asterisk indicates cross comparison between Q41 and L41 variants.

3.3.6 Sustained activation of β-AR signalling reduces the viability of HUES7-L41 cardiomyocytes:

A study of GRK5-Q41L has shown that GRK5-Leu41 can ameliorate cardiotoxicity, protecting against left ventricular remodelling during chronically administered isoproterenol in transgenic mouse models (Liggett et al., 2008). The measurement of cell death is a feature for cardiotoxicity investigation which is induced during sustained β-AR activation. The relative quantification of viable cardiomyocytes was estimated by CardioECR based on changes in CI signals. Additionally, the direct quantification of cell death and viability was performed by flow cytometry with Ethidium homodimer-1 (EthD-1) and Calcein AM dyes, respectively.

3.3.6.1 CM viability was enhanced in the GRK5-L41 variant during chronic ISO stress using CI measurement by xCELLigence RTCA CardioECR.

As explained in the introduction, CI signal measurement with the xCELLigence RTCA CardioECR platform is not only used to investigate contractility responses of cardiomyocytes but also to estimate cell survival via cell attachment, which is an indirect quantification for cell viability. In this way, the number of viable cardiomyocytes attached to electrodes is relatively proportional to the impedance produced by cardiomyocytes. The baseline time point, at 0h, was set as 100 % of viable starting cardiomyocytes and changes in CI indicated for % changes of viable cardiomyocytes during the experiment.

In the vehicle control treatment, a reduction of approximately 20 % CI was observed in both HUES7-GRK5-Q41 and HUES7-GRK5-L41 CMs at the endpoint of the experiment (**figure 3.24,** $p_{Q41} = 0.06$ and $p_{L41} = 0.07$). This may indicate a reduction of cell attachment during the experiment. During prolonged ISO exposure duration, a significant reduction in CI levels was

obtained in HUES7-GRK5-Q41 CMs in both low and high ISO concentrations (* $p < 0.05$). Indeed, CI of HUES7-Q41 CMs (~ 43.2 %) was 2-fold lower than CI of HUES7-L41 CMs (~ 86.3%) after 72h of 100 nM ISO incubation (** $p < 0.01$). At 1 μM ISO, CI levels of HUES7-Q41 CMs were significantly reduced from 47.4 % to 20.3 % between 48h and 72h, which are significantly lower than CI level of HUES7-GRK5-L41 CMs (~83 %) at 72h time point (**figure 3.24**).

The idea of using β-blockers to rescue cardiotoxicity effects during β-AR induction by ISO in HUES7-GRK5-Q41 CMs was also proven in this experiment. There was no significant increase in CI, indirectly imply for cell death in the propranolol and ICI treatments during long-term 100 nM ISO exposure. A certain level of cell death was observed in the CGP treatment, when there is a reduction of 18.4 % CI level in HUES7-GRK5-Q41 compared to HUES7-GRK5-L41 CMs at 72 h time point ($p = 0.08$). This result correlated with the beat rate reduction in the CGP treated HUES7-GRK5-Q41 CMs (**figure 3.23**). This observation illustrates that the sustained activation of β2-AR signalling may have deleterious effects for hPSC-CMs. Importantly, the GRK5-L41 variant showed cardioprotective functions by reducing cell death induced by prolonged ISO exposure. This function of the GRK5-L41 variant exhibited similar effects to propranolol and ICI treatment by reducing the cardiotoxicity of chronic catecholamines stress on hPSC-CMs.

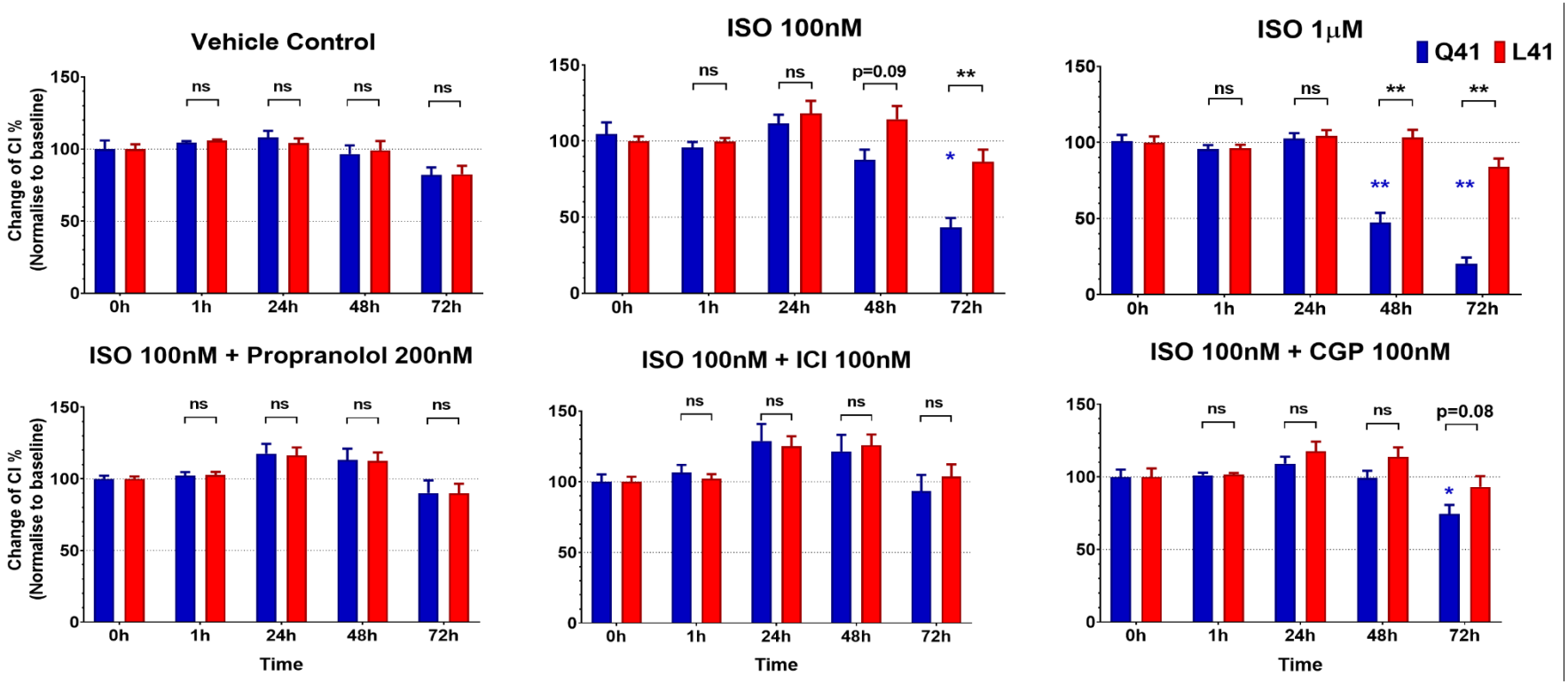

Figure 3.24. Estimation of viability levels of in HUES7-GRK5-Q41L CMs during chronic ISO stress with the presence of β-blockers by xCELLigence RTCA CardioECR.

Analysis of CI measurement in HUES7-Q41 CMs (blue) and HUES7-L41 CMs (red) indicates viability changes during 72 h exposure of ISO, with and without the presence of β-blockers, representing means ± SEM, n ≥ 4 biological replicates. *p<0.05, **p < 0.01 Two-way ANOVA with Dunnett's multiple comparison tests. Colour-coded according to duration treatment compared within the same cell lines; black asterisk indicates cross-comparison between Q41 and L41 variants

3.3.6.2 GRK5-L41 SNP enhances CM survival in both isogenic and heterogenic hIPSC-CMs during prolonged ISO stress.

Live and dead cardiomyocytes were also investigated by flow cytometry, which provides direct measurement of live and dead cells. EthD-1 is a red fluorescent dye with its signal enhanced when it binds to DNA by entering the broken membrane of dead cells. Intact live cells exclude nonfluorescent EthD-1 dyes. Calcein AM (Cal AM) is a cell-permeable dye that is catalysed into intensely green fluorescent calcein only with the presence of ubiquitous intracellular esterase in live cells. By measuring the fluorescent signals of cells, dead cells and live cells in the isogenic and hIPSC models could be estimated during chronic ISO exposure.

The procedure to estimate live and dead cardiomyocytes is illustrated in **figure 3.25**. Single colour stained cells with either Calcein AM or EthD-1 dye were used to set up the thresholds for EthD-1^+ cardiomyocytes (indicating dead cardiomyocytes) and Calcein AM^+ cardiomyocytes (indicating live cardiomyocytes). Cells positive to both Calcein AM and EthD-1 could be live cells bound by DNA fragments that have conjugated with florescent EthD-1 dyes. Doxorubicin (Dox) is an anti-cancer drug that can induce cardiac death (Burridge et al., 2016). The percentage of dead cells and live cells was calculated based on their distribution to the total counted cardiomyocytes, excluding debris treated with 10 μM Dox was used as the positive control for dead cells.

The unstained control showed no positive cells in either green or red channels, indicating that cardiomyocytes have no autofluorescent signals (**figure 3.25.A & B**). The single stain of Calcein AM dye showed no cardiomyocytes positive to EthD-1 (**figure 3.25.C**). Similarly, no cells in the single stain of EthD-1 were positive to Calcein AM (**figure 3.25.D**). The positive control for dead cardiomyocytes, treated with Dox, exhibited almost

61 % cardiomyocytes positive EthD-1 (**figure 3.25.F)**. The high cell death level observed in Dox-treated cardiomyocytes proved that this EthD-1/ Calcein AM assay could be used to quantify dead cells and live cells. Results in the previous experiments showed more distinct phenotype differences of GRK5-Q41L SNP at 1 μM ISO. This experiment focused on cell death responses of both isogenic and hIPSC models during chronic exposure of 1 μM ISO.

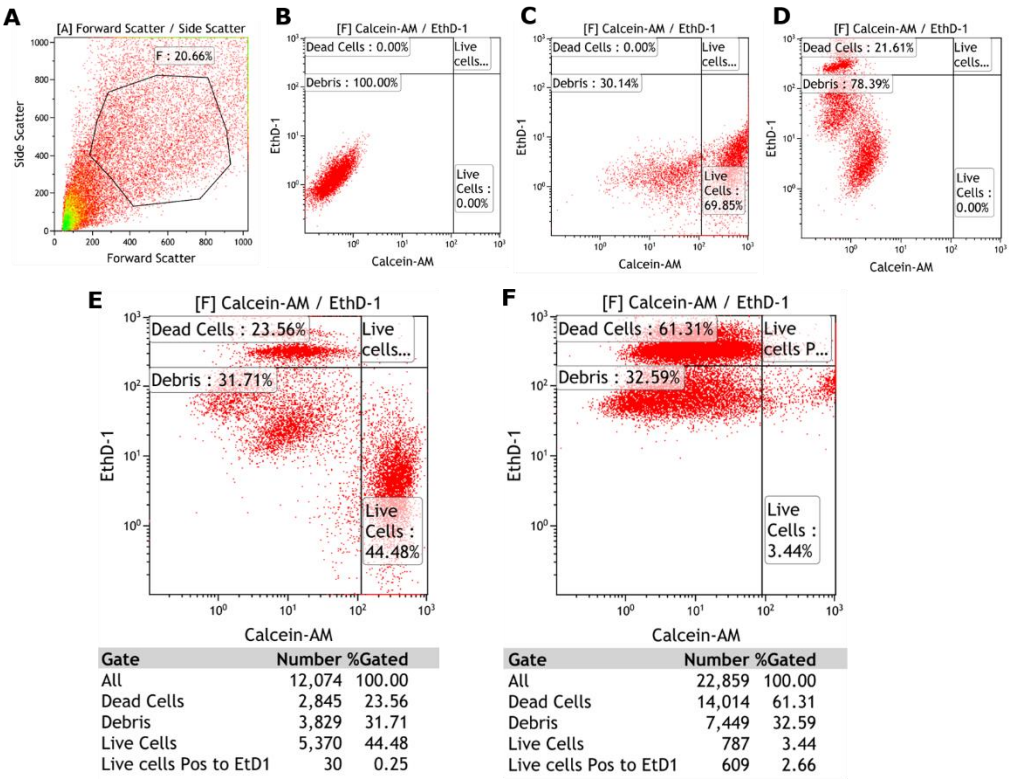

Figure 3.25. Procedure to estimate live CMs and dead CMs by flow cytometry.

Algorithm to quantify live cells and dead cells (A) Forward scatter and Side scatter were used for gating cardiomyocytes from debris. (B) Unstained control showed no autofluorescent cardiomyocytes (C) Single colour stained with Calcein AM (green colour) was used for gating of viable cardiomyocytes (D) Single colour stained with EthD-1 (red colour) was used for gating of dead cardiomyocytes (E) Dead cardiomyocytes were obtained in all samples induced during cardiomyocytes dissociations process (F) Dox-treated cardiomyocytes were used as a control for dead cardiomyocytes.

Cardiomyocytes of the isogenic and hIPSC models were treated with 1 μM ISO for different durations, ranging from 0 h to 96 h. At the endpoint of ISO treatment, cardiomyocytes were dissociated and incubated with the-1 and Calcein AM dyes. During the cardiomyocytes dissociation process, a certain level of cell death was obtained (**figure 3.25.E**). This cell death level in the vehicle-treated samples (termed 0h) was set as the baseline for each sample set. The number of dead cells induced by ISO treatment was normalised to the vehicle-treated samples in each haplotype.

Increases in cell death (2.3-14.6 %) were obtained in HUES7-GRK5-Q41 CMs during long-term ISO induction, which corresponds to significant reductions in live cells detected at 72 h (13.9 %) and 96 h (15.5%) (**Figure 3.26**, * $p < 0.05$). There were some elevations of cell death obtained in HUES7-GRK5-L41 and HUES7-GRK5-Q/L41 CMs during the ISO treatment, but these changing levels were not significantly different compared to the 0 h sample (~1-4.5% in HUES7-GRK5-L41 and ~3.7 – 11% in HUES7-GRK5-Q/L41). These results show a similar reduction pattern of cell death obtained in GRK5-Q41 CMs in the CardioECR experiment.

A reduction of live cells in hIPSC-GRK5-Q41 CMs was also detected during 96 h of 1μM ISO exposure, ranging from 18.5 % to 26.3 %. Significant increases in dead cells were observed after 48 h of ISO induction (**figure 3.27,*** $p < 0.05$). Different cell death levels (7-10 %) were also observed in hIPSC-GRK5-L41 CMs. However, these changing levels in live and dead cells were not significant compared to the vehicle control at 0 h.

Direct comparisons of changes in cell survival and cell death responses between Q41 and L41 variants at 72 h and 96 h post ISO treatments illustrated the cardioprotective functions of L41 SNP over Q41 SNP during chronic catecholamine stress (**figure 3.28**). In the isogenic model, L41 and Q/L41 CMs showed significant enhancement in cell survival compared to Q41

cardiomyocytes ($p < 0.05$). However, this gain-of-function phenotype of L41 was not demonstrated in the hIPSC model. Whereas the survival rate of hIPSC-GRK5-L41 cardiomyocytes was enhanced, these rates were not significantly better compared to hIPSC-GRK5-Q41 CMs ($p > 0.05$).

Overall, this data illustrates that the GRK5-L41 haplotype exhibits a cardioprotective function, where this variant can ameliorate the cardiotoxicity induced during chronic catecholamine stress produced by 1 μM ISO in the isogenic hESC model and even in the heterogenic hIPSC model. This observation emphasises the dominant protective effects of the L41 variant in cardiomyocytes.

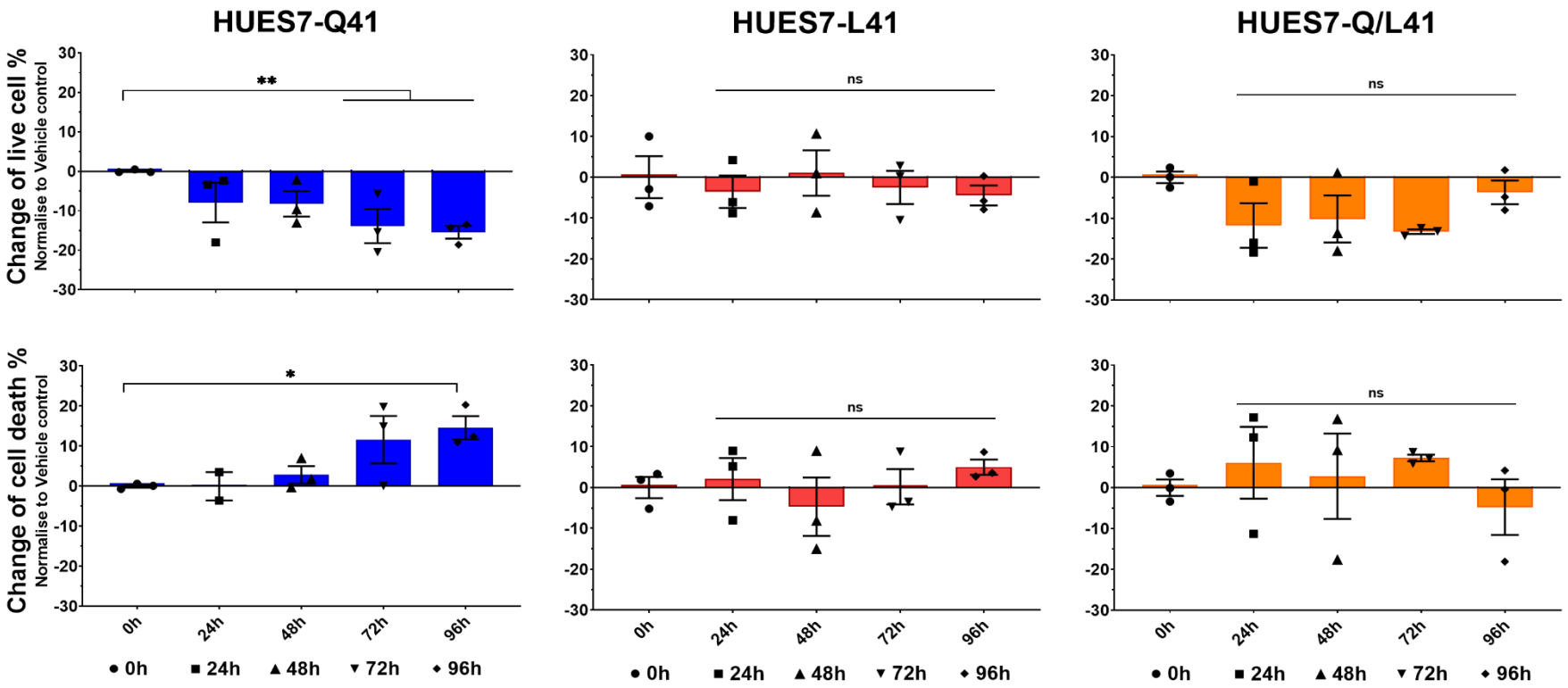

Figure 3.26. Quantification of live cells and dead cell in the isogenic model by flow cytometry.

Analysis of changes in live cells (A) and dead cells (B) of isogenic HUES7-GRK5-Q41L CMs during chronic ISO, representing means ± SEM, n=3 biological replicates. ns not significant difference, *p<0.05, **p<0.01. One-way ANOVA with Dunnett's multiple comparison tests.

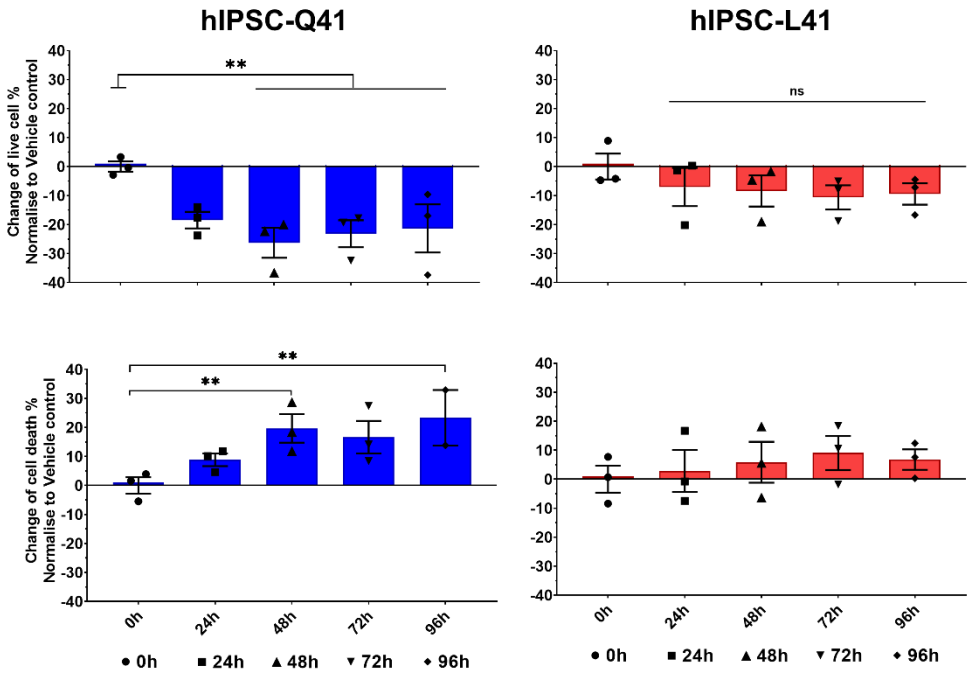

Figure 3.27. Quantification of live cells and dead cell in hIPSC model

Analysis of changes in live cells (A) and dead cells (B) of hIPSC-GRK5-Q41L CMs during chronic ISO, representing means ± SEM, n=3 biological replicates. ns not significant difference, *p<0.05, **p<0.01. One-way ANOVA with Dunnett's multiple comparison tests.

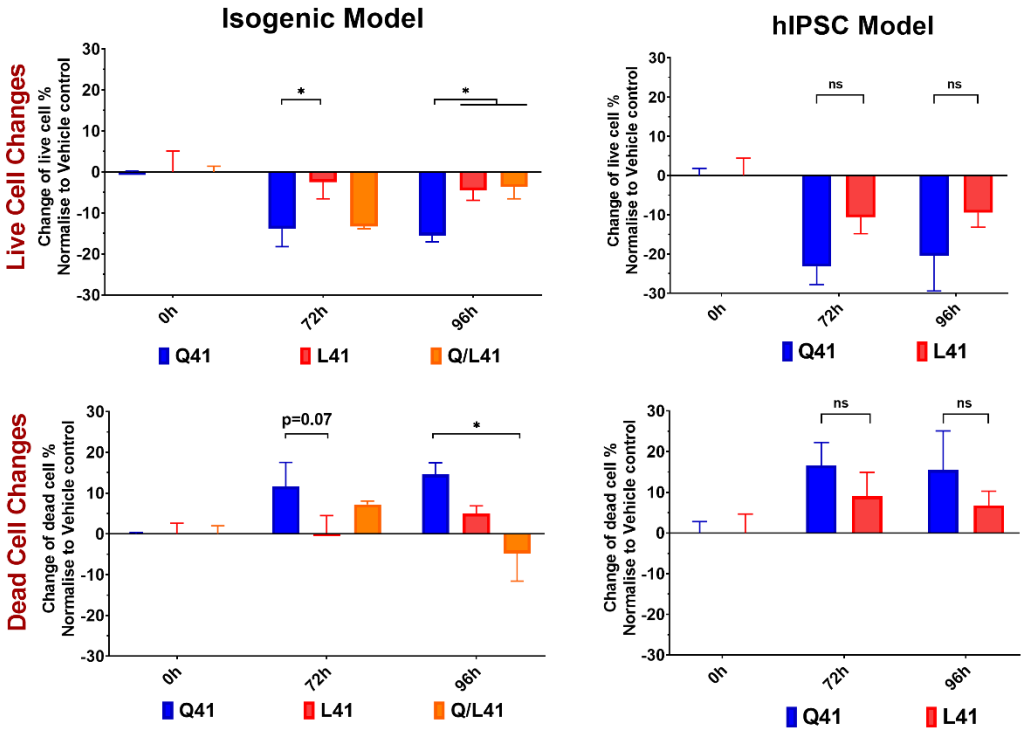

Figure 3.28. Effects of GRK5-Q41L SNP in cell death responses during chronic ISO stress at 72 and 96 h in isogenic and hIPSC model

Cross comparison of changes in live cells (A) and dead cells (B) of Q41 and L41 variants in isogenic and hIPSC model at 72h and 96h post-ISO-exposure represent means ± SEM, n=3 biological replicates. ns not significant difference, *p<0.05, **p<0.01. Two-way ANOVA with Dunnett's multiple comparison tests.

3.4 Discussion:

In the experiment described in this chapter, the hIPSC lines and gene-edited HUES7 lines in the isogenic set were characterized, and the cardiac differentiation of all lines was performed. Cardiomyocytes of the isogenic model and hIPSC models were characterized in terms of purity and RNA expression of *GRK5*. The GRK5-L41 variant helped cardiomyocytes maintain their contractility functions compared to the reduced contractility amplitude observed in GRK5-Q41 CMs by CellOPTIQ quantification. Real-time measurement of contractility response by CardioECR for isogenic HUES7-GRK5-Q41L model was performed with and without β-blockers during chronic ISO stress. These analyses confirmed the gain-of-function of the GRK5-L41 variant and also showed similar β-AR blocking effects of this variant to enhance contractility response and cell survival during prolonged ISO treatment. The direct measurement of live cells and dead cells of GRK5-Q41L variants in both isogenic set and hIPSC set, by flow cytometry, again confirmed the cardioprotective effects of the GRK5-L41 variant to reduce cell death induced by chronic catecholamine stress. This high throughput phenotype analysis of GRK5-Q41L for contractility response and cell death response in many cases showed statistically significant changes in the isogenic model, but not in the hIPSC model. The heterogenic hIPSC model did not always mirror the changes in the isogenic set; the lack of significant differences in the hIPSC models could be accounted for by the differences in genetic background and by the epigenetic modulation during the reprogramming process. These observations, therefore, highlight the importance of isogenic background in studying SNP functions.

3.4.1 Immaturity of hPSC-CMs.

Over the last decade, CM differentiation processes have rapidly evolved to more efficient, scalable and reproducible protocols. However, there are still challenges in terms of the maturation of hPSC-CMs (Chang and Mummery, 2018; Denning et al., 2016; Dunn and Palecek, 2018). The immaturity of hPSC-CMs is the defining drawback, which may bias the interpretation of the data. However, this challenge is shared by the whole field and emphasises the importance of hPSC-CM model characterizations for specific phenotyping studies. In the hPSC-CM models in this study, *GRK5* mRNA expression was significantly upregulated in differentiated hPSC-CMs, which was close to the expression level in VHH even in the early stage on day 20 post-differentiation (**figure 3.10**). The physiological expression level of *ADRB2* (β2-AR) and some increased mRNA expression level of *ADRB1* (β1-AR) showed that our hPSC-CMs could be used to study phenotype and effects of GRK5-Q41L variant in β-AR signalling system during HF. However, the absence of AT1 receptor with deficient *AGTRII* expression showed that our hPSC-CM model could not be used to study the effects of the GRK5-Q41L variant in AT signalling.

Although our hPSC-CMs exhibited foetal-like CMs, they showed a positive chronotropic response to ISO, but positive inotropic was not observed (**figure 3.23**). By using blockers specific for β1-AR and β2-AR during ISO treatment, β2-AR is observed as the major component response to ISO (**figure 3.22**). This observation is consistent with mRNA expression results, which are similar to other studies associated with the β-AR system in our hPSC-CM model (Robertson et al., 2013; Wu et al., 2015). These results state the difference of our hPSC-CM model to adult cardiomyocytes, in which β1-AR (~80%) is the dominant subtypes compared to β2-AR (~20%) and β3-AR (< 1%) (Lohse et al., 2003b; Madamanchi, 2007).

Even though β1-AR was less dominant in hPSC-CMs, their positive chronotropic responses were still observed with ISO induction in the presence of ICI, with ~ 10 % of beat rate increase in the contractility assay conducted by the CardioECR system (**figure 3.23**). Additionally, the CGP treatment during ISO induction in this assay also showed an enhancement of cell viability (**figure 3.24**). This partially rescued the effects of the CGP treatment, as shown by the efficient blocking of the activation of β1-ARs in our hPSC-CMs. The real-time analysis of beat rate by CardioExcyte, performed by Dr Hoang Minh Duc for isogenic and hIPSC sets, also showed β1-AR responses in our hPSC-CMs model (**figure 3.29.A**). Also, cAMP production was obtained during ISO exposure supplemented with ICI (**figure 3.29.B**) In comparison to the Wu study, B1-AR in our hPSC-CMs responded to ISO exposure (**figure 3.29.C**, Wu et al., 2015). This could be explained by differences in differentiation protocols, batch-to-batch variation and inter-lab variation.

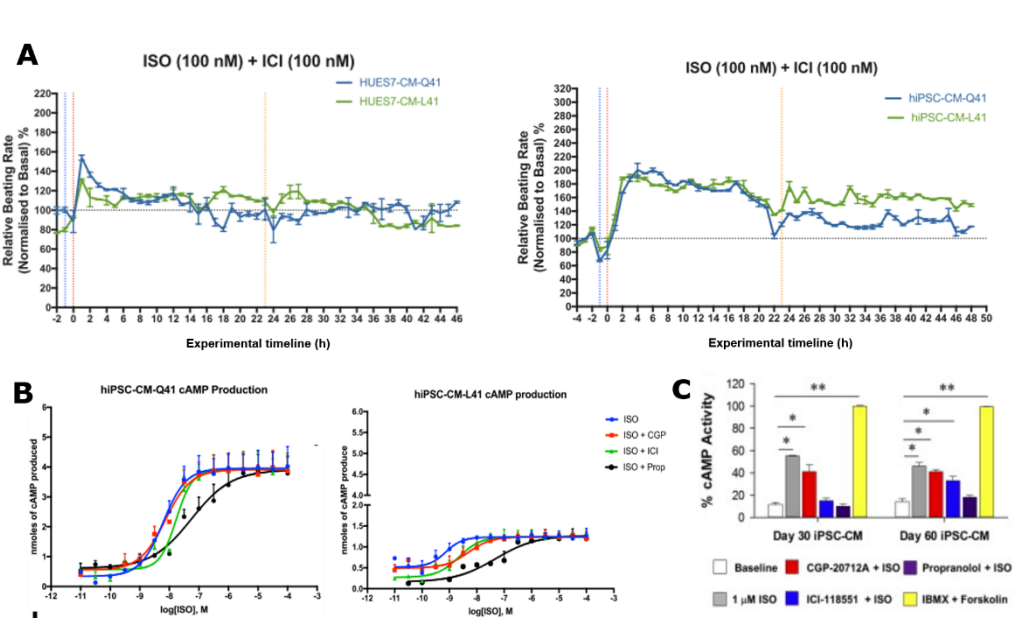

Figure 3.29. Evidences of β1-AR responses in our hPSC-CMs

(A) Real-time analysis of the beat rate of CMs using CardioExcyte 96 in isogenic and hIPSC models showed beat rate increases in response to ISO induction during ICI administration, n = 2 biological replicates. Represent means ± SEM (courtesy of Dr Hoang Minh Duc) (B) cAMP production of hPSC-CM on day 30 during ISO induction with the presence of β-blockers indicated for β1-AR signalling responses, n=3 biological replicates (C) Taken from Wu et al., 2015, cAMP production in hIPSC-CM day 30 and day 60 post differentiation. The importance of isogenic background.

The effects of the GRK5-Q41L variant in isogenic hESC-CMs sets reveals statistically significant phenotype differences associated with genetic studies, while the heterogenic hIPSC set in some aspects did not exhibit consistent phenotypes (Dorn and Liggett, 2009; Kang et al., 2015, p. 5; Liggett et al., 2008). This emphasises the importance of genetic backgrounds in phenotype studies of SNPs, when the heterogenic backgrounds, harbouring different polymorphisms, could hinder or bias the interpretation of phenotyping results. Indeed, the hIPSC set harbours different polymorphisms in β1-AR. hIPSC-Q41 is homozygous in *ADRB1*-G49S and *ADRB1*-R389G, but hIPSC-L41 is heterozygous in these two polymorphisms (**figure 3.7**). These polymorphisms had different effects on risks for HF

progression, myocardial ischemia and β-AR resistance, which consequently are associated with the survival rate of patients (Dorn, 2010a; Dorn and Liggett, 2009). The hIPSC set also harboured different polymorphisms in β2-AR compared to the isogenic set, where ADRB2-G16R and ADRB2-Q16E also exhibited their phenotyping differences on desensitization and downregulation (Dorn, 2010a; Dorn and Liggett, 2009). As β1-AR and β2-AR are the first-line targets during ISO induction, these polymorphisms and other undefined polymorphisms of the heterogenic background of the hIPSC model could alter or hide GRK5-Q41L phenotypes. This could explain the inconsistent phenotype results between the isogenic model and the hIPSC model.

Theoretically, the cardiac differentiation of hESC and hIPSC is the same as they went through the same differentiating process. Practically, cardiac differentiation of hiPSCs exhibited line-to-line variation, which could be explained by the effects of the reprogramming process associated with epigenetic modulations and the sources of somatic cells (Burridge et al., 2014; Yester and Kühn, 2017). These observations, therefore, explain why we focused on the isogenic set of GRK5-Q41L SNP for further phenotyping assays and the mechanistic study described in the subsequent chapters.

3.4.2 Methods for the phenotype analysis of CMs harbouring GRK5-Q41L variants during catecholamine stress:

The gain-of-function effects of the GRK5-L41 over the GRK5-Q41 variant, in which the GRK5-Q41 variant exhibited disrupted contractility function by significant contraction amplitude reductions, were observed in both the optical-based CellOPTIQ platform and the impedance-based CardioECR platform. However, more deleterious phenotypes of HUES7-Q41 CMs were obtained from the CardioECR platform than the CellOPTIQ

platform. This raises an issue regarding the technical differences between these two platforms.

The first technical difference observed was due to the cell density, which affects the confluency of the monolayer of beating cardiomyocytes. While the CellOPTIQ platform works on partial and thin monolayers of cardiomyocytes, cell impedance-based signals in the CardioECR system required a fully confluent monolayer of beating cardiomyocytes to achieve the best coverage of electrodes by cells. CI signals were not well detected when cells and electrodes had poor contact. However, this feature later induced the detachment of beating sheets of cardiomyocytes during long-term culture (after 2 weeks). These features may explain the more severe phenotype in CardioECR due to either poor cell-electrode contact or cell detachment, leading to no cell contraction being detected. In contrast, the real-time analysis of CardioECR would be more consistent with the internal control to the baseline of the same sample at the starting point continuing to the endpoint, which provides more detail and more consistent data. The CellOPTIQ, on the other hand, was more subjective as frames of cardiomyocytes were manually picked for analysis. The use of both CellOPTIQ and CardioECR platforms could complement or support each other. Indeed, similar phenotype responding patterns were observed in the isogenic set for both platforms, which strongly illustrates the gain-of-function effects of GRK5-L41 during chronic ISO stress.

Contraction traces at the control without treatment (0h) showed variation across the cell lines in both isogenic and hIPSC sets (**Figure 3.12 & 3.16**). A direct comparison of the absolute contraction amplitude across the haplotype at the same timepoint could lead to miss-interpret data. Therefore, all absolute measurements conducted by CellOPTIQ and Cardio ECR were normalised with their basal readings at the control treatments to

obtain the percentage changes during the treatment. The phenotype difference across haplotypes was then investigated on the changes which were induced during the chronic ISO treatment. In the isogenic set, the absolute contraction amplitude of Q41 and Q/L41 at 0h were 3-fold and 2-fold higher than L41 (**Figure 3.12 & 3.13)**. This greater contraction amplitude of Q41 over L41 in the isogenic set gave notice that the GRK5-Q41L variants could constitutively induce some level of phenotype differences at the vehicle control condition (**Figure 3.16 & 3.17)**. The difference in the beat length at the vehicle control condition of the hIPSC model could be accounted for by the differences in genetic background between these cell lines. Also, variation in cell density and cell survival can be induced by human error in conducting the technique during cell preparation. Therefore, normalisation of the data with the internal control (0h) is important to avoid miss-interpret the data.

CI from the CardioECR system could be used indirectly for the evaluation of viable cells, based on their attachment or coverage with electrodes. Because of this feature, viable detached cardiomyocytes and electrode-poor contacted cells could cause false-negative results, which could show low survival rates where no CI was detected. Given the awareness of this assay feature, a live/death assay by flow cytometry is a direct measurement of the percentage of live and dead cells. This direct quantification overcomes and complements the cell death measurement via CI. Similar patterns, with significant elevation of dead cells by prolonged ISO exposure on HUES7-GRK5-Q41 CMs, were obtained from both experiments.

However, the CI-based CardioECR exhibited more extreme cell death induction, which could be explained by the natural reduction of attachment cardiomyocytes during experiment time (seen in vehicle-treated samples, **figure 3.24**). The uses of different assays to approach the same questions,

even though they gave some variation in phenotype results, provides more precise and accurate interpretation of phenotypes, given that there is no single experiment that can fit all purposes.

3.4.3 GRK5-Q41L variants in hPSC-CMs revealed its gain-of-function effects during catecholamine stress in contractility and cell death responses:

hPSC-CMs are known to exhibit several hallmarks of immaturity, including rounded shape, disorganised sarcomeres and lack of ultrastructural transverse tubules (T-tubules) (Bhogal et al., 2018; Denning et al., 2016). The presence of T-tubules was important for phosphorylated β2-AR and Gi coupling, which account for the cardioprotective function of β2-AR during catecholamine stress-induced myocardial toxicity (Gorelik et al., 2013; Paur Helen et al., 2012). Indeed, loss of T-tubules disturbs localized β2-AR signalling in failing human and rat ventricular myocytes (Lyon et al., 2009; Schobesberger et al., 2017). hPSC-CMs exhibited foetal-like cardiomyocytes with almost no T-tubules, which is similar to what is seen in the failing heart. The lack of compartmentalization of β2-AR-cAMP signalling and Gi coupling raised a question as to whether β2-AR signalling in hPSC-CMs may function differently from its cardioprotective function in adult human cardiomyocytes. β2-Ars, on the other hand, may act as β1-ARs, which induces cardiotoxicity effects during cardiac remodelling in HF (Dorn, 2010b; Lohse et al., 2003b). This would explain why the dominant β2-AR signalling activation in hPSC-CMs does not have negative chronotropic effects and seems to not have cardioprotective functions against cardiac death induced by sustained β2-AR-cAMP signalling. Cardiac death consequently led to a reduction in contractility functions via reduced contraction amplitude and beat rate (**figure 3.20, 3.23 & 3.24**).

Quicker desensitization of β-ARs was the most significant feature of the GRK5-L41 variant, which explains how cardioprotective effects act to reduce a deleterious Gs-cAMP-PKA cascade during catecholamine stress (Liggett et al., 2008; Wang et al., 2008). In the hPSC-CM model in this study, positive inotropic responses were not observed during ISO exposure, which is a foetal-like feature of hPSCs. However, ISO induced positive chronotropic was observed. Also, the Gs-cAMP-PKA cascade induced by ISO is known as the main mechanism of cardiotoxicity in catecholamine stress. PKA accelerated contractility via transmitting to calcium-regulatory machinery, which then induced a reduction of contraction time (UP90). The GRK5-L41 variant with hydrophobic leucine group has a stronger affinity to plasma membrane than glycine. The GRK5-L41 variant enhanced its association with activated β-ARs and its phosphorylation function, to reduce Gs-cAMP-PKA induction.

In our lab, the measurement of the desensitisation rate was not stable to facilitate characterisation of GRK5-L41 variant phenotype, even though both GRK5-Q41L CMs showed faster contraction time (Up90). However, the significant reduction of contraction time in GRK5-Q41 CMs indirectly correlated to the higher amount of PKA levels produced in GRK5-Q41 CMs than in GRK5-L41 CMs for both the isogenic and hIPSC models (**figure 3.14 & 3.18**). These results indirectly show that the GRK5-L41 variant may more efficiently and quickly desensitise β-ARs than GRK5-Q41. Supposingly, a smaller amount of Gs-cAMP-PKA cascade was induced in GRK5-L41 during catecholamine stress (**figure 3.14 & 3.18**). Overall, all the phenotype results together prove that our hPSC-CM model could be used to study phenotypes of the GRK5-Q41L variant in β-AR signalling during HF. The GRK5-L41 variant showed a cardioprotective function as endogenous β-blocker effects, due to faster desensitisation of β-ARs, which enhanced cell survival by reducing the Gs-cAMP-PKA signalling cascade.

Chapter 4 Phenotyping of GRK5-Q41L in hPSC-CM models during catecholamine stress

4.1 Introduction:

4.1.1 Canonical function of GRK5 in the heart:

GRKs are classically known for their phosphorylation activity on membrane receptors; however, GRKs can also phosphorylate non-receptor substrates (Gurevich and Gurevich, 2016; Penela et al., 2006; Schumacher and Koch, 2017; Traynham et al., 2016). Phosphorylation of agonist bound GPCRs located within the plasma membrane is defined as canonical role GRKs, while the noncanonical activities of GRKs account for their phosphorylation of nonreceptor targets.

Conversely, GRK5 was reported to promote cardiomyocytes survival during catecholamine-induced β-AR stimulation (Dorn, 2009; Liggett et al., 2008; Noma et al., 2007). These beneficial effects are due to the conventional role of GRKs in terminating GPCR signalling by mediating the uncoupling of GPCRs with G protein (known as desensitisation). Phosphorylation of GPCRs by GRK5 (or other GRKs) does not only terminate G protein coupling but also recruit β-arrestin binding, followed by receptor internalisation and downstream signalling of a β-arrestin dependent pathway. β-arrestin can function as signal transducers to regulate normal and compromised cardiomyocytes functions such as myocyte survival and myocytes hypertrophy (Cahill et al., 2017; Jean-Charles et al., 2017; Nobles et al., 2011; Noma et al., 2007; Schumacher and Koch, 2017).

4.1.2 Noncanonical functions of GRK5 in the heart:

GRK5 also have noncanonical functions which phosphorylate non-receptor targets to induce intracellular responses. Reduction of GRK5 mediated phosphorylation of the tumour protein 53 (p53) showed inhibition of DNA damage-induced apoptosis in osteosarcoma cells (Chen et al., 2010). GRK5 also exhibited phosphorylation of tubulin, centrin and pericentrin for

regulation of cell cycle progression, microtubule fraction and nucleation in COS-1, HEK293 and HeLa cells (Carman et al., 1998; Michal et al., 2012).

Indeed, the noncanonical function of GRK5 in the nucleus has been explored in more detail during the last decade. Gold et al. reported the new GRK5 activity when it translocated to the nucleus (Gold et al., 2013). The accumulated nuclear GRK5 induced by Phenylephrine (PE) and Angiotensin II (AngII) via the Gq pathway can phosphorylate HDAC5. This phosphorylation of HDAC5 results in its translocation from the nucleus to the cytoplasm, which in turn activates the hypertrophic transcription factors MEF2 (**Figure 4.1**). A recent study in mice cardiomyocytes reported that chronic ISO exposure increased exchange protein directly activated by cAMP 1 (Epac1) - GRK5 interaction and induced nuclear GRK5 accumulation, following by HDAC5 nuclear export and MEF2 upregulation (Laudette et al., 2019).

More studies have revealed that nuclear localisation of GRK5 in cardiomyocytes is attributed to the development of hypertrophy and the progression of HF (Hullmann et al., 2014; Traynham et al., 2015). Cardiac GRK5-overexpressing mice showed an increase in hypertrophy, which later progressed to HF, due to its translocation to the nucleus (Martini et al., 2008). Moreover, nuclear GRK5 was shown to interact with nuclear factor of activated T-cells (NFAT) pathway to regulate the hypertrophic growth of myocardium during the induction of pathological hypertrophy, but not physiological hypertrophy (Hullmann et al., 2014).

Also, nuclear GRK5 was also report to interact with the inhibitor of kappa B alpha (IκBα) in HEK293 cells (Sorriento et al., 2008). This interaction promoted the accumulation of IκBα in the nucleus and resulted in impaired protection against apoptosis due to the inhibition of NF-κB signalling. The roles of GRK5 in the regulation of NF-κB signalling during

cardiac hypertrophy remains poorly understood. Moreover, GRK5 contains a nuclear localization sequence (NLS), thus GRK5 showed the direct binding to DNA (Johnson et al., 2013, 2004). The direct binding GRK5 to the Bcl-2 promoter showed inhibitory effects on transcription of BCL2 on human neuroblastoma SHSY5Y cells (Liu et al., 2010).

These findings revealed that the canonical role of GRK5 to phosphorylate agonist bound GPCRs occurred at the plasma membrane and are associated with cardioprotective effects. In contrast, non-canonical actions of GRK5 are induced by its nuclear accumulation resulting in pathological hypertrophy (Pfleger et al., 2019a; Schumacher and Koch, 2017; Traynham et al., 2016). The noncanonical functions of GRK5 in noncardiomyocyte studies also exhibited deleterious effects.

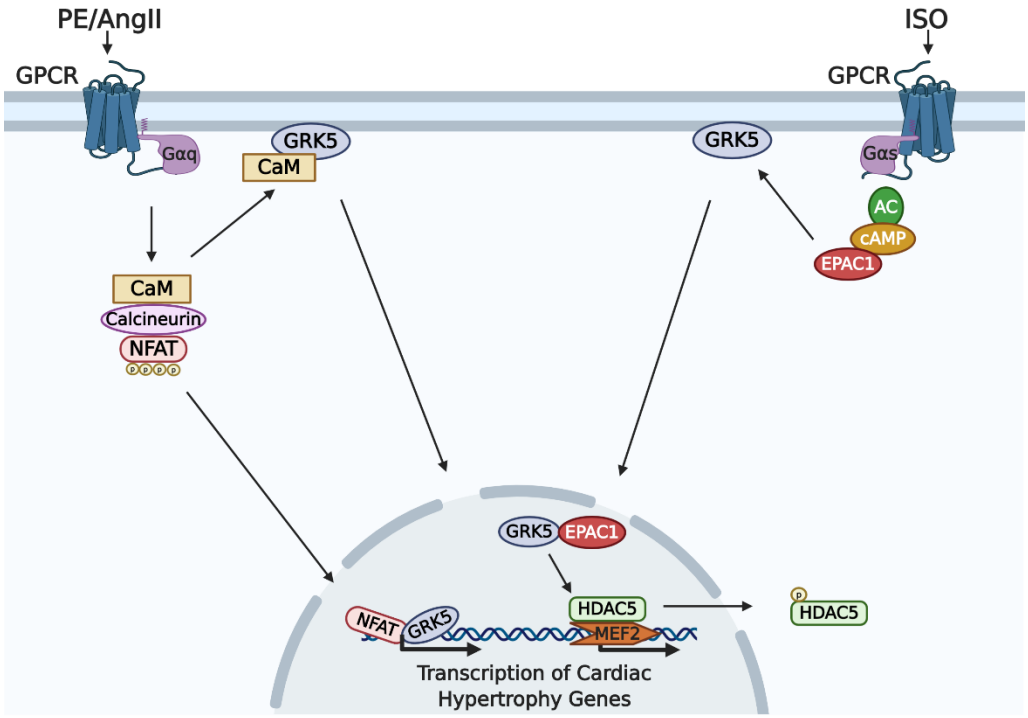

Figure 4.1.Summary diagram illustrating the GRK5's role in cardiac hypertrophy.

Gq activation due to PE and AngII stimulation of α1-AR or AT-1R, respectively, causes CaM to bind GRK5 leading to translocation to the nucleus via Gq dependent pathway. Upon β-ARs stimulation by ISO, Epac1 interacts with GRK5-Epac1 complex translocate to the nucleus. Once in the nucleus, GRK5 can act as an HDAC5 kinase, relieving repression of MEF2 and inducing hypertrophic gene transcription. Abbreviations: PE, Phenylephrine (PE); AngII, Angiotensin II; ISO, Isoprenaline; CaM, Calmodulin; HDAC5, histone deacetylase 5; MEF2, myocyte enhancer factor-2; Epac1, exchange protein directly activated by cAMP 1. (Adapted Laudette et al., 2019; Traynham et al., 2016).

4.1.3 The nuclear translocation of GRK5:

GRK5 contains two calmodulin (CaM) binding domains that reside in the N-terminal and C-terminal (Johnson et al., 2013; Komolov et al., 2015; Traynham et al., 2016). Although the exact mechanism of CaM binding to GRK5 is unknown, the nuclear translocation and accumulation of GRK5 inducing upregulated transcription of hypertrophic gene MEF2 requires CaM binding to the N-terminal domain (Gold et al., 2013; Martini et al., 2008).

The CaM binds to N- and C-terminal regions of GRK5 at amino acid 20–39 and 546–562 residues, respectively (Komolov et al., 2015). These regions also overlap with the membrane-binding determinants. Therefore, this study suggested that CaM binding would block GRK5 association with GPCRs on membranes in response to elevation of intracellular Ca^{2+} levels. The binding of CaM showed reduced GRK5 binding to the membrane and GRK5-mediated phosphorylation of β2-AR (Chuang et al., 1996; Tran et al., 2007). The nuclear export sequence (NES) and NLS of GRK5 protein both localised in the catalytic domain (Johnson et al., 2013, 2004). CaM binding to the N-terminal region exposes NES, promoting the export of GRK5 from the nucleus to the cytoplasm.

The membrane-binding determinant in the N-terminal is at amino acid 22–35 residues (Komolov et al., 2015). The GRK5-Q41L variant, which resides at the α1 helix of the RH domain, is close to the membrane-binding determinant and CaM binding domain in the N-terminal. This GRK5-Q41L variant may affect the nuclear translocation of GRK5 and its noncanonical function on hypertrophic responses in cardiomyocytes. In this chapter, the change of nuclear and cytoplasm compartment of GRK5 in GRK5-Q41L variants was investigated to identify the association of subcellular distribution changes of GRK5-Q41L with their cardioprotective phenotypes during chronic catecholamine stress.

4.2 Chapter Aims and Objectives:

The increase of accumulated GRK5 in the nucleus has been revealed to induce pathological hypertrophy in cardiomyocytes. This chapter aimed to inspect the distribution of GRK5 between the nuclei and the cytoplasm of hPSC-CMs and to investigate hypertrophic responses of GRK5-Q41L CMs via BNP production during chronic catecholamines stress. The following objectives were:

1. Quantify the nuclear and cytoplasm compartment of GRK5 in hPSC-CMs using western blot and immunocytochemistry (ICC) analysis to explore the association of cardioprotective phenotypes in GRK5-Q41L variants with their subcellular GRK5 distribution changes during chronic catecholamine stress.
2. Evaluate BNP induction in hPSC-CM models using high content imaging analysis to investigate the association of hypertrophic responses in GRK5-Q41L variants with their nuclear GRK5 fraction changes.

4.3 Results:

4.3.1 Optimisation for subcellular GRK5 analysis by western blot:

The presence of GRK5 on the cell membrane is known to mediate the uncoupling and internalisation of GPCRs. While recent studies of GRK5 functions showed that the increased accumulation of GRK5 in the nuclei attributes to the development of hypertrophy and the progression of HF (Hullmann et al., 2014; Traynham et al., 2015). The nuclear and cytoplasm distribution of GRK5 in the isogenic and hIPSC cardiomyocytes models were quantified to investigate whether the reduced contractility and cell death phenotypes of GRK5-Q41L have relations to their subcellular localisation. In this chapter, western blot was employed to investigate the total distribution of nuclear and cytoplasmic GRK5 fraction while immunocytochemistry (ICC) imaging was performed to illustrate GRK5 localisation in GRK5-Q41L CMs at the single-cell level.

To quantify the distribution of GRK5 between the nuclei and the cytoplasm during chronic catecholamine stress, the nuclear protein fraction and the cytoplasm protein fraction of GRK5-Q41L CMs were extracted by using the commercial NE-PER Nuclear and Cytoplasm Extraction Reagent (Thermo Fisher, #78833). Nuclear and cytoplasmic protein from CMs, which had been exposed to ISO for 24h, 48h and 72h, were subjected to western blot and compared with vehicle-treated control CMs.

Subcellular localisation of GRK5 protein in the nuclei and the cytoplasm was successfully illustrated by western blot (**Figure 4.2.A**). Clear bands of nuclear and cytoplasmic GRK5 were well defined at 68 kDa. However, the chemiluminescent signals of GRK5 occasionally appeared to be quickly faded after 1 min post-detection time (**Figure 4.2.B**) and brownish bands were also visibly observed. The quick loss of signal indicated that there was no

problem with immunoblotting process but the chemiluminescent signal production.

To approach this problem, the "blue light test" was performed to check if the ECL reagent functioned properly. The test was conducted by simply adding 1 µL of Horseradish Peroxidase (HRP) conjugated secondary antibody into 1 mL of the detection ECL reagent in a tube and mixing well in a dark room. Visible bluish-white light was quickly produced and lost after 5 min indicated that the ECL reagent functioned. The visibly brownish bands of GRK5 suggested the presence of abundant HRP reactions.

Free radicals, which are produced during the oxidation reaction of the HRP molecules with luminol in the ECL substrate, can speed the probability of HRP inactivation. To reduce excessively abundant HRP reactions, we diluted the HRP antibody from 1:5000 to 1:10000 dilution and the incubation time with ECL reagent was also reduced from 5 min to 2 min. The chemiluminescent signal of GRK5 presented more stably indicated that the short-lived signal issue was due to excessively abundant free radicals produced during HRP reactions (**Figure 4.2.C**).

To perform densitometry quantification of subcellular GRK5, multiple proteins used as loading controls for the cytoplasm and nuclear protein fraction was investigated. The GRK5 probed membranes were incubated with stripping buffer to remove GRK5 and HRP antibodies. These blotted membranes of cytoplasmic protein fraction were then re-probed with common cytoplasm loading controls, such as β-Tubulin, β-Catenin and β-Actin, as well as cardiac-specific cytoskeleton proteins, α-Actinin and cTnT (**Figure 4.2.D**). Bands of β-Tubulin (55 kDa), β-Catenin (92 kDa) and β-Actin (42 kDa) were detected at corrected sizes. However, cardiac-specific cytoplasmic proteins, α-Actinin (105 kDa) and cTnT (36 kDa), were not

detected by western blot, while more than 80% of the same source of cells in all cell lines was positive to α-Actinin in ICC experiment (**Figured 4.2.F**).

Multiple loading controls for nuclear protein fractions, such as Lamin A/ Lamin C, Histone 3 and TATA-binding protein (TBP), were tested and shown in **Figure 4.2.E.** Among three nuclear loading controls, Lamin A/Lamin C and TBP subsequently showed clear bands at 74 kDa, 63 kDa and 38 kDa, while no signal was detected for Histone 3. β-Actin and TBP were then chosen for the cytoplasmic and nuclear loading control for this western blot experiment.

Together, the results identified the optimal working conditions for the western blot analysis of nuclear and cytoplasmic GRK5 compartments. β-Actin and TBP could be used for the cytoplasmic and nuclear loading control for quantification of subcellular GRK5. These experiments also highlighted the need for close monitoring of antibody dilution and duration for chemiluminescent signal development to avoid the short-lived signals due to excessively abundant free radicals produced during HRP reactions.

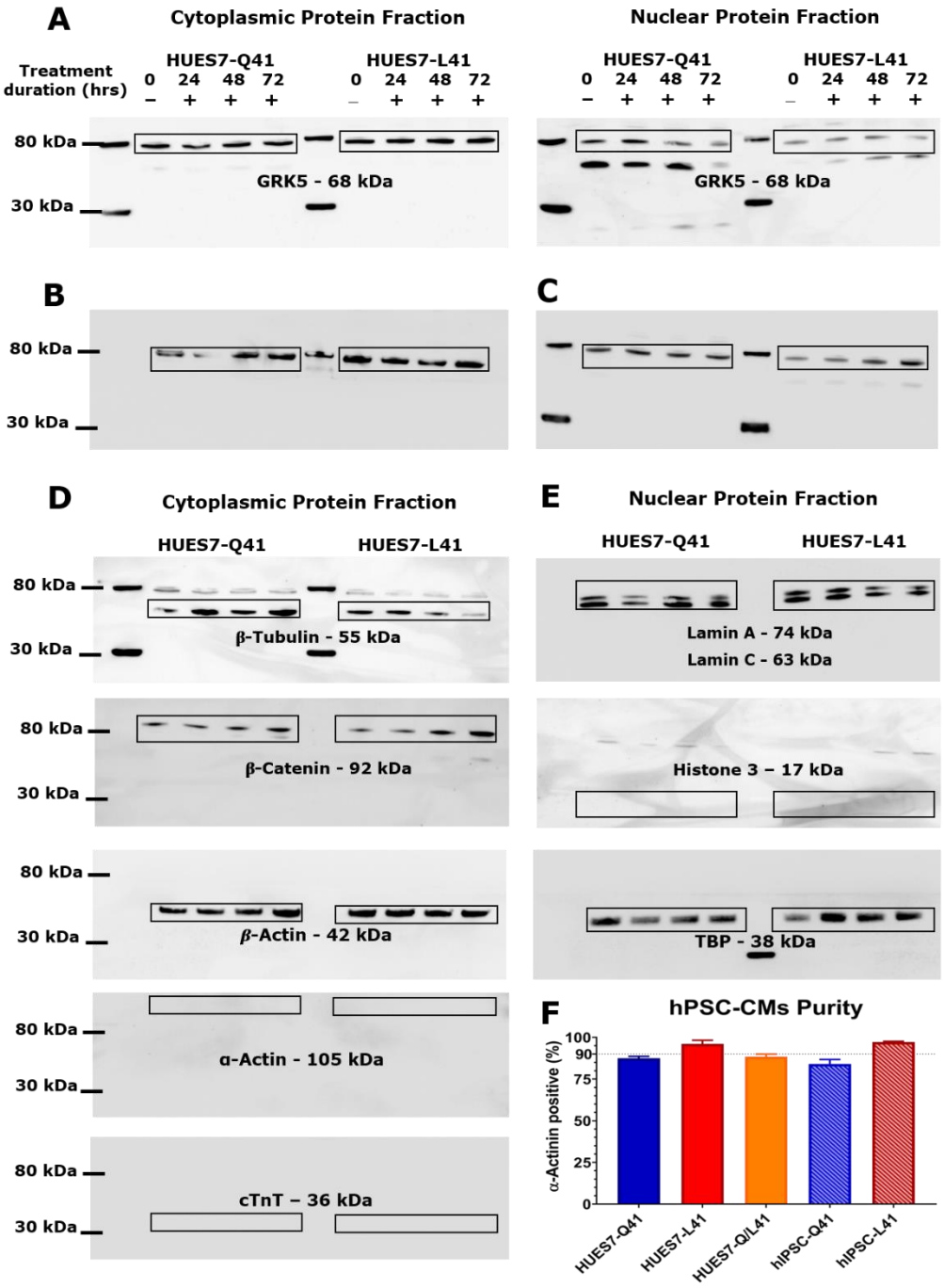

Figure 4.2. Loading control optimisation using for GRK5 quantification in the nuclei and the cytoplasm.

(A) Blot of cytoplasmic and nuclear GRK5 present in the defined box at 68 kDa. (B) Short-lived chemiluminescent signal occurred due to excessively abundant reactive oxidation reactions of HRP. (C) Reduction of HRP dilution and incubation time with ECL reagent enhanced signal stability. (D) Multiple proteins for cytoplasm loading controls, including β-Tubulin, β-Catenin, β-Actin, α-Actinin and cTnT were probed and showed their presence at specific sizes in the defined boxes. (E) Multiple loading controls for the nuclear protein fraction, including Lamin A/Lamin C, Histon 3 and TBP, were tested and showed their presence in the defined boxes at correct size (F) Purity of hPSC-CMs for all lines used in western blot experiments, n = 3 biological replicates, mean ± SE.

4.3.2 Investigation of GRK5 distribution in the nuclear and cytoplasm compartments using western blot:

To investigate the changes of GRK5 distribution in the nuclei and cytoplasm during chronic catecholamines stress, cardiomyocytes of isogenic and hIPSC models were exposed to ISO at 100 nM and 1 μM for 0h, 24h, 48h and 72 h. The nuclear and cytoplasm protein fractions of cardiomyocytes were blotted and probed with either GRK5, nuclear TBP and cytoplasmic β-actin antibodies.

The blotted membranes showed that nuclear and cytoplasm GRK5 can be successfully detected by western blot. An increase of nuclear GRK5 fraction was obtained in HUES7-Q41 CMs during catecholamine exposure at both 100 nM (**Figure 4.3.A**) and 1 μM (**Figure 4.3.B**). This increased accumulation of nuclear GRK5 was not obtained in HUE7-L41 and HUES7-Q/L41 CMs. Defined bands of TBP and β-actin illustrated that these loading controls could be used for densitometry analysis.

The absolute changes of subcellular GRK5 distribution were investigated by densitometry quantification of western blot bands. As the blots in **Figure 4.2**, densitometry analysis of nuclear GRK5 fraction showed that distribution of GRK5 in the nuclear extracts of HUES7-Q41 CMs increased upon ISO exposure, with 24h: 194%, 48h: 127%, and 72h: 283% at ISO 100 nM compared to vehicle-treated (termed 0h): 100 % (**Figure 4.3.A**). The increase of nuclear GRK5 was more significant at ISO 1 μM, where an increase of 183%, 226% and 137% was observed at 24h, 48h and 72h compared to 0h (**Figure 4.4.C**, $*p < 0.05$,$**p < 0.01$).

In contrast, nuclear GRK5 fraction of HUES7-L41 and HUES7-Q/L41 CMs did not show significant increases upon ISO incubation at both ISO 100 nM and 1 μM (**Figure 4.4.A & C**). Nuclear distribution of GRK5 in HUES7-L41 CMs exhibited slight reductions in nuclear GRK5 during chronic ISO

exposure, where their nuclear GRK5 extracts were 24 h: 111%, 48 h: 47%, 72 h: 36% at ISO 100 nM and 24 h: 102 %, 48 h: 94 %, 72 h: 87 % at ISO 1 μM. HUES7-Q/L41 CMs showed varied levels of nuclear GRK5 upon ISO treatment at 100 nM (24 h: 113 %, 48 h: 137 %, 72 h: 80 %) and ISO 1 μM (24 h: 141 %, 48 h: 150 %, 72 h: 58 %). However, these variations of nuclear GRK5 levels in both HUES7-L41 and HUES7-Q/L41 CMs were not significantly different compared it their vehicle-treated control (ns, $p \geq 0.05$). Thus, the analysis of the nuclear compartment in the isogenic model showed that the HUES7-L41 variant prevented a significant increase of nuclear GRK5 fraction observed in HUES7-Q41 during chronic ISO exposure.

The cytoplasm fraction of GRK5 in HUES7-Q41 CMs showed some levels of increase range from 11 % to 25 % at ISO 100nM (**Figure 4.4.B**). At ISO 1 μM, analysis of cytoplasm GRK5 distribution in HUES7-Q41 CMs were relatively low with 48h: 48 % and 72h: 88 % compared to vehicle-treated control at 0h (**Figure 4.4.D**). However, the changes of cytoplasmic GRK5 distribution were not significantly different upon catecholamine stress. Cytoplasmic GRK5 of HUES7-L41 and HUES7-Q/L41 CMs showed some levels of increase. HUES7-L41 CMs showed slight increases of cytoplasmic GRK5 at ISO 100 nM (24h: 100 %, 48h: 96 %, 72h: 121 %) and ISO 1 μM (24h: 96 %, 48h: 124 %, 72h: 130%). Similarly, cytoplasmic GRK5 of HUES7-Q/L41 CMs showed varied levels at ISO 100 nM (24h: 109 %, 48h: 138 %, 72h: 335 %) and ISO 1 μM (24h: 96 %, 48h: 124 %, 72h: 130%). There were no significant changes of cytoplasm GRK5 in HUES7-Q41L CMs upon chronic catecholamine stress.

Western blot analysis of subcellular GRK5 distribution in the isogenic model showed that chronic catecholamine stress induced a significant increase of nuclear GRK5 in HUES7-Q41, while HUES7-L41 and HUES7-Q/L41 CMs did not show these nuclear GRK5 accumulations. From these

data, the conclusion was drawn that GRK5 distribution in the cytoplasm showed no significant changes detected during the long-term catecholamine stress.

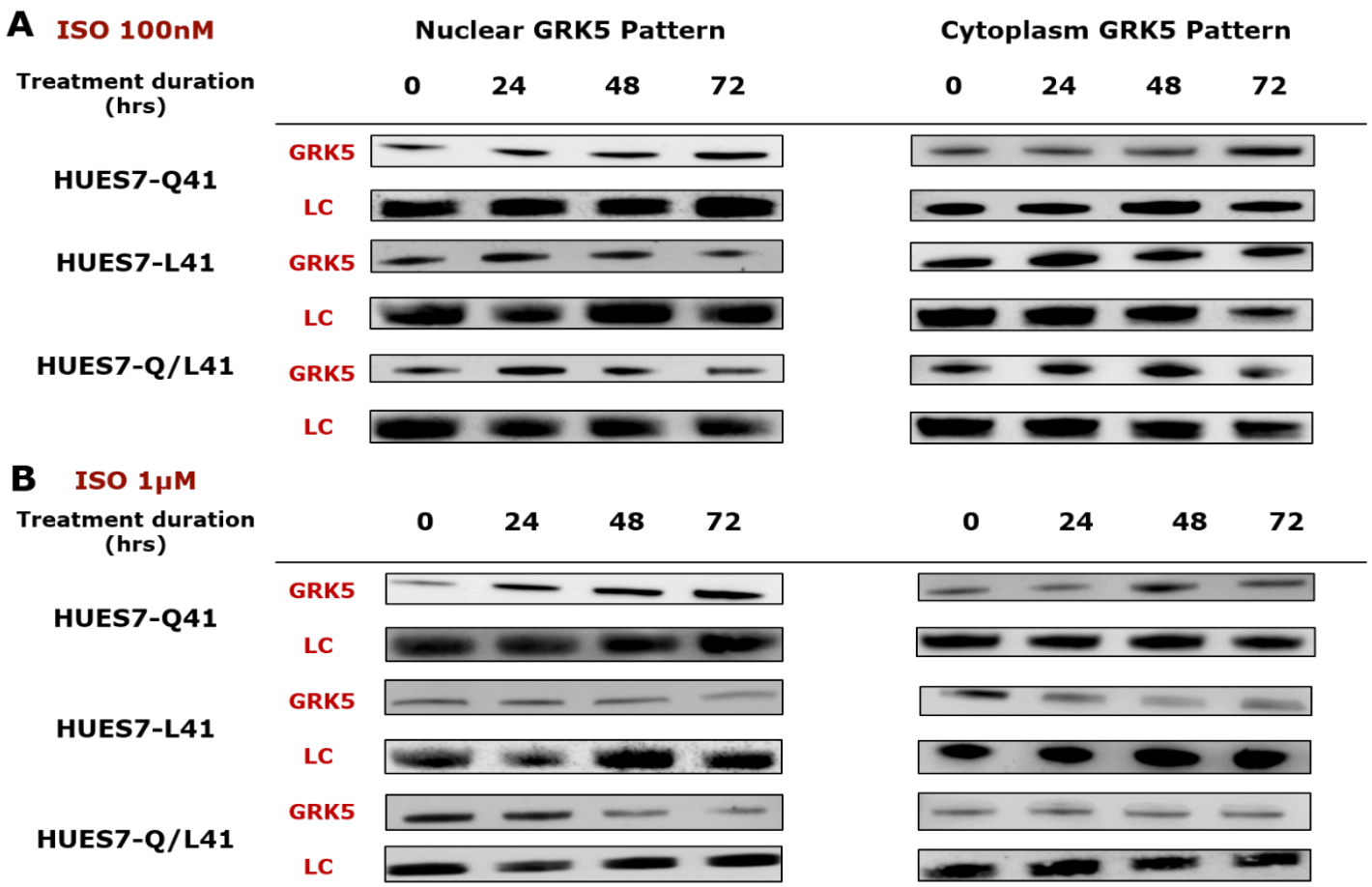

Figure 4.3. Nuclear and cytoplasm blot of GRK5 in the isogenic model.

Representative nuclear and cytoplasm blots of GRK5 and its loading controls with TBP (nuclear protein fraction) and β-actin (cytoplasm protein fraction) in isogenic GRK5-Q41L cardiomyocytes during chronic catecholamine stress at ISO 100 nM (A) and 1 μM (B).

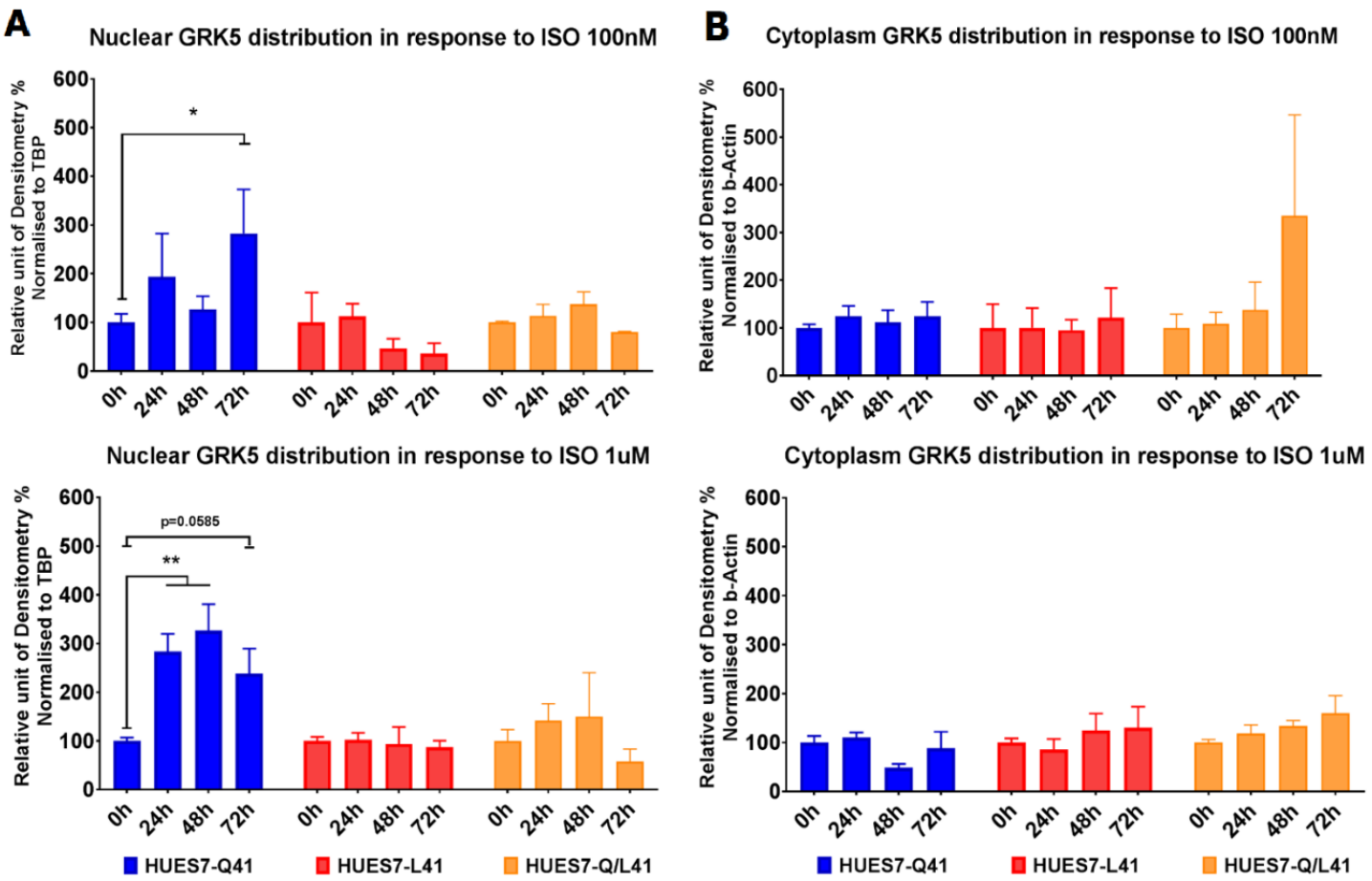

Figure 4.4. Densitometry analysis of western blot of nuclear and cytoplasm GRK5 in the isogenic model.

Densitometry analysis of GRK5 distribution in the nuclei (A) and cytoplasm (B) at ISO 100 nM and ISO 1 μM, present as mean ± SEM, n = 3 biological replicates. *p<0.05, **p < 0.01 Two-way ANOVA with Dunnett's multiple comparison tests

The distribution of subcellular GRK5 in hIPSC-Q41L CM models was subjected to western blot during long term catecholamine stress induced by ISO at 100 nM and 1 μM (**Figure 4.5.A & B**). Densitometry analysis of western blot in the hIPSC-Q41L model showed no significant changes of nuclear GRK5 extracts in both hIPSC-Q41 and hIPSC-L41 upon ISO stress (ns, $p \geq 0.05$). Although there were some increased levels of nuclear GRK5 detected in hIPSC-Q41 CMs range from 156 % to 241 % during 72h of ISO exposure at both ISO 100 nM and 1 μM, these changes were not significant (ns, $p \geq 0.05$). The relatively low levels of nuclear GRK5 in hIPSC-L41 CMs at ISO 100 nM (24h: 84 %, 48h: 93 %, 72h: 95 %) and ISO 1 μM (24h: 45 %, 48h: 45 %, 72h: 52 %) were also not significant (**Figure 4.6.A,** ns, $p \geq 0.05$). Cytoplasm GRK5 showed varied levels in both hIPSC-Q41 and hIPSC-L41 upon ISO stress. These varied levels of cytoplasm GRK5 were not significantly different from the vehicle-treated controls.

In summary, western blot analysis provided a useful tool to investigate changes in nuclear and cytoplasmic GRK5 distribution upon catecholamine stress. An interesting observation was an increase of GRK5 accumulated in the nuclei of HUES7-Q41 CMs during the chronic ISO stress, but these accumulations of nuclear GRK5 was not detected in HUES7-L41 or Q/L41. There were no significant changes in cytoplasmic GRK5 distribution between variants in both isogenic and hIPSC CM models.

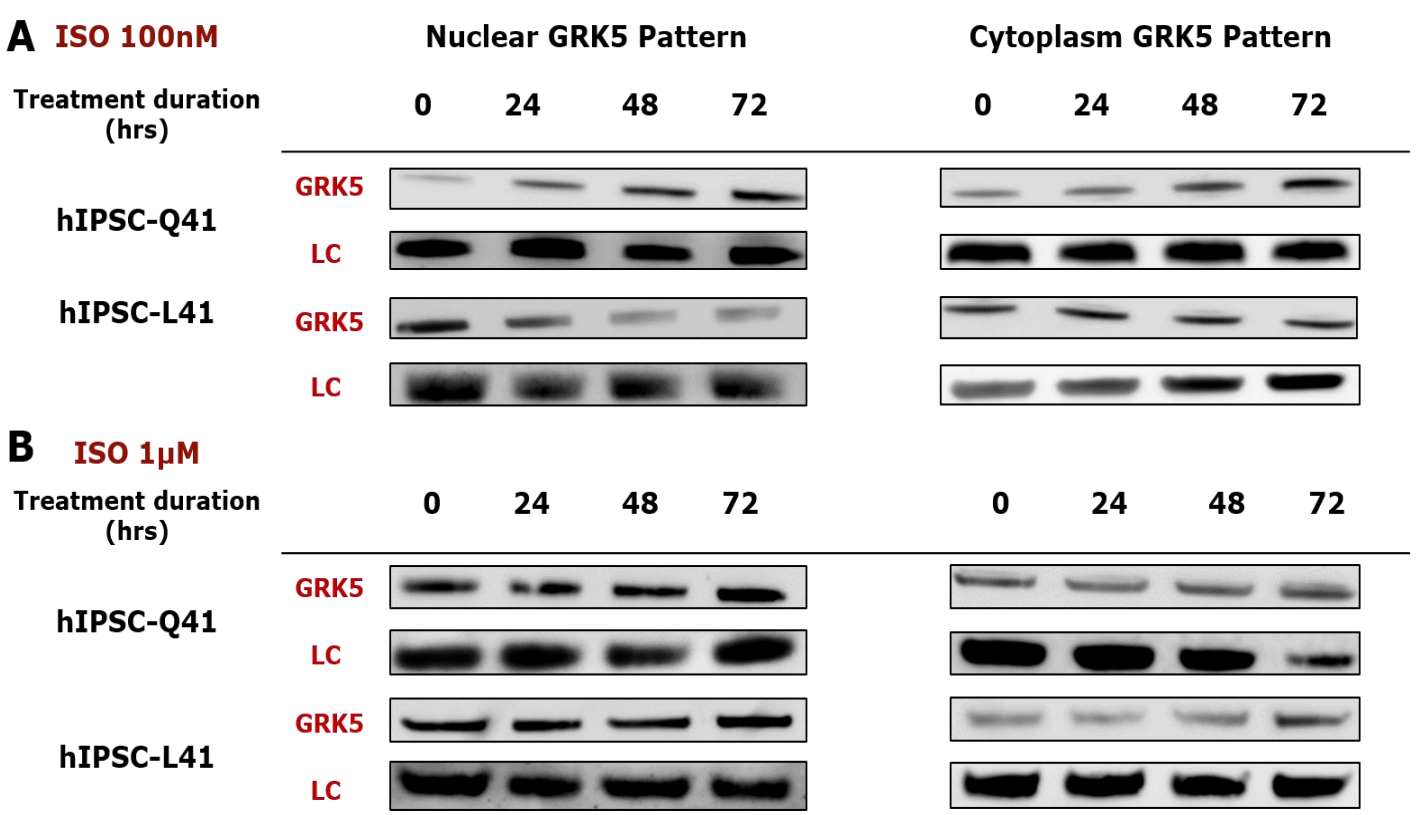

Figure 4.5. Nuclear and cytoplasm blot of GRK5 in the hIPSC model.
Representative nuclear and cytoplasm blots of GRK5 and its loading controls with TBP (nuclear protein fraction) and β-actin (cytoplasm protein fraction) in hIPSC GRK5-Q41L cardiomyocytes during chronic catecholamine stress at ISO 100 nM (A) and 1 μM (B).

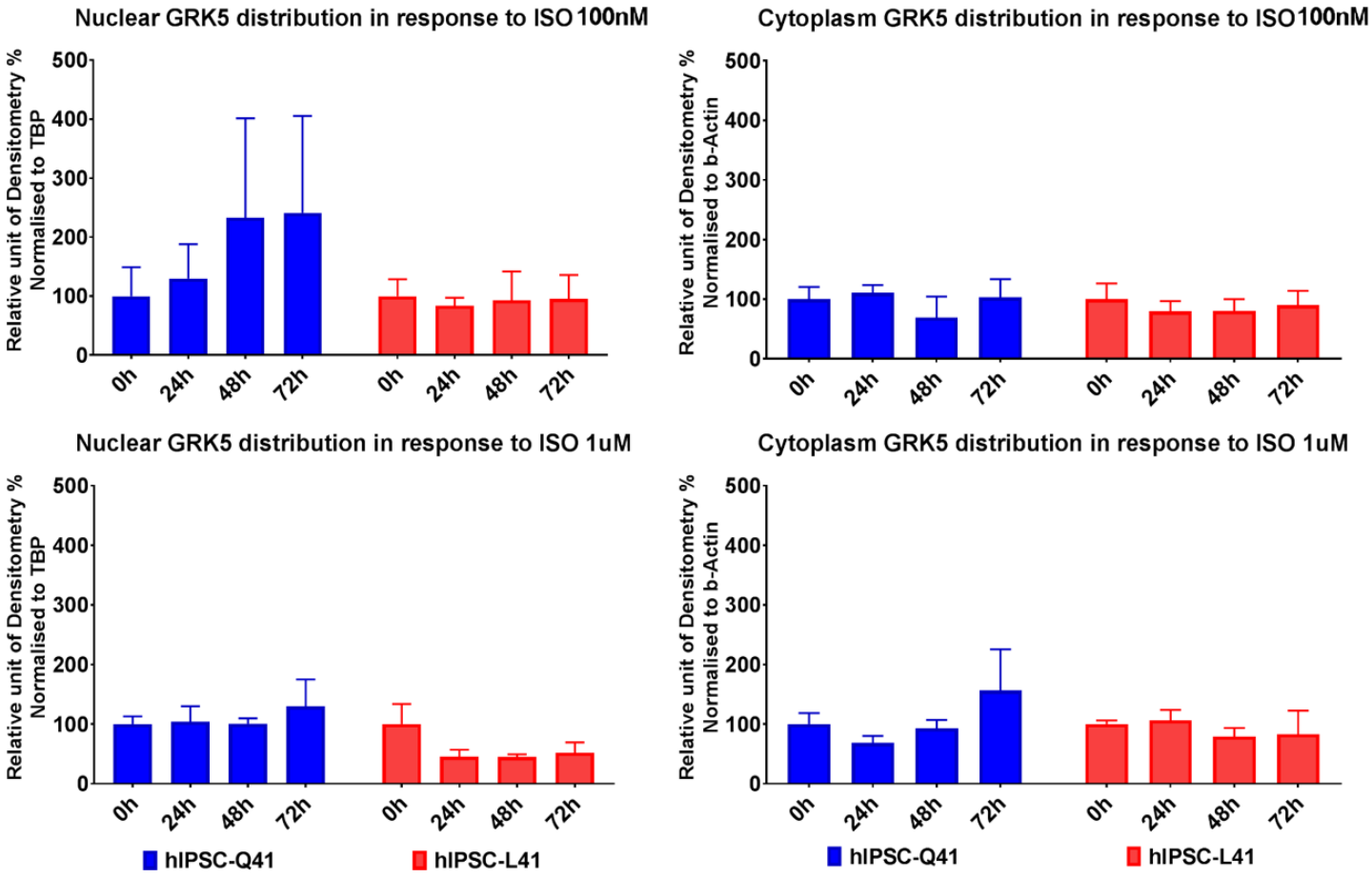

Figure 4.6. Densitometry analysis of western blot of nuclear and cytoplasm GRK5 in the hIPSC model.

Densitometry analysis of GRK5 distribution in the nuclei (A) and cytoplasm (B) at ISO 100 nM and ISO 1 µM, present as mean ± SEM, n = 3 biological replicates. *p < 0.05, **p < 0.01 Two-way ANOVA with Dunnett's multiple comparison tests.

4.3.3 ImageJ Macro writing for intensity quantification of subcellular GRK5 analysis by immunocytochemistry:

Western blot analysis in the previous section showed an interesting observation of increased nuclear GRK5 accumulation in HUES7-Q41 CMs, but similar increases of nuclear GRK5 fraction were not observed in hIPSC-Q41 CMs. Because the bulk analysis of western blot could be contaminated by α-actinin^{-} cells, ICC staining for GRK5 and α-actinin was performed to validate western results and to visualise the localisation of GRK5 in α-actinin^{+} cells for the isogenic and hIPSC models. A Zeiss 780 superresolution confocal microscope was used to achieve high-resolution images illustrating GRK5 localization in cardiomyocytes.

Cardiomyocytes of both isogenic and hIPSC were exposed to 1 μM ISO for 72h or treated with 0.4 μM HCl as the vehicle-treated control. High-resolution images of isogenic and hIPSC CMs with 100 to 250 cells (α-actinin^{+} ^{cells}) per condition were taken for quantification of subcellular GRK5 intensity from 3 biological replicates. These images were analysed by ImageJ to investigate the effects of GRK5-Q41L variants on the subcellular GRK5 distribution during chronic catecholamine stress.

The distribution of GRK5 of a single CM and CM cluster is illustrated in **Figure 4.7**, where cardiomyocytes were identified by α-actinin. 2D and 3D images showed that GRK5 was present both in the nuclei and the membrane cytoplasm. In the nuclei, GRK5 protein appeared concentrated and abundant in granular patterns (white arrow), which likely suggested the nucleoli localisation. Strategies to investigate GRK5 distribution in the nuclei and the cytoplasm were shown in **Figure 4.8**. In detail, DAPI stain (the blue channel) was used to create the nuclear mask to calculate nuclear GRK5 intensity (**Figure 4.8.B**), while α-actinin was utilised to generate the cytoplasm mask for cytoplasm GRK5 intensity quantification (**Figure 4.8.C**).

An ImageJ Macro using this strategy was written to get a consistent and reproducible workflow for quantification of nuclear and cytoplasm GRK5 intensity. Since cardiomyocytes are large-volume cells so a single plane image was difficult to display their 3D data so that the 3D data was processed to a maximum intensity project 2D image by ZEN Black software. The projection took the brightest pixel in each plane and displayed the intensity value into the 2D image. All the analysis were applied to the maximum intensity images. By using Macro Recording, the workflow was automatically recorded. The workflow was started by splitting a multi-channel image into single-channel images (**Figure 4.8.A**), where channel 1 (C1) displayed for DAPI (blue), channel 2 (C2) was α-actinin (green) and channel 3 (C3) was GRK5 (red).

A C1 – DAPI image was used to create the nuclei mask. "Gaussian Blur, sigma=3" filter and "Triangle white stack" were used for nuclei segmentation (**Figure 4.9**). The segmentation after thresholding always displayed as white (value =255). By subtracting to 244, the value of the segmented nuclei was 1 and the background was 0. The segmented nuclei were used as the nuclei mask (C1 – Nuclei mask). By using "Image Calculator", C1 - Nuclei mask (nuclei = 1, background = 0) was multiple with C3 image, which contained data of GRK5 (value = n). In the result image after calculation, segmented nuclei contained intensity data GRK5 data (nuclei = 1 x n = n, background = 0 x n =0). "NaN background" was used to convert the non-threshold pixel of background into Not a Number (NaN) value so that the mean value did not contain zero value of the background. These images were saved as "Nuclei_title" and the measurement of these images was calculated for only nuclei GRK5 data with NaN background. The results and images of interest were saved with relevant name by "File.directory()+title+" code. Unnecessary images and windows were closed.

Next, a C2 – the α-actinin image was used to generate the cytoplasm mask (**Figure 4.10**). "Gaussian Blur, sigma=5" filter and "Huang white stack" were optimal conditions for cytoplasm segment mentation (**Figure 4.8.C**). Applying the same principle, cytoplasm segmentation was converted into 1 (cytoplasm =1), while the background turned into NaN value. Measurement of the resulting image "Cytoplasm_title" was calculated the mean of cytoplasm GRK5 with NaN background and empty nuclei pattern (**Figure 4.8.C**). Results and images of interest were saved and unnecessary windows were closed.

This section explained the establishment of ICC analysis of subcellular GRK5 compartment by using ImageJ Macro. This ImageJ Macro was optimised and successfully quantified nuclear and cytoplasm GRK5 fraction as an illustration in figure 4.8.

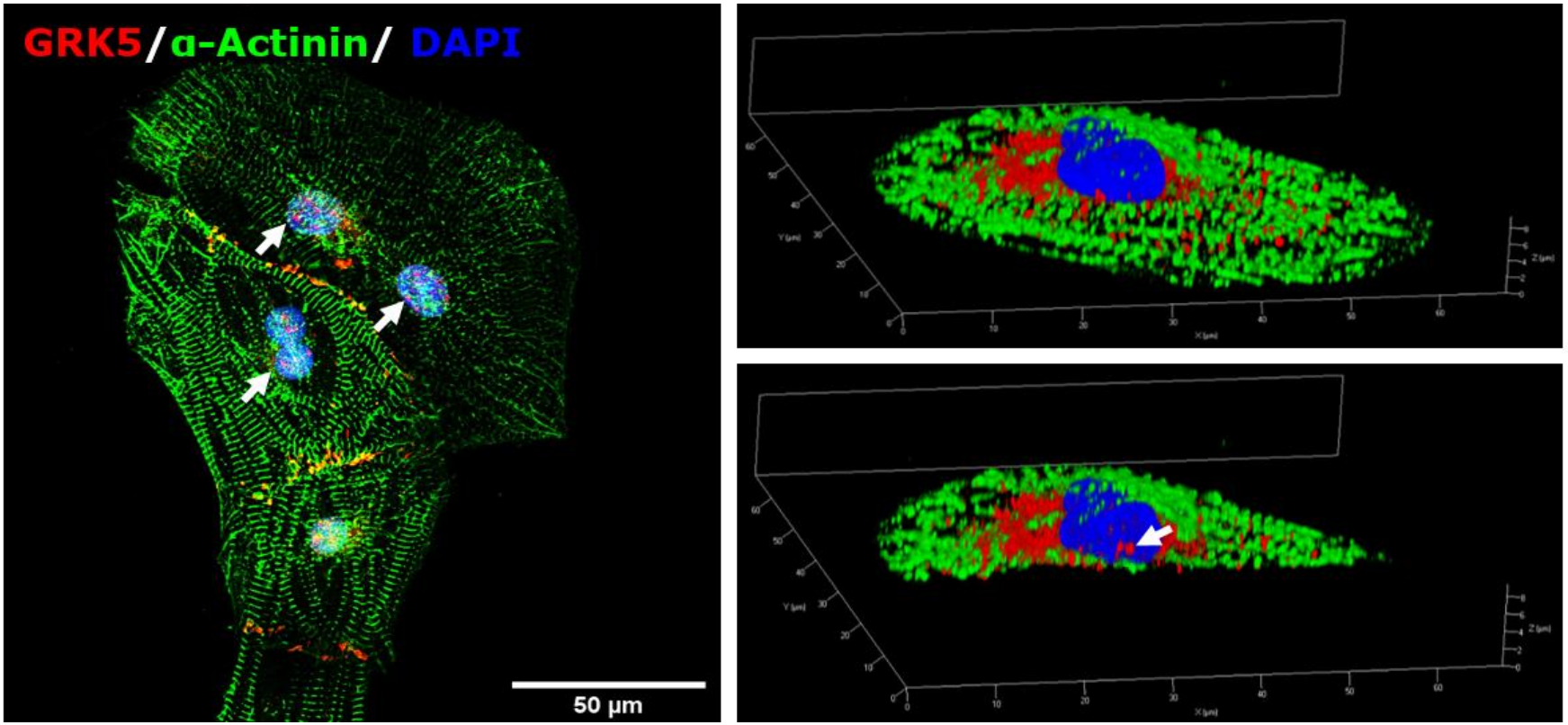

Figure 4.7.Localization of GRK5 protein in hPSC-CMs.

Representative 2D and 3D immunofluorescent images of cardiomyocytes staining with DAPI (Blue), α-actinin (Green) and GRK5 (red) illustrated for localisation of GRK5 protein in hPSC-CMs, scale bar 50 µm. 2D and 3D images showed that GRK5 present both in the nuclei and the cytoplasm (membrane). GRK5 protein displayed concentratedly and abundantly in special pattern (white arrow) in the nuclei.

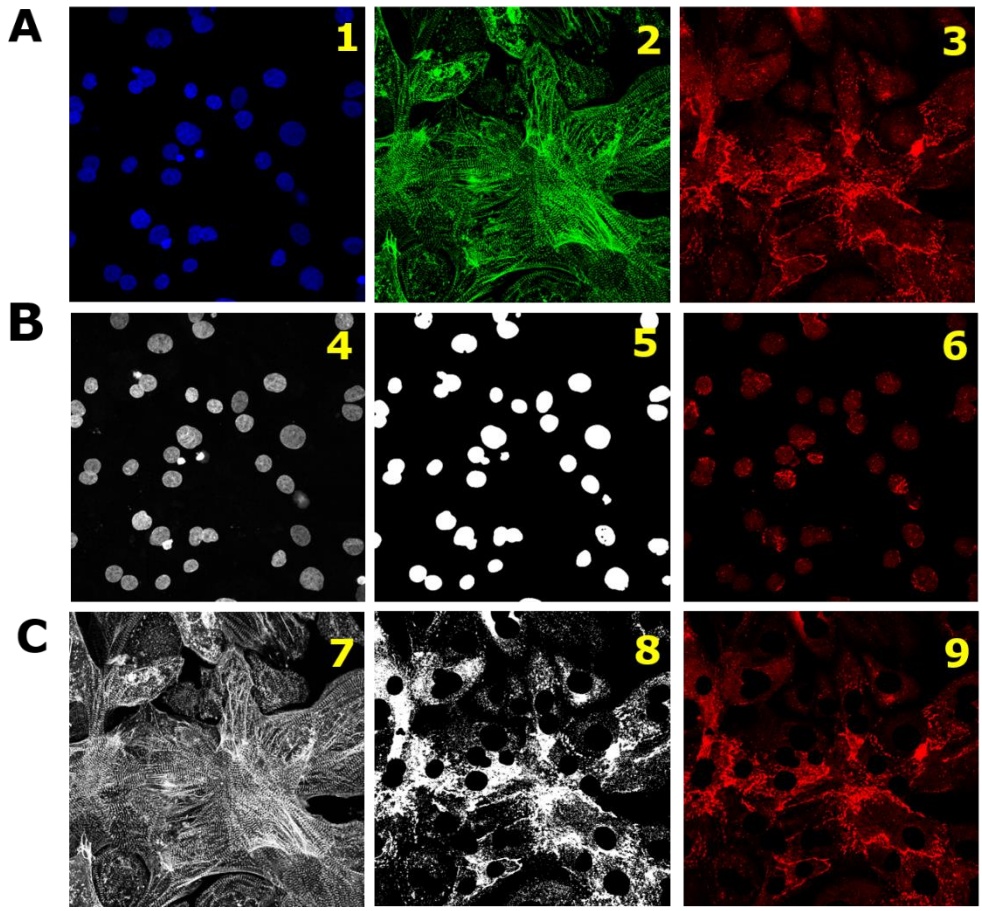

Figure 4.8. Intensity quantification of GRK5 in cardiomyocytes using high-resolution microscopy and ImageJ analysis.

(A) ImageJ algorithm to quantify nuclear and cytoplasm GRK5 started by splitting a multichannel image into single-channel images, DAPI nuclear dye (blue), α-actinin (green) and GRK5 (red). (B) DAPI channel was used to generate nuclei mask, while (C) α-actinin stain was used for cytoplasm segmentation to quantify cytoplasm GRK5 intensity.

NucleiCytoplasm_GRK5_Intensity_Quantification.ijm

File Edit Language Templates Run Tools Tabs

NucleiCytoplasm_GRK5_Intensity_Quantification.ijm

```
title=getTitle();
// Separating the 3 channels and naming them
run("Split Channels"); selectWindow("C1-"+title);run("Blue");
selectWindow("C2-"+title);run("Green");
selectWindow("C3-"+title);run("Red");
//Making NUCLEI  Mask
selectWindow("C1-"+title);
run("Gaussian Blur...", "sigma=3 stack");
run("8-bit");
run("Auto Threshold", "method=Triangle white stack");
run("Subtract...", "value=254");
run("Duplicate...", "title="+title+"_Nuclei mask");
rename("Nuclei mask_" + title);
run("Invert", "stack");
run("Subtract...", "value=254");
// Using mask we keep only the nuclei fraction of the red channel
imageCalculator("Multiply create 32-bit", "C1-"+title,"C3-"+title);
selectWindow("Result of C1-"+title);
setAutoThreshold("Li dark");
run("NaN Background"); // REMOVING 0  values from the background therefore measure will
rename("Nuclei_" + title);
run("Red");
selectWindow("Nuclei_" + title);
run("Measure");
saveAs("Results",File.directory()+title+"Results_Nuclei.xls");
selectWindow("Nuclei_" + title);
saveAs("Tiff",File.directory()+title+"_Nuclei32bit");
// converting and saving for windows friendly visualisation
run("RGB Color");
saveAs("Tiff",File.directory()+title+"_Nuclei");
run("Close");
run("Clear Results");
close("C1-"+title)
close("Result of C1-"+title);
close("Results",File.directory()+title+"Results_Nuclei.xls")
```

Run Kill Show Errors Clear

Figure 4.9.Macro script panel for quantification of nuclear GRK5

Workflows start by splitting a multi-channel image into single-channel images. C1 DAPI channel was used to create the Nuclei Mask. The Nuclei mask was used to calculate the nuclear fraction of GRK5 (red channel). Results and images of interest were saved with a relevant name and unnecessary windows were closed.

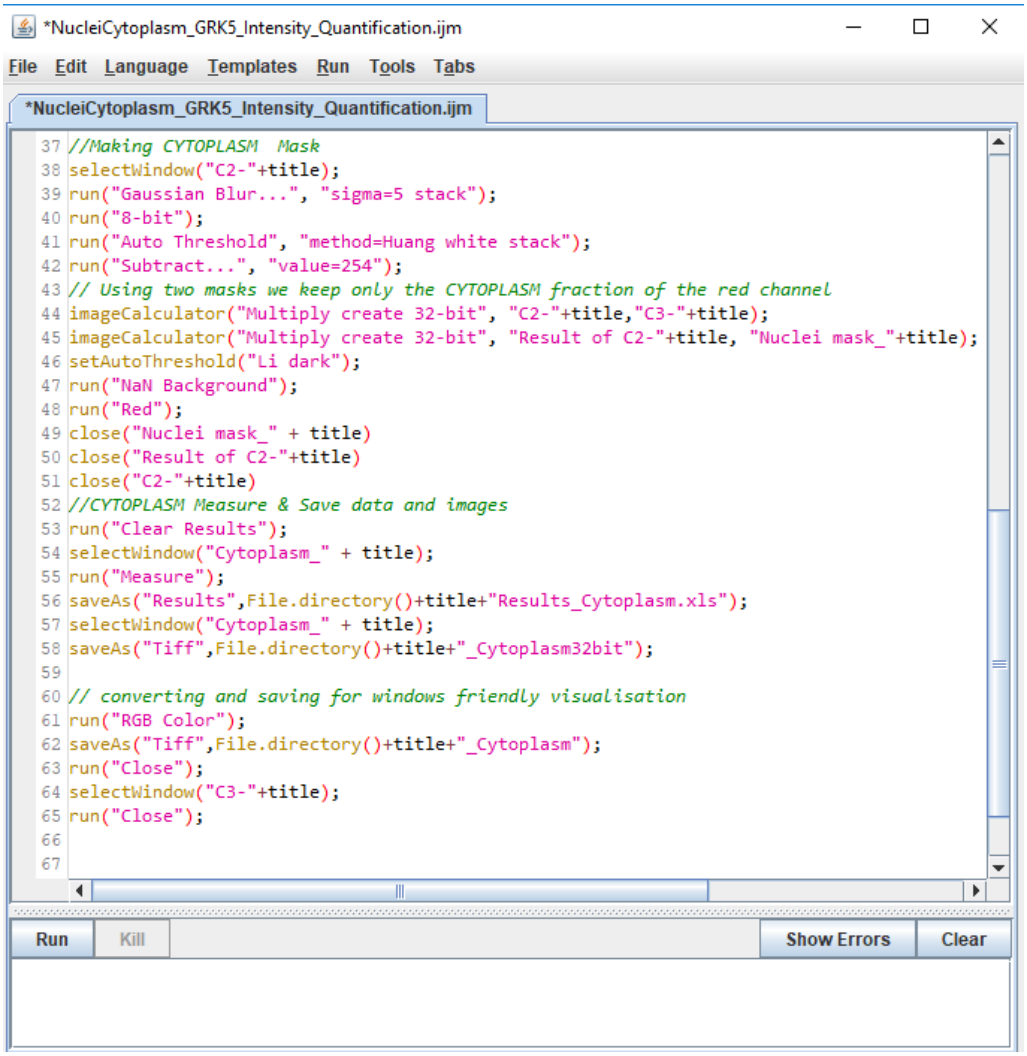

Figure 4.10. Macro script panel for quantification of cytoplasmic GRK5

C2 α-actinin (green) channel was used to create the cytoplasm mask. The cytoplasm mask was used to calculate the cytoplasmic fraction of GRK5 (red channel). Results and images of interest were saved with a relevant name and unnecessary windows were closed.

4.3.4 Changes in subcellular GRK5 distribution during chronic catecholamine stress:

An ImageJ Macro was previously optimised to quantify GRK5 intensity in the nuclei and cytoplasm of cardiomyocytes. To investigate the effects of GRK5-Q41L variants on the subcellular GRK5 distribution during chronic catecholamine stress, the intensity of subcellular GRK5 in different variants after 72h exposure to ISO 1μM stress was normalised with their vehicle control. The difference in GRK5 intensity during ISO treatment illustrated the changes in the distribution of GRK5 in Q41L variants during the stress.

The changes of subcellular GRK5 intensity in the isogenic and hIPSC models during 72h of ISO 1 μM exposure was illustrated in **Figure 4.11.A**. In the isogenic model, the HUES7-Q41 CM variant exhibited a significant increase of nuclear GRK5 fraction with 26.7% higher compared with vehicle-treated cardiomyocytes. In contrast, analysis of nuclear GRK5 intensity showed a reduction of 10.7 % in HUES7-L41, but a slight increase of 3.2% in HUES7-Q/L41. The changes of nuclear GRK5 fraction intensity in HUES7-Q41 was significantly increased compared to HUES7-L41 and HUES7-Q/L41 haplotypes during chronic catecholamine stress (**Figure 4.11.A**, ** $p < 0.01$). These results of nuclear GRK5 fraction changes were relatively consistent with the previous western blot analysis in **Figure 4.4**, where HUES7-L41 and HUES7-Q/L41 showed prevention of nuclear GRK5 accumulation during catecholamine stress. The 2.5D illustration of GRK5 localisation and GRK5 intensity pixel in the HUES7-Q41L isogenic model upon ISO stress was illustrated in **Figure 4.12**, where GRK5 protein presented both in the nuclei and the cytoplasm in cardiomyocytes. These 2.5D images were generated by Zen Blue software. Upon catecholamine stress, a visible increase of GRK5 in nuclei was observed in HUES7-Q41 CMs but not HUES7-L41 or HUES7-L41 CMs.

In contrast, hIPSC-Q41 CMs did not show an increase of nuclear GRK5 accumulation as HUES7-Q41 CMs during chronic ISO stress with 2.4% reduction of nuclear GRK5 fraction. However, hIPSC-L41 CMs exhibited a reduction of 17.5 % nuclear GRK5 intensity during the ISO treatment. This reduction pattern in hIPSC-L41 was similar to the isogenic HUES7-L41 CMs, it was significantly lower compared to the hIPSC-L41 variant (**Figure 4.11.A**, * $p < 0.05$). The 2.5D illustration of GRK5 distribution and pixel intensity in the hIPSC model also displayed less GRK5 accumulation in the nuclei of the hIPSC-L41 variant compared to the hIPSC-Q41 variant (**Figure 4.12**).

Changes in cytoplasm GRK5 distribution of both models displayed in **Figure 4.11.B**. In the isogenic model, ISO-treated HUES7-Q41 and HUES7-L41 CMs showed a reduction of cytoplasm GRK5 fraction with -25.3% and -16.2% respectively, while the HUES7-Q/L41 variant showed almost no difference compared to vehicle-treated cardiomyocytes. hIPSC-L41 variant showed a significant reduction in cytoplasm GRK5 compared to the hIPSC-Q41 variant (**Figure 4.11.B**,** $p < 0.01$). However, the decrease of cytoplasm GRK5 intensity in the isogenic and hIPSC systems did not well illustrated in these 2.5D images.

In general, the analysis of nuclear GRK5 distribution showed that GRK5-L41 variants prevented the increase of nuclear GRK5 accumulation in both isogenic and hIPSC models. Consistent with western blot analysis, nuclear GRK5 accumulation was only observed in the HUES7-Q41 but not in the hIPSC model. All GRK5-Q41L haplotypes showed decreased levels in cytoplasm GRK5 fraction upon ISO stress. GRK5 protein was shown to localise both in the nuclei and the cytoplasm of cardiomyocytes with the relatively abundant localisation of GRK5 in the cell membrane.

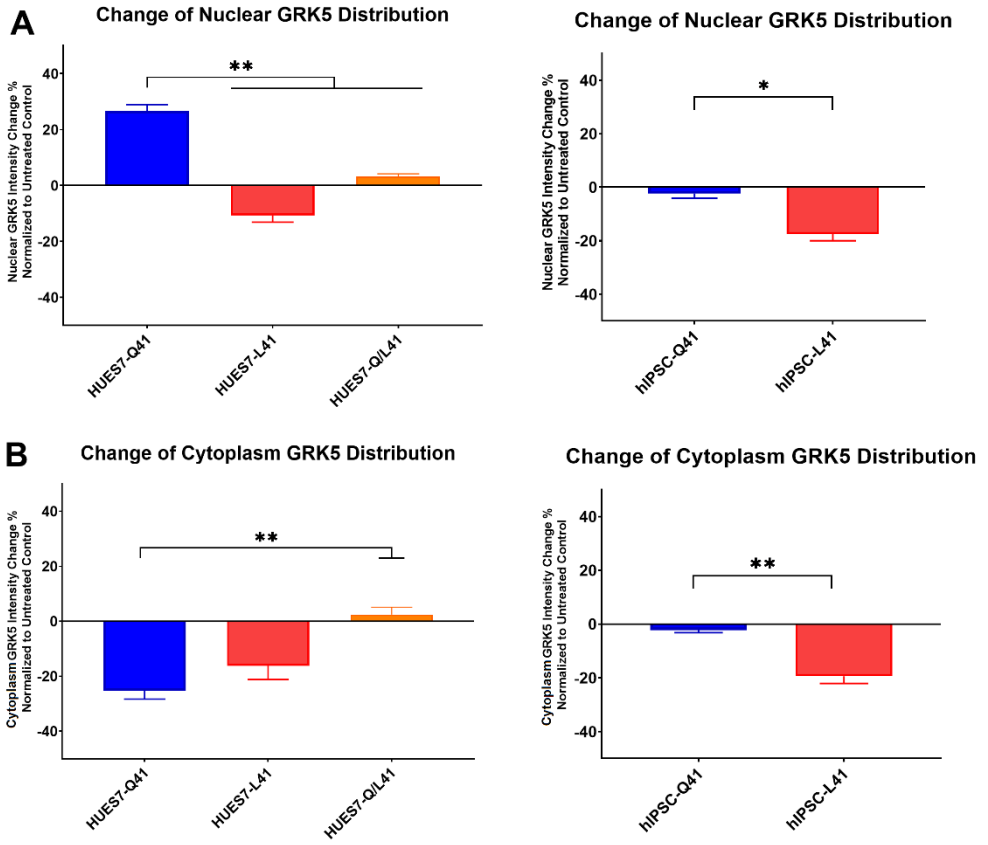

Figure 4.11.Changes of nuclear and cytoplasm GRK5 distribution upon 72h of ISO 1 µM in the isogenic and hIPSC model.

(A) Comparison of nuclear GRK5 fraction changes in isogenic and hIPSC model exhibited a reduction of nuclear GRK5 accumulation in L41 variant in both isogenic and hIPSC model. (B) Analysis of cytoplasmic GRK5 fraction changes in isogenic and hIPSC models showed a varied reduction of cytoplasmic GRK5 upon ISO treatment, represent means ± SEM, n=3 biological replicates. *p < 0.05, **p < 0.01 One-way ANOVA with Dunnett's multiple comparison tests.

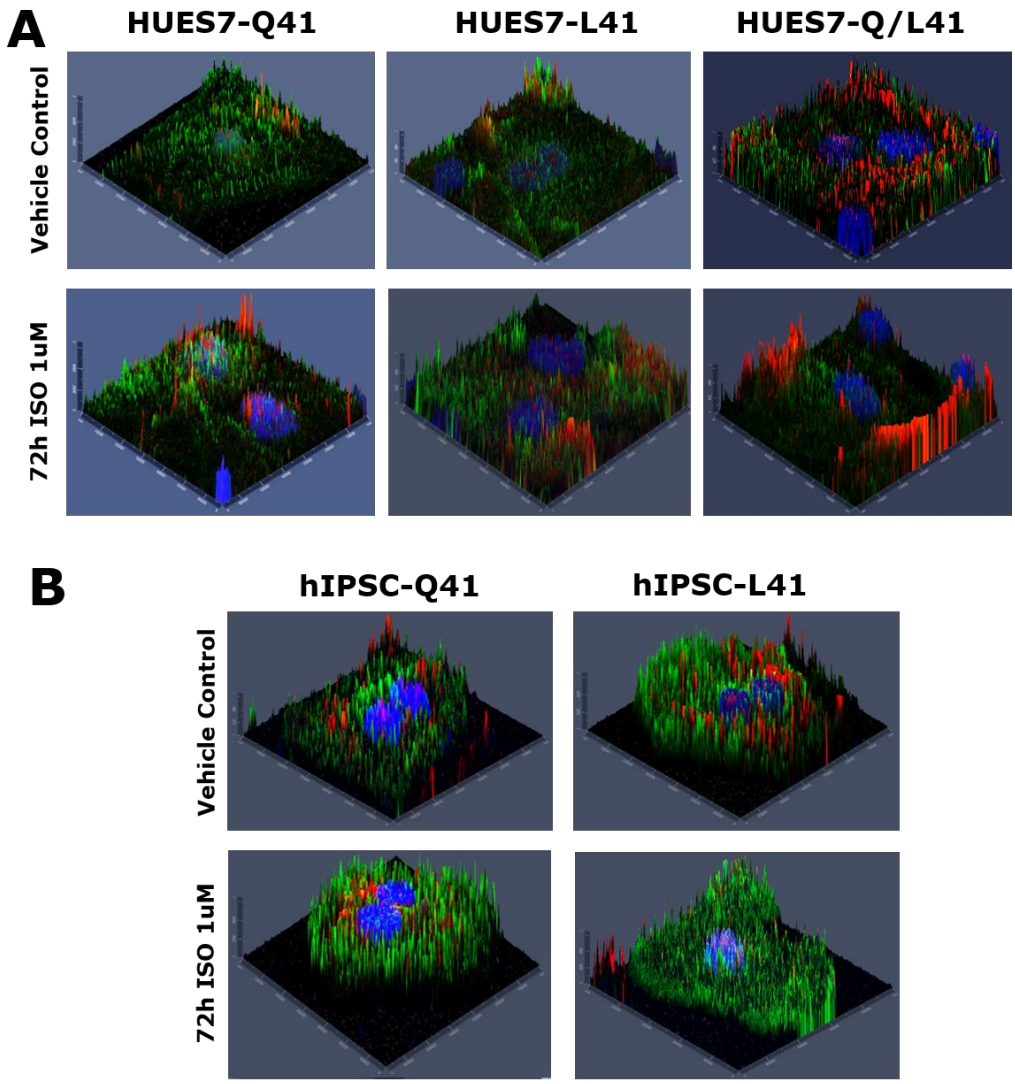

Figure 4.12.Localisation of GRK5 protein in cardiomyocytes during chronic ISO stress.

Representative images illustrate the localisation of GRK5 protein in cardiomyocytes upon 72h exposure to ISO 1 μM in the isogenic model (A) and hIPSC model (B); DAPI (blue), α-actinin (green), GRK5 (red).

4.3.5 Develop BNP assay to investigate hypertrophic responses of cardiomyocytes.

The increase of GRK5 accumulation was reported to attribute to the development of hypertrophy and HF progression (Hullmann et al., 2014; Traynham et al., 2015). Western blot and ICC analysis in previous sections showed increases of nuclear GRK5 accumulation in the HUES7-Q41 variant of the isogenic model. This thesis next investigated the hypertrophic responses of GRK-Q41L variants in the isogenic and hIPSC model by quantifying BNP protein production during chronic catecholamine stress. Cardiomyocytes exposed to chronic ISO stress was subjected to ICC staining with BNP antibody to quantify BNP protein production, which is a method of choice to investigate hypertrophic responses in cardiomyocytes.

Endothelin 1 (ET-1) was reported as hypertrophic stimuli, which upregulated BNP expression in cardiomyocytes after 18h treatment. Along with ET-1, Phenylephrine (PE) and Angiotensin II (AngII) were also tested to trigger the hypertrophic response in cardiomyocytes via the Gαq pathway (Traynham et al., 2015). Optimisation of treatment with different drugs or 18h for stimulating hypertrophic responses was performed in the hIPSC model. A quantitative analysis pipeline using high-content confocal screening platform Operetta was optimised to quantify the number of CMs positive to BNP protein expression through BNP intensity measurement (**Figure 4.13.A**). The untreated hPSC-CM culture has a basal proportion of cardiomyocytes positive to BNP at approximately 20 % - 30 % of the total culture. This indicated that in-vitro culture of hPSC-CMs could induce basal induction of hypertrophic response.

Optimisation for hypertrophic responses by chemical stimuli with ET-1, AngII and PE for 18h in the hIPSC model showed in **Figure 4.13.B**. ET-1 treated hIPSC-Q41L CMs both exhibited over 60 % positive to BNP. This

indicated ET-1 could be used to stimulate BNP induction in hPSC-CMs. The maximum BNP induced by ET-1 was detected at 10 nM, while a significant reduction of BNP production was detected at ET-1 1 μM in both hIPSC-Q41 and hIPSC-L41 CMs. ET-1 10 nM was so used as the optimal concentration for BNP induction (**Figure 4.14.A & B**). In contrast, the BNP production levels of PE and Ang-II in both Q41 and L41 variants were both close to the basal BNP expression level in vehicle-treated condition. These low BNP production could be due to the concentration of these compounds out of dynamic range or their low receptor expression levels in hPSC-CMs. Since AngII 10 μM and PE 100 μM were relatively too high, we decided to use ET-1 10nM as a positive hypertrophic stimulation in hPSC-CMs.

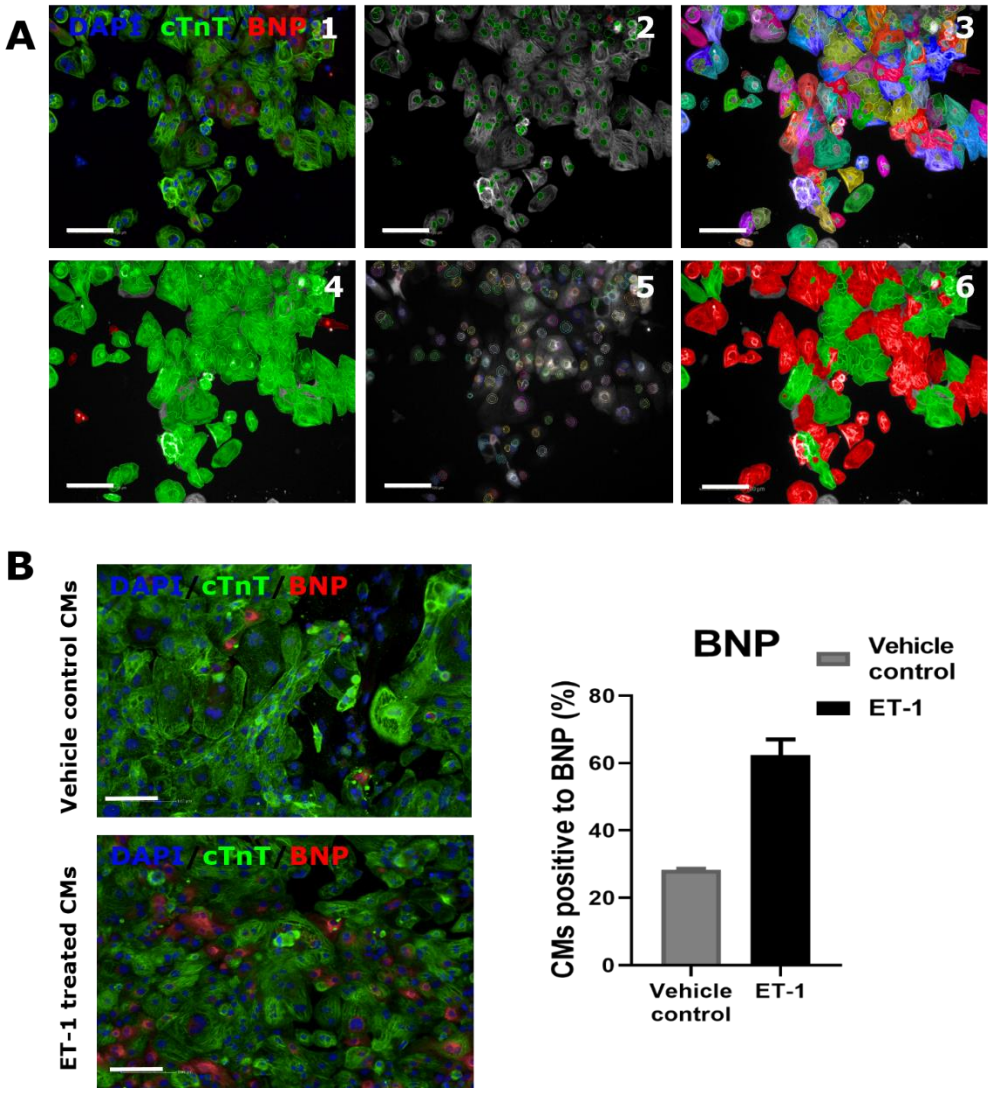

Figure 4.13. Quantification of BNP production in hPSC-CMs.

(A) The high content imaging algorithm to quantified BNP expression in hPSC-CMs using Operratte Immunostaining image of hPSC-CMs staining with DAPI (blue), cTnT (green) and BNP (red). The analysis pipeline was first to find nuclei fraction (2), cytoplasm fraction (3), then next identified CMs by cardiac cTnT marker (4). BNP was measured in the perinuclear region (5) to identify CMs positive to BNP expression (6) based on BNP negative control staining. (B) Representative images illustrated BNP expression in untreated cultures and hypertrophic stimulated condition by 10 nM ET-1 for 18h in hIPSC-Q41 CMs, scale bar 100 µm, present mean ± SEM, n=2 biological replicates.

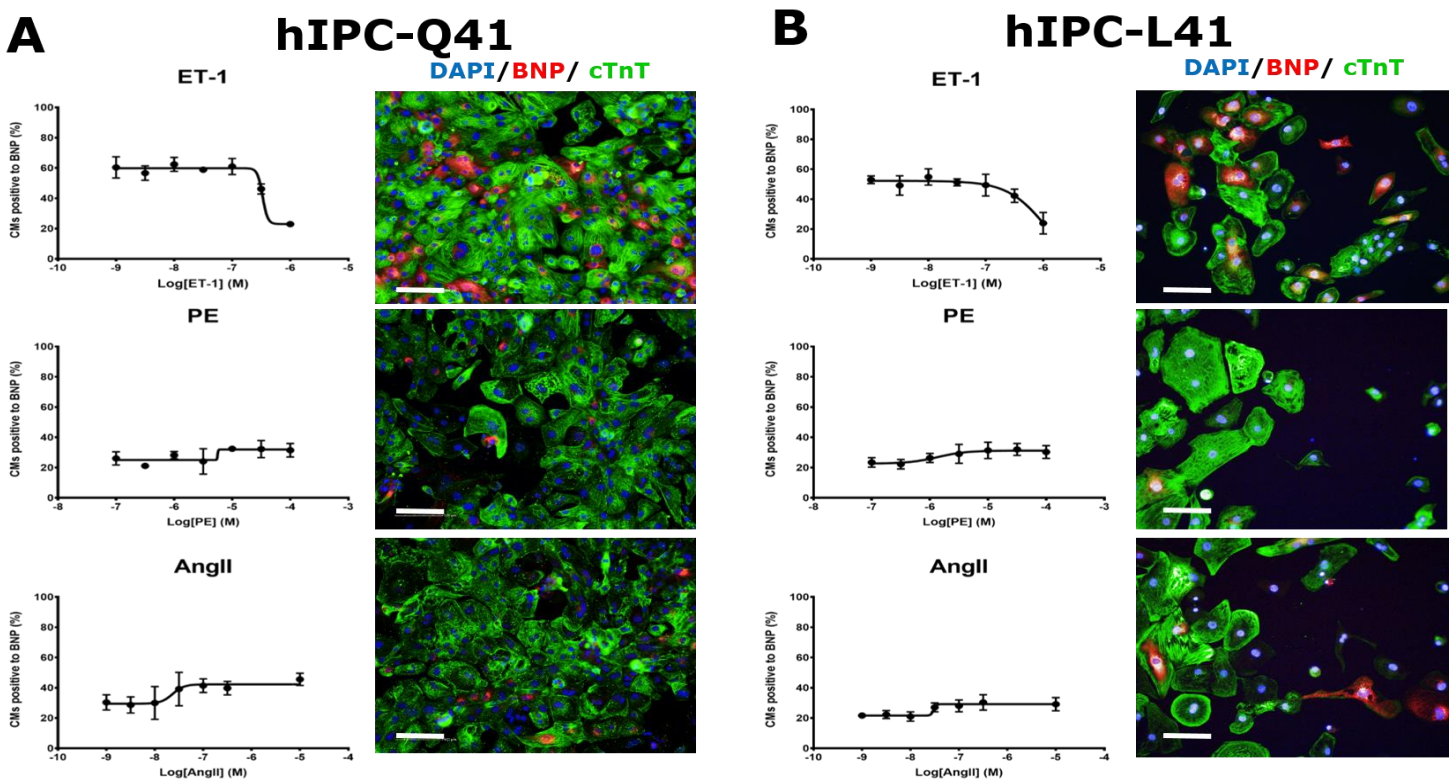

Figure 4.14. The BNP production response curve of hypertrophic drugs.

The BNP production response curve was conducted for different hypertrophic drugs, including ISO, ET-1, PE and AngII by detecting ICC signal of BNP in hPSC-CMs. The percentage of cardiomyocytes positive to BNP was plotted against the logarithmic values of the drug concentration for hIPSC-GRK5-Q41 (A) and hIPSC-GRK5-L41 (B). staining with cTnT (Green), BNP (Red) and nuclear dye DAPI (Blue) in the ET-1 treatment at 10 nM for 18h. The data represent means ± SEM, n=2 biological replicates.

4.3.6 HUES7-L41 cardiomyocytes exhibited beneficial effects in contractile performances during chronic catecholamine stress

To investigate the correlation of nuclear accumulation of GRK5 and hypertrophic responses in hPSC-CMs, BNP expression of GRK5-Q41L variants was quantified for both the isogenic and hIPSC models during long term ISO exposure at 100 nM and 1 μM upon 96h. The percentage of cardiomyocytes positive to BNP expression was quantified by using the pipe-line in **Figure 4.13.A**. The effects of GRK5-Q41L variants during chronic ISO and ET-1 treatment on BNP expression were analysed by normalisation to the vehicle-treated cardiomyocytes.

Summary of percentage change of BNP response in the isogenic and hIPSC models during chronic ISO and ET-1 treatment was shown in **table 4.1**. Interestingly, HUES7-L41 and HUES7-Q/L41 haplotypes produced significantly higher BNP expression during chronic ISO 100 nM and 1 μM exposure after 24h (**Figure 4.15.A**, * $p < 0.05$, ** $p < 0.01$). These L41 and Q/L41 variants maintained this increased BNP production during chronic ISO treatment. At 100 nM, increases of BNP expression in HUES7-L41 and HUES7-Q/L41 ranged from 11% - 14.2% and 6.5% - 11.9% respectively. At ISO 1 μM, these upregulated BNP levels were even higher in HUES7-L41 (~13% - 18%) and HUES7-Q/L41 (~10.5% - 12.8%). In contrast, maximum BNP production in HUES7-Q41 CMswas detected at 24h and reduced to basal BNP level after longer ISO exposure. Under ET-1 treatment, BNP expression reaches the maximum at 24h in both HUES7-Q41 (~16.7%) and HUES7-Q/L41 (~36.1%). HUES7-Q/L41 has maximum ET-1 induced BNP expression at 48h (~12.8%). The representative images illustrated for high BNP expression in HUES7-Q41 and HUES7-Q/L41 CMs during chronic ISO and ET-1 induction for 72h (**Figure 4.16**).

The hIPSC-Q41L model exhibited opposite responses compared to the isogenic model (**Figure 4.15.A**). Indeed, hIPSC-Q41 CMs produced higher BNP levels compared to hIPSC -L41 CMs. At 100nM, the significant high BNP expression was detected at 48h (~14.5%) while the maximum BNP of ISO 1 μM was at 96h (~13.3%) (* $p < 0.05$, ** $p < 0.01$). BNP expression of hIPSC-L41 varied and stayed relatively close to the basal BNP expression of vehicle-treated cardiomyocytes. The significant-high BNP production of hIPSC-L41 was detected at 9.2% at 96h ISO 100 nM exposure. In the same response pattern, hIPSC-Q41 produced significant higher BNP expression levels (~ 19.6% - 25.1%) than hIPSC-L41 (~ 3.2% - 10.7%). The representative images illustrated for high BNP expression in the hIPSC model during chronic ISO and ET-1 induction for 72h (**Figure 4.17**).

The upregulation of BNP expression during chronic ISO stress indicated that ISO could stimulate hypertrophic responses in hPSC-CMs. The L41 and Q/L41 variant in the isogenic HUES7 model exhibited higher BNP induction than HUES7-Q41L. However, hIPSC-L41 showed lower BNP induction compared to hIPSC-Q41 during chronic ISO stress. The opposite response of the isogenic and hIPSC could be accounted for by the genetic background.

% Change normalised to vehicle 0h		**The Isogenic Model**			**The hIPSC Model**	
		Q41	**L41**	**Q/L41**	**Q41**	**L41**
ISO 100nM	24h	6.4	11.0	6.5	4.1	-1.3
	48h	4.0	11.5	11.9	14.5	1.9
	72h	1.6	14.2	8.5	6.0	2.4
	96h	2.0	10.9	8.0	9.5	9.2
ISO 1μM	24h	3.5	14.6	12.5	6.2	-0.1
	48h	2.1	17.7	12.8	7.0	2.7
	72h	0.7	17.9	12.2	11.0	2.2
	96h	0.9	13.0	10.5	13.3	2.5
ET-1 10nM	24h	16.7	36.1	7.0	24.3	3.2
	48h	7.7	22.6	12.8	25.1	7.6
	72h	6.9	17.7	7.5	21.7	10.5
	96h	6.1	16.0	8.2	19.6	10.7

Table 4.1. Percentage change of BNP hypertrophic response in the isogenic and hIPSC models during chronic ISO and ET-1 treatment.

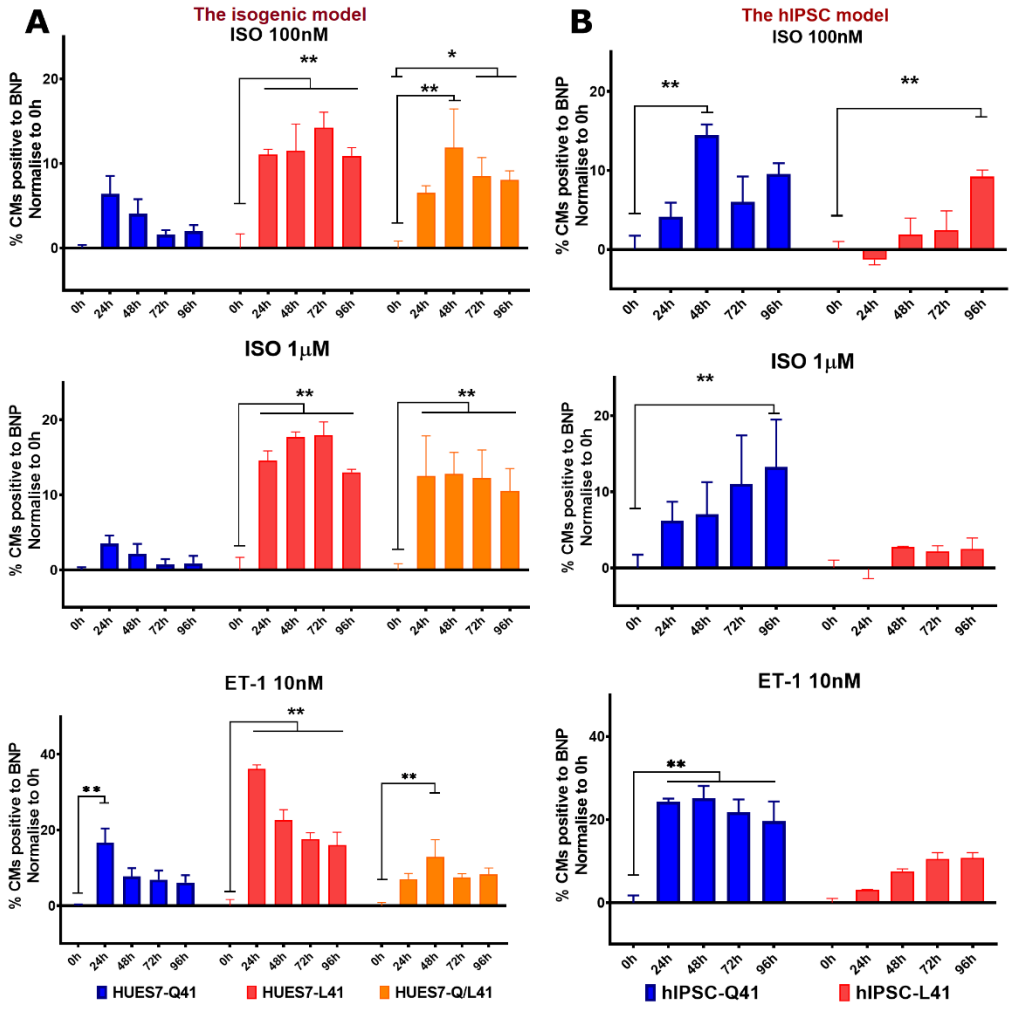

Figure 4.15. Investigation of hypertrophic response in the isogenic and hIPSC models during chronic ISO and ET-1 treatment.

BNP expressed CMs were quantified to investigate hypertrophic responses of GRK5-Q41L variant in the HUES7 isogenic model (A) and hIPSC model (B). The increase of BNP induction during chronic ISO and ET-1 treatment were normalised to vehicle-treated control (0h), present mean ± SEM, n = 3 biological replicates. *p<0.05, **p < 0.01 Two-way ANOVA with Dunnett's multiple comparison tests

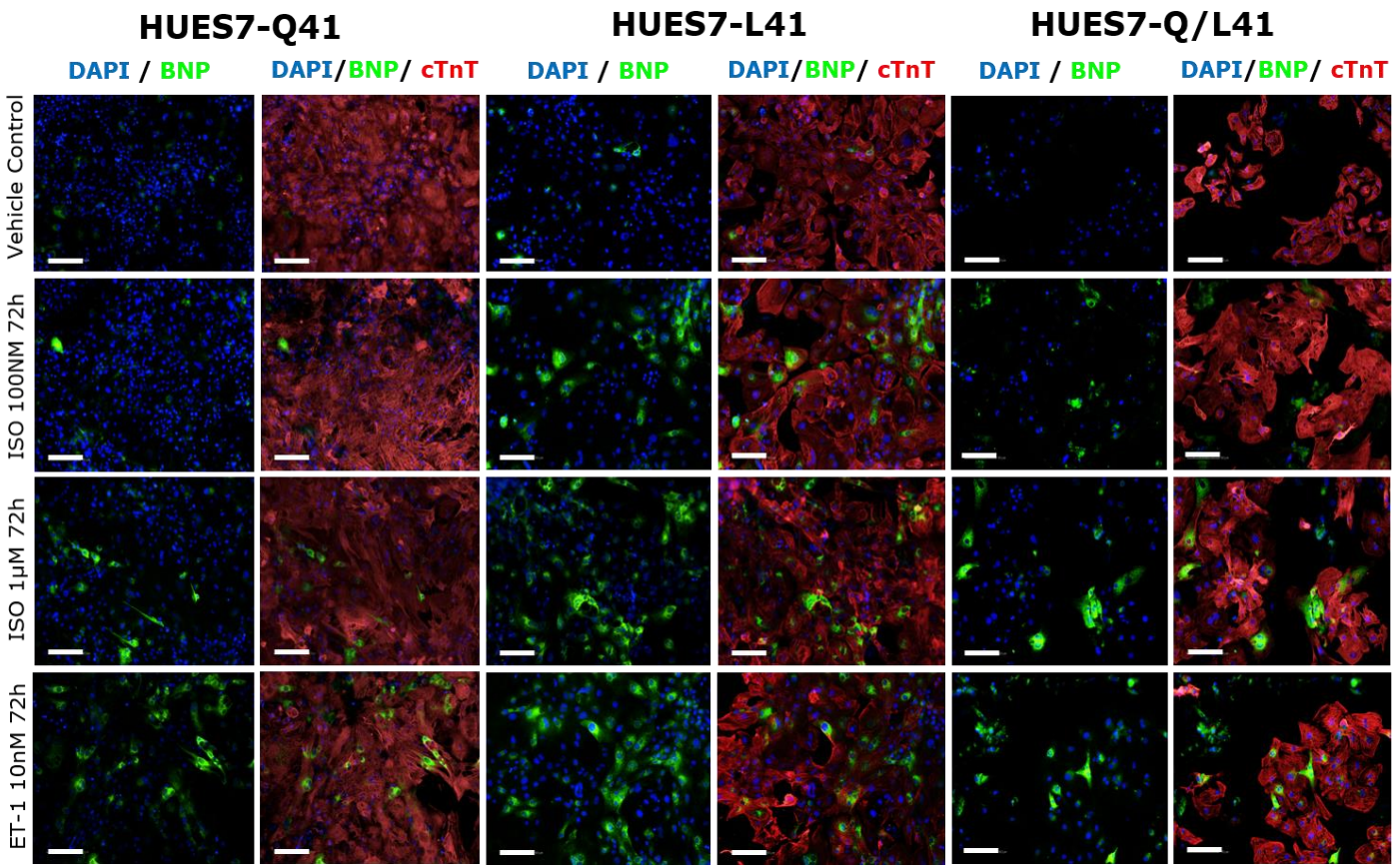

Figure 4.16. Hypertrophic response of the isogenic HUES7-Q41L model during chronic ISO and ET-1 treatment.

Representative immunofluorescent images of BNP expressed CMs with DAPI (blue), cTnT (red) and BNP (green), scale bar 100 µM. The chronic ISO and ET-1 treatments for 72h showed upregulation of BNP production in all haplotypes, where BNP expressions of L41 and Q/L41 variants were observed higher than Q41 variant.

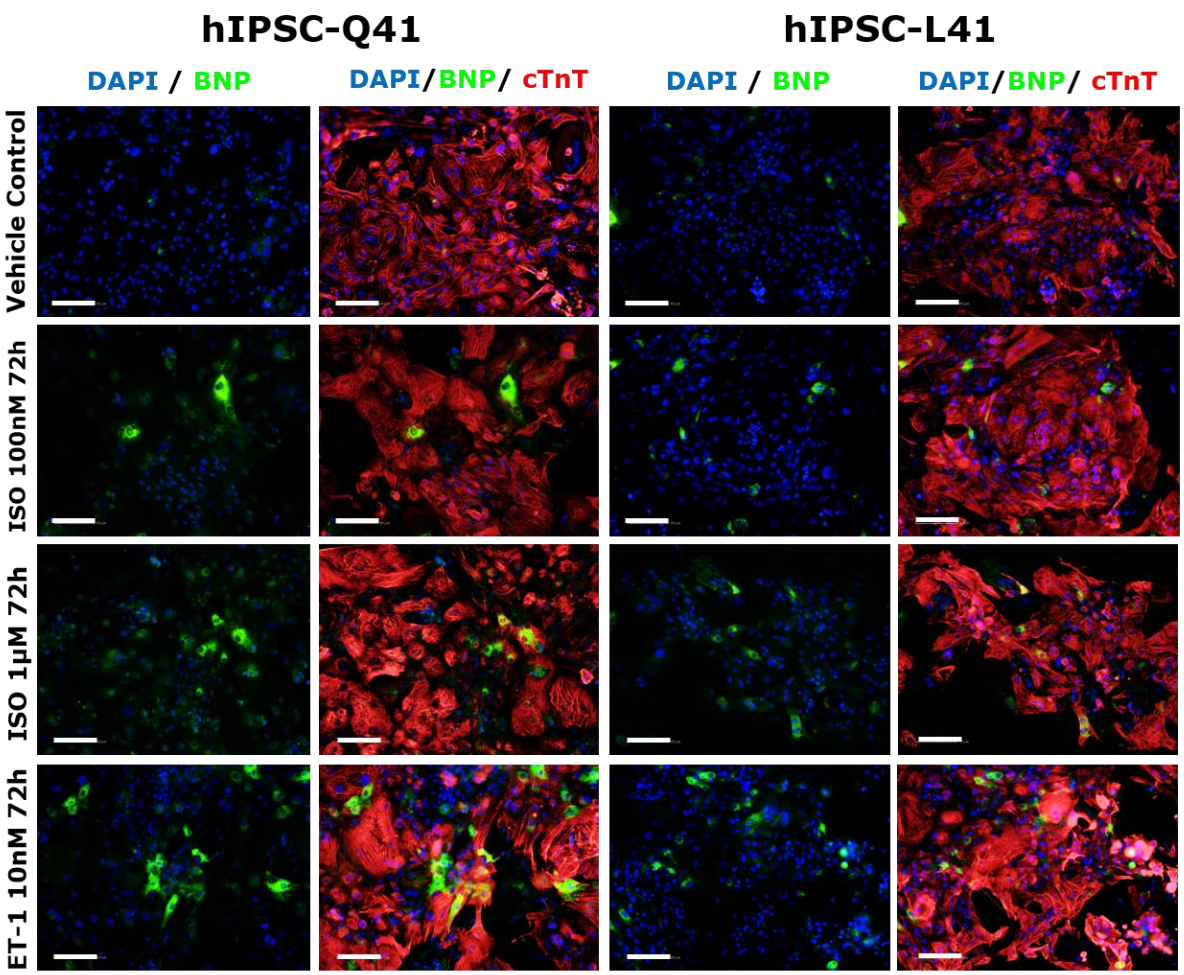

Figure 4.17. Hypertrophic response of the hIPSC-Q41L model during chronic ISO and ET-1 treatment.

Representative immunofluorescent images of BNP expressed CMs with DAPI (blue), cTnT (red) and BNP (green), scale bar 100 µM. The chronic ISO and ET-1 treatments for 72h showed upregulation of BNP production in all haplotypes, where BNP expressions of L41 and Q/L41 variants were observed higher than Q41 variant

4.4 Discussion:

The GRK5-L41 variant showed cardioprotective phenotypes in reducing cell death and maintaining cardiac contractility function during chronic catecholamine stress. In this chapter, the changes of GRK5 distribution in the nuclei and cytoplasm during chronic catecholamine stress was examined to investigate the correlation between the previous phenotypes and subcellular GRK5 distribution. Changes in subcellular GRK5 distribution was inspected by western blot analysis and quantification of fluorescence GRK5 intensity. In both assays, the GRK5-Q41 variant in the isogenic model showed an increase in the nuclear GRK5 fraction upon chronic ISO stress, but this nuclear accumulation was not observed in the hIPSC model. Since noncanonical functions of accumulated nuclear GRK5 could attribute to hypertrophy and HF progression, the hypertrophic responses of GRK5-Q41L variants of isogenic and hIPSC systems were next examined by quantifying BNP expression induced during chronic ISO stress. The BNP induction related to hypertrophic responses, however, showed conflicting responses between the isogenic and hIPSC models. These results together suggested that the reduction of non-canonical localisation of nuclear GRK5 in the L41 variant may not the main pathway that accounted for their cardioprotective effects.

4.4.1 Investigation of subcellular GRK5 distribution by western blot and immunocytochemistry:

The optimisation for the nuclear and cytoplasmic loading control was important for densitometry analysis of subcellular GRK5. To avoid the stripping and reprobing process, β-Actin and TBP were chosen because their protein bands (~ 40 kDa) were relatively separated from GRK5 bands (68 kDa). Therefore, each blotted membrane could be cut and be separately

probed for GRK5 and its subcellular loading control. The purity of cardiomyocytes, which were more than 84% purity in all lines, was important to prove that the obtained results are representative in cardiomyocytes (**Figure 4.2.F**).

The immunofluorescent staining of GRK5 protein was used to visualise the localisation of GRK5 in hPSC-CMs. GRK5 protein presented both in the nuclei and cytoplasm, where it was preferentially located in the cell membrane (**Figure 4.7 & Figure 4.12**). The intense GRK5 in defined granular patterns in the nuclei may suggest its localization in the nucleoli. GRK5 was reported to colocalise with Coilin, where this protein can bind to nucleoli (Yi et al., 2002). To further confirm the localisation of GRK5 in the nucleoli, GRK5 staining would need to be colocalised with a nucleolar marker. Coilin was reported to be involved in the transcription and processing of nuclear RNA suggesting that GRK5 may function in RNA biogenesis and post-transcriptional regulation in hypertrophy (Machyna et al., 2015). However, this aspect has not been well studied.

The subcellular distribution of cardiac GRK5 in unstimulated GRK5-Q41 and GRK5-L41 mice was not significantly different (Liggett et al., 2008), but there was no study of subcellular GRK5 distribution of cardiac GRK5-Q41L variant during chronic ISO stress. GRK5 translocation to the nuclei induced during ISO stress does not consistently occur when an increase of nuclear GRK5-Q41 fraction was only observed in the isogenic lines but not in the hIPSC (**Figure 4.4 & 4.11**). The GRK5-L41 variant of both isogenic and hIPSC models in immunocytochemistry assay (**Figure 4.11**) exhibited a reduction of nuclear GRK5 accumulation upon the ISO stress; however, these significant reductions of nuclear GRK5 was not significantly detected in western blot analysis (**Figure 4.4 & 4.6**). The changes of nuclear GRK5

distribution in GRK5-Q41L in the isogenic and hIPSc were not reproducible and consistently robust to considered as a phenotype of GRK5-Q41L.

4.4.2 The fetal phenotype of hPSC-CMs make them not an ideal model to study nuclear GRK5 translocation:

The hypertrophic response assay was developed by quantification of BNP intensity expression in hPSC-CMs during hypertrophic stimulation by ET-1, PE and AngII (**Figure 4.14**). Among three hypertrophic stimuli, only ET-1 efficiently induced upregulated BNP expression, while AngII and PE with varied concentration range exhibited no significant increase of BNP expression. The saturated induction level of ET-1 indicated that this dilution range is out of dynamic range and the lower dilutions should be conducted for the ET-1 dose-response curve. In contrast, the higher dilutions of PE and AngII may be necessary for BNP induction. Indeed, our qPCR of Angiotensin Receptor type II mRNA in section 3.3.4 were not detected in the hPSC-CM d30 model (**Figure 3.12**). The absence of *AGTRII* mRNA may be a feature of fetal cardiomyocytes and explained for the low BNP induction by AngII treatment. The low BNP induction response during PE treatment could be explained by the silence of α-AR (*ADRA1A*) in hIPSC-CMs during cardiac differentiation (Földes et al., 2014). Nuclear translocation of GRK5 in pathological hypertrophy was reported to occur via Gq dependent pathway during AngII and PE treatment, while ET-1 does not cause nuclear GRK5 translocation (Gold et al., 2013; Hullmann et al., 2014; Traynham et al., 2015). The hPSC-CMs was not an ideal model to study the effects of GRK5-Q41L variants on the nuclear GRK5 translocation during AngII and PE treatment.

4.4.3 Quantify BNP expression intensity to investigate hypertrophic response in hPSC-CMs:

The chronic ISO treatment could stimulate a hypertrophic response in hPSC-CMs. In the isogenic model, HUES7-L41 and HUES7-Q/L41 exhibited significantly higher BNP upregulation compared to HUES7-Q41 (**Figure 4.15)**. Even though BNP was used as a hypertrophy marker, BNP was proved to have antihypertrophic and antifibrotic effects on cardiomyocytes. Indeed, BNP protects the heart from adverse consequences of overload and inhibits the renin-angiotensin-aldosterone system, and counteracting cardiac hypertrophy and fibrosis (Gardner, 2003; Li et al., 2015; Vuolteenaho et al., 2005). The consistent high expression of BNP expression in HUES7-L41 and HUES7-Q/L41 could be regarded as a compensatory mechanism affording beneficial myocardial effects to slow the progression of heart failure. The high BNP production in L41 shows positive effects to compensate in response to hypertrophic stress.

As BNP is an endocrine hormone synthesized by human cardiac myocytes, BNF mRNA was found upregulated and was released at 18h after myocardial infarction induced by isoproterenol injections in rats (Sergeeva and Christoffels, 2013). Therefore, the measurement of BNP intensity during chronic ISO and ET-1 may not present for the total BNP production of cardiomyocytes. This may explain why the general maximum BNP intensity was detected at 24h and this intensity then reduced during treatment (**Figure 4.15**). Therefore, quantification of BNP released in the spent media by other ELISA-base assays may be necessary to enhance the accuracy of BNP production quantification for any long-term treatment.

Chapter 5 Mechanism of GRK5-Q41L

5.1 Introduction:

5.1.1 Extracellular signal-regulated kinase 1/2 (ERK1/2) is a regulator of cardiac hypertrophy:

5.1.1.1 The mitogen-activated protein kinase (MAPK) signalling pathways

Cardiac hypertrophy is a compensatory mechanism to enhance the cardiac output during detrimental stress (Gallo et al., 2019; Kontaridis et al., 2015). The mitogen-activated protein kinase (MAPK) signalling pathway plays an important role in the regulation of cardiac hypertrophy. The MAPK pathway, also known as RAS-RAF-MEK-ERK, is activated by receptor tyrosine kinase (RTKs) upon the binding by extracellular mitogenic ligands. MAPK signalling is generally categorized into three main subclasses, including ERK1/2, p38 kinase and c-Jun N-terminal kinase (JNK). Indeed, ERK1/2 is known to be activated in response to almost every hypertrophic- or stress-stimulation suggesting this role as a central regulator in the early phase of hypertrophy response (**Figure 5.1**). ERK1/2 signalling induces adaptive concentric hypertrophy and cell death prevention (Gallo et al., 2019; Kang et al., 2016). However, specific ERK-associated scaffold protein is also associated with the pathological form of hypertrophy. Meanwhile, JNK and p38 kinase, are involved in the maladaptive hypertrophy

5.1.1.2 Extracellular signal-regulated kinase 1/2 (ERK1/2):

ERK1/2 signalling is activated in cardiac myocytes in response to stress stimulation (Gallo et al., 2019; Mutlak et al., 2018). During β-AR signalling stimulation, ERK1/2 is activated via numerous pathways (**Figure 5.2**). The most thoroughly studied β-AR stimulating ERK pathway is via G protein-dependent pathway, where Gαs activation generates cAMP/PKA, which then

activates RAS/RAF/MEK1/ERK1/2 signalling (Lefkowitz et al., 2002). The Gαi-mediated stimulation of ERK via β2-AR use a Gβγ subunit-mediated mechanism to trigger Ras-dependent ERK1/2 activation (Lefkowitz et al., 2002; O'Hayre et al., 2017). In the last decades, more studies have proven that ERK1/2 can also be activated via G protein independent pathway or β-arrestin dependent pathway for both β1-AR and β2-AR, where this pathway mediates transactivation of epidermal growth factor receptor (EGFR) (Grisanti et al., 2014; Luttrell et al., 2018; Noma et al., 2007). ERK1/2 can phosphorylate their cytosolic substrates or can translocate to the nucleus and phosphorylate multiple substrates, including transcription factors as CREB, c-Myc, GATA4 or Elk1. The activation of ERK1/2 signalling has been shown to induce cardioprotection through modulation of apoptosis (Bueno et al., 2000; Grisanti et al., 2014; Noma et al., 2007). The direct mechanism of cardioprotective functions of ERK1/2 from apoptosis has not definitively identified. However, an association of ERK1/2 level and BCL2 protein family, including BCL2, BAD and Bcl-xl protein has been shown (Ahn et al., 2009; Aries et al., 2004; Ding et al., 2005, p. 3; Shin et al., 2014; Wang Yibin, 2007).

On the other hand, specific ERK-association scaffold protein associated with pathological hypertrophy, whereby the ERK1/2 autophosphorylates at Threonine 188 (ERK^{Thr188}) (Lorenz et al., 2009; Ruppert et al., 2013; Vidal et al., 2012). This autophosphorylation of ERK induces its nuclear accumulation and mediates maladaptive cardiac hypertrophy. The autophosphorylation of Thr188 is produced via the G protein-dependent pathway by direct interaction between the Gαs-derived Gβγ subunits of the activated receptor and the activated ERK. Thus, targeting this autophosphorylation was indicated as a promising pharmacological

therapeutic to manage the pathological hypertrophy progression (Gallo et al., 2019; Vidal et al., 2012).

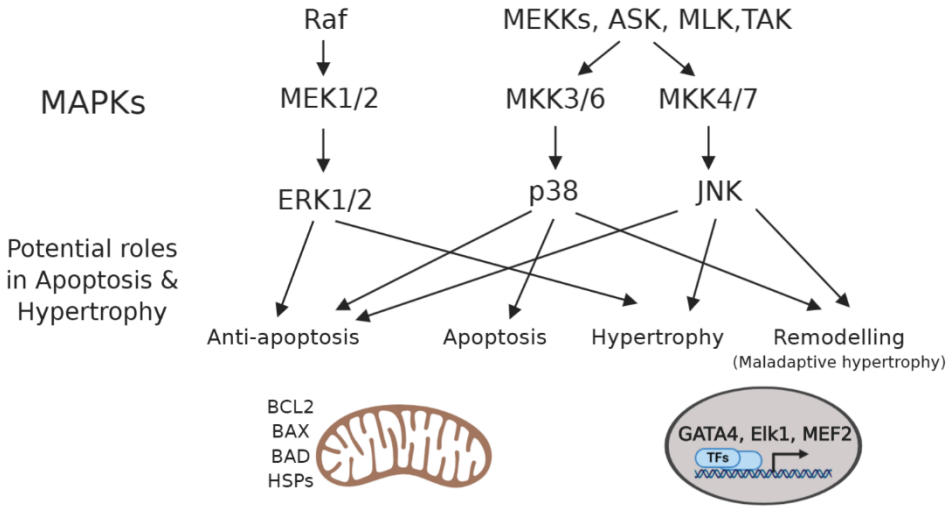

Figure 5.1.MAP kinases and their potential roles in cardiac survival and hypertrophy regulation.

The three major subclasses of MAPK are ERK1/2, p38 and JNK and their potential roles in apoptosis and hypertrophy response. MEKK, MAP kinase, kinase, kinase; MLK, mixed-lineage kinase; ASK, apoptosis signal-regulating kinase; TAK, TGF-β–activated kinase; MEK or MKK, MAP kinase, kinase; HSP, heat shock proteins; GATA, GATA binding transcription factor; MEF, myocyte-specific enhancer-binding nuclear factor; Elk1, ETS Like-1 protein. (Adapted from Wang, 2007)

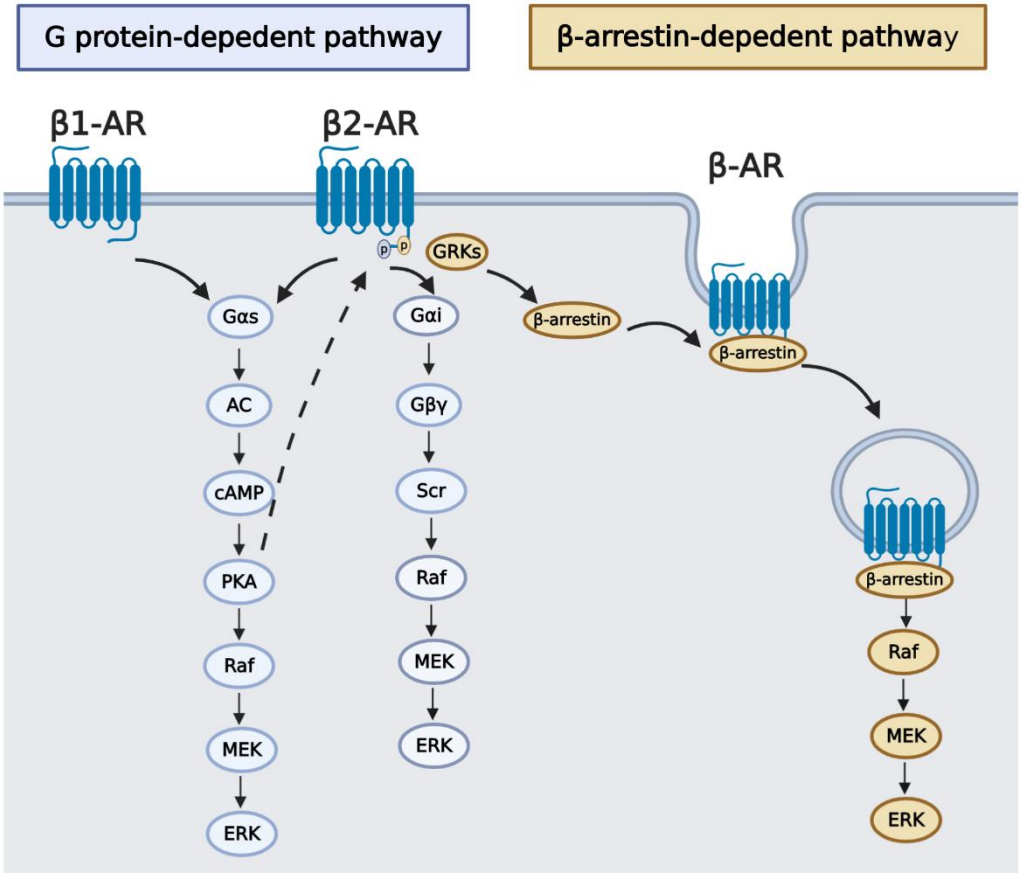

Figure 5.2. Scheme of ERK activation by the β-AR via G protein-dependent pathway and β-arrestin dependent pathway.

β1-AR mediate ERK activation via the Gs pathway, while β2-AR can mediate ERK activation via Gs and Gi. The phosphorylation of β2-AR by Gi switch β2-AR coupling to Gi in T-tubules of cardiomyocytes. ERK activation can be mediated via β-arrestin pathways, when β-arrestins bind to different effectors, subsequently inducing ERK signalling. (Adapted from Lefkowitz et al., 2002).

5.1.2 Roles of GRKs in regulation GPCR signalling:

5.1.2.1 The roles of GRKs in GPCR desensitisation:

In the classical paradigm, GPCRs transduce signalling through G proteins, also referred to as a G protein-dependent mechanism (Lefkowitz et al., 2002; Pierce et al., 2002). However, studies have shown that GPCR function and signalling are regulated through GRK/β-arrestin dependent mechanisms. β-arrestin1 (or arrestin2) or β-arrestin 2 (or arrestin 3) are ubiquitously expressed cytosolic adaptor proteins. Their roles were originally discovered as inhibitors of GPCRs after phosphorylation by GRKs

The process of GPCR desensitisation involves phosphorylation at certain serine and threonine residues on the third intracellular loop (ICL) and the carboxyl-terminal tail (C terminus) by the second messenger-dependent kinases (e.g, PKA or PKC) and –independent kinases (GRKs) (Pierce et al., 2002; Wang Jialu et al., 2018) (**Figure 5.3**). In β-AR signalling, heterologous desensitisation is mediated by second messenger kinases to uncouple their associated G proteins and thus terminating signalling. PKA phosphorylated β-ARs do not recruit β-arrestin and thereby receptor internalisation is not mediated. However, PKA-mediated phosphorylation of β2-ARs decreases affinity to Gαs thereby promoting its coupling to Gαi protein and Gαi pathway instead of Gαs pathway. However, the lack of T-tubules, which is important for β2-AR and Gαi coupling, in hPSC-CMs may change the classical cardioprotective function of β2-AR via the Gαi signalling pathway (Dorn, 2010b; Gorelik et al., 2013; Paur Helen et al., 2012; Schobesberger et al., 2017).

Homologous desensitization is mediated by phosphorylation of GRKs, which is second messenger-independent, at serine and threonine residues at the C-terminus of GPCRs (Nobles et al., 2011; Wang Jialu et al., 2018; Yang

et al., 2017) (**Figure 5.3**). Upon phosphorylation of GPCRs by GRKs, β-arrestins are recruited to GPCRs and form GPCR-β-arrestin complex. The binding of β-arrestin not only inhibits G protein coupling but also promotes receptor internalisation. β-arrestins in the GPCR-β-arrestin complex interact with clathrin and the clathrin adaptor protein 2 (AP2). These interactions thereby target the attached receptor to the clathrin-coated pits and promote internalisation of the activated receptor. The internalised GPCRs can be rapidly recycled to the plasma membrane, or go through prolonged internalisation to the late endosome, where they can slowly recycle to the membrane or undergo degradation in the endosome (Lefkowitz et al., 2006; Luttrell and Lefkowitz, 2002; Rockman et al., 2002). In this paradigm, the chronic induction of this signalling pathway induces cardiac apoptosis so that internalised β-ARs will not be available for persistent catecholamine stimulation to reduce Gαs signalling (Dries et al., 2016; Kang et al., 2016; Lohse Martin J. et al., 2003; Shin et al., 2014).

Recent studies have shown β-arrestins not only mediate GPCR desensitisation and internalisation to regulate G protein-dependent signalling amplification but also function as signal transducers for the second wave signalling occurring in endosomes via G protein-independent/ or β-arrestin- dependent mechanism (A. Grisanti et al., 2019; Carr et al., 2016; Gurevich and Gurevich, 2019; Luttrell et al., 2018; Noma et al., 2007). In Oakley *et al.* study of the interaction between GPCRs and arrestins, GPCRs are divided into two classes based on the stability of the GPCR-arrestin complex (Oakley et al., 2000). Class A GPCRs, such as β-ARs, interact with β-arrestin transiently and form a weak GPCR-β-arrestin binding complex, while class B GPCRs, such as Vasopressin receptor 2 (V2R), form a strong interaction with β-arrestin. β-arrestins function as multifunctional adaptors

and signalling transducers, linking to signalling molecules, such as MAPK, Scr, PDE and Akt, whereby ERK1/2 and Akt enhance cardiac survival and PDE4 negatively regulate cAMP during β-AR signalling stimulation (A. Grisanti et al., 2019; Baillie et al., 2003; Gurevich and Gurevich, 2019; Lefkowitz et al., 2006; Luttrell et al., 2018).

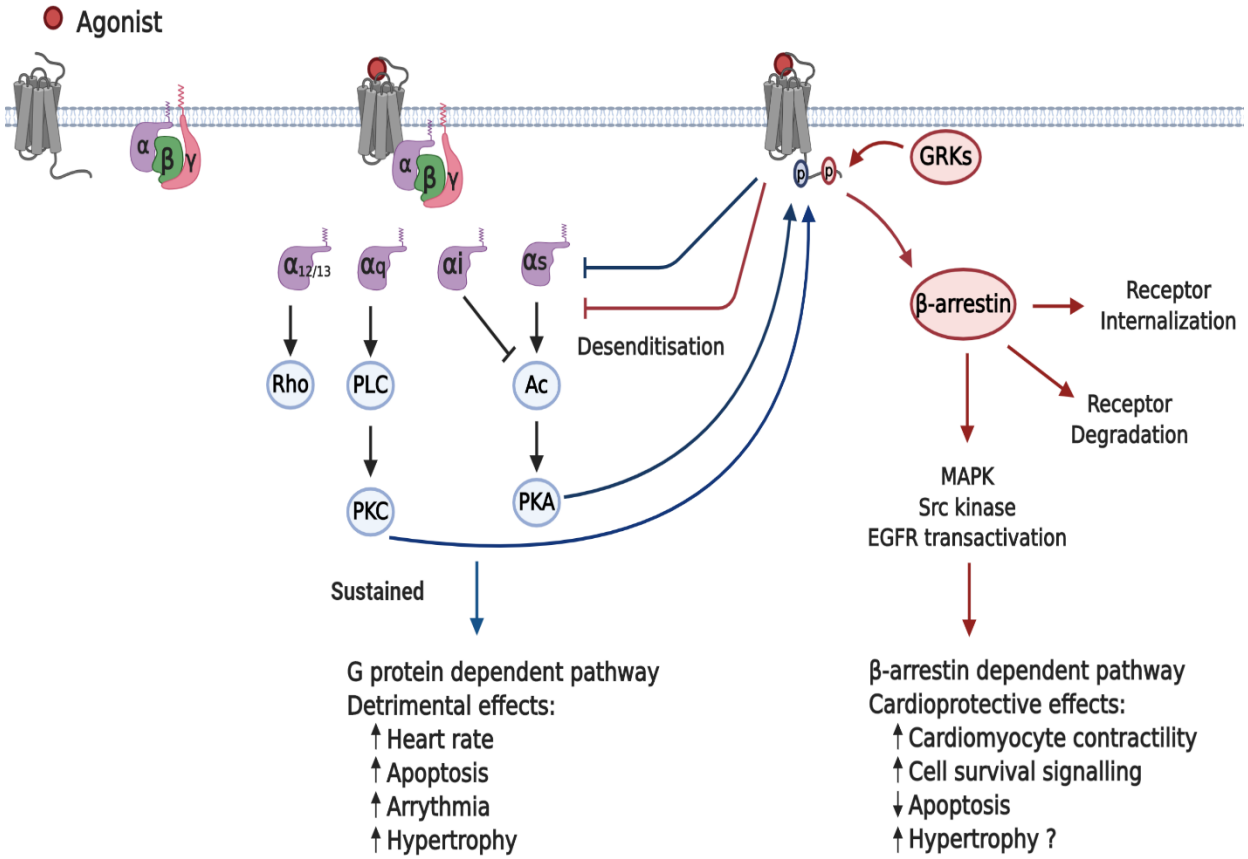

Figure 5.3. Scheme of GPCR signalling via G protein-dependent pathway and β-arrestin dependent pathway.
Activated GPCRs interact with heterotrimeric G proteins, whereby the α and βγ subunits then dissociate and subsequently activate downstream signalling effectors. G-protein–activated PKC (protein kinase C) and PKA (protein kinase A) in turn phosphorylates the receptor and turns off the G-protein signalling (heterologous desensitization, blue line, and blue phosphate). GRKs mediated GPCR phosphorylation leads to the recruitment of β-arrestins, resulting in homologous desensitization (red line and red phosphate), subsequent receptor internalization and degradation. This also activates β-arrestin–mediated signalling. Sustained G protein signalling (β-AR and AT1R) is associated with deleterious cardiac effects, while β-arrestin signalling may be beneficial for cardiac function. AC indicates adenylate cyclase; EGFR, epidermal growth factor receptor; MAPK, mitogen-activated protein kinase; Src non-receptor tyrosine kinases. (Adapted from Wang Jialu et al., 2018)

5.1.2.2 Distinct phosphorylation sites on the GPCR establish barcode encoding differential function of β-Arrestin

As explored in the previous section, activated GPCRs can be phosphorylated by either second-messenger kinases or GRKs following by β-arrestin binding. GPCR phosphorylation by different kinases can differentially regulate G protein signalling or mediate distinct downstream signalling.

These findings introduce the hypothesis whereby the phosphorylation by different kinases/GRKs imprint "barcodes" to instruct the bound β-arrestins to regulate receptor desensitisation, receptor recycling and subsequent endosome signalling (Xiao and Liu, 2016; Yang et al., 2017). Using mass spectrometry, Nobles identified multiple phosphorylation sites of β2-AR and used β2-AR as a model receptor to prove the "barcode" hypothesis (Nobles et al., 2011) (**Figure 5.4**). This study on HEK293 cells identified twelve phosphorylation sites mediated by PKA, GRK2 and GRK6 upon ISO stimulation. Indeed, S261/S262 and S345/S346 are sites for ISO-promoted phosphorylation by PKA. GRK2 is mainly responsible for the phosphorylation of T360, S364, S396, S401, S407, and S411, while GRK6 is mainly responsible for phosphorylation of S355 and S356. This study also showed GRK6 is responsible for ERK1/2 activation mediated via β-arrestin, while GRK2 is opposed to it. In other studies on baculovirus-infected Spodoptera frugiperda cells and COS-7 cells, GRK5 phosphorylate β2-AR at S355, S356, T360, S364, T384, T393, S396, S401, S407, and S411 (Fredericks et al., 1996; Komolov et al., 2017; Millman et al., 2004).

Furthermore, more detailed studies showed that β2-AR phosphorylated by either GRK2 or GRK6 stimulated distinct conformational changes of β-arrestin and elicit subsequent differential signalling responses (Charest et al., 2005; Shukla et al., 2008). In particular, these studies showed GRK2

phosphorylated β2-AR promotes β-arrestin1/clathrin complex formation leading to receptor internalisation. GRK6 phosphorylated β2-AR promotes β-arrestin1/Scr complex inducing ERK1/2 activation. In contrast, β2-AR phosphorylated by PKA did not promote formation with either β-arrestin1/clathrin or β-arrestin1/Scr. In line with Nobles *et al* study, these results explained why GRK6 is important for ERK1/2 activation, whereby S355 and S356 phosphorylation sites would be important for β-arrestin1/Scr complex recruitment. There was no study of β2-AR phosphorylated by GRK5 in promoting ERK1/2 signalling; however, V2R and Angiotensin II type 1 receptor (AT-1R) phosphorylated by GRK5 and/or GRK6 induced ERK1/2 activation via β-arrestin2 mediating pathway (Heitzler et al., 2012; Nobles et al., 2007, p. 1; Xiao et al., 2004, p. 2). In line with these studies, Norma showed that GRK5 and GRK6 phosphorylation, but not GRK2 and GRK3, are required in promoting β1-AR-mediated EGFR transaction and ERK activation (Noma et al., 2007). This study on HEK293, U2S sarcoma cells and adult mice myocytes proved that the EGFR transactivation-mediated by β1-AR via β-arrestin pathway confers cardioprotection to counteract the cardiotoxicity effects from sustained induction of the G protein pathway. These studies prove the barcode theory, wherein different ligands stabilized different receptor conformations which subsequently recruit unique GRKs to imprint distinct phosphorylation barcodes on the receptor (**Figure 5.4.C**). As a consequence, these distinct phosphorylation barcodes promote β-arrestin binding and induce differential conformation changes on β-arrestin, which in turn, promote binding of different signalling transducer molecules to activate specific downstream signalling in endosomes. There are not many studies on these pathways for β1-AR. Rapacciuolo showed that PKA-mediated phosphorylation of β1-AR induced receptor internalization via a caveolae

pathway, while GRK-mediated phosphorylation promoted it through clathrin-coated pits (Rapacciuolo et al., 2003).

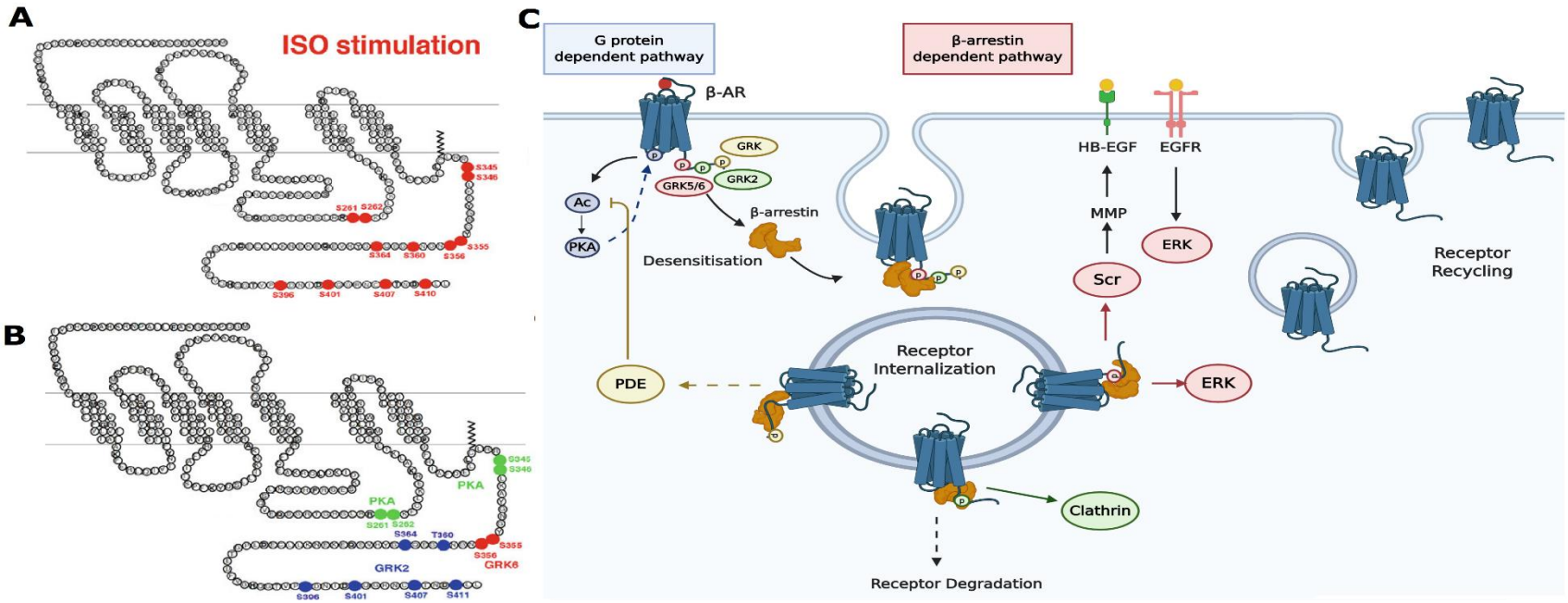

Figure 5.4. Modes of phosphorylation barcoding.

(A) Mass spectrometry analysis of ISO stimulated β2-AR phosphorylation. (B) Mass spectrometry analysis of GRK2 and 6 phosphorylate different sites on the β2-AR stimulated by ISO. (C) Model of β-AR phosphorylation at multiple sites upon ISO stimulation, resulting β-arrestin recruitment, which mediates receptor desensitisation and internalisation. Different phosphorylation patterns encoded by different GRKs transduced specific information to dictate distinct β-arrestin conformation and functional outcomes. Whereas the GRK2-mediated (green) phosphorylation sites recruit clathrin, the GRK5/GRK6 mediated (red) phosphorylation pattern selectively activates ERK1/2 signalling. The interactions of arrestin and other effectors, such as PDE(phosphodiesterase) are potentially regulated by different (yellow) phosphor-barcodes (Adapted from Nobles et al., 2011).

5.2 Chapter Aims and Objectives:

ERK1/2 signalling, which is activated during catecholamine stress, plays critical roles in myocyte survival and hypertrophy regulation. The aim of this chapter was to investigate the effects of the GRK5-Q41L variant on ERK1/2 activation and provide insight into the mechanism for the gain-of-function of GRK5-Q41L. Further experiments in this chapter focused on the isogenic HUES7-Q41L model because the hIPSC-Q41L model has a heterogenic background and exhibited an inconsistent phenotype. The objectives were:

1. Characterise activation of ERK1/2 activation in isogenic HUES7-Q41L CMs during ISO stimulation.
2. Investigate how GRK5 is involved in ERK1/2 activation in our isogenic HUES-Q41L model during ISO stimulation by inhibiting GRK5 activity and ERK1/2 activation with chemical inhibitors.
3. Investigate roles of GRK5 activity and ERK1/2 activation in contractility response and cell survival response during chronic catecholamine stress by inhibiting either GRK5 or ERK activity to explore the association of the GRK5-Q41L variant on ERK1/2 activation.

5.3 Results:

5.3.1 Characterise kinetics of ISO induced stimulation of ERK1/2 signalling:

The ERK1/2 signalling, which is activated during catecholamine stress, plays critical roles in myocyte survival and hypertrophy regulation (Gallo et al., 2019; Luttrell et al., 2018). To characterise the kinetics of ERK1/2 activation during ISO stimulation in our hPSC-CM model, cardiomyocytes were incubated with vehicle treatment (0h) and 1 μM ISO for 5, 10, 30 and 60 min. Equal amounts of cell lysate were subjected to western blot analysis to quantify the amount of phosphorylated ERK1/2 (pERK) activation over total ERK1/2 using densitometry analysis.

The blotted membranes of the timecourse of ISO stimulating pERK activation in our isogenic HUES7-Q41L are presented in **figure 5.5.A**. In the vehicle-treated condition (0 h), there was a low amount of pERK activated in both the Q41 and L41 variants. Activation of ERK1/2 was observed after 1 μM ISO adding at 5 min and the maximum pERK activation peaked at 10 min after ISO stimulation.

Interestingly, densitometry analysis showed the amount of pERK activation obtained in the HUES7-L41 variant was consistently higher compared to HUES7-Q41 after normalisation to their vehicle treatment at both 5 and 10 min. The amount of pERK production in HUES7-L41 CMs significantly increased 9.7-fold and 13.3-fold after 5 min and 10 min of ISO stimulation (**Figure 5.5.B**, * $p < 0.05$, ** $p < 0.01$). HUES7-L41 CMs only showed a significant increase of pERK activation after 10 min of ISO induction (~8.7-fold), in which fold-increase was lower than the fold-increase of pERK in the L41 variant at 5 min. The amount of pERK activation in both haplotypes declined quickly after 30 min of ISO addition and was

close to basal level at 60 min after the treatment. These western blot analysis showed that ERK1/2 activation was stimulated during ISO treatment and the L41 variant mediated a higher amount of pERK activation compared to the Q41 variant.

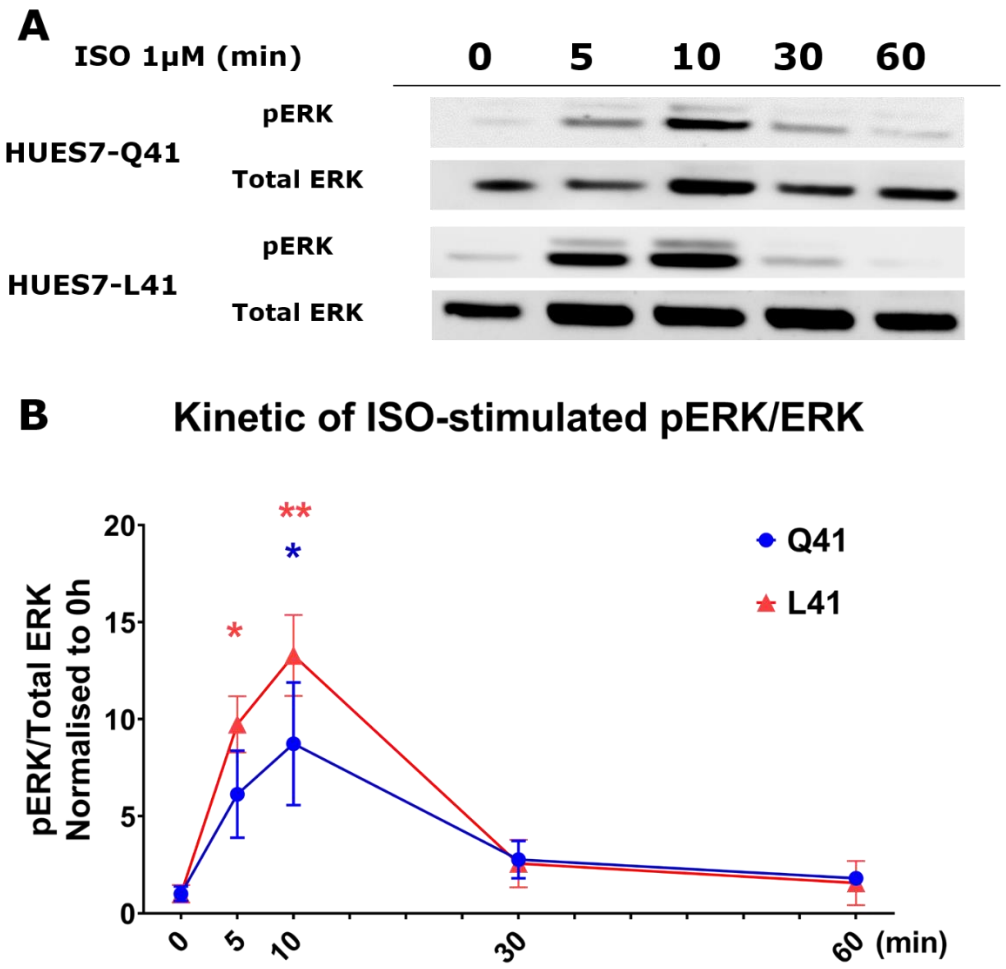

Figure 5.5.Kinetics of ERK1/2 activation in isogenic HUES7-Q41L CMs during ISO stimulation.

(A) Western blot of phosphorylated ERK1/2 (pERK) and total ERK presented at 44 kDa and 42 kDa. (B) Densitometry analysis of pERK activation during timecourse ISO-stimulated 5, 10, 30, 60 min and vehicle control was analysed, represent means ± SEM, n=3 biological replicates. *p<0.05, **p<0.01. Colour-coded according to ISO induction time compared vehicle control within the same cell lines; Two-way ANOVA with Dunnett's multiple comparison tests.

5.3.2 Identify an appropriate ISO concentration to stimulate ERK1/2 signalling in the isogenic HUES7-Q41L CM model:

To avoid using an oversaturating ISO concentration, which may erase the phenotype difference in pERK activation, half log dilution of ISO was conducted to produce an ISO-stimulating pERK curve. In the previous experiment, the maximum ISO-stimulating pERK was observed at 10 min after induction, HUES7-Q41L CMs were thereby exposed to different ISO concentration and vehicle treatment for 10 min.

The western blot analysis of pERK stimulated by different ISO concentration is illustrated in **figure 5.6.** A and further densitometry analysis is shown in **figure 5.6.B**. The blotted membranes showed that the pERK stimulation was increased in a concentration-dependent manner during 10 min incubation with ISO. The apparent increases of pERK activation were first observed at 30 nM ISO in both Q41 and L41 haplotypes. Using densitometry analysis of these blots to produce the ISO-stimulating pERK curve, we identified half-maximal effective concentration (EC_{50}) of ISO in both Q41 and L41 variant at 300 nM. ISO at 1 μM was subsaturated and induced ~ 70 % - 80 % of pERK activation, hence this ISO concentration was used to investigate the effects of Q41L variants on ERK1/2 signalling activation. Also, the densitometry analysis showed that the amount of pERK activation was significantly higher in L41 compared to Q41 in the ISO concentration at 1, 3 and 10 μM (**figure 5.6.C,** * $p < 0.05$, ** $p < 0.01$). The consistently higher induction of pERK in the L41 over Q41 variant was also observed in the previous experiment. This observation suggested that pronounced activation of ERK1/2 signalling in L41 over Q41 may be a phenotype for the gain-of-function of the L41 variant enhancing the cell survival during chronic ISO stress.

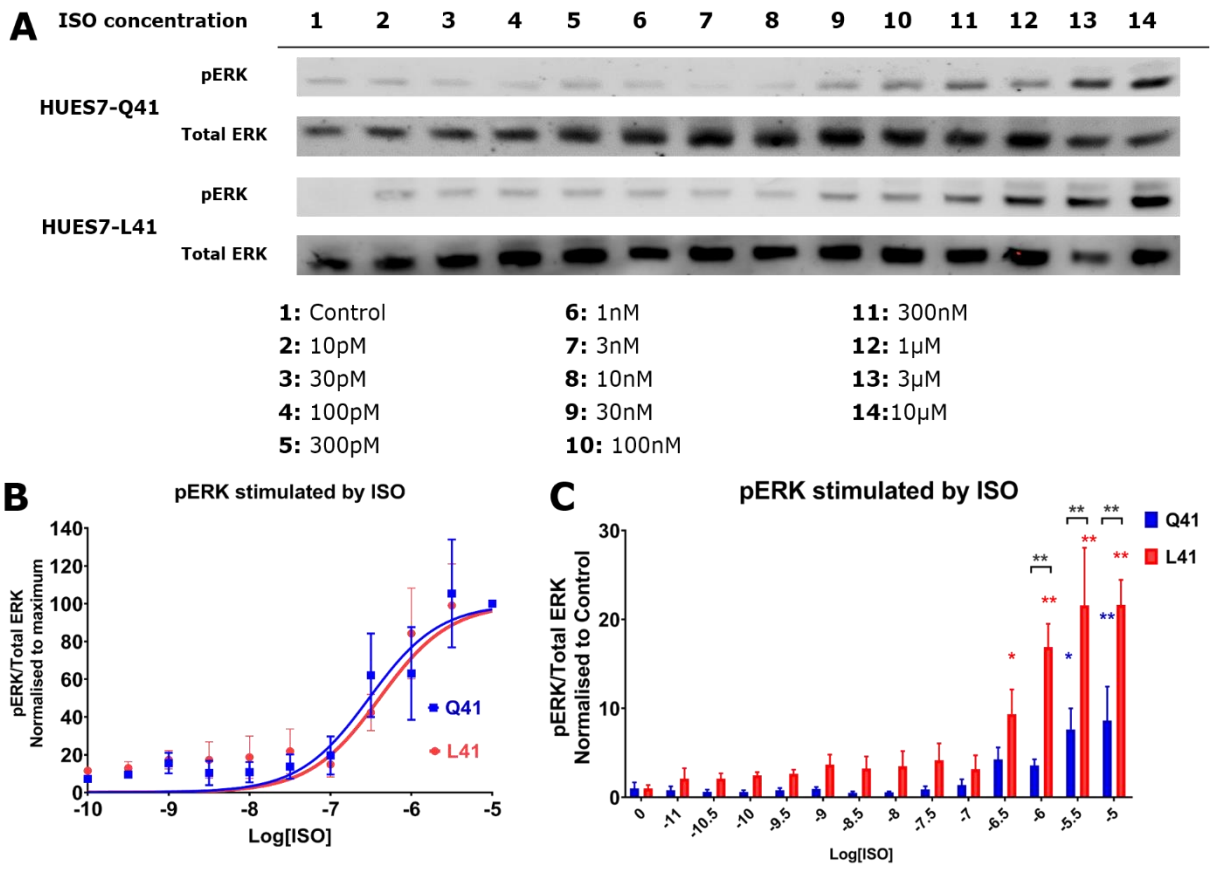

Figure 5.6. Western blot analysis of ERK1/2 activation in isogenic HUES7-Q41L CMs by different ISO concentration.

(A) Western blot analysis of pERK and total ERK were performed for various ISO concentration to avoid oversaturated ISO concentration during 10 min treatment (B) Half log stimulation curve of ISO activating pERK (C) Densitometry analysis of pERK activation for various ISO concentration after 10 min treatment, represent means ± SEM, n=3 biological replicates. *p<0.05, **p<0.01. Black asterisks indicated cross-comparison between Q41 and L41 variants. Colour-coded according to ISO induction time compared vehicle control within the same cell lines. Two-way ANOVA with Dunnett's multiple comparison test

5.3.3 Optimisation for inhibiting ERK1/2 signalling activation by chemicals to investigate roles of ERK1/2 signalling during chronic catecholamine stress:

In previous experiments, pERK1/2 activation was more pronounced in the L41 variant compared to the Q41 variant. To investigate the effects of ERK1/2 signalling on apoptosis responses in our HUES7-Q41-L CMs, different chemical inhibitors of activation of ERK1/2 were investigated.

PD98059 is a specific inhibitor of the activation of MEK1/MEK2, which is the upstream activator of the ERK1/ERK2 (Alessi et al., 1995). A concentration of 50 μM PD98059 sufficiently inhibited ~50 - 98 % of ERK1/2 activation in various cell types, including in mice and rat cardiomyocytes (Alessi et al., 1995; Ruppert et al., 2013; Stoll et al., 2002; Xiao et al., 2001; Yue et al., 2000). However, half-maximum inhibitory concentration (IC50) of PD98059 is relatively high at 50 μM and the maximum solubility of PD98059 in DMSO is 6.5 mg/ml (~ 24 mM stock). This means that a 50 μM concentration made in medium, which has a half-maximum inhibitory effect, already contains more than 0.2 % DMSO (v/v). This concentration of DMSO is toxic to the hPSC-CMs, particularly for long term experiments.

PD98059 at 50 μM was examined for its inhibitory effects on ERK1/2 activation. At these concentrations, apparent cell death was already observed without ISO stimulation in both haplotypes after 48h incubation (**Figure 5.7.A**). The issues of high IC_{50} and low solubility in PD98059 make it an inappropriate inhibitor for long term experiments.

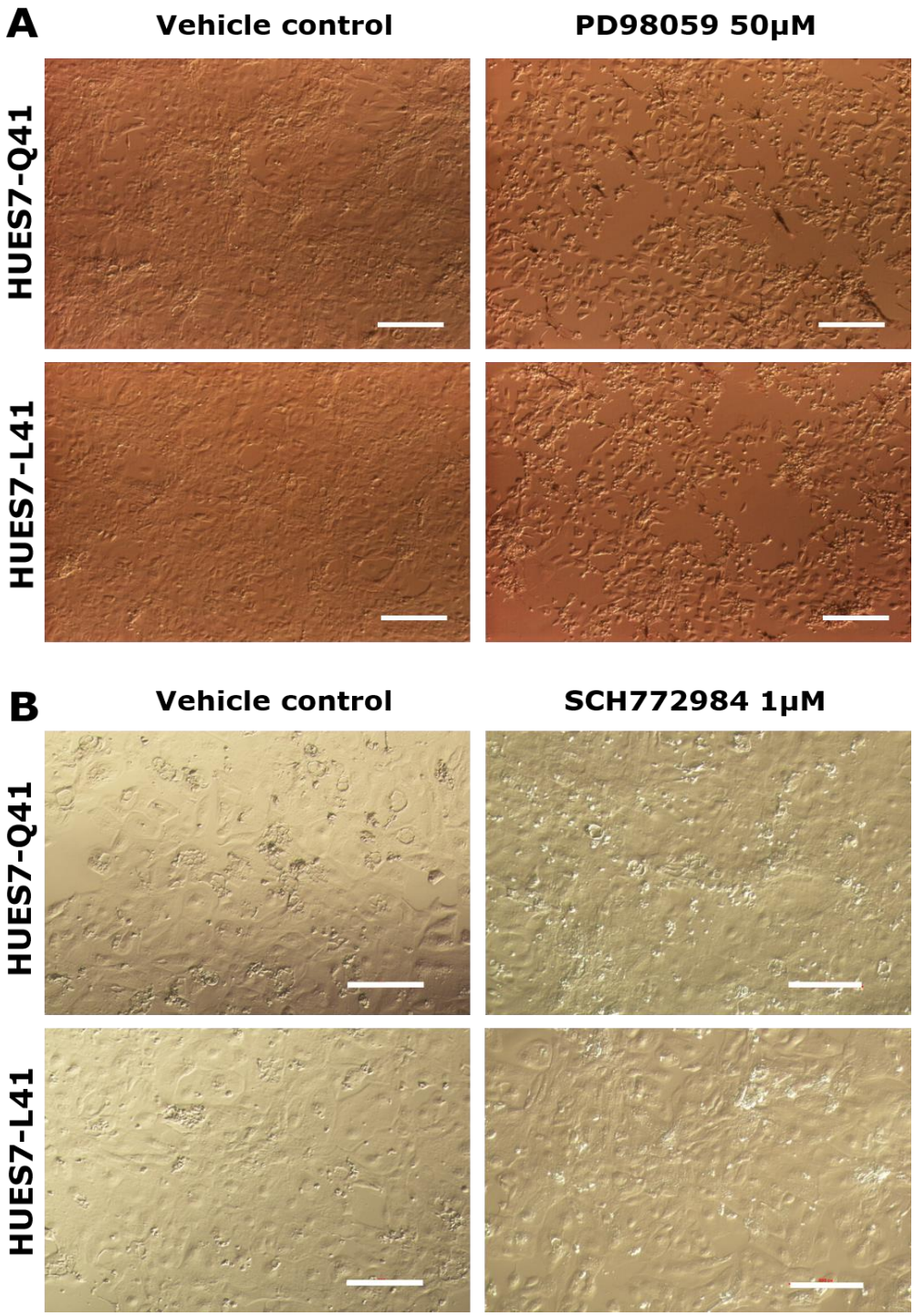

Figure 5.7. Cell death response during PD98059 and SCH772984 incubation for 48h.

Bright-field images of HUES7-Q41L CMs incubated with(A) 50 μM PD98059, scale bar 500μm, and (B) 0.3 μM SCH772984, scale bar 100 μm.

SCH772984 is another highly selective inhibitor of ERK1/2 activity with low IC_{50}, hence this was investigated (Chaikuad et al., 2014; Morris et al., 2013; Tong and Seeliger, 2015). SCH772984 simultaneously binds to the ATP binding pocket and the allosteric pocket of the kinase and has low IC_{50} for ERK1 (8.3 nM) and ERK2 (2.7 nM). This inhibitor was also 400-fold more selective for ERK1/2 over the off-target JNK1, which is also a member in MAPKs signalling (Chaikuad et al., 2014; Tong & Seeliger, 2015). SCH772984 at 1 and 5 μM was used to inhibit ERK1/2 activity in mice and rat cardiomyocytes (Kashihara et al., 2017; Wu et al., 2017). Incubation of 1 μM SCH772984 for 48h did not appear to induce cell death as had been seen with PD98059 (**Figure 5.7.B**). The half log dilution of SCH772984 (10nM -3 μM) was conducted for inhibiting ERK1/2 activation stimulated by 1 μM ISO exposure for 10 min. Cells were incubated with the SCH772984 inhibitor for 1h prior to ISO induction.

The blots presenting inhibitory effects of SCH772984 on ERK1/2 activation are shown in **figure 5.8**. Inhibition by SCH772984 in both Q41 and L41 variant was firstly observed at concentrations of 100 nM, whilst 300 nM inhibited ~ 90 % of pERK activation. Next, the stability of SCH772984 activity for 12h and 24h was examined to investigate how long the inhibitory effect was maintained. As SCH772984 showed similar inhibitory effects for both haplotypes, these experiments were only performed on the HUES7-L41 variant, since this had previously shown (**Figure 5.8**) a higher level of pERK action with ISO treatment.

HUES7-L41 CMs were incubated with SCH772984 at 300 nM, 1 μM and 3 μM for either 12h or 24h (**Figure 5.9.A & B**). The SCH772984 treated cardiomyocytes was then exposed to 1 μM ISO for 10 min to stimulate ERK1/2 phosphorylation. The blotted membrane and the densitometry

analysis showed that 300 nM SCH772984 could effectively maintain inhibitory effects of ERK1/2 activation for 24h. This stability of SCH772984 was important because the ISO treatment was also refreshed every 24h.

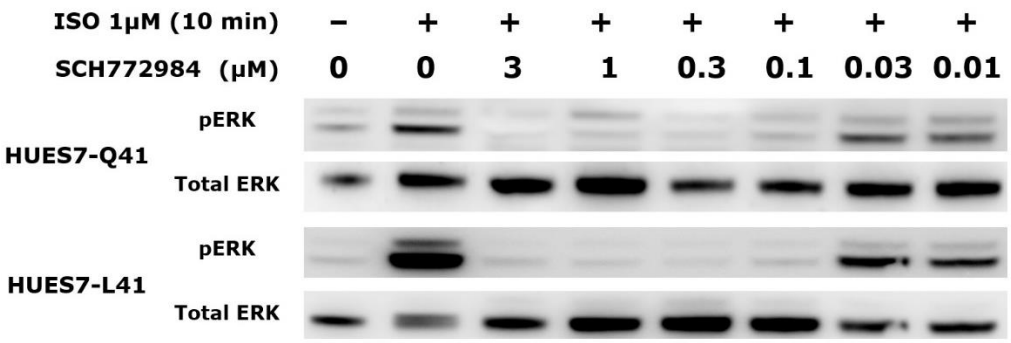

Figure 5.8. Western blot analysis for the inhibitory effect of different SCH772984 concentration on ERK1/2 activation stimulated by 1 μM ISO in isogenic HUES7-Q41L CMs.

Western blot analysis of pERK and total ERK were performed for various SCH772984 concentration during 1 μM ISO treatment for 10 min, n=2 biological replicates.

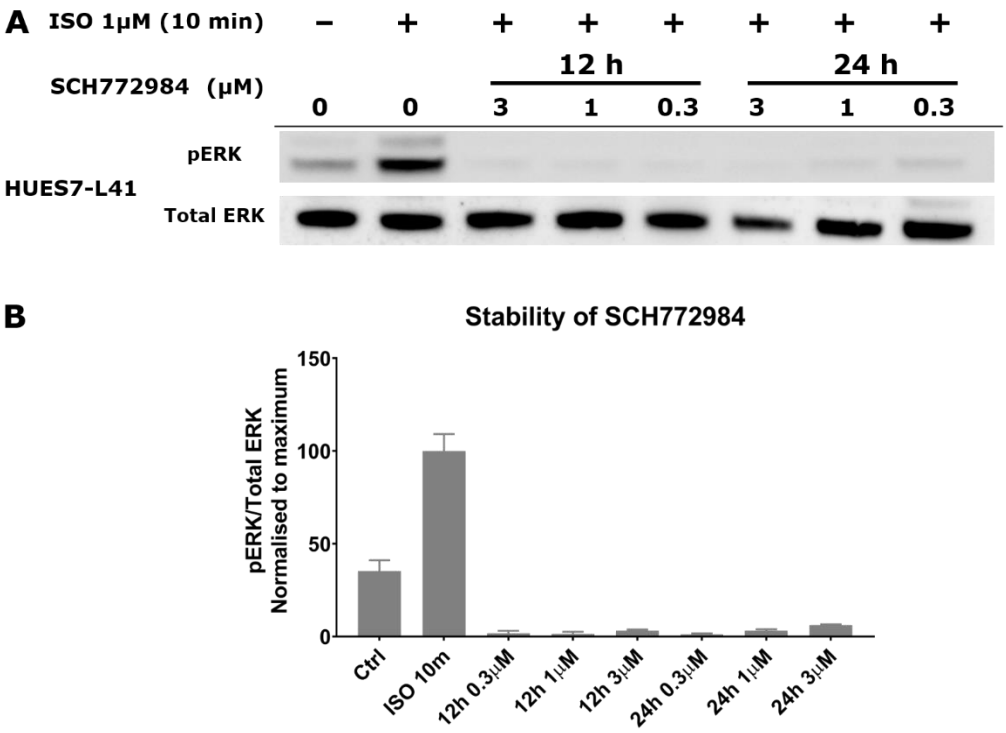

Figure 5.9. Stability analysis for the inhibitory effect of SCH772984 on ERK1/2 activation stimulated by 1 μM ISO in isogenic HUES7-L41 CMs.

(A) Western blot analysis of pERK and total ERK were performed for various SCH772984 concentration incubated for 12 h and 24 h before 1 μM ISO treatment for 10 min (B) Densitometry analysis of the blots showed that SCH772984 can effectively inhibit pERK activation up to 24 h, represent means ± SEM, n=2 biological replicates.

5.3.4 Optimisation for inhibiting GRK5 activity to investigate GRK5 roles in activating ERK1/2 signalling during chronic catecholamine stress:

The ERK1/2 activation stimulated by ISO treatment was characterised in previous experiments. To investigate the role of GRK5 in ERK1/2 activation during ISO treatment, we inhibited GRK5 activity by chemicals during ISO treatment and then investigate the amount of pERK production when the GRK5 activity was removed.

Relative to ERK signalling, far fewer specific inhibitors have been reported for GRK5. Homan screened 4480 compounds to identify selective inhibitor for GRK5, and he found Amlexanox as the best hit (Homan et al., 2014; Pfleger et al., 2019b). Further experiments showed Amlexanox inhibited GRK5 with 5-fold to 10-fold selectivity over the other GRKs, whereby Amlexanox was also found to directly bind to the active site of GRK5 to prevent downstream signalling. In their study, the use of 50 μM Amlexanox efficiently inhibited its downstream MEF2 signalling during PE-mediated α-AR signalling activation(Homan et al., 2014).

To reduce the off-target effects and avoid the use of oversaturating concentration, a half-log dilution curve of Amlexanox (0.5 μM - 500 μM) was produced for inhibiting GRK5 activity during 1 μM ISO exposure for 10 min (**Figure 5.10)**. Cardiomyocytes in both haplotypes were incubated with different Amlexanox concentration for 1h prior to ISO treatment. In this experiment, a basal level of pERK activation was observed in vehicle-treated control on both haplotypes.

In general, the GRK5 inhibitor, Amlexanox, did not completely inhibit all of the pERK activations. However, Amlexanox treatment from 50 μM to 500 μM efficiently reduced a large amount of pERK activated by ISO

treatment. 50 μM of Amlexanox was chosen for further experiments because this concentration was effective in inhibiting GRK5 activity in these two experiments. Also, Amlexanox at 150 μM to 500 μM was high, which raise concerns about off-target effects.

To investigate the role of GRK5 in ERK1/2 activation during ISO stimulation, cardiomyocytes in the isogenic HUES7-Q41L model were treated with 50 μM Amlexanox during ISO treatment. At a concentration of 300 nM SCH772984, inhibition of pERK activation occurred during 1 μM ISO treatment for 10 min. Besides vehicle-treated control (with 0.1% DMSO), cardiomyocytes treated with only SCH772984 or Amlexanox were considered as the control for ERK1/2 inhibition (Ei) and GRK5 inhibition (Gi) respectively. All the inhibitor-treated samples were preincubated for 1 h before the ISO treatment.

The blots presenting the roles of GRK5 in ERK1/2 activation during acute ISO treatment are shown in **figure 5.11**. There was very little pERK activation observed in the vehicle-treated control, SCH772984-treated (termed Ei) and Amlexanox-treated controls (termed Gi) in **figure 5.11**. Interestingly, the activation of ERK1/2 phosphorylation was removed in both Q41 and L41 haplotypes when their GRK5 activity was inhibited (**Figure 5.11**, Gi-10). This removal of GRK5 activity had similar effects as the SCH772984 inhibitor during the ISO treatment (**Figure 5.11,** Ei-10). These results suggested that GRK5 was involved in activating ERK1/2 signalling during ISO stimulation.

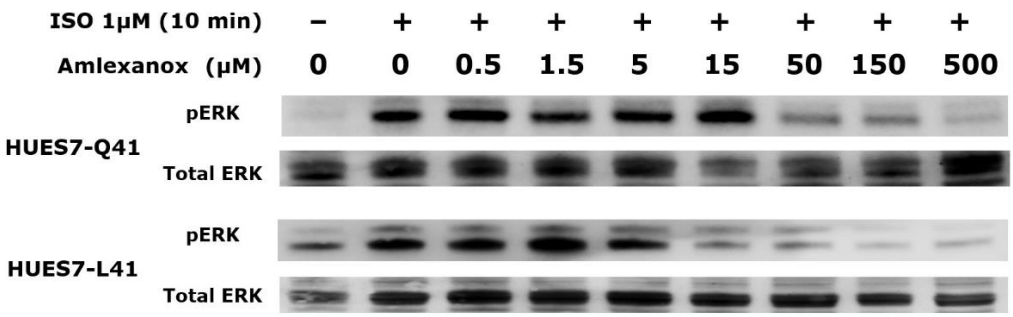

Figure 5.10. Western blot analysis for the inhibitory effect of different Amlexanox concentration on ERK1/2 activation stimulated by 1 μM ISO in isogenic HUES7-Q41L CMs.

Western blot analysis of pERK and total ERK were performed for various Amlexanox concentrations during 1 μM ISO treatment for 10 min, n=2 biological replicates.

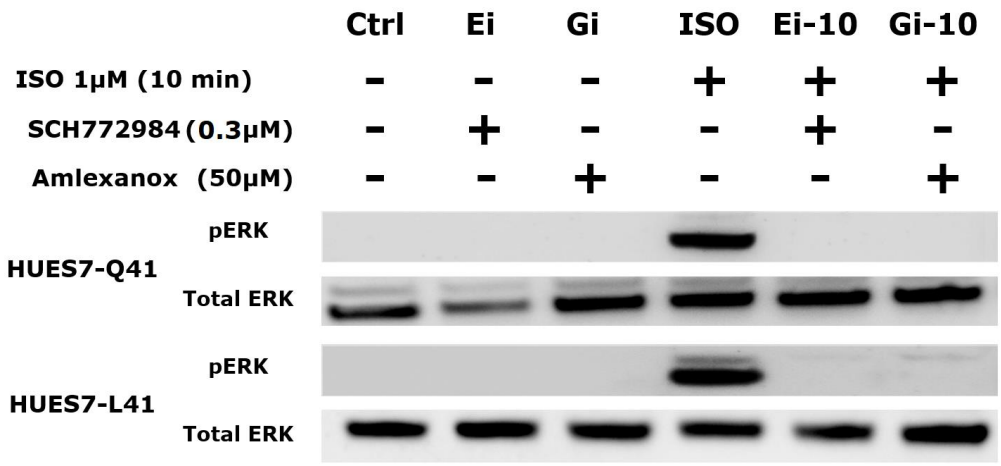

Figure 5.11. Evidence for roles of GRK5 on ERK1/2 activation stimulated by 1 μM ISO in isogenic HUES7-Q41L CMs.

Western blot analysis of pERK and total ERK for cardiomyocytes was stimulated with 1 μM ISO treatment (ISO) without or with either ERK inhibitor (Ei-10, SCH772984 0.3 μM) or GRK5 inhibitor (Gi-10, Amlexanox 50 μM). All of the vehicle-treated control, the ERK inhibitor-treated only control (Ei, SCH772984 0.3 μM) and the GRK5 inhibitor-treated only control (Gi, Amlexanox 50 μM) showed very low levels of pERK1/2 activation. n=2 biological replicates.

5.3.5 Experimental set up to investigate roles of GRK5-Q41L activity and ERK1/2 signalling during chronic catecholamine stress:

Molecular analysis using western blot suggested that GRK5 was responsible for the activation of ERK1/2 signalling in cardiomyocytes during ISO treatment (**Figure 5.11**). The higher amount of pERK induction in the L41 over the Q41 variant may be associated with the gain-of-function of this variant. To explore the roles of the GRK5-Q41L variant and ERK1/2 signalling during chronic catecholamine stress, contractility and cell index analysis were investigated in conditions where either GRK5 or ERK signalling activity were inhibited.

HUES7-Q41L CMs were dissociated and seeded in the 48 CardioECR plates as described in section 3.3.5.2. Once the contractility signals in most of the wells were detected, usually 3 to 5-day post-seeding, cardiomyocytes at day 30+ were pretreated with either ERK1/2 inhibitor (ERKi, treated with SCH772984 at 300 nM) or GRK5 inhibitor (GRK5i, treated with Amlexanox at 50 μM) for 1 h prior the ISO treatment. The cells were then exposed to 1 μM ISO with or without inhibitors for 72 h, and the cultured medium was refreshed every 24 h. The vehicle control was treated with 4 μM of HCL and 0.1% DMSO (v/v). The cells treated with only SCH772984 or Amlexanox were also included and used as the controls for the treatment with ERK inhibitor (ERKi) and GRK5 inhibitor (ERKi).

5.3.5.1 Inhibiting GRK5-Q41L activity and ERK1/2 signalling removed the beneficial effects of HUES7-L41 cardiomyocytes on contractility functions during chronic catecholamine stress

The inhibition of GRK5 activity or ERK1/2 signalling did not impact the chronotropic effects of ISO (**Figure 5.12**). At 1 h of treatment with 1 μM ISO, the beat rate rose to 150 % in HUES7-Q41 and 170 % in HUES7-L41 (**Figure 5.13.A**). During the inhibitory treatment of GRK5 activity, the beat rate increased to 169 % in HUES7-Q41 and 177 % in HUES7-L41. Under ERK1/2 signalling inhibition, similar increases of beat rates in HUES7-Q41 and HUES7-L41 were 165% and 173 % respectively.

The inhibition of GRK5 activity and ERK1/2 signalling has removed the beneficial effect of the HUES7-L41 variant (**Figure 5.12**). Indeed, the inhibitory treatment even had even more detrimental effects than the ISO treatment itself. Under the ISO treatment, HUES-Q41 CMs maintained regular beat rate and 2-fold reduction of beating amplitude at 48h compared to the baseline at 0h (**Figure 5.13.A&B**). Significant reduction of HUES-Q41 contractility responses was only observed at 72h with ~4.5-fold reduction of beat rate and ~9-fold decline of beating amplitude. Under GRK5 inhibitory treatment, the gain-of-function of L41 was removed and a significant reduction in beat rate and beating amplitude was observed in both haplotypes. At 48h exposure of ISO under GRK5 inhibition, the beat rate of HUES7-Q41 and HUES7-L41 both decreased to 55 % and 84 % respectively. While the beating amplitude of these two variants was significantly reduced with only ~ 20 % of beating amplitude maintaining compared to their baseline. At 72 h, there were no signals in beat rate and beating amplitude response.

Inhibiting ERK1/2 activation during ISO treatment exhibited similar responses to the blocking of GRK5 activity, whereby the cardioprotection of HUES7-L41 was not observed (**Figure 5.12**). The beating amplitude of both variants significantly reduced by more than 80 % at 48h and no amplitude signals were detected at 72h in both haplotypes (**Figure 5.13.B**). The beat rate of HUES7-Q41 and HUES7-L41 maintained at 38 % and 66 % at 48h and no beat rate signal was detected after 72h exposure to ISO stress with the inhibition of ERK1/2 signalling (**Figure 5.13.A**).

HUES7-Q41 and HUES7-L41 CMs in the vehicle treatment showed a similar beating rate pattern to the GRK5i control and the ERKi control during the experimental timecourse, where there were modest reductions (~ 25-45 %) observed in beating rate and beating amplitude at the 72 h endpoint (**Figure 5.14 & 5.15**). The ERKi control of these haplotypes also exhibited a reduction in beat rate (~ 45%) at 72h time point; however, these beating patterns were still close to the vehicle-treated control. These observations were similar to the results in section 3.3.5.2. These results suggested that the treatment with ERK inhibitor and GRK5 inhibitor only did not cause significantly harmful effects on contractility responses compared to their baselines.

The gain-of-function of the L41 variant in maintaining contractility compared with the Q41 variant was reviewed in **figure 3.17**, with the detailed analysis as described in section 3.3.5.2. Surprisingly, when the GRK5 activity was removed during ISO treatment, this also removed the gain-of-function effects of the L41 variant, where impaired contractility responses in L41 CMs exhibited similarly to Q41 CMs (**Figure 5.12**). These responses of both Q41 and L41 variants under GRK5 activity inhibition showed similar responses to the inhibited ERK signalling responses. These

observations suggested the gain-of-function of L41 was associated with its activity in activating ERK1/2 signalling. Therefore, blocking GRK5 activity exhibited similar effects as blocking ERK1/2 signalling and the inhibition of these targets erased the beneficial effects of L41 in contractility response.

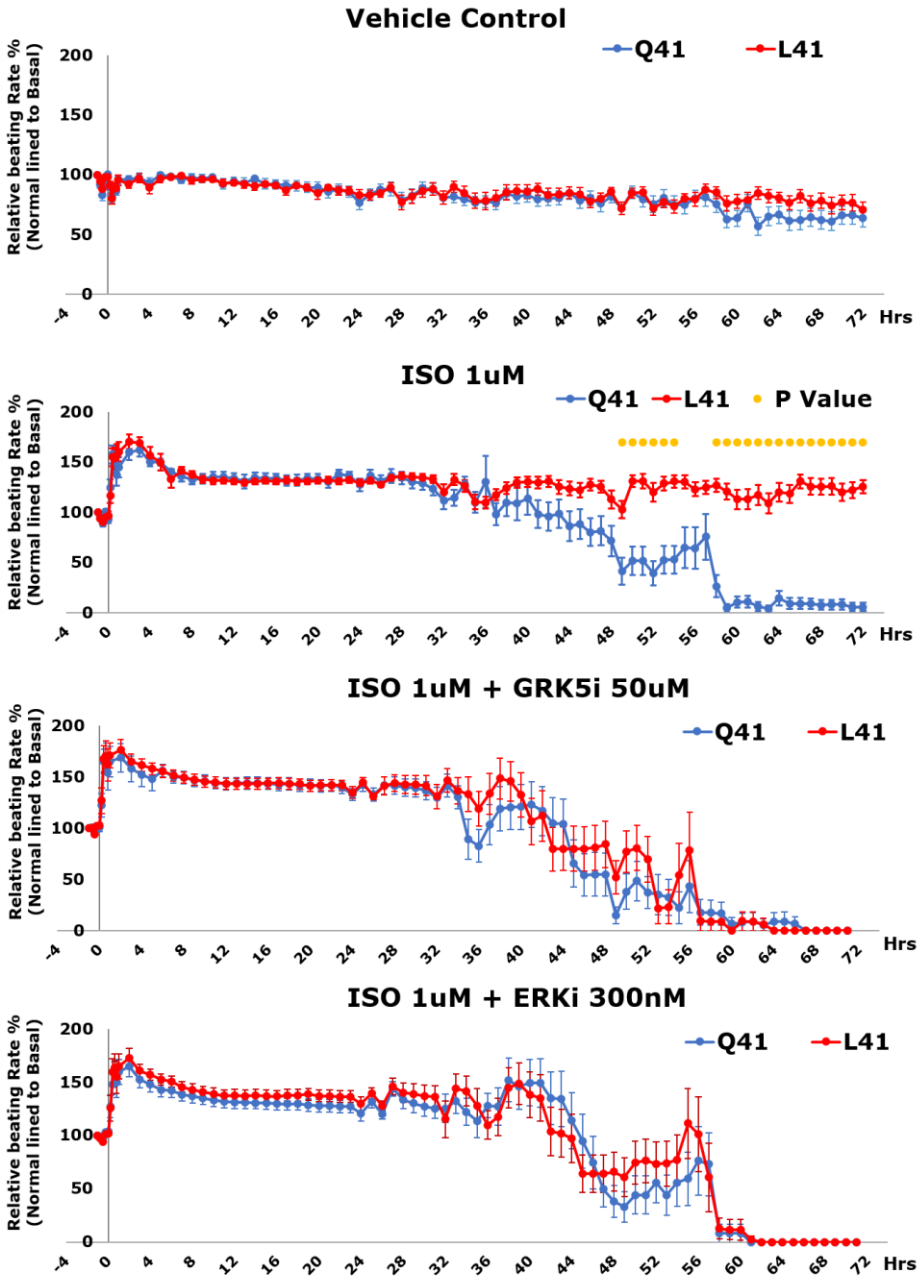

Figure 5.12. Real-time measurement of the beat rate of HUES7-Q41L CMs during chronic ISO stress.

Real-time analysis of beat rate in HUES7-Q41 CMs (blue) and HUES7-L41 (red) CMs at vehicle treatment, SCH772984 300 nM treatment (ERKi) and Amlexanox 50 μM treatment (GRK5i), represent means ± SEM, n = 3 biological replicates

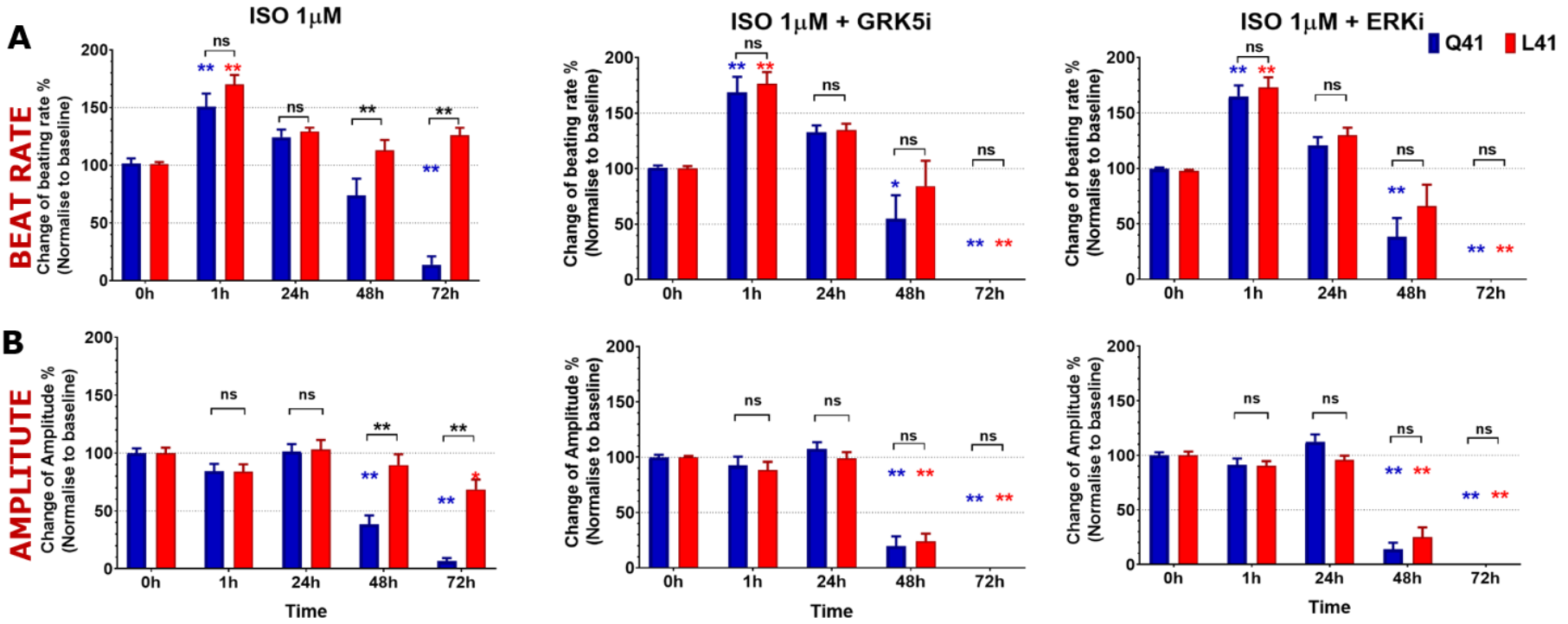

Figure 5.13. Analysis of beat rate and beating amplitude in HUES7- Q41L CMs during inhibition of GRK5 activity and ERK signalling using CardioECR

Analysis of beat rate (A) and beating amplitude (B) in HUES7-Q41 CMs (blue) and HUES7-L41 CMs (red) during 1μM ISO stimulation with either Amlexanox treatment (GRK5i) or SCH772984 (ERKi) for 72 h represent means ± SEM, n = 3 biological replicates. ns not significant difference, *p<0.05, **p < 0.01. Two-way ANOVA with Dunnett's multiple comparison tests.

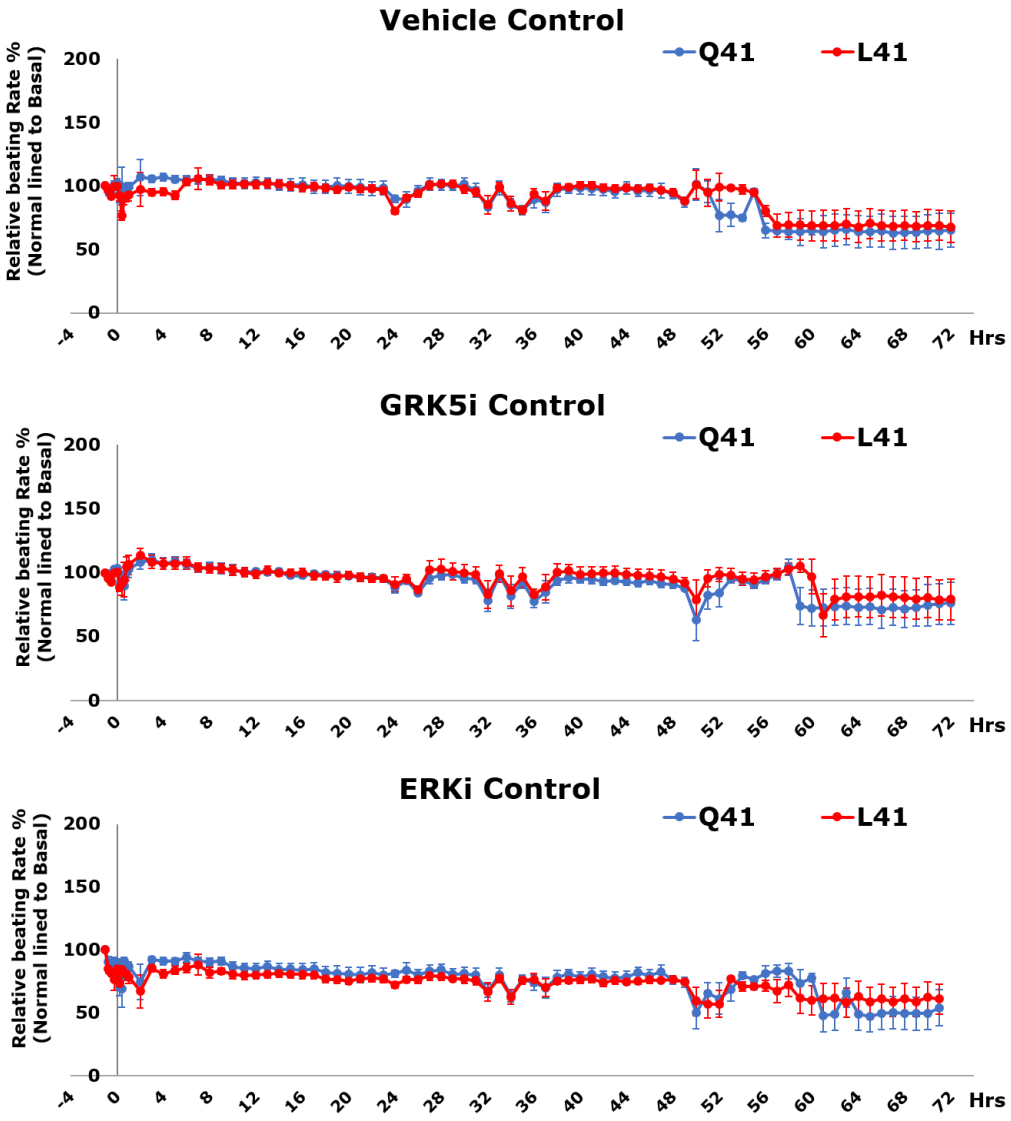

Figure 5.134. Real-time measurement of the beat rate of HUES7-Q41L CMs.

Real-time analysis of beat rate in HUES7-Q41 CMs (blue) and HUES7-L41 (red) CMs at vehicle treatment, 50 μM Amlexanox control treatment (GRK5i control), and 300 nM SCH772984 control treatment (ERKi Control); represent means ± SEM, n = 3 biological replicates.

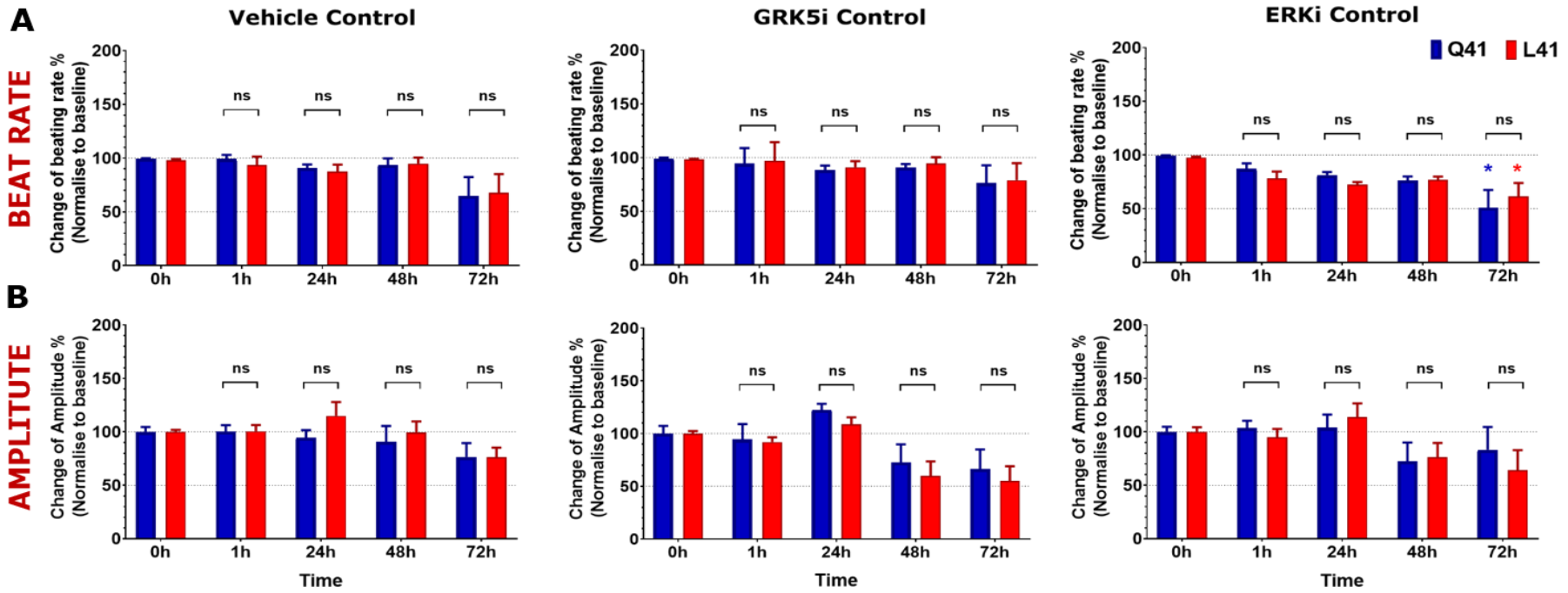

Figure 5.15. Analysis of beat rate and beating amplitude in HUES7- Q41L CMs during inhibition of GRK5 activity and ERK signalling using CardioECR.

Analysis of beat rate (A) and beating amplitude (B) in HUES7-Q41 CMs (blue) and HUES7-L41 CMs (red) at vehicle treatment, Amlexanox treatment (GRK5i) and SCH772984 (ERKi) for 72 h, represent means ± SEM, n = 3 biological replicates, ns not significant difference, *p<0.05, **p < 0.01. Two-way ANOVA with Dunnett's multiple comparison tests.

5.3.5.2 Blocking GRK5 activity and activation of ERK1/2 signalling erase the cardioprotective effects of HUES7-L41 cardiomyocytes on cell survival during chronic catecholamine stress

The cell index analysis is the indirect indicator for cell attachment and cell survival. Approximately 20 % reduction of CI was observed for the vehicle-treated control and the GRK5i controls for both HUES7-Q41 and HUES7-L41 variant (**Figure 5.16**). The treatment with ERK inhibitor may induce some effects on cells where CI of HUES7-Q41 (~68%) and HUES7-L41 (~74%) were relatively lower than the vehicle control.

In the ISO treatment, the L41 variant maintains its CI level (~ 84 %) close to vehicle-treated control. Whereas HUES7-Q41 CMs exhibited some cell loss level during the ISO treatment when CI of Q41 was 2-fold reduced at 48h and ~4-fold reduced at 72h. When GRK5 activity was inhibited, the cardioprotective effects of the L41 variant were removed and exhibited similar responses to the Q41 variant. Indeed, CI of both variants reduced ~ 2.5-fold at 48h and significantly decreased 8-fold – 9-fold at 72h for both haplotypes.

In the same manner, the inhibition of ERK1/2 signalling removed the beneficial effect of L41 and proved that ERK1/2 activation was important signalling and was mainly responsible for the cardioprotective effects of this variant. Whereby the ERK inhibition induced 2-fold reduction of CI for both haplotypes at 48h and 8-fold decrease of CI at 72h. In line with contractility results, the inhibition of GRK5 activity and ERK signalling remove the beneficial effects of the L41 variant during catecholamine stress.

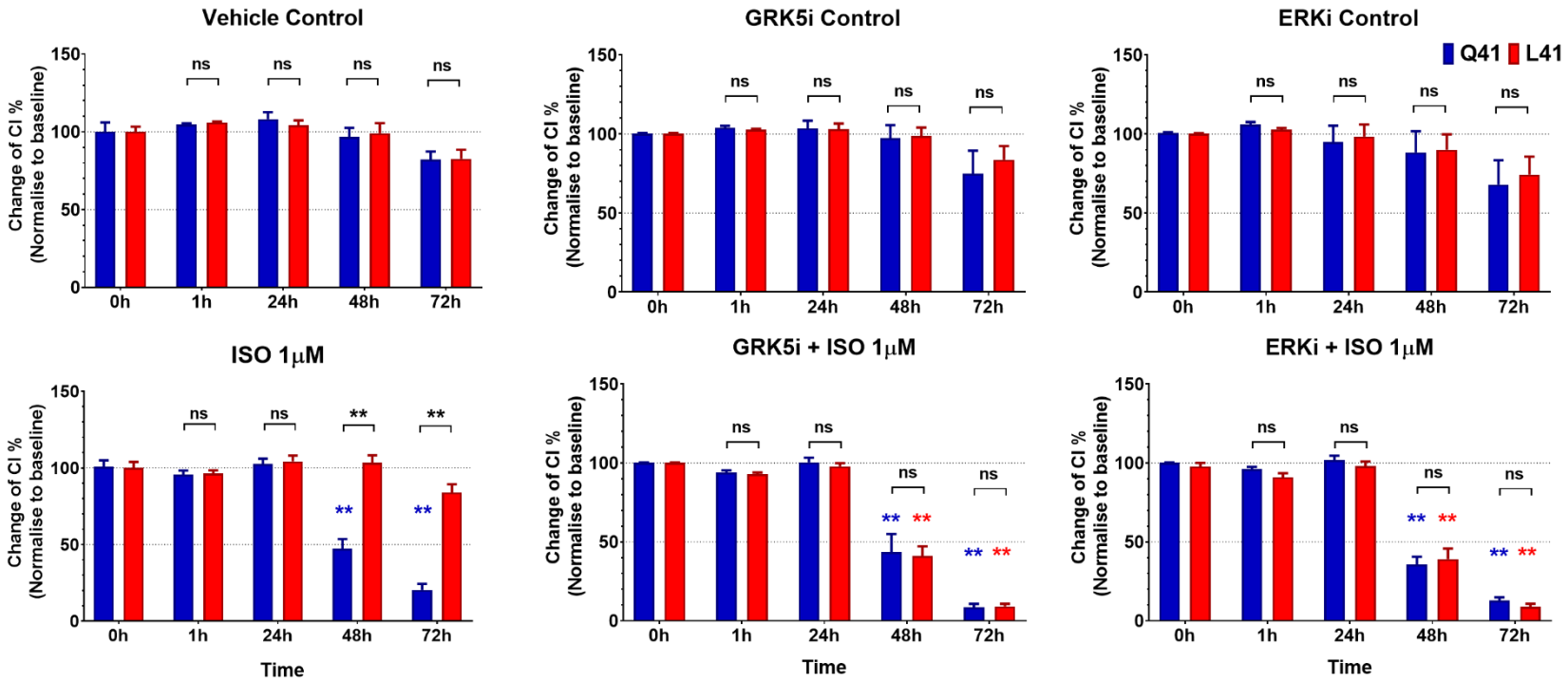

Figure 5.14. CI analysis in HUES7- Q41L CMs during inhibition of GRK5 activity and ERK signalling using CardioECR

CI analysis for HUES7-Q41 CMs (blue) and HUES7-L41 CMs (red) during 1μM ISO stimulation with either Amlexanox treatment (GRK5i) or SCH772984 (ERKi) for 72 h represent means ± SEM, n = 3 biological replicates. ns not significant difference, *p<0.05, **p < 0.01. Two-way ANOVA with Dunnett's multiple comparison tests.

5.4 Discussion:

The GRK5-L41 variant showed cardioprotective phenotypes in reducing cell death response and maintaining cardiac contractility functions during chronic catecholamine stress in section 3.3. In this chapter, molecular analysis using western blot was applied to investigate the association between these cardioprotective phenotypes and ERK1/2 signalling, which is the main regulatory signalling pathway for cardiac hypertrophy and cardiac survival in response to stress.

Western blot analysis showed that the ERK1/2 signalling was activated during ISO treatment. Interesting, the HUES7-L41 variant showed a higher amount of pERK induction compared to the HUES7-Q41 variant during the ISO stress stimulation. This observation suggested that the cardioprotective phenotypes of the L41 variant were hypothesised due to the pronounced ERK1/2 induction during chronic ISO stress. Further investigations showed that GRK5 may be responsible for ERK1/2 activation in cardiomyocytes during ISO treatment. Thus, removing ERK signalling withdrew the cardioprotective effects of the GRK5-L41 variant and the inhibition of GRK5 activity also exhibited similar responses as the ERK signalling inhibition.

These results together suggested that the cardioprotective function of the GRK5-L41 variant was associated with its increased induction of ERK1/2 phosphorylation, which may probably account for antiapoptotic responses, via the β-arrestin pathway during chronic ISO exposure. This observation was also consistent with the previous study of the GRK5-L41 polymorphism during catecholamine stress (Liggett et al., 2008) when it promoted faster receptor desensitisation to reduce deleterious effects of chronic induction of Gs protein-dependent signalling and induced receptor internalisation via β-

arrestin signalling, where ERK1/2 signalling was mainly activated in endosomes.

5.4.1 Activation of ERK1/2 signalling in the hPSC-CM model was mainly induced by GRK5 mediated phosphorylation:

Western blot analysis showed that the ERK1/2 signalling was activated in response to ISO treatment (**Figure 5.5**). The inhibition of GRK5 activity did not block ERK1/2 phosphorylation which may indicate that ISO stimulated ERK1/2 phosphorylation in our model via both G protein-dependent and β arrestin-dependent pathways (**Figure 5.11**).

In a detailed study of β-arrestin and G protein-dependent ERK1/2 activation by β2-AR on HEK293 cells, the G protein-dependent pathway mediated pERK1/2 activation quickly and was responsible for this early onset of pERK induction (Shenoy et al., 2006). In that study, β-arrestin1 and β-arrestin2 were inhibited by siRNA, G protein-dependent ERK1/2 induction occurred within 5 min and their maximum pERK production peaked at 2 or 5 min. In contrast, ERK1/2 activation mediated via β-arrestin is the later set of pERK induction, where pERK induction emerged at the later time point after 5 min and was sustained until 30 min (Shenoy et al., 2006). Analysis of the kinetics of ERK1/2 activation in the hPSC-CM model showed the maximum phosphorylated ERK1/2 (pERK) induction was observed at 10 min with some levels of pERK activation was still detected at 30 min after ISO induction (**Figure 5.5**).

Besides, inhibiting GRK5 activity showed a massive reduction of ERK1/2 phosphorylation (**Figure 5.11**). These observations suggested that the major pERK1/2 activation in hPSC-CM during ISO stimulation was mediated via β-arrestin. In contrast, ERK1/2 signalling activation on HEK293 cells in the Shenoy study was mainly mediated via G protein-dependent

pathway, where the H89 treatment removed the major pERK induction and the maximum pERK was also detected at 5 min after ISO induction (Shenoy et al., 2006). Since GRK2-mediated β2-AR phosphorylation leads to receptor internalisation but not ERK1/2 signalling activation (Charest et al., 2005; Shukla et al., 2008; Xiao and Liu, 2016), ERK1/2 activation via a β-arrestin pathway in our hPSC-CM model was likely to be mainly mediated by GRK5 and GRK6. GRK2,3,5 and 6 are all present in the heart; however, GRK2 and GRK5 are the most abundant GRK isoforms in the myocardium (Huang et al., 2011; Pfleger et al., 2019). These results together suggest that activation ERK1/2 signalling in the hPSC-CM model was mainly induced by GRK5 mediated phosphorylation.

5.4.2 Methods for studying individual GRK mediated phosphorylation of GPCRs during chronic stress experiment:

There are different approaches applied to study the loss-of-function of a protein, which target different level of gene expression. At the DNA level, CRISPR/Cas9 and TALEN are used to generate gene knockout cell lines that can completely turn off the gene. Thus, no mRNA and protein could be encoded. At the RNA level, morpholino and RNA interference (siRNA or shRNA) are used to mediated gene knockdown. These methods act to cause inactivation or degradation of the target mRNA, which in turn reduce the levels of the encoded protein. Western blot and RT-PCR are used to check protein and mRNA expression to quantify the efficiency of these knockout and knockdown method. At the protein level, chemical inhibitors are used to inactivate the function of the target protein. In my study, Amlexanox was used to inhibit the phosphorylation activity of GRK5 instead of removing the

presence of these proteins, whereby the presence of their downstream targets determined the blocking efficiency of an inhibitor.

In my thesis, pERK1/2, which is a downstream target of the β2-GRK/β-arrestin pathway, was investigated to quantify the inhibitory effect of Amlexanox on GRK5 activity during ISO stimulation. Whereas MEF2 has been used as the downstream target for GRK5 activity during PE stimulation (Homan et al., 2014). The knockout methods can completely remove the protein function; however, the generation of GRK5-knockout cell lines take several months. Because of the time limitation, this approach was not appropriate.

siRNA method can reduce from 80 -90 % expression of the targeted protein with less than 20 % off-target. The efficiency of this method relies on transfection efficiency and the fast turnover of the protein. To my knowledge, there is no study characterising the half-life of GRK5. For the long term experiment (up to 96h), these methods may require more than one round of siRNA transfection, which may cause increased cytotoxicity. Therefore, using a chemical inhibitor would be the most appropriate approach for this study.

The major issue of using chemical inhibitor is the specificity to the target, therefore the concentration optimisation for Amlexanox was performed to reduce the off-target effect (**Figure 5.11**). ERK1/2 signalling could also be activated via G protein-dependent pathway and there was always some low pERK level at the basal (untreated) culture condition. pERK was not a completely perfect downstream target to quantify the inhibitory effect of Amlexanox on inhibiting GRK5 activity. Therefore, we peaked at 50 μM Amlexanox, which removed more than half of pERK induction stimulated by ISO, and this concentration also efficiently reduced MEF2 activity during PE stimulation (Homan et al., 2014).

5.4.3 Insight mechanism of the gain-of-function of GRK5-L41 in the hPSC-CM model:

Phenotype analysis of the GRK5-L41 variant in chapter 3 showed the cardioprotective response in maintaining cardiac contractility functions and antiapoptotic response during chronic catecholamine stress induced by ISO treatment. Molecular analysis using western blot exhibited that GRK5-L41 induced a higher level of pERK1/2 activation compared to the GRK5-Q41 variant during ISO stimulation (**Figure 5.5 & 5.6**). Further investigation illustrated that blocking ERK1/2 activation reduces the beneficial effects of the GRK5-L41 variant, resulting in reduced contractility and increased cell death responses, which were similarly observed as the GRK5-Q41 variant during the chronic ISO stress. ERK1/2 signalling has been reviewed to have an important cardioprotective role to enhance myocytes survival and reduce HF progression (A. Grisanti et al., 2019; Harris Ian S. et al., 2004; Wang Yibin, 2007; Yamaguchi et al., 2004). Interesting, the inhibition of GRK5 activity also exhibited similar effects to those with the blocking of ERK1/2 phosphorylation, which removed the cardioprotective effects of the GRK5-L41 variant.

This molecular evidence and phenotype analysis together suggested that the gain-of-function of the GRK5-L41 variant is due to its higher activation of ERK1/2 phosphorylation during the ISO stimulation, with the GRK5-L41 haplotype promoting higher receptor desensitisation and internalisation via GRK5/β-arrestin pathway followed by ERK1/2 activation. By preferring the GRK5/β-arrestin pathway, the GRK5-L41 CMs would efficiently reduce the classical Gs protein-dependent signalling pathway and its deleterious impacts induced by the chronic ISO induction. Also, the higher ERK1/2 action in GRK5-L41 provided positive effects on improving cardiac survivals and may also facilitate the adaptive hypertrophy response to

enhance cardiac function in response to stress. Whereas the chronic ISO treatment may promote induction of the classical Gs protein-dependent signalling pathway rather than the GRK5/β-arrestin pathway in GRK5-Q41 CMs. The chronic ISO stimulation would amplify the minor differences from the initial signallings between the haplotypes, where GRK5-L41 promotes GRK5/β-arrestin signalling pathway over the GRK5-Q41, and induce the phenotype difference at the endpoint of the chronic catecholamine stress.

As explored in the introduction section 5.1.3, β2-AR phosphorylated by GRK6 promotes Src binding, which is a component of ERK1/2 signalling activation (Charest et al., 2005; Jean-Charles et al., 2017; Shukla et al., 2008). Shenoy et al. also illustrated that β2-AR phosphorylated by GRK5 during ISO treatment enhanced β-arrestin recruitment and pERK induction over GRK2 (Shenoy et al., 2006). In a cell-free assay and HEK293 studies, GRK5 mediated particular phosphorylation of β2-AR at Ser 355 and Ser 356, which is interesting the phosphorylation site mediated by Carvedilol treatment, to activate ERK1/2 activation (Millman et al., 2004; Nobles et al., 2007; Tran et al., 2007).

A survey of the literature suggests that there is no detailed study on GRK5-Q41L directly mediated β1-AR phosphorylation. However, Norma showed that GRK5 and GRK6 phosphorylation, but not GRK2 and GRK3, are required in promoting β1-AR-mediated EGFR transaction and ERK activation (Noma et al., 2007). This study on HEK293, U2S sarcoma cells and adult mice myocytes proved the EGFR transactivation-mediated by β1-AR via GRK5/6/β-arrestin pathway confers cardioprotection to counteract the chronic catecholamine toxicity from the G protein pathway. Detail studies of GRK5-Q41L interaction with β2-AR during Carvedilol and ISO treatment on HTL and CHO cells showed that GRK5-L41 exhibited more robust interaction with β2-AR rather than GRK5-Q41 (He et al., 2017; Wang et al., 2008).

These reports explain and support our hypothesis that GRK5-L41 promotes more robust β-ARs desensitisation and internalisation, and induced the B-arrestin dependent pathway, followed by induction of higher ERK1/2 signalling and reduction of the Gs protein-dependent pathway.

Another question is why a single amino acid change can cause these differences. Glutamine (Q) is a polar and hydrophilic amino acid while Leucine (L) is a hydrophobic amino acid. The substitution of Leucine in amino acid 41 located in the α1 helix of the RH domain, which is an important domain that mediates the GRK5 interaction with the phospholipid membrane and CaM. Indeed, the association with phospholipid membrane is important for interaction with GPCRs (β-ARs) while the interaction with CaM is required for GRK5 translocation to the nuclei (Komolov et al., 2015; Tran et al., 2007). In this regard, a recent study on the structure of GRK5 bound to β2-AR illustrated the conformational changes that occur in the GRK5 RH domain and catalytic domain interface upon receptor binding (Komolov et al., 2017). These conformation changes facilitate contacts between ICL2, ICL3 and C terminus of β2-AR with the GRK5 RH bundle subdomain. GRK5 RH domain is suggested to serve as a docking site for GPCRs and to help to control kinase activation via transient contacts of the RH bundle and kinase subdomains. This may explain the enhanced activity of GRK5-L41 on β2-AR (Wang et al., 2008).

Therefore, a hypothesis is proposed to explain the gain-of-function benefits of GRK5-L41 via two mechanisms: (1) GRK5-L41 enhances its activity on β-AR by facilitating faster desensitisation by increasing the hydrophobicity and thus the interaction with the phospholipid membrane, and (2) GRK5-L41 preferably promotes β-arrestin signalling and ERK1/2 activation to increase cell survival and possibly activate adaptive hypertrophic responses to enhance contractility performance. These gain-of-

function benefits of GRK5-L41 have similar effects to carvedilol in accounting for the cardioprotective effects on β-AR via β-arrestin dependent signalling to enhance contractility function and cardiac survivals. The mechanism in which GRK5-L41 promote faster receptor desensitisation was already illustrated to have similar effects as the β-blocker, propranolol (Liggett et al., 2008). To my knowledge, the work in my thesis has, for the first time, characterised the ERK1/2 activation of GRK5-Q41L variants on hPSC-CMs and linked the cardioprotective effect of GRK5-L41 with the higher induction of ERK1/2 activation during ISO stimulation.

The CaM binding to the GRK5 RH domain is suggested to block GRK5 association with membranes in response to elevation of intracellular calcium levels (Komolov et al., 2015; Tran et al., 2007). The GRK5-L41 polymorphism in the RH domain may also alter affinity to CaM binding interaction, which is associated with the nuclear translocation and non-canonical function of GRK5 in the nuclei. This may explain the increase of nuclear GRK5 fraction in HUES7-Q41 but not HUES-L41 during chronic ISO treatment (**Figure 4.3**). The higher hydrophobicity of GRK5-L41 may enhance interaction with β-ARs on the membrane and possibly decrease CaM binding, which is involved in nuclear GRK5 translocation.

The increase of nuclear GRK5 fraction during β-AR stimulation by ISO was also observed in a recent study on mouse myocytes model (Laudette et al., 2019). However, this increase of GRK5 nuclear fraction was only observed in the isogenic HUES7 model, but not in the hIPSC model. Also, results of the blocking ERK1/2 signalling and GRK5 activity shown in section 5.3.5 indicated that the gain-of-function effects of GRK5-L41 were mainly accounted for by its canonical action on the cell membrane. Thus, my work adds new knowledge by characterising the changes in subcellular distribution of GRK5-Q41L variants during chronic catecholamine stress by ISO. Even

though the reduction of nuclear fraction of GRK5-L41 over GRK5-Q41 during chronic ISO maybe not the major mechanism for its gain-of-function effects.

Chapter 6 General Discussion

This study aims to use new human cellular models, established by (1) introducing a single polymorphism GRK5-L41 on HUES7-GRK5-Q41 to create an isogenic hPSC model and (2) generating hIPSC lines harbouring homogenous GRK5-Q41 and GRK5-L41 from lymphoblastoid cells, to study the phenotype of the putative effect of GRK5-Q41L polymorphism and then derive mechanistic insight.

Using monolayer cardiac differentiation as a tool, we generated cardiomyocytes from these two hPSC systems as the relevant cellular models to characterise the function of GRK5-Q41L polymorphism. The relevance of the established hPSC-CMs and key results of each chapter will be discussed along with experimental considerations and limitations. Discussion of key findings is contextualised within the literature, with a proposed mechanism for the putative effects of GRK5-Q41L on hPSC-CMs during chronic catecholamine stress.

6.1 Validation of the generated hPSC-GRK5-Q41L CM models

Rodent models and cardiomyocytes isolated from neonatal rats/mice are the most widely used *in vivo* and *in vitro* models in cardiovascular research due to their easy handling, low maintenance cost and availability for genetic manipulation (Overington et al., 2006; Savoji et al., 2019). The physiological differences between these animal models and human are the main concerns for the relevance of these models. Human primary cells derived from donors are the gold standard model for representing human cardiomyocytes. However, their usage is restricted due to non-proliferative capacity, finite lifespan and limited viable source from small biopsies (Overington et al., 2006; Savoji et al., 2019).

Human PSCs, with their unlimited source due to long-term proliferation, can provide a relevant human cellular model on account of efficient cardiac differentiation, ease of genetic modification and integration into multi-cell complexes. These attributes make hPSC-CMs promising alternative models, which have been applied for cardiac safety evaluation of drugs and have successfully recapitulated different cardiomyopathy disease *in vitro* (Fermini et al., 2016; Giacomelli et al., 2017; Mulder et al., 2018; Savoji et al., 2019).

The generation of GRK5-L41 SNP on HUES7-GRK5-Q41 was performed by Dr Hoang Minh Duc by using a novel footprint-free method (Kondrashov et al., 2018). The use of CRISPR/Nickase and the *PiggyBac* system reduces the likelihood of off-targets and the time required for introducing the site-specific modification in GRK5 locus via gene editing. The isogenic and hIPSC models were characterised and shown to exhibit accepted criteria relating to pluripotent marker expression, proliferation rate and genomic stability during culture maintaining. The genotype of GRK5 confirmed the successful establishment of the isogenic and hIPSC model.

The establishment of the isogenic model added more confidence on the phenotype differences induced by GRK5-Q41L SNP because cell lines in this model have the same genetic background. The hIPSC model with heterogenic genetic background did not consistently mirror phenotype as the isogenic model in contractility response, hypertrophic response and subcellular GRK5 distribution assay. This highlight the importance of the genetic background on phenotype responses.

The efficient cardiac differentiation protocol provided a tool to generate the relevant cellular model hPSC-CM for cardiovascular research. The high purity culture of hPSC-CMs (> 85% α-actinin^{+} cells) enabled the evaluation of phenotype and molecular signalling. GRK5-L41 was proposed to function

as a genetic β-blocker to improve left ventricular function during HF (Liggett et al., 2008). Although the herein protocol is a non-subtype cardiac specification differentiation protocol, ~80% of CMs at day 60 are MLC2v$^+$ and the MLC2v$^+$ proportion increases with time in culture (courtesy by Dr Hoang Minh Duc). This indicated the majority of generated cells are ventricular cardiomyocytes, whereby the use of XAV939 and KY02111 as WNT inhibitor direct the cardiac differentiation toward ventricular subtype (Minami et al., 2012).

6.2 Development of phenotyping assay studies the putative functions of GRK5-L41 during chronic catecholamine exposure.

Human associated studies showed that patients harbouring the GRK5-L41 variant were associated with decreased mortality during cardiac ischemia and HF (Dorn and Liggett, 2009; Liggett et al., 2008). The cell-based and transgenic mouse studies suggested that GRK5-L41 expressing mice were protected from impaired contractile function and left ventricular dilation with performance similar to the propranolol treatment. These studies suggested that the GRK5-L41 variant does not affect the kinase activity but rather serves to improve the desensitisation rate of activated β-ARs. Therefore, an enhancement of receptor desensitisation protects GRK5-L41 expressing mice from adverse consequences of chronic β-AR stimulation.

A study on human GRK5-Q41L transfected Cos7 suggested that GRK5—mediated Q41L does not affect the nuclear function of GRK5-mediate HDAC5 phosphorylation during 1h treatment of AngII (Zhang et al., 2011). In this thesis, phenotypes of GRK5-Q41L variants associated with the canonical and noncanonical function of GRK5 were characterised to validate the use of hPSC-CM models. Further investigations were performed to

provide insight into the mechanism for the gain-of-function of the GRK5-L41 variant.

In this thesis, different phenotyping assays were developed to examine the contractility response and cell death response of hPSC-Q41L-CMs during chronic ISO exposures. The optical trace by CellOTIQ analysis and impedance by CardioECR analysis was successfully used to investigate contractility responses in hPSC-CMs carrying Q41L variants. Indeed, reduction of contraction amplitude and beating rate was observed in Q41 CMs at 72h of ISO exposure in both the CellOTIQ and CardioECR experiment. In contrast, L41 CMs prevented the adverse effects of chronic ISO treatment to maintain physiological contractility function and cell survival, at which performance was similar to propranolol treatment.

In hPSC-CMs, ISO has performed its positive effects on chronotropy but not inotropy. Q41 CMs in both isogenic and hIPSC models showed significant faster contraction time compared to L41 CMs, which may imply the higher PKA phosphorylation in Q41 CMs over L41 CMs. The cell death responses were directly quantified by a Cal AM/ EthD-1 assay and by indirect analysis through cell impedance using the CardioECR. L41 CMs in both assays showed lower cell death levels compared to Q41 CMs during chronic ISO exposure. These results support the cardioprotective function of the L41 haplotype.

Noncanonical functions of accumulated GRK5 in the nucleus reveal a role in pathological hypertrophy and progression to HF (Gold et al., 2013; Hullmann et al., 2014; Traynham et al., 2016). An increase of nuclear GRK5 accumulation in isogenic HUES7-Q41 CMs was observed in western blot and confocal imaging analysis during chronic ISO treatment. However, hIPSC-Q41 CMs did not show a similar increase of nuclear GRK5 fraction. In contrast, the L41 variant in both isogenic and hIPSC models did not show

any accumulation of nuclear GRK5 fraction, but some reduction level of nuclear GRK5 fraction was observed.

Measurement of BNP expression by high content imaging analysis was conducted to illustrate the hypertrophic responses of hPSC-CMs in association with changes in nuclear GRK5 fraction. HUES7-L41 and HUESQ/L41 CMs associated with low nuclear GRK5 accumulation showed significantly higher BNP expression than HUES7-Q41 CMs. Indeed, HUES7-Q41 CMs exhibited increased nuclear GRK5 accumulation. The high BNPs expression in HUES7-L41 and HUES7-Q/L41 CMs was regarded as a compensatory mechanism to slow the HF progress because BNP has antihypertrophic and antifibrotic effects to protect the heart from adverse consequences of overload.

However, the GRK5-Q41L variant in the hIPSC model did not show similar changes either in nuclear GRK5 fraction or BNP expression, although L41 CMs in both isogenic and hIPSC models showed cardioprotection effects in phenotyping assays. The inconsistent results between isogenic and hIPSC models suggested changes of nuclear GRK5 may not the main pathway that accounted for the cardioprotection of the GRK5-L41 variant. To my knowledge, this thesis is the first study characterising the effects of GRK5-Q41L on the canonical and noncanonical function of GRK5 on the human cardiac model at the endogenous level during chronic catecholamine exposure.

Further investigation on the isogenic HUES7-GRK5-Q41L model showed that GRK5 is responsible for the major induction of pERK phosphorylation in hPSC-CMs during ISO stimulation. The cardioprotection of the GRK5-L41 variant was suggested to associate with the higher pERK activation in GRK5-L41. The inhibition of GRK5-L41 activity responded

similarly to when ERK activation was inhibited, resulting in loss of cardioprotection by the L41 variant.

Glutamine (Q41) is a polar and hydrophilic amino acid while Leucine (L41) is a high hydrophobic amino acid. The substitution of a hydrophobic amino acid L41 in the α1helix in the RH domain of GRK5, which is an important domain mediating GRK5 interaction with phospholipid membrane and CaM, is suggested to enhancing interaction with GPCRs on the membrane (Komolov et al., 2015).

This L41 variant exerts the gain-of-function by (1) facilitating faster GRK5-mediated β-ARs phosphorylation and desensitisation to reduce adverse effects of chronic β-AR induction (Liggett et al., 2008) and (2) promoting stimulation of β-arrestin dependent pathway over Gs protein-dependent pathway during catecholamine stress. This hypothesis was supported by the faster contraction time of Q41 CMs during ISO treatment compared to L41 CMs, implying the higher PKA phosphorylation in Q41 CMs.

The proposed mechanism for the cardioprotection effects of GRK5-Q41L is illustrated in Figure 6.1. Contextualization with the literature, the effects of the GRK5-L41 variant exerted similar responses to carvedilol treatment by promoting β-arrestin dependent pathway stimulation. Further experiments required to prove the association of the GRK5-L41 variant with carvedilol treatment.

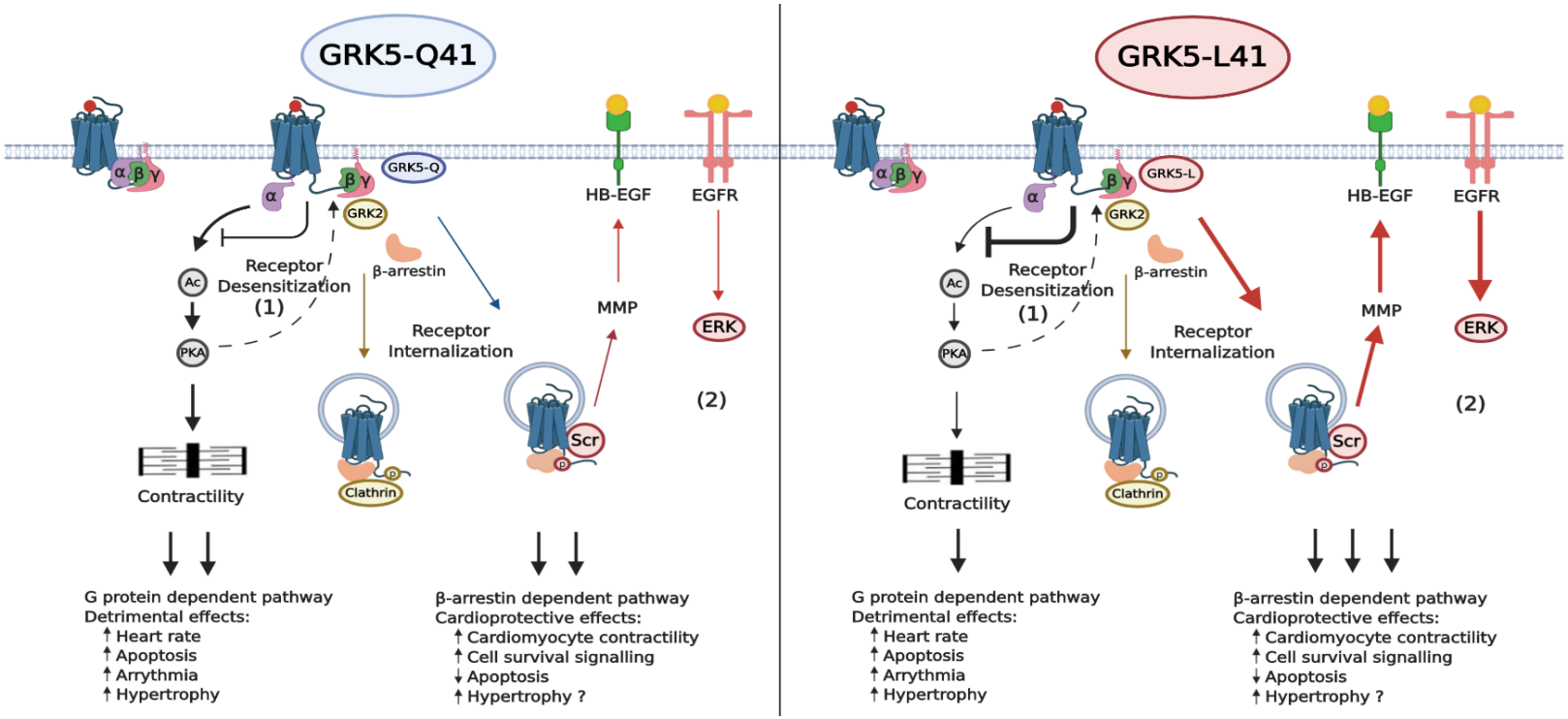

Figure 6.1. ***A mechanism for the gain-of-function of GRK5-Q41L preferably mediated ERK1/2 activation via the β-arrestin pathway.***

Simulation of β-ARs by ISO mediates both G protein-dependent and β-arrestin dependent pathway. During sustained ISO induction, GRK5-L41 mediated cardioprotective effects via two mechanisms (1) GRK5-L41 promote faster desensitisation to reduce deleterious effects from sustained induction of G-protein signalling (2) GRK5-L41 preferably mediated β-arrestin signalling and ERK1/2 activation to increase cell survival and possibly activate adaptive hypertrophic responses. GRKs mediated β-ARs phosphorylation recruit β-arrestin binding and subsequently receptor internalisation, while PKA-phosphorylated receptor mediates receptor desensitisation. GRK2-mediated (yellow) phosphorylation sites recruit clathrin, GRK5-mediated (red) phosphorylation pattern selectively activates ERK1/2 signalling.

6.3 Study limitations:

6.3.1 hPSC models to study GRK5-Q41L function:

Using a novel short-cut strategy helped to reduce the time for the establishment of the isogenic HUES7-GRK5-Q41L models. However, this strategy did not generate the intermediated GRK5 knockout lines as the conventional gene-editing CRISPR/Cas9 strategy. Inconsistent phenotypes between the hIPSC-GRK5-Q41L model and isogenic model indicated the importance of (epi)genetic background. The heterogeneous background between hIPSC could also hinder GRK5-Q41L phenotypes and imply the importance of isogenic background in studying SNP functions.

In this approach, isogenic pairs should be established for hIPSC lines to study the phenotype of GRK5-Q41L SNP. Epigenetic modulations during reprogramming and clonal variation due to the gene-editing process could add heterogeneity to the phenotype of the SNP study (Burridge et al., 2014; Dimmeler et al., 2014; Hartman et al., 2016; Luttrell et al., 2018; Yester and Kühn, 2017). However, idealism needs to be balanced with realism; studying multiple lines, each of which has isogenic pairs and/or several clones encounters practical issues in terms of time- and labour-intensiveness.

6.3.2 The immature phenotype of hPSC-CMs

Although the protocol used in this thesis efficiently generates high purity cardiomyocytes, wherein ~80% are $MLC2v^+$, the immature morphology of these cells is a key consideration. This is a defining drawback shared by the whole hPSC field, irrespective of the desired targeted cell type. In this thesis, immature phenotypes of hPSC-CMs may affect the cardioprotective function of β2-AR because T-tubules are important for phosphorylated β2-AR and Gi coupling (Lyon et al., 2009; Schobesberger et al., 2017). The loss of T-tubules disturbs localised β2-AR signalling in failing

human and rat ventricular myocytes. This means β2-ARs may act as β1-ARs-like Gs-cAMP-PKA signalling, which induces cardiotoxicity effects during cardiac remodelling in HF.

Different strategies have been employed for *in vitro* maturation of hPSC-CMs including mechanical or electrical stimulation, topography or modulating substrate stiffness, applying biochemical cues within maturation matrices and genetic manipulation (Denning et al., 2016). Recent studies in hPSC-CMs maturation have shown improvements in promoting T-tubule formation and in generating a uniform calcium transient Ca^{2+} wave propagation by treating with Tri-iodo-L-thyronine (T3) and dexamethasone combining with 5 days culture on a matrigel mattress (Parikh et al., 2017).

Such protocols to enhance the maturity of hPSC-CMs may benefit from studying the phenotype of the GRK5-Q41L variant on β-AR signalling. The low mRNA expression of *AGTR1*, which encodes AT-1R, and the absence of α1-AR (Földes et al., 2014) may indicate that the hPSC-CM model is not an optimal model for studying effects of GRK5-Q41L variants on AT-1R and α1-AR signalling pathways. Indeed, these two signalling pathways were revealed to stimulate noncanonical effects of GRK5 in the nucleus (Gold et al., 2013, p. 5; Hullmann et al., 2014; Traynham et al., 2016; Zhang et al., 2011).

6.3.3 Contractility assays by CellOPTIQ and CardioECR.

Optimization for cell seeding density were required for both CellOPTIQ (~ 100,000 cells/cm^2) and CardioECR (~ 180,000 cells/cm^2) platforms. Different seeding densities between these systems is due to their working principle. In the CellOPTIQ system, a dense confluent monolayer creates multiple contraction peaks, which can cause false-negative results. As a large number of images are required for data analysis, the CellOPTIQ platform

generates huge data content and is only optimised for the endpoint assay. In the CardioECR system, the signal detection depends on the contact between cells and electrodes. Therefore, the fully confluent monolayer maximises signal detection by the electrodes in the CardioECR plate. However, cell detachment was observed earlier in the timecourse using the CardioECR relative to the CellOPTIQ.

The CardioECR plate is also very expensive (~ £350 for each plate of 48 wells), which is much more costly than the conventional 96-well tissue culture plastic plates needed for CellOPTIQ experiments.

Although the CardioECR platform offers real-time analysis of contractility and cell survival response, non-continuous measurements between sweeps should be considered, otherwise the 10GB data limit is rapidly exceeded and this interferes with long-term experiments. Also, the absence of contractility signals of the beating cardiomyocytes was observed, which required more caution in data analysis. Because the CardioECR system was on load from the xCELLigence company, the access time and technical supports were restricted to perform more replicates for the hIPSC model. Replicating this experiment for the hIPSC model would add confidence in the reported data for phenotype study.

6.3.4 Cell survival analysis by cell impedance signals.

CI (cell impedance or cell index) signal sensitivity depends on the contact between electrodes so that this platform can only function for 2D monolayer culture. Cell detachment was also observed during the long time culture, and seeding density would so require further optimisation.

Besides, CI measurement by CardioECR is an indirect analysis for cell survival. CI signals were also associated with cell adhesion, whereby β2-AR and Ca^{2+} have shown effects on cell adhesion (Gargiulo et al., 2014; Janmey,

1994; Noh et al., 2017; van Roy and Berx, 2008). Activation of β2-AR and intracellular Ca^{2+} changes during ISO stimulation may add complexity in CI analysis. Moreover, a general reduction of CI during culture time on the CardioECR system was observed in the untreated cardiomyocytes and was also revealed in a study by Zhang and colleagues (Zhang et al., 2016). Effects of β2-AR activation, intracellular Ca^{2+} changes on CI and a general reduction of CI during culture time may explain the drastic changes in CI analysis compared to Cal AM/EthD-1 assay by flow cytometry. Nevertheless, both CardioECR and flow cytometry experiments confirmed the cardioprotection of the GRK5-L41 variant during chronic ISO exposure.

6.3.5 Hypertrophic response assay

BNP is an endocrine hormone synthesized in cardiomyocytes and is released to target its receptors on endothelial cells, kidney, vascular smooth muscle cells, and adrenal gland (Sergeeva and Christoffels, 2013; Sturgill et al., 2011). BNP mRNA was found to be upregulated and released at 18 h after MI induced by isoproterenol injection in rats (Sergeeva and Christoffels, 2013). Therefore, quantification of BNP intensity at any specific time does not present for the total BNP production in hPSC-CMs. This may explain why the general maximum percentage of cells producing BNP during chronic ISO or ET-1 treatment was < 40% at 24 h, whereas treatment with ET-1 for 18h activated 60% of cardiomyocytes producing BNP in both Q41 and L41 variant. Therefore, quantification of BNP in spent media would further enhance the accuracy of BNP production quantification.

6.4 Future work:

Although the study has developed various assays to characterise and validate the phenotype of GRK5-Q41L variants on the isogenic and heterogenic hPSC-CM models, additional experiments should be performed to increase the phenotyping and to elucidate the molecular mechanism associated with the gain-of-function phenotype of GRK5-L41:

1. Characterizing hypertrophic responses of GRK5-Q41L variant using high content imaging analysis of cell area or flow cytometer analysis of cell volumes to identify an association of cell size/volume changes with the levels of BNP induction and ERK phosphorylation in GRK5-Q41L CMs. The flow cytometry approach has the advantage that cell volume is quantified and overcomes the artefact of cell spreading and cell density in 2D (Mosqueira et al., 2019, 2018).
2. Confirming the proposed mechanism by additional contractility assay by CellOPTIQ, qPCR and cell death assay by flow cytometry when inhibiting GRK5-Q41L activity and ERK1/2 activation.
3. Reproducing experiments studying the mechanism of GRK5-Q41L variant on hIPSC models to add confidence to the proposed mechanism(s).
4. Developing an immunoprecipitation assay to quantify the interaction of GRK5 with β1-AR, β2-AR and CaM to determine the impact of the GRK5-Q41L variant on canonical and noncanonical functions of GRK5 in the hPSC-CM model during acute and chronic ISO exposure.
5. RNA sequencing and phosphor-proteomic analysis to identify the candidate signalling targets and pathways between GRK5-Q41 and GRK5-L41 haplotypes.

6. Generating isogenic pair for hIPSC-GRK5-Q41L then applying the same experimental layout to further confirmation and understanding the phenotype of GRK5-Q41L on different genetic background.

References

A. Grisanti, L., A. Talarico, J., Carter, R.L., E. Yu, J., A. Repas, A., Radcliffe, S.W., Tang, H., Makarewich, C.A., Houser, S.R., G. Tilley, D., 2019. beta-adrenergic receptor-mediated transactivation of EGFR decreases cardiomyocyte apoptosis through differential subcellular activation of ERK and Akt.pdf. https://doi.org/10.25376/hra.7819955.v1

Ahles, A., Engelhardt, S., 2014. Polymorphic Variants of Adrenoceptors: Pharmacology, Physiology, and Role in Disease. Pharmacol. Rev. 66, 598–637. https://doi.org/10.1124/pr.113.008219

Ahn, S., Kim, J., Hara, M.R., Ren, X.-R., Lefkowitz, R.J., 2009. β-Arrestin-2 Mediates Anti-apoptotic Signaling through Regulation of BAD Phosphorylation. J. Biol. Chem. 284, 8855–8865. https://doi.org/10.1074/jbc.M808463200

Alessi, D.R., Cuenda, A., Cohen, P., Dudley, D.T., Saltiel, A.R., 1995. PD 098059 Is a Specific Inhibitor of the Activation of Mitogen-activated Protein Kinase Kinase in Vitro and in Vivo. J. Biol. Chem. 270, 27489–27494. https://doi.org/10.1074/jbc.270.46.27489

Anderson, D., Self, T., Mellor, I.R., Goh, G., Hill, S.J., Denning, C., 2007. Transgenic Enrichment of Cardiomyocytes From Human Embryonic Stem Cells. Mol. Ther. 15, 2027–2036. https://doi.org/10.1038/sj.mt.6300303

Andersson, D.C., Fauconnier, J., Yamada, T., Lacampagne, A., Zhang, S.-J., Katz, A., Westerblad, H., 2011. Mitochondrial production of reactive oxygen species contributes to the β-adrenergic stimulation of mouse cardiomycytes. J. Physiol. 589, 1791–1801. https://doi.org/10.1113/jphysiol.2010.202838

Aries, A., Paradis, P., Lefebvre, C., Schwartz, R.J., Nemer, M., 2004. Essential role of GATA-4 in cell survival and drug-induced cardiotoxicity. Proc. Natl. Acad. Sci. 101, 6975–6980. https://doi.org/10.1073/pnas.0401833101

Baillie, G.S., Sood, A., McPhee, I., Gall, I., Perry, S.J., Lefkowitz, R.J., Houslay, M.D., 2003. β-Arrestin-mediated PDE4 cAMP phosphodiesterase recruitment regulates β-adrenoceptor switching from Gs to Gi. Proc. Natl. Acad. Sci. 100, 940–945. https://doi.org/10.1073/pnas.262787199

Balligand, J.-L., 2013. Beta3-Adrenoreceptors in Cardiovasular Diseases: New Roles for an “Old” Receptor [WWW Document]. URL https://www.ingentaconnect.com/content/ben/cdd/2013/00000010/00000001/art00011 (accessed 8.1.19).

Ban, H., Nishishita, N., Fusaki, N., Tabata, T., Saeki, K., Shikamura, M., Takada, N., Inoue, M., Hasegawa, M., Kawamata, S., Nishikawa, S.-I., 2011. Efficient generation of transgene-free human induced pluripotent stem cells (iPSCs) by temperature-sensitive Sendai virus vectors. Proc. Natl. Acad. Sci. 108, 14234–14239. https://doi.org/10.1073/pnas.1103509108

Bhogal, N.K., Hasan, A., Gorelik, J., 2018. The Development of Compartmentation of cAMP Signaling in Cardiomyocytes: The Role of T-Tubules and Caveolae Microdomains. J. Cardiovasc. Dev. Dis. 5, 25. https://doi.org/10.3390/jcdd5020025

Blinova, K., Dang, Q., Millard, D., Smith, G., Pierson, J., Guo, L., Brock, M., Lu, H.R., Kraushaar, U., Zeng, H., Shi, H., Zhang, X., Sawada, K., Osada, T., Kanda, Y., Sekino, Y., Pang, L., Feaster, T.K., Kettenhofen,

R., Stockbridge, N., Strauss, D.G., Gintant, G., 2018. International Multisite Study of Human-Induced Pluripotent Stem Cell-Derived Cardiomyocytes for Drug Proarrhythmic Potential Assessment. Cell Rep. 24, 3582–3592. https://doi.org/10.1016/j.celrep.2018.08.079

Blinova, K., Stohlman, J., Vicente, J., Chan, D., Johannesen, L., Hortigon-Vinagre, M.P., Zamora, V., Smith, G., Crumb, W.J., Pang, L., Lyn-Cook, B., Ross, J., Brock, M., Chvatal, S., Millard, D., Galeotti, L., Stockbridge, N., Strauss, D.G., 2017. Comprehensive Translational Assessment of Human-Induced Pluripotent Stem Cell Derived Cardiomyocytes for Evaluating Drug-Induced Arrhythmias. Toxicol. Sci. 155, 234–247. https://doi.org/10.1093/toxsci/kfw200

Bourque, K., Jones-Tabah, J., Mnasri, N., Martin, R.D., Hébert, T.E., 2018. Combining Optical Approaches with Human Inducible Pluripotent Stem Cells in G Protein-Coupled Receptor Drug Screening and Development. Biomolecules 8, 180. https://doi.org/10.3390/biom8040180

Bristow, M.R., 2000. β-Adrenergic Receptor Blockade in Chronic Heart Failure. Circulation 101, 558–569. https://doi.org/10.1161/01.CIR.101.5.558

Bristow, M.R., Ginsburg, R., Umans, V., Fowler, M., Minobe, W., Rasmussen, R., Zera, P., Menlove, R., Shah, P., Jamieson, S., 1986. Beta 1- and beta 2-adrenergic-receptor subpopulations in nonfailing and failing human ventricular myocardium: coupling of both receptor subtypes to muscle contraction and selective beta 1-receptor down-regulation in heart failure. Circ. Res. 59, 297–309. https://doi.org/10.1161/01.RES.59.3.297

Brito-Martins, M., Harding, S.E., Ali, N.N., 2008. β1- and β2-adrenoceptor responses in cardiomyocytes derived from human embryonic stem cells: comparison with failing and non-failing adult human heart. Br. J. Pharmacol. 153, 751–759. https://doi.org/10.1038/sj.bjp.0707619

Brodde, O.-E., 2008. β-1 and β-2 adrenoceptor polymorphisms: Functional importance, impact on cardiovascular diseases and drug responses. Pharmacol. Ther. 117, 1–29. https://doi.org/10.1016/j.pharmthera.2007.07.002

Brodde, O.-E., 2007. β-adrenoceptor blocker treatment and the cardiac β-adrenoceptor-G-protein(s)-adenylyl cyclase system in chronic heart failure. Naunyn. Schmiedebergs Arch. Pharmacol. 374, 361–372. https://doi.org/10.1007/s00210-006-0125-7

Bueno, O.F., De Windt, L.J., Tymitz, K.M., Witt, S.A., Kimball, T.R., Klevitsky, R., Hewett, T.E., Jones, S.P., Lefer, D.J., Peng, C.-F., Kitsis, R.N., Molkentin, J.D., 2000. The MEK1–ERK1/2 signaling pathway promotes compensated cardiac hypertrophy in transgenic mice. EMBO J. 19, 6341–6350. https://doi.org/10.1093/emboj/19.23.6341

Burkhalter, M.D., Fralish, G.B., Premont, R.T., Caron, M.G., Philipp, M., 2013. Grk5l Controls Heart Development by Limiting mTOR Signaling during Symmetry Breaking. Cell Rep. 4, 625–632. https://doi.org/10.1016/j.celrep.2013.07.036

Burridge, P.W., Keller, G., Gold, J.D., Wu, J.C., 2012. Production of De Novo Cardiomyocytes: Human Pluripotent Stem Cell Differentiation and Direct Reprogramming. Cell Stem Cell 10, 16–28. https://doi.org/10.1016/j.stem.2011.12.013

Burridge, P.W., Li, Y.F., Matsa, E., Wu, H., Ong, S.-G., Sharma, A., Holmström, A., Chang, A.C., Coronado, M.J., Ebert, A.D., Knowles, J.W., Telli, M.L., Witteles, R.M., Blau, H.M., Bernstein, D., Altman, R.B., Wu, J.C., 2016. Human induced pluripotent stem cell-derived

cardiomyocytes recapitulate the predilection of breast cancer patients to doxorubicin-induced cardiotoxicity. Nat. Med. 22, 547–556. https://doi.org/10.1038/nm.4087

Burridge, P.W., Matsa, E., Shukla, P., Lin, Z.C., Churko, J.M., Ebert, A.D., Lan, F., Diecke, S., Huber, B., Mordwinkin, N.M., Plews, J.R., Abilez, O.J., Cui, B., Gold, J.D., Wu, J.C., 2014. Chemically defined generation of human cardiomyocytes. Nat. Methods 11, 855–860. https://doi.org/10.1038/nmeth.2999

Burridge, P.W., Thompson, S., Millrod, M.A., Weinberg, S., Yuan, X., Peters, A., Mahairaki, V., Koliatsos, V.E., Tung, L., Zambidis, E.T., 2011. A Universal System for Highly Efficient Cardiac Differentiation of Human Induced Pluripotent Stem Cells That Eliminates Interline Variability. PLoS ONE 6, e18293. https://doi.org/10.1371/journal.pone.0018293

Cahill, T.J., Thomsen, A.R.B., Tarrasch, J.T., Plouffe, B., Nguyen, A.H., Yang, F., Huang, L.-Y., Kahsai, A.W., Bassoni, D.L., Gavino, B.J., Lamerdin, J.E., Triest, S., Shukla, A.K., Berger, B., Little, J., Antar, A., Blanc, A., Qu, C.-X., Chen, X., Kawakami, K., Inoue, A., Aoki, J., Steyaert, J., Sun, J.-P., Bouvier, M., Skiniotis, G., Lefkowitz, R.J., 2017. Distinct conformations of GPCR–β-arrestin complexes mediate desensitization, signaling, and endocytosis. Proc. Natl. Acad. Sci. 114, 2562–2567. https://doi.org/10.1073/pnas.1701529114

Carman, C.V., Som, T., Kim, C.M., Benovic, J.L., 1998. Binding and Phosphorylation of Tubulin by G Protein-coupled Receptor Kinases. J. Biol. Chem. 273, 20308–20316. https://doi.org/10.1074/jbc.273.32.20308

Carr, R., Schilling, J., Song, J., Carter, R.L., Du, Y., Yoo, S.M., Traynham, C.J., Koch, W.J., Cheung, J.Y., Tilley, D.G., Benovic, J.L., 2016. β-arrestin–biased signaling through the β2-adrenergic receptor promotes cardiomyocyte contraction. Proc. Natl. Acad. Sci. 113, E4107–E4116. https://doi.org/10.1073/pnas.1606267113

Chaikuad, A., Tacconi, E.M.C., Zimmer, J., Liang, Y., Gray, N.S., Tarsounas, M., Knapp, S., 2014. A unique inhibitor binding site in ERK1/2 is associated with slow binding kinetics. Nat. Chem. Biol. 10, 853–860. https://doi.org/10.1038/nchembio.1629

Chang, Y.X., Mummery, C.L., 2018. Human-Induced Pluripotent Stem Cell-Derived Cardiomyocytes in the Evaluation of Cardiotoxic Potential of Drugs, in: Delgado-Morales, R. (Ed.), Stem Cell Genetics for Biomedical Research: Past, Present, and Future. Springer International Publishing, Cham, pp. 173–194. https://doi.org/10.1007/978-3-319-90695-9_8

Charest, P.G., Terrillon, S., Bouvier, M., 2005. Monitoring agonist-promoted conformational changes of β-arrestin in living cells by intramolecular BRET. EMBO Rep. 6, 334–340. https://doi.org/10.1038/sj.embor.7400373

Chen, H., Ma, N., Xia, J., Liu, J., Xu, Z., 2012. β2-Adrenergic receptor-induced transactivation of epidermal growth factor receptor and platelet-derived growth factor receptor via Src kinase promotes rat cardiomyocyte survival. Cell Biol. Int. 36, 237–244. https://doi.org/10.1042/CBI20110162

Chen Mai, Sato Priscila Y., Chuprun J. Kurt, Peroutka Raymond J., Otis Nicholas J., Ibetti Jessica, Pan Shi, Sheu Shey-Shing, Gao Erhe, Koch Walter J., 2013. Prodeath Signaling of G Protein–Coupled Receptor Kinase 2 in Cardiac Myocytes After Ischemic Stress Occurs Via Extracellular Signal–Regulated Kinase-Dependent Heat Shock Protein 90–Mediated Mitochondrial Targeting. Circ. Res. 112, 1121–1134. https://doi.org/10.1161/CIRCRESAHA.112.300754

Chen, X., Zhu, H., Yuan, M., Fu, J., Zhou, Y., Ma, L., 2010. G-protein-coupled Receptor Kinase 5 Phosphorylates p53 and Inhibits DNA Damage-induced Apoptosis. J. Biol. Chem. 285, 12823–12830. https://doi.org/10.1074/jbc.M109.094243

Chuang, T.T., Paolucci, L., Blasi, A.D., 1996. Inhibition of G Protein-coupled Receptor Kinase Subtypes by Ca2+/Calmodulin. J. Biol. Chem. 271, 28691–28696. https://doi.org/10.1074/jbc.271.45.28691

Cipolletta, E., Dl, G., Lc, A., Annunziata, R., Iaccarino, G., 2013. B2 Adrenergic Receptor Polymorphisms and Treatment- Outcomes in Cardiovascular Diseases. Int. J. Cardiovasc. Res. 02. https://doi.org/10.4172/2324-8602.1000119

Communal, C., Singh, K., Sawyer, D.B., Colucci, W.S., 1999. Opposing Effects of β1- and β2-Adrenergic Receptors on Cardiac Myocyte Apoptosis : Role of a Pertussis Toxin–Sensitive G Protein. Circulation 100, 2210–2212. https://doi.org/10.1161/01.CIR.100.22.2210

Corbi, G., Conti, V.P., Russomanno, G., Longobardi, G., Furgi, G., Filippelli, A., Ferrara, N., 2013. Adrenergic signaling and oxidative stress: a role for sirtuins? Front. Physiol. 4. https://doi.org/10.3389/fphys.2013.00324

Cotarlan, V., Brofferio, A., Gerhard, G.S., Chu, X., Shirani, J., 2013. Impact of β1- and β2-Adrenergic Receptor Gene Single Nucleotide Polymorphisms on Heart Rate Response to Metoprolol Prior to Coronary Computed Tomographic Angiography. Am. J. Cardiol. 111, 661–666. https://doi.org/10.1016/j.amjcard.2012.11.015

De Los Angeles, A., Ferrari, F., Xi, R., Fujiwara, Y., Benvenisty, N., Deng, H., Hochedlinger, K., Jaenisch, R., Lee, S., Leitch, H.G., Lensch, M.W., Lujan, E., Pei, D., Rossant, J., Wernig, M., Park, P.J., Daley, G.Q., 2015. Hallmarks of pluripotency. Nature 525, 469–478. https://doi.org/10.1038/nature15515

Denning, C., Allegrucci, C., Priddle, H., Barbadillo-munoz, M.D., Anderson, D., Self, T., Smith, N.M., Parkin, T., Young, L.E., 2006. Common culture conditions for maintenance and cardiomyocyte differentiation of the human embryonic stem cell lines, BG01 and HUES-7. Int. J. Dev. Biol. 50, 27–37. https://doi.org/10.1387/ijdb.052107cd

Denning, C., Borgdorff, V., Crutchley, J., Firth, K.S.A., George, V., Kalra, S., Kondrashov, A., Hoang, M.D., Mosqueira, D., Patel, A., Prodanov, L., Rajamohan, D., Skarnes, W.C., Smith, J.G.W., Young, L.E., 2016. Cardiomyocytes from human pluripotent stem cells: From laboratory curiosity to industrial biomedical platform. Biochim. Biophys. Acta BBA - Mol. Cell Res., Cardiomyocyte Biology: Integration of Developmental and Environmental Cues in the Heart 1863, 1728–1748. https://doi.org/10.1016/j.bbamcr.2015.10.014

Dimmeler, S., Ding, S., Rando, T.A., Trounson, A., 2014. Translational strategies and challenges in regenerative medicine. Nat. Med. 20, 814–821. https://doi.org/10.1038/nm.3627

Ding, B., Abe, J., Wei, H., Xu, H., Che, W., Aizawa, T., Liu, W., Molina, C.A., Sadoshima, J., Blaxall, B.C., Berk, B.C., Yan, C., 2005. A positive feedback loop of phosphodiesterase 3 (PDE3) and inducible cAMP early repressor (ICER) leads to cardiomyocyte apoptosis. Proc. Natl. Acad. Sci. U. S. A. 102, 14771–14776. https://doi.org/10.1073/pnas.0506489102

Dixon, J.E., Dick, E., Rajamohan, D., Shakesheff, K.M., Denning, C., 2011. Directed Differentiation of Human Embryonic Stem Cells to Interrogate the Cardiac Gene Regulatory Network. Mol. Ther. 19, 1695–1703. https://doi.org/10.1038/mt.2011.125

Dolatshad, N.F., Hellen, N., Jabbour, R.J., Harding, S.E., Földes, G., 2015. G-protein Coupled Receptor Signaling in Pluripotent Stem Cell-derived Cardiovascular Cells: Implications for Disease Modeling. Front. Cell Dev. Biol. 3. https://doi.org/10.3389/fcell.2015.00076

Dorn, G.W., 2010a. Adrenergic Signaling Polymorphisms and Their Impact on Cardiovascular Disease. Physiol. Rev. 90, 1013–1062. https://doi.org/10.1152/physrev.00001.2010

Dorn, G.W., 2010b. Refugee Receptors Switch Sides. Science 327, 1586–1587. https://doi.org/10.1126/science.1188538

Dorn, G.W., 2009. GRK mythology: G-protein receptor kinases in cardiovascular disease. J. Mol. Med. 87, 455–463. https://doi.org/10.1007/s00109-009-0450-7

Dorn, G.W., Liggett, S.B., 2013. G-protein coupled receptor kinase-5 polymorphism. US8530160 B2.

Dorn, G.W., Liggett, S.B., 2009. Mechanisms of Pharmacogenomic Effects of Genetic Variation within the Cardiac Adrenergic Network in Heart Failure. Mol. Pharmacol. 76, 466–480. https://doi.org/10.1124/mol.109.056572

Dries, E., Santiago, D.J., Johnson, D.M., Gilbert, G., Holemans, P., Korte, S.M., Roderick, H.L., Sipido, K.R., 2016. Calcium/calmodulin-dependent kinase II and nitric oxide synthase 1-dependent modulation of ryanodine receptors during β-adrenergic stimulation is restricted to the dyadic cleft. J. Physiol. 594, 5923–5939. https://doi.org/10.1113/JP271965

Duncan, G., Firth, K., George, V., Hoang, M.D., Staniforth, A., Smith, G., Denning, C., 2017. Drug-Mediated Shortening of Action Potentials in LQTS2 Human Induced Pluripotent Stem Cell-Derived Cardiomyocytes. Stem Cells Dev. 26, 1695–1705. https://doi.org/10.1089/scd.2017.0172

Dunn, K.K., Palecek, S.P., 2018. Engineering Scalable Manufacturing of High-Quality Stem Cell-Derived Cardiomyocytes for Cardiac Tissue Repair. Front. Med. 5. https://doi.org/10.3389/fmed.2018.00110

El-Armouche, A., Eschenhagen, T., 2008. β-Adrenergic stimulation and myocardial function in the failing heart. Heart Fail. Rev. 14, 225. https://doi.org/10.1007/s10741-008-9132-8

Empel, V.P.M. van, Windt, L.J.D., 2004. Myocyte hypertrophy and apoptosis: a balancing act. Cardiovasc. Res. 63, 487–499. https://doi.org/10.1016/j.cardiores.2004.02.013

Fermini, B., Hancox, J.C., Abi-Gerges, N., Bridgland-Taylor, M., Chaudhary, K.W., Colatsky, T., Correll, K., Crumb, W., Damiano, B., Erdemli, G., Gintant, G., Imredy, J., Koerner, J., Kramer, J., Levesque, P., Li, Z., Lindqvist, A., Obejero-Paz, C.A., Rampe, D., Sawada, K., Strauss, D.G., Vandenberg, J.I., 2016. A New Perspective in the Field of Cardiac Safety Testing through the Comprehensive In Vitro Proarrhythmia Assay Paradigm. J. Biomol. Screen. 21, 1–11. https://doi.org/10.1177/1087057115594589

Földes, G., Matsa, E., Kriston-Vizi, J., Leja, T., Amisten, S., Kolker, L., Kodagoda, T., Dolatshad, N.F., Mioulane, M., Vauchez, K., Arányi, T., Ketteler, R., Schneider, M.D., Denning, C., Harding, S.E., 2014. Aberrant α-Adrenergic Hypertrophic Response in Cardiomyocytes from Human Induced Pluripotent Cells. Stem Cell Rep. 3, 905–914. https://doi.org/10.1016/j.stemcr.2014.09.002

Fredericks, Z.L., Pitcher, J.A., Lefkowitz, R.J., 1996. Identification of the G Protein-coupled Receptor Kinase Phosphorylation Sites in the Human β2-Adrenergic Receptor. J. Biol. Chem. 271, 13796–13803. https://doi.org/10.1074/jbc.271.23.13796

Fredriksson, R., Lagerström, M.C., Lundin, L.-G., Schiöth, H.B., 2003. The G-Protein-Coupled Receptors in the Human Genome Form Five Main Families. Phylogenetic Analysis, Paralogon Groups, and Fingerprints. Mol. Pharmacol. 63, 1256–1272. https://doi.org/10.1124/mol.63.6.1256

Fujio Yasushi, Nguyen Thao, Wencker Detlef, Kitsis Richard N., Walsh Kenneth, 2000. Akt Promotes Survival of Cardiomyocytes In Vitro and Protects Against Ischemia-Reperfusion Injury in Mouse Heart. Circulation 101, 660–667. https://doi.org/10.1161/01.CIR.101.6.660

Fusaki, N., Ban, H., Nishiyama, A., Saeki, K., Hasegawa, M., 2009. Efficient induction of transgene-free human pluripotent stem cells using a vector based on Sendai virus, an RNA virus that does not integrate into the host genome. Proc. Jpn. Acad. Ser. B 85, 348–362. https://doi.org/10.2183/pjab.85.348

Fusco, A., Santulli, G., Sorriento, D., Cipolletta, E., Garbi, C., Dorn, G.W., Trimarco, B., Feliciello, A., Iaccarino, G., 2012. Mitochondrial localization unveils a novel role for GRK2 in organelle biogenesis. Cell. Signal. 24, 468–475. https://doi.org/10.1016/j.cellsig.2011.09.026

Gainetdinov, R.R., Bohn, L.M., Walker, J.K.L., Laporte, S.A., Macrae, A.D., Caron, M.G., Lefkowitz, R.J., Premont, R.T., 1999. Muscarinic Supersensitivity and Impaired Receptor Desensitization in G Protein–Coupled Receptor Kinase 5–Deficient Mice. Neuron 24, 1029–1036. https://doi.org/10.1016/S0896-6273(00)81048-X

Gallo, S., Vitacolonna, A., Bonzano, A., Comoglio, P., Crepaldi, T., 2019. ERK: A Key Player in the Pathophysiology of Cardiac Hypertrophy. Int. J. Mol. Sci. 20, 2164. https://doi.org/10.3390/ijms20092164

Gardner, D.G., 2003. Natriuretic peptides: markers or modulators of cardiac hypertrophy? Trends Endocrinol. Metab. 14, 411–416. https://doi.org/10.1016/S1043-2760(03)00113-9

Gargiulo, L., Copsel, S., Rivero, E.M., Galés, C., Sénard, J.-M., Lüthy, I.A., Davio, C., Bruzzone, A., 2014. Differential β2-adrenergic receptor expression defines the phenotype of non-tumorigenic and malignant human breast cell lines. Oncotarget 5, 10058–10069. https://doi.org/10.18632/oncotarget.2460

Giacomelli, E., Mummery, C.L., Bellin, M., 2017. Human heart disease: lessons from human pluripotent stem cell-derived cardiomyocytes. Cell. Mol. Life Sci. 74, 3711–3739. https://doi.org/10.1007/s00018-017-2546-5

Ginsburg, K.S., Bers, D.M., 2004. Modulation of excitation-contraction coupling by isoproterenol in cardiomyocytes with controlled SR Ca2+ load and Ca2+ current trigger. J. Physiol. 556, 463–480. https://doi.org/10.1113/jphysiol.2003.055384

Gold, J.I., Martini, J.S., Hullmann, J., Gao, E., Chuprun, J.K., Lee, L., Tilley, D.G., Rabinowitz, J.E., Bossuyt, J., Bers, D.M., Koch, W.J., 2013. Nuclear Translocation of Cardiac G Protein-Coupled Receptor Kinase 5 Downstream of Select Gq-Activating Hypertrophic Ligands Is a Calmodulin-Dependent Process. PLOS ONE 8, e57324. https://doi.org/10.1371/journal.pone.0057324

Gorelik, J., Wright, P.T., Lyon, A.R., Harding, S.E., 2013. Spatial control of the βAR system in heart failure: the transverse tubule and beyond. Cardiovasc. Res. 98, 216–224. https://doi.org/10.1093/cvr/cvt005

Grisanti, L.A., Schumacher, S.M., Tilley, D.G., Koch, W.J., 2018. Designer Approaches for G Protein–Coupled Receptor Modulation for Cardiovascular Disease. JACC Basic Transl. Sci. 3, 550–562. https://doi.org/10.1016/j.jacbts.2017.12.002

Grisanti, L.A., Talarico, J.A., Carter, R.L., Yu, J.E., Repas, A.A., Radcliffe, S.W., Tang, H., Makarewich, C.A., Houser, S.R., Tilley, D.G., 2014. β-Adrenergic receptor-mediated transactivation of epidermal growth factor receptor decreases cardiomyocyte apoptosis through differential subcellular activation of ERK1/2 and Akt. J. Mol. Cell. Cardiol. 72, 39–51. https://doi.org/10.1016/j.yjmcc.2014.02.009

Gurevich, V.V., Gurevich, E.V., 2019. GPCR Signaling Regulation: The Role of GRKs and Arrestins. Front. Pharmacol. 10. https://doi.org/10.3389/fphar.2019.00125

Gurevich, V.V., Gurevich, E.V., 2016. G Protein-Coupled Receptor Kinases (GRKs) History: Evolution and Discovery, in: G Protein-Coupled Receptor Kinases, Methods in Pharmacology and Toxicology. Humana Press, New York, NY, pp. 3–22. https://doi.org/10.1007/978-1-4939-3798-1_1

Hanania, N.A., Sharafkhaneh, A., Barber, R., Dickey, B.F., 2002. β-Agonist Intrinsic Efficacy. Am. J. Respir. Crit. Care Med. 165, 1353–1358. https://doi.org/10.1164/rccm.2109060

Harris Ian S., Zhang Shaosong, Treskov Ilya, Kovacs Attila, Weinheimer Carla, Muslin Anthony J., 2004. Raf-1 Kinase Is Required for Cardiac Hypertrophy and Cardiomyocyte Survival in Response to Pressure Overload. Circulation 110, 718–723. https://doi.org/10.1161/01.CIR.0000138190.50127.6A

Hartman, M.E., Dai, D.-F., Laflamme, M.A., 2016. Human pluripotent stem cells: Prospects and challenges as a source of cardiomyocytes for in vitro modeling and cell-based cardiac repair. Adv. Drug Deliv. Rev., Tissue engineering of the heart: from in vitro models to regenerative solutions 96, 3–17. https://doi.org/10.1016/j.addr.2015.05.004

Hauser, A.S., Chavali, S., Masuho, I., Jahn, L.J., Martemyanov, K.A., Gloriam, D.E., Babu, M.M., 2018. Pharmacogenomics of GPCR Drug Targets. Cell 172, 41-54.e19. https://doi.org/10.1016/j.cell.2017.11.033

He, Y., Gao, X., Goswami, D., Hou, L., Pal, K., Yin, Y., Zhao, G., Ernst, O.P., Griffin, P., Melcher, K., Xu, H.E., 2017. Molecular assembly of rhodopsin with G protein-coupled receptor kinases., Molecular assembly of rhodopsin with G protein-coupled receptor kinases. Cell Res. Cell Res. 27, 27, 728, 728–747. https://doi.org/10.1038/cr.2017.72, 10.1038/cr.2017.72

Heitzler, D., Durand, G., Gallay, N., Rizk, A., Ahn, S., Kim, J., Violin, J.D., Dupuy, L., Gauthier, C., Piketty, V., Crépieux, P., Poupon, A., Clément, F., Fages, F., Lefkowitz, R.J., Reiter, E., 2012. Competing G protein-coupled receptor kinases balance G protein and β-arrestin signaling. Mol. Syst. Biol. 8, 590. https://doi.org/10.1038/msb.2012.22

Hill, S.J., Baker, J.G., 2003. The ups and downs of Gs- to Gi-protein switching. Br. J. Pharmacol. 138, 1188–1189. https://doi.org/10.1038/sj.bjp.0705192

Ho, D., Yan, L., Iwatsubo, K., Vatner, D.E., Vatner, S.F., 2010. Modulation of β-Adrenergic Receptor Signaling in Heart Failure and Longevity: Targeting Adenylyl Cyclase Type 5. Heart Fail. Rev. 15, 495–512. https://doi.org/10.1007/s10741-010-9183-5

Homan, K.T., Wu, E., Cannavo, A., Koch, W.J., Tesmer, J.J.G., 2014. Identification and Characterization of Amlexanox as a G Protein-Coupled Receptor Kinase 5 Inhibitor. Molecules 19, 16937–16949. https://doi.org/10.3390/molecules191016937

Hullmann, J., Traynham, C.J., Coleman, R.C., Koch, W.J., 2016. The expanding GRK interactome: Implications in cardiovascular disease

and potential for therapeutic development. Pharmacol. Res. 110, 52–64. https://doi.org/10.1016/j.phrs.2016.05.008

Hullmann, J.E., Grisanti, L.A., Makarewich, C.A., Gao, E., Gold, J.I., Chuprun, J.K., Tilley, D.G., Houser, S.R., Koch, W.J., 2014. GRK5-Mediated Exacerbation of Pathological Cardiac Hypertrophy Involves Facilitation of Nuclear NFAT ActivityNovelty and Significance. Circ. Res. 115, 976–985. https://doi.org/10.1161/CIRCRESAHA.116.304475

Janmey, P.A., 1994. Phosphoinositides and Calcium as Regulators of Cellular Actin Assembly and Disassembly. Annu. Rev. Physiol. 56, 169–191. https://doi.org/10.1146/annurev.ph.56.030194.001125

Jean-Charles, P.-Y., Kaur, S., Shenoy, S.K., 2017. G Protein–Coupled Receptor Signaling Through β-Arrestin–Dependent Mechanisms: J. Cardiovasc. Pharmacol. 70, 142–158. https://doi.org/10.1097/FJC.0000000000000482

Jiménez-Sainz, M.C., Murga, C., Kavelaars, A., Jurado-Pueyo, M., Krakstad, B.F., Heijnen, C.J., Mayor, F., Aragay, A.M., 2005. G Protein-coupled Receptor Kinase 2 Negatively Regulates Chemokine Signaling at a Level Downstream from G Protein Subunits. Mol. Biol. Cell 17, 25–31. https://doi.org/10.1091/mbc.e05-05-0399

Johnson, L.R., Robinson, J.D., Lester, K.N., Pitcher, J.A., 2013. Distinct Structural Features of G Protein-Coupled Receptor Kinase 5 (GRK5) Regulate Its Nuclear Localization and DNA-Binding Ability. PLOS ONE 8, e62508. https://doi.org/10.1371/journal.pone.0062508

Johnson, L.R., Scott, M.G.H., Pitcher, J.A., 2004. G Protein-Coupled Receptor Kinase 5 Contains a DNA-Binding Nuclear Localization Sequence. Mol. Cell. Biol. 24, 10169–10179. https://doi.org/10.1128/MCB.24.23.10169-10179.2004

Kale, J., Osterlund, E.J., Andrews, D.W., 2018. BCL-2 family proteins: changing partners in the dance towards death. Cell Death Differ. 25, 65–80. https://doi.org/10.1038/cdd.2017.186

Kang, J.H., Lee, H.-S., Kang, Y.-W., Cho, K.-H., 2016. Systems biological approaches to the cardiac signaling network. Brief. Bioinform. 17, 419–428. https://doi.org/10.1093/bib/bbv039

Kang, P.M., Yue, P., Liu, Z., Tarnavski, O., Bodyak, N., Izumo, S., 2004. Alterations in apoptosis regulatory factors during hypertrophy and heart failure. Am. J. Physiol. - Heart Circ. Physiol. 287, H72–H80. https://doi.org/10.1152/ajpheart.00556.2003

Kang, S., Hong, X., Ruan, C., Yu, P., Yu, S., Chen, M., Zhang, D., Fan, H., Liu, Z., 2015. Effects of GRK5 and ADRB1 polymorphisms influence on systolic heart failure. J. Transl. Med. 13, 44. https://doi.org/10.1186/s12967-015-0402-7

Kashihara, T., Nakada, T., Kojima, K., Takeshita, T., Yamada, M., 2017. Angiotensin II activates CaV1.2 Ca2+ channels through β-arrestin2 and casein kinase 2 in mouse immature cardiomyocytes. J. Physiol. 595, 4207–4225. https://doi.org/10.1113/JP273883

Katritch, V., Cherezov, V., Stevens, R.C., 2013. Structure-Function of the G Protein–Coupled Receptor Superfamily. Annu. Rev. Pharmacol. Toxicol. 53, 531–556. https://doi.org/10.1146/annurev-pharmtox-032112-135923

Keung, W., Boheler, K.R., Li, R.A., 2014. Developmental cues for the maturation of metabolic, electrophysiological and calcium handling properties of human pluripotent stem cell-derived cardiomyocytes. Stem Cell Res. Ther. 5, 17. https://doi.org/10.1186/scrt406

Khan, J.M., Lyon, A.R., Harding, S.E., 2013. The case for induced pluripotent stem cell-derived cardiomyocytes in pharmacological screening. Br.

J. Pharmacol. 169, 304–317. https://doi.org/10.1111/j.1476-5381.2012.02118.x

Koch, W.J., Rockman, H.A., Samama, P., Hamilton, R.A., Bond, R.A., Milano, C.A., Lefkowitz, R.J., 1995. Cardiac function in mice overexpressing the beta-adrenergic receptor kinase or a beta ARK inhibitor. Science 268, 1350–1353. https://doi.org/10.1126/science.7761854

Kolenko, V., Teper, E., Kutikov, A., Uzzo, R., 2013. Zinc and zinc transporters in prostate carcinogenesis. Nat. Rev. Urol. 10, 219–226. https://doi.org/10.1038/nrurol.2013.43

Komolov, K.E., Benovic, J.L., 2018. G protein-coupled receptor kinases: Past, present and future. Cell. Signal., In Honor of Bob Lefkowitz 41, 17–24. https://doi.org/10.1016/j.cellsig.2017.07.004

Komolov, K.E., Bhardwaj, A., Benovic, J.L., 2015. Atomic Structure of GRK5 Reveals Distinct Structural Features Novel for G Protein-coupled Receptor Kinases. J. Biol. Chem. 290, 20629–20647. https://doi.org/10.1074/jbc.M115.647297

Komolov, K.E., Du, Y., Duc, N.M., Betz, R.M., Rodrigues, J.P.G.L.M., Leib, R.D., Patra, D., Skiniotis, G., Adams, C.M., Dror, R.O., Chung, K.Y., Kobilka, B.K., Benovic, J.L., 2017. Structural and Functional Analysis of a β2-Adrenergic Receptor Complex with GRK5. Cell 169, 407-421.e16. https://doi.org/10.1016/j.cell.2017.03.047

Kondrashov, A., Duc Hoang, M., Smith, J.G.W., Bhagwan, J.R., Duncan, G., Mosqueira, D., Munoz, M.B., Vo, N.T.N., Denning, C., 2018. Simplified Footprint-Free Cas9/CRISPR Editing of Cardiac-Associated Genes in Human Pluripotent Stem Cells. Stem Cells Dev. 27, 391–404. https://doi.org/10.1089/scd.2017.0268

Kontaridis, M.I., Geladari, E.V., Geladari, C.V., 2015. Pathways to Myocardial Hypertrophy, in: Cokkinos, D.V. (Ed.), Introduction to Translational Cardiovascular Research. Springer International Publishing, Cham, pp. 167–186. https://doi.org/10.1007/978-3-319-08798-6_10

Laudette, M., Coluccia, A., Sainte-Marie, Y., Solari, A., Fazal, L., Sicard, P., Silvestri, R., Mialet-Perez, J., Pons, S., Ghaleh, B., Blondeau, J.-P., Lezoualc'h, F., 2019. Identification of a pharmacological inhibitor of Epac1 that protects the heart against acute and chronic models of cardiac stress. Cardiovasc. Res. 115, 1766–1777. https://doi.org/10.1093/cvr/cvz076

Lefkowitz, R.J., Pierce, K.L., Luttrell, L.M., 2002. Dancing with Different Partners: Protein Kinase A Phosphorylation of Seven Membrane-Spanning Receptors Regulates Their G Protein-Coupling Specificity. Mol. Pharmacol. 62, 971–974. https://doi.org/10.1124/mol.62.5.971

Lefkowitz, R.J., Rajagopal, K., Whalen, E.J., 2006. New Roles for β-Arrestins in Cell Signaling: Not Just for Seven-Transmembrane Receptors. Mol. Cell 24, 643–652. https://doi.org/10.1016/j.molcel.2006.11.007

Lewin, G., Matus, M., Basu, A., Frebel, K., Rohsbach, S.P., Safronenko, A., Seidl, M.D., Stümpel, F., Buchwalow, I., König, S., Engelhardt, S., Lohse, M.J., Schmitz, W., Müller, F.U., 2009. Critical Role of Transcription Factor Cyclic AMP Response Element Modulator in β1-Adrenoceptor–Mediated Cardiac Dysfunction. Circulation 119, 79–88. https://doi.org/10.1161/CIRCULATIONAHA.108.786533

Li, D., Lu, C.-J., Hao, G., Wright, H., Woodward, L., Liu, K., Vergari, E., Surdo, N.C., Herring, N., Zaccolo, M., Paterson, D.J., 2015. Efficacy of B-Type Natriuretic Peptide Is Coupled to Phosphodiesterase 2A in Cardiac Sympathetic NeuronsNovelty and Significance. Hypertension 66, 190–198. https://doi.org/10.1161/HYPERTENSIONAHA.114.05054

Liggett, S.B., 2010. Pharmacogenomics of β1-Adrenergic Receptor Polymorphisms in Heart Failure. Heart Fail. Clin., Pharmacogenetics in Heart Failure: How It Will Shape the Future 6, 27–33. https://doi.org/10.1016/j.hfc.2009.08.011

Liggett, S.B., Cresci, S., Kelly, R.J., Syed, F.M., Matkovich, S.J., Hahn, H.S., Diwan, A., Martini, J.S., Sparks, L., Parekh, R.R., Spertus, J.A., Koch, W.J., Kardia, S.L.R., Dorn Ii, G.W., 2008. A GRK5 polymorphism that inhibits β-adrenergic receptor signaling is protective in heart failure. Nat. Med. 14, 510–517. https://doi.org/10.1038/nm1750

Liu, P., Wang, X., Gao, N., Zhu, H., Dai, X., Xu, Y., Ma, C., Huang, L., Liu, Y., Qin, C., 2010. G protein-coupled receptor kinase 5, overexpressed in the α-synuclein up-regulation model of Parkinson's disease, regulates bcl-2 expression. Brain Res. 1307, 134–141. https://doi.org/10.1016/j.brainres.2009.10.036

Liu, S., Premont, R.T., Kontos, C.D., Zhu, S., Rockey, D.C., 2005. A crucial role for GRK2 in regulation of endothelial cell nitric oxide synthase function in portal hypertension. Nat. Med. 11, 952–958. https://doi.org/10.1038/nm1289

Liu, Y., Li, Z., Guo, X., Jing, X., Zhang, X., Shao, H., Guan, Y., Abraham, M.R., 2017. Recent Advances in Hypertrophic Cardiomyopathy: A System Review. Genet. Polymorph. https://doi.org/10.5772/intechopen.69620

Lohse Martin J., Engelhardt Stefan, Eschenhagen Thomas, 2003. What Is the Role of β-Adrenergic Signaling in Heart Failure? Circ. Res. 93, 896–906. https://doi.org/10.1161/01.RES.0000102042.83024.CA

Lohse, M.J., Engelhardt, S., Eschenhagen, T., 2003a. What Is the Role of β-Adrenergic Signaling in Heart Failure? Circ. Res. 93, 896–906. https://doi.org/10.1161/01.RES.0000102042.83024.CA

Lohse, M.J., Engelhardt, S., Eschenhagen, T., 2003b. What Is the Role of β-Adrenergic Signaling in Heart Failure? Circ. Res. 93, 896–906. https://doi.org/10.1161/01.RES.0000102042.83024.CA

Lorenz, K., Schmitt, J.P., Schmitteckert, E.M., Lohse, M.J., 2009. A new type of ERK1/2 autophosphorylation causes cardiac hypertrophy. Nat. Med. 15, 75–83. https://doi.org/10.1038/nm.1893

Lucia, C. de, Eguchi, A., Koch, W.J., 2018. New Insights in Cardiac β-Adrenergic Signaling During Heart Failure and Aging. Front. Pharmacol. 9. https://doi.org/10.3389/fphar.2018.00904

Lundstrom, K., 2006. Latest Development in Drug Discovery on G Protein-coupled Receptors. Curr. Protein Pept. Sci. 7, 465–470. https://doi.org/10.2174/138920306778559403

Luttrell, L.M., Lefkowitz, R.J., 2002. The role of β-arrestins in the termination and transduction of G-protein-coupled receptor signals. J. Cell Sci. 115, 455–465.

Luttrell, L.M., Wang, J., Plouffe, B., Smith, J.S., Yamani, L., Kaur, S., Jean-Charles, P.-Y., Gauthier, C., Lee, M.-H., Pani, B., Kim, J., Ahn, S., Rajagopal, S., Reiter, E., Bouvier, M., Shenoy, S.K., Laporte, S.A., Rockman, H.A., Lefkowitz, R.J., 2018. Manifold roles of β-arrestins in GPCR signaling elucidated with siRNA and CRISPR/Cas9. Sci. Signal. 11, eaat7650. https://doi.org/10.1126/scisignal.aat7650

Lyon, A.R., MacLeod, K.T., Zhang, Y., Garcia, E., Kanda, G.K., Lab, M.J., Korchev, Y.E., Harding, S.E., Gorelik, J., 2009. Loss of T-tubules and other changes to surface topography in ventricular myocytes from failing human and rat heart. Proc. Natl. Acad. Sci. 106, 6854–6859. https://doi.org/10.1073/pnas.0809777106

Machyna, M., Neugebauer, K.M., Staněk, D., 2015. Coilin: The first 25 years. RNA Biol. 12, 590–596. https://doi.org/10.1080/15476286.2015.1034923

Madamanchi, A., 2007. β-Adrenergic receptor signaling in cardiac function and heart failure. McGill J. Med. MJM 10, 99–104.

Mangmool, S., Parichatikanond, W., Kurose, H., 2018. Therapeutic Targets for Treatment of Heart Failure: Focus on GRKs and β-Arrestins Affecting βAR Signaling. Front. Pharmacol. 9. https://doi.org/10.3389/fphar.2018.01336

Mangmool, S., Shukla, A.K., Rockman, H.A., 2010. β-Arrestin–dependent activation of Ca2+/calmodulin kinase II after β1–adrenergic receptor stimulation. J. Cell Biol. 189, 573–587. https://doi.org/10.1083/jcb.200911047

Marín-García, J., 2016. Cell death in the pathogenesis and progression of heart failure. Heart Fail. Rev. 21, 117–121. https://doi.org/10.1007/s10741-016-9538-7

Martini, J.S., Raake, P., Vinge, L.E., DeGeorge, B.R., Chuprun, J.K., Harris, D.M., Gao, E., Eckhart, A.D., Pitcher, J.A., Koch, W.J., 2008. Uncovering G protein-coupled receptor kinase-5 as a histone deacetylase kinase in the nucleus of cardiomyocytes. Proc. Natl. Acad. Sci. 105, 12457–12462. https://doi.org/10.1073/pnas.0803153105

Mayor, F., Cruces-Sande, M., Arcones, A.C., Vila-Bedmar, R., Briones, A.M., Salaices, M., Murga, C., 2018. G protein-coupled receptor kinase 2 (GRK2) as an integrative signalling node in the regulation of cardiovascular function and metabolic homeostasis. Cell. Signal., In Honor of Bob Lefkowitz 41, 25–32. https://doi.org/10.1016/j.cellsig.2017.04.002

Michal, A.M., So, C.H., Beeharry, N., Shankar, H., Mashayekhi, R., Yen, T.J., Benovic, J.L., 2012. G Protein-coupled Receptor Kinase 5 Is Localized to Centrosomes and Regulates Cell Cycle Progression. J. Biol. Chem. 287, 6928–6940. https://doi.org/10.1074/jbc.M111.298034

Millman, E.E., Rosenfeld, J.L., Vaughan, D.J., Nguyen, J., Dai, W., Alpizar-Foster, E., Clark, R.B., Knoll, B.J., Moore, R.H., 2004. Endosome sorting of β2-adrenoceptors is GRK5 independent. Br. J. Pharmacol. 141, 277–284. https://doi.org/10.1038/sj.bjp.0705504

Minami, I., Yamada, K., Otsuji, T.G., Yamamoto, T., Shen, Y., Otsuka, S., Kadota, S., Morone, N., Barve, M., Asai, Y., Tenkova-Heuser, T., Heuser, J.E., Uesugi, M., Aiba, K., Nakatsuji, N., 2012. A Small Molecule that Promotes Cardiac Differentiation of Human Pluripotent Stem Cells under Defined, Cytokine- and Xeno-free Conditions. Cell Rep. 2, 1448–1460. https://doi.org/10.1016/j.celrep.2012.09.015

Mockridge, J.W., Benton, E.C., Andreeva, L.V., Latchman, D.S., Marber, M.S., Heads, R.J., 2000. IGF-1 Regulates Cardiac Fibroblast Apoptosis Induced by Osmotic Stress. Biochem. Biophys. Res. Commun. 273, 322–327. https://doi.org/10.1006/bbrc.2000.2934

Morris, E.J., Jha, S., Restaino, C.R., Dayananth, P., Zhu, H., Cooper, A., Carr, D., Deng, Y., Jin, W., Black, S., Long, B., Liu, J., DiNunzio, E., Windsor, W., Zhang, R., Zhao, S., Angagaw, M.H., Pinheiro, E.M., Desai, J., Xiao, L., Shipps, G., Hruza, A., Wang, J., Kelly, J., Paliwal, S., Gao, X., Babu, B.S., Zhu, L., Daublain, P., Zhang, L., Lutterbach, B.A., Pelletier, M.R., Philippar, U., Siliphaivanh, P., Witter, D., Kirschmeier, P., Bishop, W.R., Hicklin, D., Gilliland, D.G., Jayaraman, L., Zawel, L., Fawell, S., Samatar, A.A., 2013. Discovery of a Novel ERK Inhibitor with Activity in Models of Acquired Resistance to BRAF

and MEK Inhibitors. Cancer Discov. 3, 742–750. https://doi.org/10.1158/2159-8290.CD-13-0070

Mosqueira, D., Mannhardt, I., Bhagwan, J.R., Lis-Slimak, K., Katili, P., Scott, E., Hassan, M., Prondzynski, M., Harmer, S.C., Tinker, A., Smith, J.G.W., Carrier, L., Williams, P.M., Gaffney, D., Eschenhagen, T., Hansen, A., Denning, C., 2018. CRISPR/Cas9 editing in human pluripotent stem cell-cardiomyocytes highlights arrhythmias, hypocontractility, and energy depletion as potential therapeutic targets for hypertrophic cardiomyopathy. Eur. Heart J. 39, 3879–3892. https://doi.org/10.1093/eurheartj/ehy249

Mosqueira, D., Smith, J.G.W., Bhagwan, J.R., Denning, C., 2019. Modeling Hypertrophic Cardiomyopathy: Mechanistic Insights and Pharmacological Intervention. Trends Mol. Med. https://doi.org/10.1016/j.molmed.2019.06.005

Mulder, P., de Korte, T., Dragicevic, E., Kraushaar, U., Printemps, R., Vlaming, M.L.H., Braam, S.R., Valentin, J.-P., 2018. Predicting cardiac safety using human induced pluripotent stem cell-derived cardiomyocytes combined with multi-electrode array (MEA) technology: A conference report. J. Pharmacol. Toxicol. Methods 91, 36–42. https://doi.org/10.1016/j.vascn.2018.01.003

Mummery Christine L., Zhang Jianhua, Ng Elizabeth S., Elliott David A., Elefanty Andrew G., Kamp Timothy J., 2012. Differentiation of Human Embryonic Stem Cells and Induced Pluripotent Stem Cells to Cardiomyocytes. Circ. Res. 111, 344–358. https://doi.org/10.1161/CIRCRESAHA.110.227512

Muthumala, A., Drenos, F., Elliott, P.M., Humphries, S.E., 2008. Role of β adrenergic receptor polymorphisms in heart failure: Systematic review and meta-analysis. Eur. J. Heart Fail. 10, 3–13. https://doi.org/10.1016/j.ejheart.2007.11.008

Mutlak, M., Schlesinger-Laufer, M., Haas, T., Shofti, R., Ballan, N., Lewis, Y.E., Zuler, M., Zohar, Y., Caspi, L.H., Kehat, I., 2018. Extracellular signal-regulated kinase (ERK) activation preserves cardiac function in pressure overload induced hypertrophy. Int. J. Cardiol. 270, 204–213. https://doi.org/10.1016/j.ijcard.2018.05.068

Nobles, K.N., Guan, Z., Xiao, K., Oas, T.G., Lefkowitz, R.J., 2007. The Active Conformation of β-Arrestin1 DIRECT EVIDENCE FOR THE PHOSPHATE SENSOR IN THE N-DOMAIN AND CONFORMATIONAL DIFFERENCES IN THE ACTIVE STATES OF β-ARRESTINS1 AND -2. J. Biol. Chem. 282, 21370–21381. https://doi.org/10.1074/jbc.M611483200

Nobles, K.N., Xiao, K., Ahn, S., Shukla, A.K., Lam, C.M., Rajagopal, S., Strachan, R.T., Huang, T.-Y., Bressler, E.A., Hara, M.R., Shenoy, S.K., Gygi, S.P., Lefkowitz, R.J., 2011. Distinct Phosphorylation Sites on the β2-Adrenergic Receptor Establish a Barcode That Encodes Differential Functions of β-Arrestin. Sci. Signal. 4, ra51. https://doi.org/10.1126/scisignal.2001707

Noh, H., Yu, M.R., Kim, H.J., Lee, J.H., Park, B.-W., Wu, I.-H., Matsumoto, M., King, G.L., 2017. Beta 2-adrenergic receptor agonists are novel regulators of macrophage activation in diabetic renal and cardiovascular complications. Kidney Int. 92, 101–113. https://doi.org/10.1016/j.kint.2017.02.013

Noma, T., Lemaire, A., Naga Prasad, S.V., Barki-Harrington, L., Tilley, D.G., Chen, J., Le Corvoisier, P., Violin, J.D., Wei, H., Lefkowitz, R.J., Rockman, H.A., 2007. β-Arrestin–mediated β1-adrenergic receptor transactivation of the EGFR confers cardioprotection. J. Clin. Invest. 117, 2445–2458. https://doi.org/10.1172/JCI31901

Oakley, R.H., Laporte, S.A., Holt, J.A., Caron, M.G., Barak, L.S., 2000. Differential Affinities of Visual Arrestin, βArrestin1, and βArrestin2 for G Protein-coupled Receptors Delineate Two Major Classes of Receptors. J. Biol. Chem. 275, 17201–17210. https://doi.org/10.1074/jbc.M910348199

O'Hayre, M., Eichel, K., Avino, S., Zhao, X., Steffen, D.J., Feng, X., Kawakami, K., Aoki, J., Messer, K., Sunahara, R., Inoue, A., Zastrow, M. von, Gutkind, J.S., 2017. Genetic evidence that β-arrestins are dispensable for the initiation of β2-adrenergic receptor signaling to ERK. Sci Signal 10, eaal3395. https://doi.org/10.1126/scisignal.aal3395

Overington, J.P., Al-Lazikani, B., Hopkins, A.L., 2006. How many drug targets are there? Nat. Rev. Drug Discov. 5, 993–996. https://doi.org/10.1038/nrd2199

Parikh, S.S., Blackwell, D.J., Gomez-Hurtado, N., Frisk, M., Wang, L., Kim, K., Dahl, C.P., Fiane, A., Tønnessen, T., Kryshtal, D.O., Louch, W.E., Knollmann, B.C., 2017. Thyroid and Glucocorticoid Hormones Promote Functional T-Tubule Development in Human-Induced Pluripotent Stem Cell–Derived Cardiomyocytes Novelty and Significance. Circ. Res. 121, 1323–1330. https://doi.org/10.1161/CIRCRESAHA.117.311920

Paur Helen, Wright Peter T., Sikkel Markus B., Tranter Matthew H., Mansfield Catherine, O'Gara Peter, Stuckey Daniel J., Nikolaev Viacheslav O., Diakonov Ivan, Pannell Laura, Gong Haibin, Sun Hong, Peters Nicholas S., Petrou Mario, Zheng Zhaolun, Gorelik Julia, Lyon Alexander R., Harding Sian E., 2012. High Levels of Circulating Epinephrine Trigger Apical Cardiodepression in a β2-Adrenergic Receptor/Gi–Dependent Manner. Circulation 126, 697–706. https://doi.org/10.1161/CIRCULATIONAHA.112.111591

Penela, P., Murga, C., Ribas, C., Tutor, A.S., Peregrín, S., Mayor, F., 2006. Mechanisms of regulation of G protein-coupled receptor kinases (GRKs) and cardiovascular disease. Cardiovasc. Res. 69, 46–56. https://doi.org/10.1016/j.cardiores.2005.09.011

Pfleger, J., Gresham, K., Koch, W.J., 2019a. G protein-coupled receptor kinases as therapeutic targets in the heart. Nat. Rev. Cardiol. 1–11. https://doi.org/10.1038/s41569-019-0220-3

Pfleger, J., Gresham, K., Koch, W.J., 2019b. G protein-coupled receptor kinases as therapeutic targets in the heart. Nat. Rev. Cardiol. 16, 612–622. https://doi.org/10.1038/s41569-019-0220-3

Philipp, M., Berger, I.M., Just, S., Caron, M.G., 2014. Overlapping and Opposing Functions of G Protein-coupled Receptor Kinase 2 (GRK2) and GRK5 during Heart Development. J. Biol. Chem. 289, 26119–26130. https://doi.org/10.1074/jbc.M114.551952

Pierce, K.L., Premont, R.T., Lefkowitz, R.J., 2002. Seven-transmembrane receptors. Nat. Rev. Mol. Cell Biol. 3, 639. https://doi.org/10.1038/nrm908

Pitt, G.S., Marx, S.O., 2014. 19 - Calmodulin and CaMKII as Ca2+ Switches for Cardiac Ion Channels, in: Zipes, D.P., Jalife, J. (Eds.), Cardiac Electrophysiology: From Cell to Bedside (Sixth Edition). W.B. Saunders, Philadelphia, pp. 189–195. https://doi.org/10.1016/B978-1-4557-2856-5.00019-4

Raake Philip W., Vinge Leif E., Gao Erhe, Boucher Matthieu, Rengo Giuseppe, Chen Xiongwen, DeGeorge Brent R., Matkovich Scot, Houser Steven R., Most Patrick, Eckhart Andrea D., Dorn Gerald W., Koch Walter J., 2008. G Protein–Coupled Receptor Kinase 2 Ablation in Cardiac Myocytes Before or After Myocardial Infarction Prevents Heart Failure.

Circ. Res. 103, 413–422. https://doi.org/10.1161/CIRCRESAHA.107.168336

Raake Philip W., Zhang Xiaoying, Vinge Leif E., Brinks Henriette, Gao Erhe, Jaleel Naser, Li Yingxin, Tang Mingxin, Most Patrick, Dorn Gerald W., Houser Steven R., Katus Hugo A., Chen Xiongwen, Koch Walter J., 2012. Cardiac G-Protein–Coupled Receptor Kinase 2 Ablation Induces a Novel Ca2+ Handling Phenotype Resistant to Adverse Alterations and Remodeling After Myocardial Infarction. Circulation 125, 2108–2118. https://doi.org/10.1161/CIRCULATIONAHA.111.044255

Rapacciuolo, A., Suvarna, S., Barki-Harrington, L., Luttrell, L.M., Cong, M., Lefkowitz, R.J., Rockman, H.A., 2003. Protein Kinase A and G Protein-coupled Receptor Kinase Phosphorylation Mediates β-1 Adrenergic Receptor Endocytosis through Different Pathways. J. Biol. Chem. 278, 35403–35411. https://doi.org/10.1074/jbc.M305675200

Ribas, C., Penela, P., Murga, C., Salcedo, A., García-Hoz, C., Jurado-Pueyo, M., Aymerich, I., Mayor Jr., F., 2007. The G protein-coupled receptor kinase (GRK) interactome: Role of GRKs in GPCR regulation and signaling. Biochim. Biophys. Acta BBA - Biomembr., G Protein-Coupled Receptors, Signaling Mechanisms and Pathophysiological Relevance 1768, 913–922. https://doi.org/10.1016/j.bbamem.2006.09.019

Ribeiro, M.C., Tertoolen, L.G., Guadix, J.A., Bellin, M., Kosmidis, G., D'Aniello, C., Monshouwer-Kloots, J., Goumans, M.-J., Wang, Y., Feinberg, A.W., Mummery, C.L., Passier, R., 2015. Functional maturation of human pluripotent stem cell derived cardiomyocytes in vitro – Correlation between contraction force and electrophysiology. Biomaterials 51, 138–150. https://doi.org/10.1016/j.biomaterials.2015.01.067

Robertson, C., Tran, D.D., George, S.C., 2013. Concise Review: Maturation Phases of Human Pluripotent Stem Cell-Derived Cardiomyocytes. STEM CELLS 31, 829–837. https://doi.org/10.1002/stem.1331

Rockman, H.A., Choi, D.J., Rahman, N.U., Akhter, S.A., Lefkowitz, R.J., Koch, W.J., 1996. Receptor-specific in vivo desensitization by the G protein-coupled receptor kinase-5 in transgenic mice. Proc. Natl. Acad. Sci. 93, 9954–9959. https://doi.org/10.1073/pnas.93.18.9954

Rockman, H.A., Koch, W.J., Lefkowitz, R.J., 2002. Seven-transmembrane-spanning receptors and heart function. Nature 415, 206. https://doi.org/10.1038/415206a

Rose, B.A., Force, T., Wang, Y., 2010. Mitogen-Activated Protein Kinase Signaling in the Heart: Angels Versus Demons in a Heart-Breaking Tale. Physiol. Rev. 90, 1507–1546. https://doi.org/10.1152/physrev.00054.2009

Ruppert, C., Deiss, K., Herrmann, S., Vidal, M., Oezkur, M., Gorski, A., Weidemann, F., Lohse, M.J., Lorenz, K., 2013. Interference with ERKThr188 phosphorylation impairs pathological but not physiological cardiac hypertrophy. Proc. Natl. Acad. Sci. 110, 7440–7445. https://doi.org/10.1073/pnas.1221999110

Saito, S., Hiroi, Y., Zou, Y., Aikawa, R., Toko, H., Shibasaki, F., Yazaki, Y., Nagai, R., Komuro, I., 2000. β-Adrenergic Pathway Induces Apoptosis through Calcineurin Activation in Cardiac Myocytes. J. Biol. Chem. 275, 34528–34533. https://doi.org/10.1074/jbc.M002844200

Sato, P.Y., Chuprun, J.K., Schwartz, M., Koch, W.J., 2015a. The Evolving Impact of G Protein-Coupled Receptor Kinases in Cardiac Health and Disease. Physiol. Rev. 95, 377–404. https://doi.org/10.1152/physrev.00015.2014

Sato, P.Y., Chuprun, J.K., Schwartz, M., Koch, W.J., 2015b. The Evolving Impact of G Protein-Coupled Receptor Kinases in Cardiac Health and Disease. Physiol. Rev. 95, 377–404. https://doi.org/10.1152/physrev.00015.2014

Savoji, H., Mohammadi, M.H., Rafatian, N., Toroghi, M.K., Wang, E.Y., Zhao, Y., Korolj, A., Ahadian, S., Radisic, M., 2019. Cardiovascular disease models: A game changing paradigm in drug discovery and screening. Biomaterials, Organoids and Ex Vivo Tissue On-Chip Technologies 198, 3–26. https://doi.org/10.1016/j.biomaterials.2018.09.036

Schobesberger, S., Wright, P., Tokar, S., Bhargava, A., Mansfield, C., Glukhov, A.V., Poulet, C., Buzuk, A., Monszpart, A., Sikkel, M., Harding, S.E., Nikolaev, V.O., Lyon, A.R., Gorelik, J., 2017. T-tubule remodelling disturbs localized β2-adrenergic signalling in rat ventricular myocytes during the progression of heart failure. Cardiovasc. Res. 113, 770–782. https://doi.org/10.1093/cvr/cvx074

Schumacher, S.M., Koch, W.J., 2017. Noncanonical Roles of G Protein-coupled Receptor Kinases in Cardiovascular Signaling. J. Cardiovasc. Pharmacol. 70, 129. https://doi.org/10.1097/FJC.0000000000000483

Sergeeva, I.A., Christoffels, V.M., 2013. Regulation of expression of atrial and brain natriuretic peptide, biomarkers for heart development and disease. Biochim. Biophys. Acta BBA - Mol. Basis Dis. 1832, 2403–2413. https://doi.org/10.1016/j.bbadis.2013.07.003

Shamas-Din, A., Kale, J., Leber, B., Andrews, D.W., 2013. Mechanisms of Action of Bcl-2 Family Proteins. Cold Spring Harb. Perspect. Biol. 5, a008714. https://doi.org/10.1101/cshperspect.a008714

Sheng, J.-J., Chang, H., Yu, Z.-B., 2015. Nuclear Translocation of Calpain-2 Mediates Apoptosis of Hypertrophied Cardiomyocytes in Transverse Aortic Constriction Rat. J. Cell. Physiol. 230, 2743–2754. https://doi.org/10.1002/jcp.24999

Shenoy, S.K., Drake, M.T., Nelson, C.D., Houtz, D.A., Xiao, K., Madabushi, S., Reiter, E., Premont, R.T., Lichtarge, O., Lefkowitz, R.J., 2006. β-Arrestin-dependent, G Protein-independent ERK1/2 Activation by the β2 Adrenergic Receptor. J. Biol. Chem. 281, 1261–1273. https://doi.org/10.1074/jbc.M506576200

Shiina, T., Kawasaki, A., Nagao, T., Kurose, H., 2000. Interaction with β-Arrestin Determines the Difference in Internalization Behavior between β1- and β2-Adrenergic Receptors. J. Biol. Chem. 275, 29082–29090. https://doi.org/10.1074/jbc.M909757199

Shin, S.-Y., Kim, T., Lee, H.-S., Kang, J.H., Lee, J.Y., Cho, K.-H., Kim, D.H., 2014. The switching role of β-adrenergic receptor signalling in cell survival or death decision of cardiomyocytes. Nat. Commun. 5, 5777. https://doi.org/10.1038/ncomms6777

Shukla, A.K., Violin, J.D., Whalen, E.J., Gesty-Palmer, D., Shenoy, S.K., Lefkowitz, R.J., 2008. Distinct conformational changes in β-arrestin report biased agonism at seven-transmembrane receptors. Proc. Natl. Acad. Sci. 105, 9988–9993. https://doi.org/10.1073/pnas.0804246105

Sorriento, D., Ciccarelli, M., Santulli, G., Campanile, A., Altobelli, G.G., Cimini, V., Galasso, G., Astone, D., Piscione, F., Pastore, L., Trimarco, B., Iaccarino, G., 2008. The G-protein-coupled receptor kinase 5 inhibits NFκB transcriptional activity by inducing nuclear accumulation of IκBα. Proc. Natl. Acad. Sci. 105, 17818–17823. https://doi.org/10.1073/pnas.0804446105

Sorriento, D., Gambardella, J., Fiordelisi, A., Iaccarino, G., Illario, M., 2019. GRKs and β-Arrestins: "Gatekeepers" of Mitochondrial Function in the

Failing Heart. Front. Pharmacol. 10. https://doi.org/10.3389/fphar.2019.00064

Sotoodehnia, N., Siscovick, D.S., Vatta, M., Psaty, B.M., Tracy, R.P., Towbin, J.A., Lemaitre, R.N., Rea, T.D., Durda, J.P., Chang, J.M., Lumley, T.S., Kuller, L.H., Burke, G.L., Heckbert, S.R., 2006. β2-Adrenergic Receptor Genetic Variants and Risk of Sudden Cardiac Death. Circulation 113, 1842–1848. https://doi.org/10.1161/CIRCULATIONAHA.105.582833

Später, D., Hansson, E.M., Zangi, L., Chien, K.R., 2014. How to make a cardiomyocyte. Development 141, 4418–4431. https://doi.org/10.1242/dev.091538

Stoll, S.W., Kansra, S., Elder, J.T., 2002. Metalloproteinases Stimulate ErbB-dependent ERK Signaling in Human Skin Organ Culture. J. Biol. Chem. 277, 26839–26845. https://doi.org/10.1074/jbc.M201108200

Sturgill, M.G., Kelly, M., Notterman, D.A., 2011. Chapter 25 - Pharmacology of the Cardiovascular System, in: Fuhrman, B.P., Zimmerman, J.J. (Eds.), Pediatric Critical Care (Fourth Edition). Mosby, Saint Louis, pp. 277–305. https://doi.org/10.1016/B978-0-323-07307-3.10025-4

Suzuki, T., Nguyen, C.T., Nantel, F., Bonin, H., Valiquette, M., Frielle, T., Bouvier, M., 1992. Distinct regulation of beta 1- and beta 2-adrenergic receptors in Chinese hamster fibroblasts. Mol. Pharmacol. 41, 542–548.

Takahashi, K., Tanabe, K., Ohnuki, M., Narita, M., Ichisaka, T., Tomoda, K., Yamanaka, S., 2007. Induction of Pluripotent Stem Cells from Adult Human Fibroblasts by Defined Factors. Cell 131, 861–872. https://doi.org/10.1016/j.cell.2007.11.019

Talkhabi, M., Aghdami, N., Baharvand, H., 2016. Human cardiomyocyte generation from pluripotent stem cells: A state-of-art. Life Sci. 145, 98–113. https://doi.org/10.1016/j.lfs.2015.12.023

Tanimura, A., Nezu, A., Tojyo, Y., Matsumoto, Y., 1999. Isoproterenol potentiates α-adrenergic and muscarinic receptor-mediated Ca2+ response in rat parotid cells. Am. J. Physiol.-Cell Physiol. 276, C1282–C1287. https://doi.org/10.1152/ajpcell.1999.276.6.C1282

Thomson, J.A., Itskovitz-Eldor, J., Shapiro, S.S., Waknitz, M.A., Swiergiel, J.J., Marshall, V.S., Jones, J.M., 1998. Embryonic Stem Cell Lines Derived from Human Blastocysts. Science 282, 1145–1147. https://doi.org/10.1126/science.282.5391.1145

Tomita, H., Nazmy, M., Kajimoto, K., Yehia, G., Molina, C.A., Sadoshima, J., 2003. Inducible cAMP Early Repressor (ICER) Is a Negative-Feedback Regulator of Cardiac Hypertrophy and an Important Mediator of Cardiac Myocyte Apoptosis in Response to β-Adrenergic Receptor Stimulation. Circ. Res. 93, 12–22. https://doi.org/10.1161/01.RES.0000079794.57578.F1

Tong, M., Seeliger, M.A., 2015. Targeting Conformational Plasticity of Protein Kinases. ACS Chem. Biol. 10, 190–200. https://doi.org/10.1021/cb500870a

Tran, T.M., Jorgensen, R., Clark, R.B., 2007. Phosphorylation of the β2-Adrenergic Receptor in Plasma Membranes by Intrinsic GRK5†. Biochemistry 46, 14438–14449. https://doi.org/10.1021/bi700922h

Traynham, C.J., Cannavo, A., Zhou, Y., Vouga, A.G., Woodall, B.P., Hullmann, J., Ibetti, J., Gold, J.I., Chuprun, J.K., Gao, E., Koch, W.J., 2015. Differential Role of G Protein–Coupled Receptor Kinase 5 in Physiological Versus Pathological Cardiac HypertrophyNovelty and Significance. Circ. Res. 117, 1001–1012. https://doi.org/10.1161/CIRCRESAHA.115.306961

Traynham, C.J., Hullmann, J., Koch, W.J., 2016. "Canonical and non-canonical actions of GRK5 in the heart." J. Mol. Cell. Cardiol. 92, 196–202. https://doi.org/10.1016/j.yjmcc.2016.01.027

Ungerer, M., Böhm, M., Elce, J.S., Erdmann, E., Lohse, M.J., 1993. Altered expression of beta-adrenergic receptor kinase and beta 1-adrenergic receptors in the failing human heart. Circulation 87, 454–463. https://doi.org/10.1161/01.CIR.87.2.454

van Roy, F., Berx, G., 2008. The cell-cell adhesion molecule E-cadherin. Cell. Mol. Life Sci. 65, 3756–3788. https://doi.org/10.1007/s00018-008-8281-1

Vidal, M., Wieland, T., Lohse, M.J., Lorenz, K., 2012. β-Adrenergic receptor stimulation causes cardiac hypertrophy via a Gβγ/Erk-dependent pathway. Cardiovasc. Res. 96, 255–264. https://doi.org/10.1093/cvr/cvs249

Vinge, L.E., Andressen, K.W., Attramadal, T., Andersen, G.Ø., Ahmed, M.S., Peppel, K., Koch, W.J., Freedman, N.J., Levy, F.O., Skomedal, T., Osnes, J.-B., Attramadal, H., 2007. Substrate Specificities of G Protein-Coupled Receptor Kinase-2 and -3 at Cardiac Myocyte Receptors Provide Basis for Distinct Roles in Regulation of Myocardial Function. Mol. Pharmacol. 72, 582–591. https://doi.org/10.1124/mol.107.035766

Vuolteenaho, O., Ala-Kopsala, M., Ruskoaho, H., 2005. BNP as a biomarker in heart disease. Adv. Clin. Chem. 40, 1–36.

Wang Jialu, Gareri Clarice, Rockman Howard A., 2018. G-Protein–Coupled Receptors in Heart Disease. Circ. Res. 123, 716–735. https://doi.org/10.1161/CIRCRESAHA.118.311403

Wang, J.J.-C., Rau, C., Avetisyan, R., Ren, S., Romay, M.C., Stolin, G., Gong, K.W., Wang, Y., Lusis, A.J., 2016. Genetic Dissection of Cardiac Remodeling in an Isoproterenol-Induced Heart Failure Mouse Model. PLOS Genet. 12, e1006038. https://doi.org/10.1371/journal.pgen.1006038

Wang Wang, Zhu Weizhong, Wang Shiqiang, Yang Dongmei, Crow Michael T., Xiao Rui-Ping, Cheng Heping, 2004. Sustained β1-Adrenergic Stimulation Modulates Cardiac Contractility by Ca2+/Calmodulin Kinase Signaling Pathway. Circ. Res. 95, 798–806. https://doi.org/10.1161/01.RES.0000145361.50017.aa

Wang, W.C.H., Mihlbachler, K.A., Bleecker, E.R., Weiss, S.T., Liggett, S.B., 2008. A Polymorphism of GRK5 Alters Agonist-Promoted Desensitization of β2-Adrenergic Receptors. Pharmacogenet. Genomics 18, 729–732. https://doi.org/10.1097/FPC.0b013e32830967e9

Wang, X., Cheng, Y., Xue, H., Yue, Y., Zhang, W., Li, X., 2015. Fargesin as a potential β1 adrenergic receptor antagonist protects the hearts against ischemia/reperfusion injury in rats via attenuating oxidative stress and apoptosis. Fitoterapia 105, 16–25. https://doi.org/10.1016/j.fitote.2015.05.016

Wang Yibin, 2007. Mitogen-Activated Protein Kinases in Heart Development and Diseases. Circulation 116, 1413–1423. https://doi.org/10.1161/CIRCULATIONAHA.106.679589

Warne, T., Edwards, P.C., Doré, A.S., Leslie, A.G.W., Tate, C.G., 2019. Molecular basis for high-affinity agonist binding in GPCRs. Science 364, 775–778. https://doi.org/10.1126/science.aau5595

Watson, P.A., Reusch, J.E.B., McCune, S.A., Leinwand, L.A., Luckey, S.W., Konhilas, J.P., Brown, D.A., Chicco, A.J., Sparagna, G.C., Long, C.S., Moore, R.L., 2007. Restoration of CREB function is linked to completion and stabilization of adaptive cardiac hypertrophy in

response to exercise. Am. J. Physiol. - Heart Circ. Physiol. 293, H246–H259. https://doi.org/10.1152/ajpheart.00734.2006

Wright, S.C., Schellenberger, U., Ji, L., Wang, H., Larrick, J.W., 1997. Calmodulin-dependent protein kinase II mediates signal transduction in apoptosis. FASEB J. 11, 843–849. https://doi.org/10.1096/fasebj.11.11.9285482

Wu, H., Lee, J., Vincent, L.G., Wang, Q., Gu, M., Lan, F., Churko, J.M., Sallam, K.I., Matsa, E., Sharma, A., Gold, J.D., Engler, A.J., Xiang, Y.K., Bers, D.M., Wu, J.C., 2015. Epigenetic Regulation of Phosphodiesterases 2A and 3A Underlies Compromised β-Adrenergic Signaling in an iPSC Model of Dilated Cardiomyopathy. Cell Stem Cell 17, 89–100. https://doi.org/10.1016/j.stem.2015.04.020

Wu, Q.Q., Ni, J., Zhang, N., Liao, H.H., Tang, Q.Z., Deng, W., 2017. Andrographolide Protects against Aortic Banding-Induced Experimental Cardiac Hypertrophy by Inhibiting MAPKs Signaling. Front. Pharmacol. 8. https://doi.org/10.3389/fphar.2017.00808

Wu, W., Lee, W.-L., Wu, Y.Y., Chen, D., Liu, T.-J., Jang, A., Sharma, P.M., Wang, P.H., 2000. Expression of Constitutively Active Phosphatidylinositol 3-Kinase Inhibits Activation of Caspase 3 and Apoptosis of Cardiac Muscle Cells. J. Biol. Chem. 275, 40113–40119. https://doi.org/10.1074/jbc.M004108200

Xi, B., Wang, T., Li, N., Ouyang, W., Zhang, W., Wu, J., Xu, X., Wang, X., Abassi, Y.A., 2011. Functional Cardiotoxicity Profiling and Screening Using the xCELLigence RTCA Cardio System. JALA J. Assoc. Lab. Autom. 16, 415–421. https://doi.org/10.1016/j.jala.2011.09.002

Xiao, K., Liu, H., 2016. "Barcode" and Differential Effects of GPCR Phosphorylation by Different GRKs, in: Gurevich, V.V., Gurevich, E.V., Tesmer, J.J.G. (Eds.), G Protein-Coupled Receptor Kinases, Methods in Pharmacology and Toxicology. Springer, New York, NY, pp. 75–120. https://doi.org/10.1007/978-1-4939-3798-1_5

Xiao, K., Shenoy, S.K., Nobles, K., Lefkowitz, R.J., 2004. Activation-dependent Conformational Changes in β-Arrestin 2. J. Biol. Chem. 279, 55744–55753. https://doi.org/10.1074/jbc.M409785200

Xiao, L., Pimental, D.R., Amin, J.K., Singh, K., Sawyer, D.B., Colucci, W.S., 2001. MEK1/2–ERK1/2 Mediates α1-Adrenergic Receptor-stimulated Hypertrophy in Adult Rat Ventricular Myocytes. J. Mol. Cell. Cardiol. 33, 779–787. https://doi.org/10.1006/jmcc.2001.1348

Yamaguchi, O., Watanabe, T., Nishida, K., Kashiwase, K., Higuchi, Y., Takeda, T., Hikoso, S., Hirotani, S., Asahi, M., Taniike, M., Nakai, A., Tsujimoto, I., Matsumura, Y., Miyazaki, J., Chien, K.R., Matsuzawa, A., Sadamitsu, C., Ichijo, H., Baccarini, M., Hori, M., Otsu, K., 2004. Cardiac-specific disruption of the *c-raf-1* gene induces cardiac dysfunction and apoptosis. J. Clin. Invest. 114, 937–943. https://doi.org/10.1172/JCI20317

Yang, J., Liu, Y., Fan, X., Li, Z., Cheng, Y., 2014. A pathway and network review on beta-adrenoceptor signaling and beta blockers in cardiac remodeling. Heart Fail. Rev. 19, 799–814. https://doi.org/10.1007/s10741-013-9417-4

Yang Jason H., Saucerman Jeffrey J., Winslow Raimond, 2011. Computational Models Reduce Complexity and Accelerate Insight Into Cardiac Signaling Networks. Circ. Res. 108, 85–97. https://doi.org/10.1161/CIRCRESAHA.110.223602

Yang, Z., Yang, F., Zhang, D., Liu, Z., Lin, A., Liu, C., Xiao, P., Yu, X., Sun, J.-P., 2017. Phosphorylation of G Protein-Coupled Receptors: From the Barcode Hypothesis to the Flute Model. Mol. Pharmacol. 92, 201–210. https://doi.org/10.1124/mol.116.107839

Yester, J.W., Kühn, B., 2017. Mechanisms of Cardiomyocyte Proliferation and Differentiation in Development and Regeneration. Curr. Cardiol. Rep. 19, 13. https://doi.org/10.1007/s11886-017-0826-1

Yi, X.P., Gerdes, A.M., Li, F., 2002. Myocyte Redistribution of GRK2 and GRK5 in Hypertensive, Heart-Failure–Prone Rats. Hypertension 39, 1058–1063. https://doi.org/10.1161/01.HYP.0000019130.09167.3B

Yu, J., Chau, K.F., Vodyanik, M.A., Jiang, J., Jiang, Y., 2011. Efficient Feeder-Free Episomal Reprogramming with Small Molecules. PLOS ONE 6, e17557. https://doi.org/10.1371/journal.pone.0017557

Yu, J., Thomson, J.A., 2008. Pluripotent stem cell lines. Genes Dev. 22, 1987–1997. https://doi.org/10.1101/gad.1689808

Yue, T.-L., Wang, C., Gu, J.-L., Ma, X.-L., Kumar, S., Lee, J.C., Feuerstein, G.Z., Thomas, H., Maleeff, B., Ohlstein, E.H., 2000. Inhibition of Extracellular Signal–Regulated Kinase Enhances Ischemia/Reoxygenation–Induced Apoptosis in Cultured Cardiac Myocytes and Exaggerates Reperfusion Injury in Isolated Perfused Heart. Circ. Res. 86, 692–699. https://doi.org/10.1161/01.RES.86.6.692

Zhai, C., Zhang, M., Zhang, Y., Xu, H., Wang, J., An, G., Wang, Y., Li, L., 2012. Glycyrrhizin protects rat heart against ischemia-reperfusion injury through blockade of HMGB1-dependent phospho-JNK/Bax pathway. Acta Pharmacol. Sin. 33, 1477–1487. https://doi.org/10.1038/aps.2012.112

Zhang, T., Brown, J.H., 2004. Role of Ca2+/calmodulin-dependent protein kinase II in cardiac hypertrophy and heart failure. Cardiovasc. Res. 63, 476–486. https://doi.org/10.1016/j.cardiores.2004.04.026

Zhang, X., Guo, L., Zeng, H., White, S.L., Furniss, M., Balasubramanian, B., Lis, E., Lagrutta, A., Sannajust, F., Zhao, L.L., Xi, B., Wang, X., Davis, M., Abassi, Y.A., 2016. Multi-parametric assessment of cardiomyocyte excitation-contraction coupling using impedance and field potential recording: A tool for cardiac safety assessment. J. Pharmacol. Toxicol. Methods, Focused Issue on Safety Pharmacology 81, 201–216. https://doi.org/10.1016/j.vascn.2016.06.004

Zhang, Y., Matkovich, S.J., Duan, X., Gold, J.I., Koch, W.J., Dorn, G.W., 2011. Nuclear Effects of G-Protein Receptor Kinase 5 on Histone Deacetylase 5–Regulated Gene Transcription in Heart FailureClinical Perspective. Circ. Heart Fail. 4, 659–668. https://doi.org/10.1161/CIRCHEARTFAILURE.111.962563

Zhao, G., Zhu, Y., Eno, C.O., Liu, Y., DeLeeuw, L., Burlison, J.A., Chaires, J.B., Trent, J.O., Li, C., 2014. Activation of the Proapoptotic Bcl-2 Protein Bax by a Small Molecule Induces Tumor Cell Apoptosis. Mol. Cell. Biol. 34, 1198–1207. https://doi.org/10.1128/MCB.00996-13

Appendix I - Publications and other scientific contributions

Publication:

Alexander Kondrashov, Minh Duc Hoang, James GW Smith, Jamie R Bhagwan, Gary Duncan, Diogo Mosqueira, Maria Barbadillo Munoz, **Nguyen TN Vo**, Chris Denning. Simplified footprint-free Cas9/CRISPR editing of cardiac-associated genes in human pluripotent stem cells. **Stem cells and development** 27 (6), 391-404.

Poster presentations at local conferences:

Jun, 2019: Cancer and STEM Away Day. Poster title: "Study GRK5-L41- mediated cardioprotection during catecholamine stress using footprint-free CRISPR/Cas9 edited human pluripotent stem cell-derived cardiomyocytes".

Dec 2018: MSCA Eighth Annual Scientific Meeting 2018. Poster title: "Using footprint-free CRISPR/Cas9 edited human pluripotent stem cells to study GRK5-mediated cardioprotection during catecholamine stress".

Seminars:

July 2019: COMPARE Team Science Seminar, University of Birmingham, United Kingdom. Invited talk: "Using footprint-free CRISPR/Cas9 edited human pluripotent stem cells to study GRK5-L41 mediated cardioprotection during catecholamine stress".

Dec 2018: Vinmec Research Institute of Stem cell and Gene Technology, Vietnam. Invited talk: "Understanding cardioprotective function of GRK5 polymorphism using human pluripotent stem cell-derived cardiomyocyte model".

Honors and awards

July 2019: winner for poster presentation at Cancer and STEM Away Day, University of Nottingham, United Kingdom.

Dec 2018: 1st prize for poster presentation at MSCA Eighth Annual Scientific Meeting, University of Birmingham, United Kingdom.

Oct, 2018: 3rd prize for oral presentation at Sue Watson PGR Oral Presentation Event for the work "Study roles of the GRK5-L41 polymorphism during catecholamine stress using hPSC-CMs".

Oct 2016: Vice-Chancellor's Scholarship for Research Excellence for International student year 2016, by University of Nottingham.